HIGH RESOLUTION PROTON SCATTERING AT 100 MEV

by

Yigal S. Horowitz

A thesis submitted to the Faculty of Graduate Studies and Research in partial fulfilment of the requirements for the degree of Doctor of Philosophy.

Foster Radiation Laboratory
McGill University
Montreal.

July 1968

ABSTRACT

Nuclei in the 2s-1d shell, ^{24}Mg and ^{28}Si, as well as ^{12}C in the 1p shell have been studied by means of elastic and inelastic scattering of 100 MeV protons. A lithium drifted germanium detector long enough to stop 100 MeV protons in side-entry orientation and mounted in a scattering chamber-cryostat has been used as the total absorption proton counter. This experiment constitutes the first use of germanium detectors as total absorption counters for proton energies above 60 MeV. The overall energy resolution of 0.4 MeV (FWHM) achieved is as good as the best resolutions presently attainable with magnetic spectrometers in the 100 MeV to 200 MeV energy region.

The measurements cover an angular region from 10° - 60° and excitation energies up to 16.5 MeV. Angular distributions have been extracted for 35 peaks in the energy spectra. An optical model analysis of the elastic scattering is presented. A qualitative discussion of the excited states which correspond to the observed peaks is presented and is based mainly on shapes of the distributions. Comparisons are made with results from similar experiments. Shapes of angular distributions for strongly excited 2+ and 3^- transitions appear energy and shell independent, however significant differences exist for 0+ and 4+ transitions. A comparison of proton inelastic scattering and radiative decay rates is presented. The E3 transition rate for the 10.18 MeV level in ^{28}Si is estimated.

The excitation of a previously unknown level in ^{28}Si at an energy of 11.45 ± 0.12 MeV with $J^\pi = 5^-$ has been observed. The level may be the 5^- level of the $K = 3^-$ band in ^{28}Si. The measurements confirm the $J^\pi = 3^-(1^-)$ assignment to the 10.18 MeV level in ^{28}Si (O. Sundberg *et al.* 1967) and are suggestive of a $J^\pi = 4+$ assignment to the 14.08 MeV level in ^{12}C.

ACKNOWLEDGEMENTS

I wish to acknowledge with gratitude the encouragement and valuable advice of Professor R. E. Bell which was given throughout the course of this research.

The interest and suggestions of Professor N. K. Sherman during the earlier parts of this work have proved invaluable.

The author acknowledges the help of Mr. I. Mackenzie who collaborated wholeheartedly in the measurement of the elastic scattering cross-sections. Thanks are also due to Dr. T. Y. Li for making available his optical model program and for instructions in its use and interpretation.

My thanks to Professor S. K. Mark for many valuable suggestions, one of them, the use of an old Ortec detector as the silicon target.

The skilled draftmanship and designing ability of Mr. J. Annecou are gratefully acknowledged. Mr. Annecou collaborated in the design of the scattering chamber-cryostat.

Mr. S. Doig, foreman of the Machine Shop, is thanked for his ready co-operation, Mr. S. Smith for his patient and careful construction of the scattering chamber-cryostat.

Finally, the financial support of J. W. McConnell Memorial Fellowships held during the course of this work is gratefully acknowledged.

TABLE OF CONTENTS

LIST OF ILLUSTRATIONS

LIST OF TABLES

CHAPTER 1. INTRODUCTION

1.1 EXPERIMENTAL MOTIVATION

The excitation of nuclei by protons of intermediate energy, that is, from 100 MeV to 200 MeV can be an important tool in nuclear structure studies. The impulse approximation is expected to be valid for these energies so that the microscopic model which describes nuclear states in terms of the motions of individual nucleons offers the possibility of testing nuclear wave functions. In principle this microscopic model has no free parameters at intermediate energies.

The applicability of the impulse approximation to nucleon probes of 100 MeV or higher with light nuclei was first discussed by Serber (1947). He pointed out that at these energies the de Broglie wavelength of the incident proton becomes smaller than or comparable with the average spacing of nucleons in the nucleus. For nucleons of 100 MeV a wavelength of 0.48×10^{-13} cm is to be compared with an average nucleon spacing of approximately 1.8×10^{-13} cm. The impulse approximation thus disregards the possibility of interaction of the incident nucleon with two or more nucleons at the same time. The force assumed to be producing the inelastic scattering is thus just the free two-nucleon interaction acting once. In the sense of this simplicity, proton probes of 100 MeV or greater have proved superior to lower energy protons where the nucleon-nucleon

scattering is modified appreciably, but in an unknown manner, by the presence of other nucleons in the nucleus.

Compared to electrons protons are desirable as nuclear probes because they "see" neutrons and protons equally well and because the strong spin and isospin coupling which characterizes the nucleon-nucleon interaction could concievably provide valuable information about the way in which nucleon spins are distributed in the nucleus. Moreover the measurement of inelastic scattering of protons is now being performed with high accuracy in a broad energy region extending up to 185 MeV.

An additional feature of inelastic scattering is that the matrix elements are closely related to those for radiative transitions so that information can be obtained about the spin and parity of excited states. Cohen and Rubin (1958) were the first to establish that the levels strongly excited by inelastic scattering were those strongly coupled to the ground state by the electromagnetic field.

Some of the more important studies of high energy inelastic proton scattering from complex nuclei are listed in Table 1. In many cases measurements were also made on heavier nuclei but especially prior to 1960, the inelastic spectrum showed insufficient resolved features to be analysed. It is obvious that the resolution in energy is a figure of merit for these experiments and sets a definite limit to what can be achieved regarding information on nuclear levels. Unfortunately the higher energy proton scattering experiments have

TABLE 1

SUMMARY OF INELASTIC PROTON SCATTERING EXPERIMENTS FOR ENERGIES BETWEEN 96 MeV AND 185 MeV

Ref. and Year	Energy MeV	Beam Energy Spread	Target Nuclei	Method of Energy Analysis	Total Energy Resolution MeV
1,1954	96	2	C	Range telescope	3.0
2-3, 1956	96	2	Li,Be,B,C,N,O	Range telescope	3.0
4,1956	185	1	C	Magnetic	
5-6,1957	185	1	C,O,Li,Be,B,N	Spectrometer	1.8
7,1957	135 95	---	C	Total Absorption	3.4
8,1964	155	0.5	$Li^{6,7}$,Be^{9},$B^{10,11}$ C,O	Magnetic Spectrometer	0.8
9,1964	185	0.25	ditto	Magnetic Spectrometer	0.4-0.5
10,11 1966	185	0.25	Mg, Al, Si	Magnetic Spectrometer	0.35
12, 1966	100	0.4	Li, Be, C	Total Absorption	1.8
13,1967	100	0.4	C, Mg, Si	Germanium total Absorption	0.4-0.6

1-2-3 Strauch and Titus
4-5-6 Tyren and Maris
7 Dickson and Salter
8 Jacmart et al.
9-10-11 Hasselgren et al.
12 Mark et al.
13 Horowitz et al.

in the past been severely disadvantaged because of energy resolution very often inadequate to resolve peaks corresponding to the various excited states.

The high resolution magnetic spectrometer constructed in Uppsala (Table 1) represents to date almost an order of magnitude improvement in energy resolution over the first proton inelastic scattering experiments in 1954. The importance of this advance is best illustrated by noting that Strauch and Titus in 1954 were able to extract angular distributions for only two excited states in ^{12}C (the 4.43- and 9.67 MeV levels) whereas the corresponding number of angular distributions extracted by the Uppsala group in 1965 was twelve representing inelastic scattering from the 4.4-, 7.6-, 9.7-, 12.7-, 15.1-, 16.1-, 18.2-, 19.3-, 20.4-, 21.4-, 22.1-, and 23.4 MeV levels, a twenty-five MeV region of excitation.

At the Foster Radiation Laboratory we have obtained in the past energy resolutions of 1.2% and 1.8% with NaI (Tl) and plastic scintillation counters respectively. Converted to MeV these percentages represent a resolving power quite inadequate to study even the first excited states of most s-d shell nuclei and many p shell nuclei. The need for better energy resolution in 100 MeV proton inelastic scattering experiments prompted our investigation into the use of lithium drifted germanium crystals as total absorption counters. The results have been very successful. The overall experimental resolution for A = 24, 28 is approximately 400 keV, almost all of which we believe is due to beam spread. An energy resolution of 400 keV is as good as the best energy resolution presently available with magnetic spectrometers in the 100 MeV to 200 MeV region. With the germanium detectors, however, one has

the great advantage of obtaining the entire energy spectrum simultaneously in the detector. In contrast the Uppsala group at 185 MeV obtained their energy spectra in steps of 0.4 MeV. This advantage has, for example, allowed us to easily extend the angular region studied out to 60 degrees whereas the studies at Orsay and Uppsala have usually been carried out to only 30 or 40 degrees.

The first part of this thesis describes the use of the germanium detectors as total absorption counters in our studies of 100 MeV proton inelastic scattering from the ^{12}C, ^{24}Mg and ^{28}Si nuclei. Prior to and concurrent with our work, reports have been published of total absorption detection of 29 MeV and 40 MeV protons by Pehl et al. in 1965, 59 MeV protons by Bertrand et al. in 1966, and 160 MeV protons by Gruhn et al. in 1967. Our successful total absorption detection of 100 MeV protons has been reported by Horowitz et al. also in 1967.

1.2 GENERAL DETECTOR REQUIREMENTS

The desired properties for a 100 MeV total absorption detector must include:

I - An energy resolution for 100 MeV protons better than the 700 keV we have obtained using NaI (Tl). This figure represents a best value for a selected counter used to detect a nearly monochromatic beam. This "pencil beam" was produced by a slit system described by Portner (1965) and was estimated to produce a beam with energy spread

of approximately 120 keV (FWHM). Aligned in the full beam NaI(Tl) counters yield roughly 900 keV (FWHM) resolution. If one assumes the figure of 700 keV (FWHM) to represent the detector and photomultiplier contribution to the energy resolution one obtains by subtracting in quadrature a value of approximately 600 keV (FWHM) for the energy spread of the full beam. Prior to our work this was the generally accepted value of the beam energy spread, but obviously the fact that the two contributions are roughly equal makes this estimation of the beam energy spread of dubious accuracy.

II - A high peak count to total count ratio. This consideration is as important as the intrinsic detector resolution if one expects to extract cross-sections of reasonable accuracy from the detected particle spectra. The two major effects which contribute to this ratio being less than unity are, of course, nuclear reactions in the crystal and multiple Coulomb scattering of protons out of the crystal. One cannot avoid reactions in the crystal, but proper collimation can effectively minimize the latter process. The requirement of somehow collimating the scattered protons so that they can only impinge on some central area of the detector places very definite minimum dimensions acceptable for a practical detector.

III - A consistent response over the volume irradiated, a pulse rise-time suitable for microsecond timing and a dead layer thin enough so that energy straggling contributes negligibly to the overall resolution.

IV - A reasonable lifetime under the conditions of high fluxes of high energy neutron and proton bombardment.

The ability of semi-conductor detector systems to measure a wide energy range while simultaneously providing very good energy resolution has led to their widespread use in modern nuclear spectroscopy. We were led, therefore, to consider the possible adaptation of this type of detector to the total absorption detection of 100 MeV protons.

In low energy nuclear spectroscopy the usual experimental detector configuration has the detected charged particle entering the diode in a direction perpendicular to the detector junction. In this configuration the thickness of the active volume corresponds to the depleted depth of the diode. Successful drifts to 5 mm have been reported in silicon (Pehl et al.1965), and although successful drifts to a depth of 10 mm have been reported for germanium it appears to be very difficult to produce a detector having a depth greater than 7 mm. Typically an 8 mm thick germanium detector requires 300 hours to drift (F. S. Goulding 1966). A 5 mm silicon detector can stop 29 MeV protons and a 10 mm germanium detector can stop 60 MeV protons. Since the range of a 100 MeV proton in silicon is 50 mm and in germanium 24 mm, it was obvious to us that in the p-i-n detectors sufficient stopping thickness of material could be obtained only in a configuration where the protons enter the detector in a direction parallel to the detector junction. Even if successful drifts to several centimeters could be achieved high resolution

measurements of charged particles would be severely hampered by the inability to collect all the charge within a reasonable period of time. A schematic representation of a typical detector illustrating the two configurations is shown in figure 1. The side entry technique also has the advantage that it offers little dead layer to the incident particles since the compensated region for these detectors is thought to extend to the edge of the depleted region.

FIGURE 1

FIGURE 1

Lithium drifted germanium detector in side-entry configuration required for the total absorption detection of 100 MeV protons. The detector is 26 mm long, approximately 10% longer than the range of a 100 MeV proton in germanium.

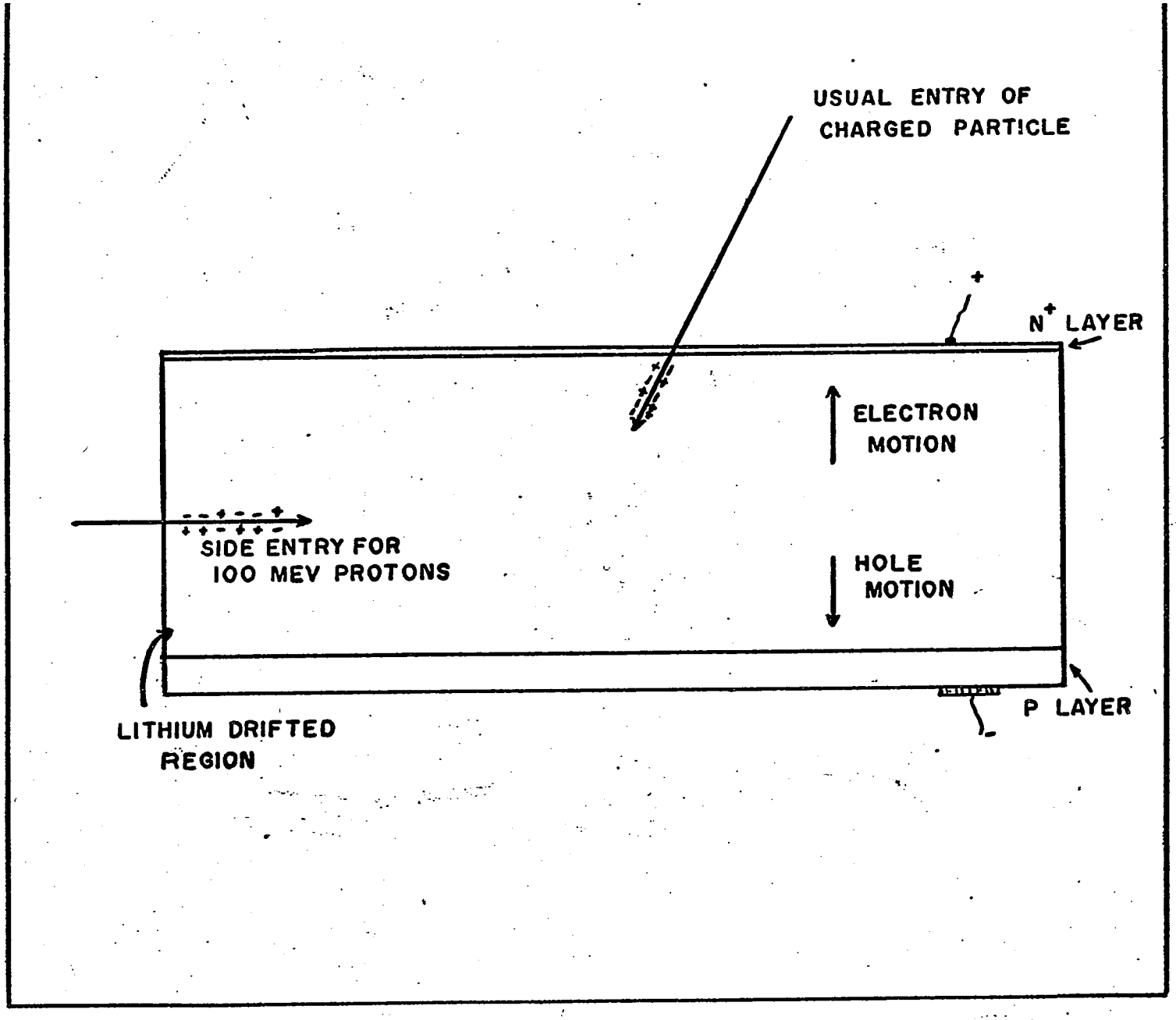
USUAL ENTRY OF
CHARGED PARTICLE
N+ LAYER
ELECTRON
MOTION
HOLE
MOTION
SIDE ENTRY FOR
100 MEV PROTONS
LITHIUM DRIFTED
REGION
P LAYER

CHAPTER 2. Ge(li) CRYSTALS - TOTAL ABSORPTION DETECTION OF 100 MeV PROTONS

2.1 INTRINSIC DETECTOR RESOLUTION

It is interesting to consider the ultimate resolution limit of germanium detectors for 100 MeV protons. Assuming no other sources of resolution spreading the ultimate resolution is determined by the statistical fluctuations in the number of electron-hole pairs created in the crystal by the incident particle.

If all the energy lost by the 100 MeV proton in the detector were converted by one unique mechanism into ionization the signal produced could show no fluctuation and there would be no statistical spread. On the other hand if much of the energy was dissipated in thermal heating of the lattice and the probability for the production of an electron-hole pair was low compared to non-ionizing events then we could expect normal statistical fluctuations in the number of hole-electron pairs produced. In this case the statistical fluctuation Δn would be given by

$$\Delta N = (E/\varepsilon)^{1/2} \quad \ldots\ldots\ldots\ldots\ldots\ldots 1$$

where E is the energy absorbed by the detector and ε is the average energy required to produce a hole-electron pair. In semi-conductors

as well as for gaseous detectors the real situation lies between these two extremes. Fano (1947) was the first to treat the process in gases and for that reason the discrepancy between the normal statistical fluctuations and the experimentally observed statistical fluctuations is called the Fano factor, F.

$$(\Delta N)^2_{exp} = F(\Delta N)^2 \quad \ldots\ldots\ldots 2$$

Combining equations 1 and 2 we obtain -

$$(\Delta E)_{FWHM} = 2.355(\varepsilon EF)^{1/2} \quad \ldots\ldots 3$$

The most recent measurements of the Fano factor in germanium have been by Mann and Bilger (1966). Their results at high electric fields of the order of 1000 volts per cm led them to conclude that the intrinsic Fano factor for γ rays or electrons in germanium at liquid N_2 temperature ($77^{\circ}K$) is $F = 0.129 \pm 0.003$ and appears to be independent of the primary energy in the investigated range, i.e., from 0.122 MeV to 4.8 MeV.

Heavier particles like protons, alphas or tritons have the added disadvantage of producing additional fluctuations through nuclear collisions. Lindhard and Nielsen (1962) have shown, however, that for protons the additional fluctuations should remain small compared to the Fano width. Siffert et al. (1966) have investigated the Fano factor for low energy protons. They get $0.1 < F < 0.5$ for various proton energies from 1 to 5 MeV and explain the rather large differences by noting that their beam energy fluctuations could have been larger than assumed. Their results consequently can neither confirm nor deny the Lindhard-Nielsen predictions.

If we assume the validity of the Lindhard-Nielsen model

and use F = 0.13 for protons also, it is then a simple matter to obtain the figure of 16.3 keV for the theoretical limitation of the energy resolution for 100 MeV protons.

Workers in the intermediate energy proton field have so far reported results which after corrections due to other sources of energy spread are still considerably higher than the theoretical limitation calculated for F = 0.13. Pehl et al. (1965), after subtracting non-detector contributions such as beam energy spread, thin entrance window, and electronic noise arrived at a spread of 21 keV for 30 MeV protons and 30 keV for 40 MeV protons, compared to a theoretical limitation of 8.9 and 10.4 keV respectively. Bertrand et al. (1966) arrived at a detector contribution of 95 keV compared to the theoretical limitation of 12.6 keV for 60 MeV protons. Gruhn et al. (1967) at 160 MeV made no effort to unfold their detector resolution from the overall energy resolution.

Our own efforts have been seriously hampered by an inadequately known beam energy width however in the following section we shall show that a value of 160 keV (FWHM) can be tentatively extracted for our detector response to 100 MeV protons. These results are summarized in figure 2. Note that the trend away from the theoretical limitation is well established for 29 MeV and 40 MeV protons detected with the same germanium crystal. Also note that only the results for the 30 MeV protons lie below the theoretical limitation based on a Fano factor of 1.

Although many more careful measurements must be made before a definitive statement could be attempted, it appears that the practical response of lithium drifted germanium detectors to high energy protons may be limited by more than purely statistical fluctuations in the number of hole-electron pairs created. In any event it is obvious that these detectors should, indeed, satisfy our first requirement of substantially better energy resolution than that obtainable with NaI(Tl) crystals.

In fact, the theoretically predicted resolution limit represents roughly a factor 15 improvement over even the most optimistic estimates recently arrived at by Houdayer et al. (1967) for a NaI(Tl) crystal coupled to the photocathode of a RCA 8575 photomultiplier in an experimental configuration which rejects the dynode multiplication factor of the photomultiplier in favour of the standard charge sensitive amplification used in semi-conductor techniques.

2.2 DETECTOR ENERGY RESOLUTION

Determination of the Ge (Li) counter optimum energy resolution was important both from the point of view of possibly obtaining additional information about the fundamental response of germanium detectors to high energy protons and also our desire to obtain the best energy resolution we could achieve with these counters. Our experimental program consisted of aligning the detector in the full

beam with the cyclotron current drastically reduced so that approximately 100 protons per second were incident upon the detector. The detector bias and amplifier shaping networks were then varied to obtain optimum resolution. Although no extremely intensive cross-check of these three inter-related parameters was carried out, some general features did emerge.

For RC integration and differentiation time constants beyond one microsecond the overall energy resolution was insensitive to increases of the detector bias above 700 volts (100 volts/mm). This is an indication that the electron-hole charge carriers have reached saturation velocity for an electric field of 100 volts/mm. This is in good agreement with a study of collection times in germanium carried out by Bertrand (1966). For values of detector bias below 700 volts the time constant had to be increased beyond one μsecond to achieve optimum resolution. For a time constant of 0.5μsecond (the next smallest value made available by the Ortec 410 amplifier) The observed resolution was 600 keV and an increase of detector bias to 1000 volts was not observed to improve this resolution - an expected result if indeed saturation velocity had been reached.

With a detector bias of 700 volts and one μsecond integration and differentiation time constants an energy resolution of 380 $\pm$ 20 keV was an easily reproducible result. The straggling due to energy loss in aluminum in the beam path contributes roughly 50 keV to the resolution

and the electronic noise contribution, as determined by the width of a 60 cycle pulser taken with the beam on was 80 keV. The energy resolution after unfolding these effects is 368 keV.

Prior to our use of a Ge (Li) detector there had been at least two attempts to estimate the energy spread of the McGill proton beam. P. M. Portner (1963) obtained a profile of the beam at the horizontal crossover downstream from the 45 degree magnet. His method was to locate a range analyser and Faraday cup after a 0.030 inch slit at the horizontal cross-over point. The slit was moved horizontally across the beam by remote control and the beam profile obtained by measuring the current in the Faraday cup at 0.025 inch intervals. The measured current was normalized using an external beam monitor cup. A range energy determination was then performed with the slit defining a small portion of the beam on either side of the profile. The measurements indicated an energy dispersion of 4.4 MeV/inch. On the basis of phase space area (for a monoenergetic beam) the horizontal size of the beam at the focus should be 0.12 inches. The close agreement between this number and the profile obtained with the range analyser as well as an independent measurement of the beam size by polaroid exposures made it reasonable to consider the profile to be a momentum distribution of the beam. Assigning this profile the energy dispersion previously mentioned Portner arrived at an energy spread of 330 $\pm$ 20 keV (FWHM).

This value was in significant disagreement with the more generally accepted value of $\sim$ 600 keV (FWHM) for the full beam energy spread. Our own result of 380 $\pm$ 20 keV is clearly compatible only with Portner's results. Our peak also displays a low energy deviation from Gaussian symmetry very similar to the form of the profile observed by Portner. Unfolding a beam energy spread of 330 keV yields a detector contribution of 160 keV. The +5% uncertainty in these measurements produces however roughly a 40% uncertainty in the final unfolded estimate of the detector resolution.

We conclude that our best estimate of the detector resolution is 160 $\pm$ 60 keV. Our lack of precise knowledge of the beam energy spread prevents a meaningful comparison between this result and the theoretical limit. A beam whose energy spread is very small and well known must be used in order to study the ultimate resolution possible using lithium drifted germanium detectors in high energy proton scattering experiments.

2.3 DETECTOR SENSITIVE VOLUME REQUIREMENTS

Recall that the second requirement involved a minimum active volume based on the necessity of collimating the detector. This collimation is absolutely necessary from two points of view. The first and perhaps most important is that the protons impinging on the detector should be confined to a central area of the detector so that the probability of their multiple Coulomb scattering out of

the active volume is very small. In NaI(Tl) crystals this problem is effectively non-existent because of their very large volume and consequent ease of effective collimation.

Another reason for the necessity of collimation arises from the variation in the collection time of the charge carriers produced in different regions of the drifted volume. This variation in collection time will cause a variation at the amplifier output for a given total charge resulting in a broadened resolution. This effect is sometimes referred to as the "ballistic defect" (Baldinger et al. 1956). In normal configurations it takes the form of a non-linearity since different energy particles penetrate the depleted area to different depths. However in the side-entry configuration the collection time (usually defined as the rise-time of an integrated pulse) for holes and electrons vary with the point of incidence of the protons. As the incident location approaches the positive side of the diode, the collection times of the electrons becomes shorter and that of the holes becomes longer while as the incident location approaches the bottom of the depleted region the relative collection times reverse. Thus there is an obvious advantage to restricting the protons to some small central area of the detector. Bertrand et al. (1966) have done some measurements illustrating this effect. Using a 1 mm collimator width, their observed resolution of 170 keV for 60 MeV protons was the same for 1.6 or 6.4 microsecond time constants. However with a 3 mm collimator width there was a 15% difference in

resolution for the same two values of amplifier time constant.

There are basically two limitations involved in the ultimate drifted depth useable in lithium drifted germanium detectors. The first is a practical one involving the rate of growth of the intrinsic region with present drifting techniques (the drift time increases as the square of the required depletion depth). The second is the problem of complete charge collection for very deeply depleted diodes in a reasonable period of time. The latter problem will be discussed in a following section.

Because of the long drift times required a depth of 7 mm was the maximum depth for which RCA Victor Co. of Montreal was prepared to quote a reasonable price ($900.00).

The range of a 100 MeV proton in germanium is 12.6 g/cm^2 (Williamson et al. 1966) equivalent to a stopping distance in germanium of 23.7 mm. To allow for the effects of range straggling and possible uncertainties in the tabulated estimates of the ranges of protons in germanium the lengths of the diodes were chosen to be 10% greater than 23.7 mm. The detectors thus had a total active volume of dimensions 26.1 x 10 mm x 7 mm.

Different factors such as beam spot size, beam stability and detector target separation enter into the design of the detector telescope which will be discussed in detail in a later section. The RMS lateral displacement due to multiple Coulomb scattering of 100 MeV protons in germanium is almost exactly one mm. Because of this and the previous geometrical considerations we decided to limit

the area of the detector upon which scattered protons are allowed to impinge to a central area of the active volume of dimensions 1.2 mm x 2.4 mm or a total area of 2.9 mm^2. In this configuration no proton can impinge on the detector in an initial direction, which if undeflected by multiple Coulomb scattering, would come within two root mean square lateral displacements of the active volume boundary. (Figure 10 illustrates the target detector geometry). This places an upper limit of 5% loss from the active volume for 100 MeV protons and indicates that these detectors can satisfy the second requirement of high peak to total ratio.

2.4 PEAK TO TOTAL RATIO

A high peak to total ratio is important for the efficient extraction of accurate cross-sections from experimental spectra. In a clean situation (i.e., negligible slit scattering or multiple scattering out of the detector) the peak to total ratio serves as a direct measurement of the efficiency correction of the detected proton in the detector material. To correct for this effect the percentage of points falling out of the peak must be added back to the peak area to obtain the correct cross-section. This problem will be treated in greater detail in section 5.2 under Data Reduction.

To determine the peak to total ratio our experimental program consisted of aligning the detector in the full beam and adjusting the cyclotron so that approximately 100 protons per

second were incident upon the detector. The detector was preceded by a counter telescope described in section 3.2. The peak to total ratio was determined from the number of counts in the total energy spectrum compared to the number of counts in the peak which was taken to extend 1 MeV below the peak channel. The best reproducible ratio obtained was 0.82 (or a ratio of tail to peak of 0.23). A typical spectrum is illustrated in figure 3. This result is too low to be attributed in its entirety to nuclear reactions in the germanium crystal.

M. Q. Makino et al. (1967) have calculated the efficiency corrections for nuclear reactions in silicon and germanium for 5 MeV to 150 MeV protons using the energy dependence of the proton total reaction cross-sections. They calculate a tail-to- peak ratio of 0.093 for 100 MeV protons in germanium.

Bertrand et al. have determined in a manner similar to ours a peak to total ratio of 0.94 for 60 MeV protons (or a tail-to peak ratio of 0.064). They attributed this ratio (because of their superior geometry) entirely to nuclear reactions in the detector. Their value of 0.064 is roughly 50% higher than the Makino value of 0.043 for 60 MeV protons. To estimate our own efficiency correction we have assumed the shape of the Makino results as a function of energy is correct but have increased the absolute correction by 50% to account for the discrepancy between the Bertrand measurement and the Makino calculation. From the point of view of estimating cross-

sections (section 5.2 for a detailed discussion) the most valuable aspect of the Makino calculations is the shape of the efficiency curve and not the absolute value of the individual efficiency corrections.

Increasing 0.093 by one-half yields a value of 0.139 for our estimate of the tail-to-peak ratio due to reactions of 100 MeV protons in germanium. Assuming an upper limit of 0.05 for points falling out of the peak due to multiple scattering leaves a figure of 0.04 to be attributed to collimator slit scattering to account for the measured tail-to-peak ratio of 0.23. These figures are approximate and are intended only to illustrate that multiple scattering out of the detector and collimator slit scattering were not serious problems for our particular geometry.

2.5 DETECTOR LINEARITY

The third requirements mentioned in the introduction involved aspects of the detector which could not easily be tested directly. The dead area at the edge of the diodes is believed by Webb of RCA Victor to have a thickness between 0.5 and 5 microns. The upper limit is at least one order of magnitude less than the thickness at which straggling effects might contribute significantly to an overall energy resolution of 400 keV.

An inconsistent response over the irradiated volume could show itself by a non-linearity in the detector response to different

proton energies. A convenient approach to test the detector linearity is then simply to observe the spectrum of protons scattered from ^{12}C. At a laboratory scattering angle of 45 degrees the Q value for exciting the first level in ^{12}C is 4.32 MeV which fixes the energy calibration per channel at 140 keV/channel. The centroid energy of each proton peak is then calculated and compared with the expected Q values based on the accurately known energy level spectrum of ^{12}C.

TABLE II

OBSERVED AND CALCULATED Q VALUES FOR PROTON INELASTIC SCATTERING FROM ^{12}C

^{12}C energy levels MeV	Calculated Q MeV	Experimentally determined Q - MeV	Difference %
7.66	7.48	7.38	-1.3
9.63	9.41	9.44	+0.4
10.84	10.59	10.52	-0.7
11.81	11.54	11.57	+0.3
12.73	12.44	12.44	-
14.05	13.74	13.84	+0.7
15.11	14.78	14.88	+0.7
16.11	15.76	15.96	+1.3

The results are shown in Table II and illustrate the very linear response of the detector to proton energies between 75- and 100 MeV.

2.6 CHARGE COLLECTION TIME

One of our criteria for a practical detector for 100 MeV proton inelastic scattering was a pulse rise-time suitable for microsecond timing. It is instructive to see how the charge collection time (which determines the amplifier time constants necessary for maximum resolution) ultimately affects the maximum experimental counting rate possible before pulse pile-up and base line shift begin to affect the system. A good rule of thumb to observe is that the counting rate be less than p/τ (Goulding 1966, page 44) where p is the fractional resolution and τ the amplifier time constant. Thus for a pulse beam of duty cycle 250:1, a fractional resolution of 0.5% and one microsecond time constants the instantaneous counting rate must be less than 20 counts/sec. to avoid adverse effects due to pulse pile-up. From Poisson statistics a counting rate of 20 counts/sec. yields 0.5% pulse pile-up.

The restriction to this counting rate can be a very serious limitation if one is attempting to extract the cross-section of weakly excited nuclear states. For example, the number of events falling under the peak corresponding to the excitation of the 16.1 MeV level in C^{12} at 35 degrees is roughly one part in five thousand of the total number of events in the spectrum. Taking into account the 3.5:1 rejection rate due to the NE 102 window collimation reduces this ratio to roughly one part in 17.5 thousand of the total number of events occurring in the detector. To acquire 400 counts under this

peak (5% statistics) one would require 100 hours of running time. This figure is impractically high and fortunately our experiments have been performed with the recently operational stretched beam with a duty cycle of approximately 20:1 lowering the required time for 5% statistics (at that particular angle) to 8 hours.

The collection time of the electron-hole pairs created in the depleted region of the detector is ultimately related to two externally controllable variables in the following manner:

$$T = \frac{W}{V} = \frac{W}{E\mu(\text{temp})} = \frac{W^2}{(\text{voltage})\mu(\text{temp})}$$

where v is the average electron or hole drift velocity in the field direction, E is the applied electric field, and μ (temp) are the electron and hole mobilities which are related to the temperature in the following manner:

$$\mu_e\ (T^o, K) = 4.9 \times 10^7\ T^{-1.66}\ \text{cm}^2/\text{V sec}$$

$$\mu_h\ (T^o, K) = 1.05 \times 10^9\ T^{-2.33}\ \text{cm}^2/\text{V sec.}$$

The former equation is true only up to a certain saturation drift velocity where further increases in the applied field no longer increase the drift velocity. This effect of saturation drift velocity

has been studied by Bertrand et al. (1966). They measured the collection times for holes and electrons with biases of 200 volts, 500 volts and 700 volts applied to the detector, and found that as the voltage was increased from 200 volts to 500 volts the drift velocity increased by a factor of 1.6. Further increases to 700 volts resulted in only a 4% increase in the velocities, indicating that a saturation voltage had been reached.

We have seen how the amplifier time constants affect the maximum possible counting rate. The amplifier time constants necessary for maximum energy resolution in turn depend on the charge collection time. Baldinger and Franzen (1956) have studied the response of a pulse shaping network consisting of an RC differentiator and an RC integrator. They considered the case in which the differentiator and integrator are isolated from each other and $(RC)_d = (RC)_i = \tau$. The output from such a network in response to an input of given amplitude, is a function of the input rise-time, T. When the input is a step function, i.e., T = 0 the output has a maximum amplitude V_m. But when an input rises to the same amplitude in time T the output pulse has an amplitude V_t which is smaller than V_m. Baldinger and Franzens showed that this relative ballistic deficit for signals which rise to their final amplitude linearly in time T can be expressed as follows:

$$\frac{\Delta N}{N_o} = \frac{V_m - V_t}{V_m} \cong \frac{1}{24}(T/\tau)^2 \quad \ldots\ldots 4$$

where $\Delta N/N_o$ is the deficit expressed as the fraction of lost pairs.

As an example if $T = 1 \times 10^{-7}$ seconds and $\tau = 1 \times 10^{-6}$ seconds we obtain $\Delta N/N_o = 4.2 \times 10^{-4}$ or roughly 100 keV additional contribution to the overall energy width. Because of the much greater beam energy spread we were not capable of observing any increases in overall resolution beyond $\tau = 1.0 \times 10^{-6}$ seconds. For $\tau = 0.5 \times 10^{-6}$ seconds we obtain a 400 keV contribution which when added in quadrature to 380 keV yields approximately 550 keV. This value is in good agreement with the 600 keV resolution we observed experimentally with a time constant of 0.5 microseconds.

For two values of the input rise-time T_1, T_2 it is easy to derive from (4) that

$$\frac{\Delta V}{V} = \frac{T_2^2 - T_1^2}{24\tau^2 - T_1^2}$$

This equation illustrates why proper collimation of the detector is important so as to reduce the spread of values in T. In an uncollimated detector the spread in rise-times could be expected to be roughly equal to the pulse duration itself which is of the order of 1×10^{-7} seconds. Because of the extended source geometry of the detector telescope and multiple Coulomb scattering effects the spread in rise-times could not be expected to be reduced by more than roughly a factor two even though only protons impinging on a 1.5 mm width (compared to 7 mm total depleted width) appear in the final detected

proton spectra.

For $T_2 = 1.5\ T_1$ and $\tau = 10\ T_1$ we obtain from equation (5) $\Delta V/V = 5 \times 10^{-4}$ or an additional 50 keV contribution to the overall energy resolution.

Since voltages in excess of 150 volts per mm often lead to surface breakdown problems it is therefore advantageous to reach saturation electron-hole velocity with a minimum applied voltage. It is therefore clearly advantageous from this point of view to operate the detectors at low temperatures ($77^{o}K$ is convenient and is generally used). Moreover since the hole mobility is a more rapidly varying function of temperature than the electron mobility the overall limiting effect of the hole collection time can be considerably reduced by operating at low temperatures.

The cryostat constructed for this work operated at a temperature of $120^{o}K$, however with one microsecond amplifier time constants no improvement in overall energy resolution was observable for voltages exceeding 100 volts per mm, i.e., 700 volts applied to a 7 mm deep detector. It is, of course, difficult for us to detect even appreciable changes in our detector resolution since it is folded in with the much greater beam energy spread. For this reason precise studies of the detector response such as those carried out by Bertrand et al. (1966) were inaccessible to us.

There are two other extremely good reasons why lithium drifted germanium detectors must always be used at low temperatures.

1 - To reduce the detector leakage current and the noise associated with it to an acceptable level.

2 - The rapid diffusion of lithium in germanium at higher

temperatures causes the detector properties to deteriorate. Even when not in use, the detectors must be stored at a low temperature (usually dry ice temperature is sufficient) to avoid redistribution and precipitation of the lithium.

2.7 DETECTOR ENCAPSULATION

Since the detectors have to be maintained at liquid nitrogen temperatures they must also be kept in vacuo to avoid problems associated with water vapour condensation on the cold detectors. Since the leakage current is extremely sensitive to surface conditions problems can arise from possible backstreaming of pump oil and condensation on the surface. We have avoided these problems by obtaining our detectors from RCA encapsulated in a hermetically sealed aluminum and stainless steel capsules which protect the surface at all times and permits easy and safe transfers from mount to storage during system repairs or modifications. It can be seen that the handling of these detectors is far more complicated than that of NaI(Tl) detectors or even silicon detectors.

Figure 4 shows a cross-section of the resistance welded "top-hat" type aluminum capsule. The material in front of the sensitive volume consists of a 0.001 inch dural window sealed to the capsule with special low temperature epoxy. A soft foil of 0.12 mm of aluminum provides good thermal contact between the diode and the case. The back contact to the undrifted p-type material ($\sim$ 2 mm thick) is made by means of a small spring wire connected to a metal to glass

hermetic terminal seal. The diode is held firmly in position in the capsule by means of a strong spring.

2.8 RADIATION DAMAGE

The gross mechanism of radiation damage in semi-conductor crystals is well understood. The changes that occur are due to introduction of impurity centers by the interaction between nuclear radiation and the nuclei of the semi-conductor. Apart from the effect of damage on the bulk resistivity of the detector material (which causes electric field changes), the levels introduced in the gap between the conduction and valence bands provide recombination and generation centers. Consequently the detector leakage current tends to increase and significant amounts of charge may disappear during the charge collection process. Since these affects may not be uniform in the whole sensitive volume of the detector, worsening of energy resolution and the appearence of multiple peaks in the amplitude spectrum are common signs of substantial radiation damage.

A confusing mass of literature exists concerning the estimated total doses required from various types of ionizing radiation before the onset of observably deteriorating crystal properties. This is partly due to the fact that most of the experimental data have been obtained under poorly controlled conditions in which the measurement of damage was a secondary objective (as indeed was the situation in our own case). Moreover the consequences of irradiation depend on the

type of detector, the details of the manufacturing process and the details of the detector environment experimentally and during storage.

It is unfortunately true that lithium-drifted detectors are specially sensitive to radiation damage because of their low internal fields and consequent short trapping lengths. An added problem which has contributed to the confusion in the literature arises from the tendancy of lithium to precipitate out on radiation-produced vacancies. Thus the donors are slowly removed and the material becomes uncompensated. The confusion arises because the effects of this damage increase by a large factor over a period of time after irradiation, depending on the storage temperature.

This high sensitivity of lithium-drifted germanium detectors to radiation damage constitutes their only serious drawback as efficient and practical total absorption detectors in high energy proton scattering experiments. This work has required in total six detectors at a total cost in excess of five thousand dollars and has been complicated by the frustration of several extended waiting periods before the detectors could be successfully encapsulated and delivered to us by RCA.

In what follows we shall give a brief description of the radiation damage mechanism in lithium drifted germanium detectors, the effect on the lifetime of our detectors, and the special precautions we observed to try to lengthen the detector lifetimes.

It is possible from general considerations (Goulding 1966)

to show that the radiation damage due to gamma rays, fast electrons, or slow neutrons is of negligible consequence for lithium drift detectors. The most important types of damage therefore in high energy proton research will likely be those due to fast protons and fast neutrons. The exposure to heavier mass charged particles such as alpha rays will generally be many orders of magnitude lower in a proton beam environment.

The principal mechanism of damage by protons or neutrons arises from collisions by which germanium atoms are displaced from their positions in the lattice to form a vacancy and a nearby interstitial. The resulting defect is called a Frenkel pair. Each of the recoiling atoms can produce further defects in subsequent collisions.

Most of the effects of radiation damage should therefore be related to the density and/or total number of Frenkel defects created. No satisfactory functional relationship exists however between electrical properties and the number of lattice defects for several reasons. The accuracy of the calculation of the total number of defects in a neutron or proton-irradiated detector is subject to large uncertainties because of the approximations involved. Moreover calculations of the total number of Frenkel pairs neglect both the local distribution of these defects and the possibility of defect annealing by thermal recombination of defects in the highly damaged "clumps" produced by the recoil nuclei. Very little

consideration has been given to any descriptive detail of these "clumps" and their effects on the surrounding lattice.

Mann and Yntema (1964) have exposed a lithium drifted silicon detector to 4 MeV protons. An initial exposure of 10^8 protons per cm^2 was sufficient to cause a slight deterioration in the response of the detectors which took the form of a low energy tail of the spectrum peaks. A further exposure to the same number of protons was sufficient to effectively destroy the response of the detector. Because no leakage current increase was observed the authors concluded that the deterioration in the response was clearly a loss in the per-cent charge collected.

Proton damage - Protons which are incident upon a germanium crystal produce defects in the germanium lattice structure via the two mechanisms of elastic and inelastic scattering. Most analyses have dealt exclusively with elastic collisions between the incident proton and the primary "knock-on" atom which is displaced from its lattice site by this collision, and with the subsequent defects produced in the lattice as the knock-on slows down through further collisions with other atoms. This approach is satisfactory for proton energies up to $\sim$ 50 MeV, however, at high energies, inelastic nuclear collisions which usually lead to spallation of the primary knock-on become very important in the production of displacements.

Following Dearnaley (1963) we have estimated the defect production for protons undertaking elastic collisions. The result

is shown in figure 5. Note that a 100 MeV proton produces roughly 2.5 times as many Frenkel defects due to elastic collisions as a 10 MeV proton, but of course, the sharp characteristic concentration of damage at the end of the track is essentially independent of the incident charged particle energy.

G. W. Simon et al. (1962) have computed the defect density in silicon due to inelastic collisions. The most significant result of their calculation is that the defect production for E_p greater than 150 MeV is dominated by the inelastic process. At 100 MeV inelastic processes contribute an additional 40% to the total number of defects. This figure reduces to less than 5% for E_p = 20 MeV. Since the elastic and inelastic contributions are essentially independent it is clear that for E_p greater than $\sim$ 50 MeV the inelastic contribution cannot be neglected.

Neutron damage - In Frenkel defect production by fast neutrons the intense defect density at the end of the track is absent since the collisions are mainly of the hard sphere type, i.e., with a cross-section which is essentially independent of neutron energy with a value of about 4 barns for germanium. Again following Dearnaley one finds that an average value of 5000 defects is not unreasonable for the number of Frenkel pairs created by a recoiling germanium atom after a collision with a 10 MeV neutron. Since a 10 MeV neutron has roughly a 30% probability of interacting in a length of germanium

sufficient to stop 100 MeV protons we see that a 10 MeV neutron produces on the average 1.3×10^3 Frenkel defects compared to approximately 200 Frenkel defects for a 10 MeV proton. Above 10 MeV the damage for protons increases roughly at a rate of 40 Frenkel pairs for every 10 MeV whereas a 20 MeV neutron produces roughly twice as many pairs as a 10 MeV neutron.

At first glance one would assume that fast neutrons are by far the more damaging to germanium cyrstals. The very different distribution of Frenkel defect density - uniform density in the neutron case versus approximately two orders of magnitude variation from the start of the track to the very dense damage at the end of the track for protons - probably enhances the destructive character of the proton damage. It is consequently impossible to postulate any dominant factor in our detector viability as being due to either one type of damage or the other.

Conclusion

Effects of Damage - In the course of our experiments we monitored the total number of protons incident on one detector over its lifetime. An accumulated dose of 5×10^7 protons per cm^2 over a period of $\sim$ 2 months together with an unknown total dose of fast neutrons was sufficient to render the detector unuseable.

The detector characteristics effected by the radiation were increasing leakage current and, of course, worsening of the energy resolution. No multiple peaking was observed over the entire course of the experiment. The leakage current of a typical detector increased by an order of magnitude (from approximately one nanoampere to ten nanoamperes) at 700 volts bias. In one detector this increase in leakage current was not observed but in any event fluctuations in the leakage current itself were not a contributing factor to the deteriorating energy resolution since the pulser resolution was not observed to significantly worsen over the detector lifetime. The energy resolution deterioration was most likely due therefore to charge loss during collection although no improvement was observed at detector fields up to 150 volts per mm. Higher bias than this figure was usually impossible to achieve because of surface breakdown leading to vastly increased leakage currents.

Precautions to maximize detector viability - During beam extraction high fluxes of fast neutrons are known to originate at the target, collimating slits and carbon absorber of the Faraday cup. To reduce fast neutron damage as much as possible the in beam Faraday cup was not used and the beam was allowed to be absorbed in a wood stop as far away from the chamber as possible. In between experimental runs the chamber and detector were removed from the experimental area to eliminate damage due to fluxes of neutrons originating from other

experiments. During beam alignment and optimization the detector was always placed at 90 degrees to remove it as much as possible from the forward flux of fast neutrons originating at the television camera screens. To avoid the possibility of swinging the beam through the detector or through the target holder all the magnet currents were present as accurately as possible before extracting the beam. At no time did we observe the initial beam position to be laterally displaced by more than one cm from the target center.

These precautions resulted in a practical lifetime of $\sim$100 hours experimental running time for the detectors compared to $\sim$40 hours for the first detector we used. Even the former figure is disappointingly low, and represents an unfortunate drawback of these detectors when compared with the effectively infinite lifetime of NaI(Tl) detectors.

2.9 TRIANGULAR WEDGE - BEAM ENERGY SPREAD

Portner's study of the beam profile indicated that the horizontal cross-over point downstream from the 45 degree magnet was a focal point with a good spatial momentum distribution of the beam. This suggested to us the following possibility for reducing the beam energy spread.

The idea was to place a triangular aluminum wedge at the focal point designed so as to remove a negligibly small amount of energy from the low energy side of the beam and approximately 660 keV (2 x FWHM)

from the high energy side of the beam. The choice of aluminum was motivated by the very accurately known dE/dX for high energy protons in aluminum. Even with an additional contribution of $\sim$ 200 keV to the beam width due to energy straggle in the thickest part of the wedge we considered the idea of sufficient merit to be attempted.

The single great difficulty was to pinpoint the exact location of the focal point and introduce the wedge at that point. To accomplish this an apparatus was constructed in which the wedge could be moved in the beam pipe with two degrees of freedom, perpendicular and parallel to the beam axis.

The experimental procedure was as follows. The beam was initially focussed at the scattering chamber target position and viewed on a zinc sulphide fluorescent screen in the usual manner. A peak corresponding to protons elastically scattered from gold was accumulated and the peak channel position and FWHM recorded. Our choice of target was gold because its high mass results in negligible contribution to the overall resolution from kinematic broadening. The wedge was then moved in a direction perpendicular and edge first into the beam. It was possible to determine when the wedge began to enter the beam because the beam spot on the fluorescent screen soon disappeared. This effect was presumably due to spreading out of the beam spot at the focal point because of multiple scattering of the protons in the wedge.

The beam was refocussed and the wedge adjusted so that the elastic peak channel moved down in energy 3 to 4 channels corresponding roughly to 300 keV - 400 keV removed from the centroid proton energy by the wedge. The wedge was then moved parallel to the beam in steps of 0.1 inches in a 1 inch region where the focal point was believed to be. The peak channel did not migrate showing that the wedges were indeed being moved parallel to the beam direction. Elastic peaks were accumulated at each of these positions. After each movement of the wedge the position and size of the beam spot at the target was checked.

Unfortunately the spectra accumulated showed no significant improvement at any of the positions chosen. The overall resolution of the system remained approximately 400 keV in good agreement with previous elastic spectra accumulated from gold under normal running conditions. The only available conclusion therefore is that the focus is a "quasi" focus without sufficiently well defined momentum dispersion for the idea to be successful. This conclusion casts some doubt on the 5% accuracy Portner attributed to his measurement of the full beam energy spread.

FIGURE 2

FIGURE 2

Experimentally observed energy resolution of high energy protons detected in germanium.

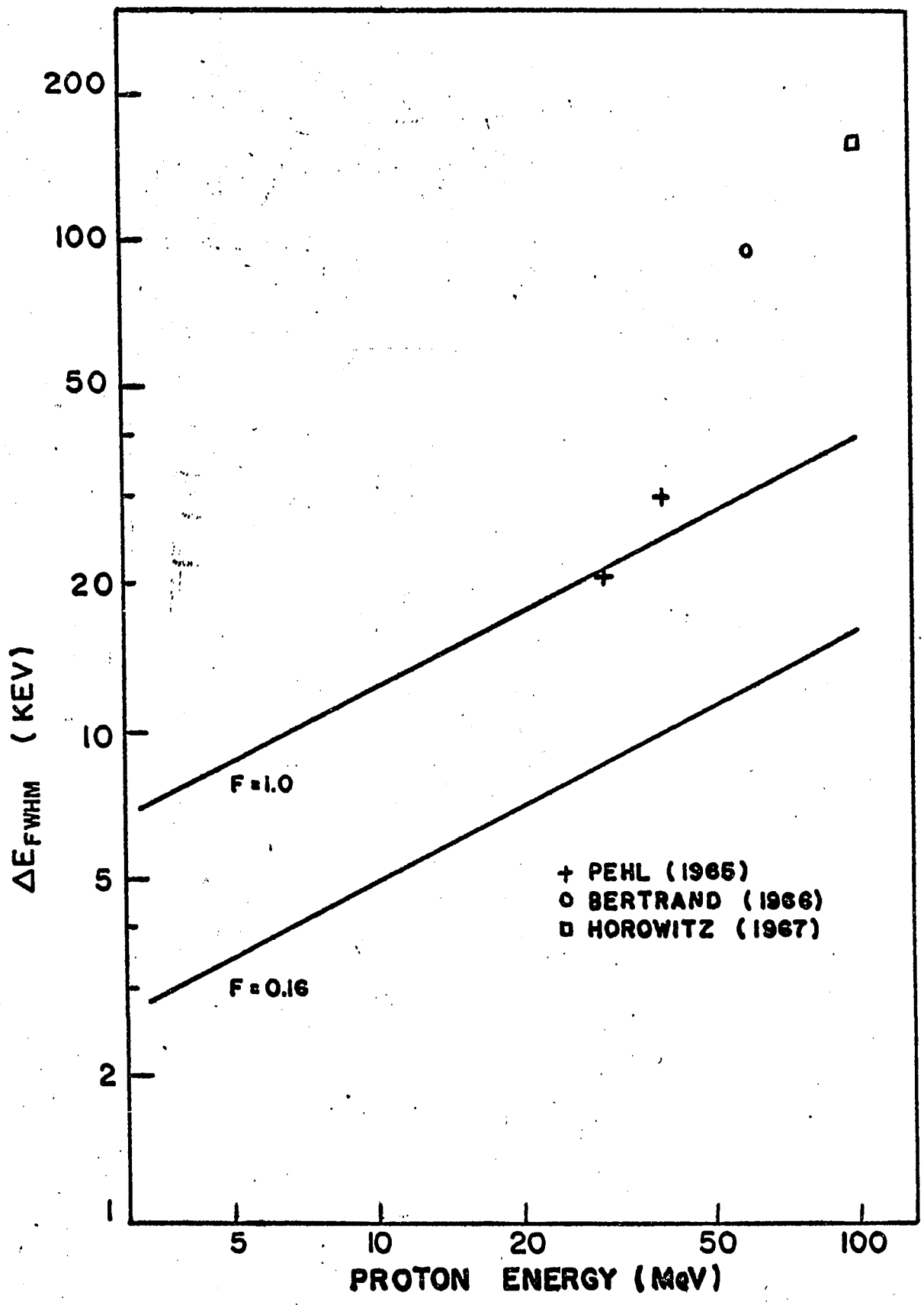
200
100
50
20
10
5
2
1
5
10
20
50
100
PROTON ENERGY (MeV)
ΔE FWHM (KEV)
F = 1.0
F = 0.16
+ PEHL (1965)
o BERTRAND (1966)
□ HOROWITZ (1967)

FIGURE 3

FIGURE 3

Energy spectrum obtained with the germanium detector directly aligned in the proton beam. Below channel 850 each plotted point is the sum of 10 channels. A tail-to-peak ratio of 0.23 was extracted from this spectrum.

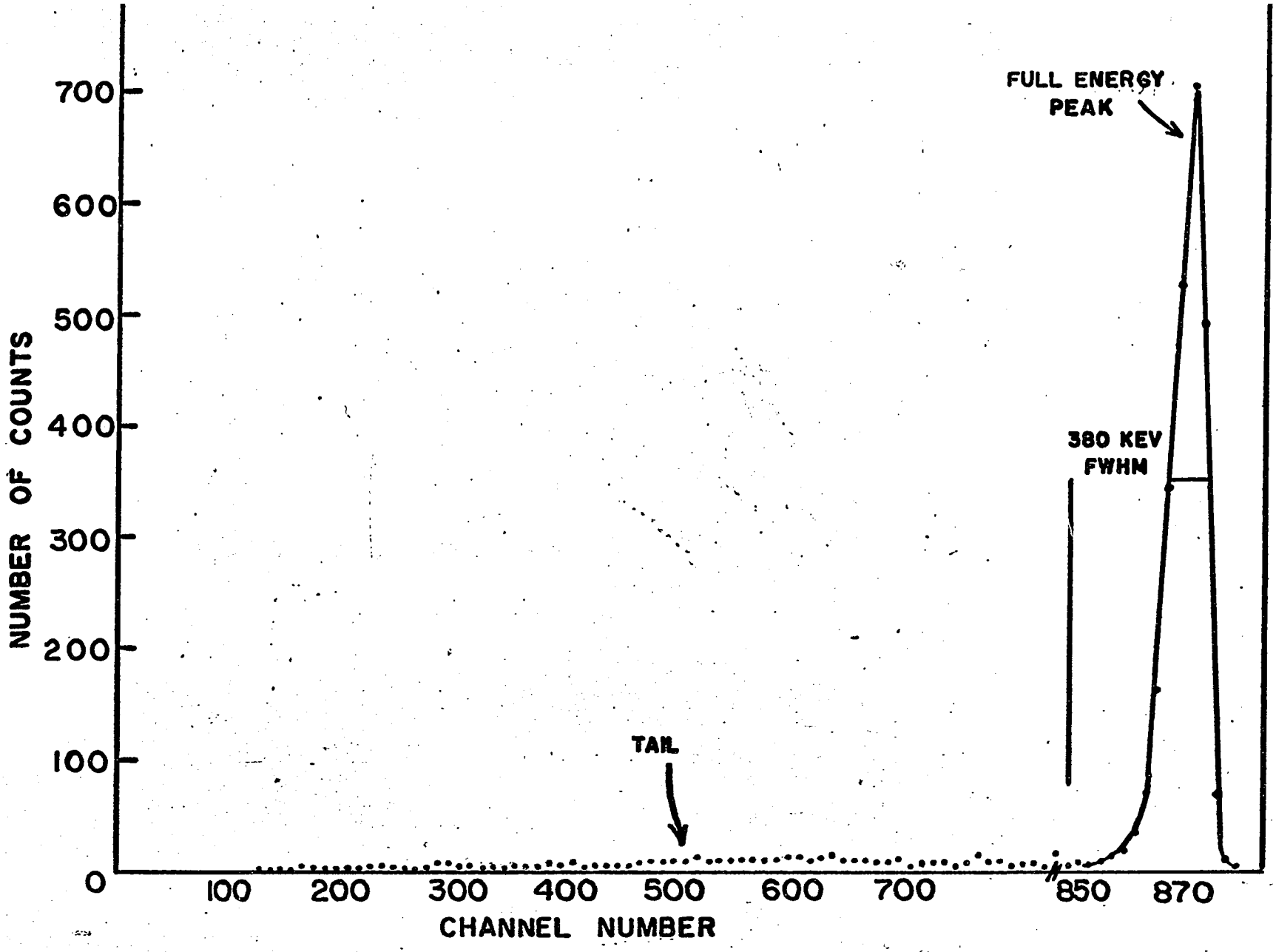
FULL ENERGY PEAK
380 KEV FWHM
TAIL
NUMBER OF COUNTS
CHANNEL NUMBER
0
100
200
300
400
500
600
700
850
870

FIGURE 4

FIGURE 4

Germanium detector hermetically encapsulated in a stainless steel "top-hat" capsule. The entrance window is 0.001 inch thick dural.

ENCAPSULATED GERMANIUM DETECTOR

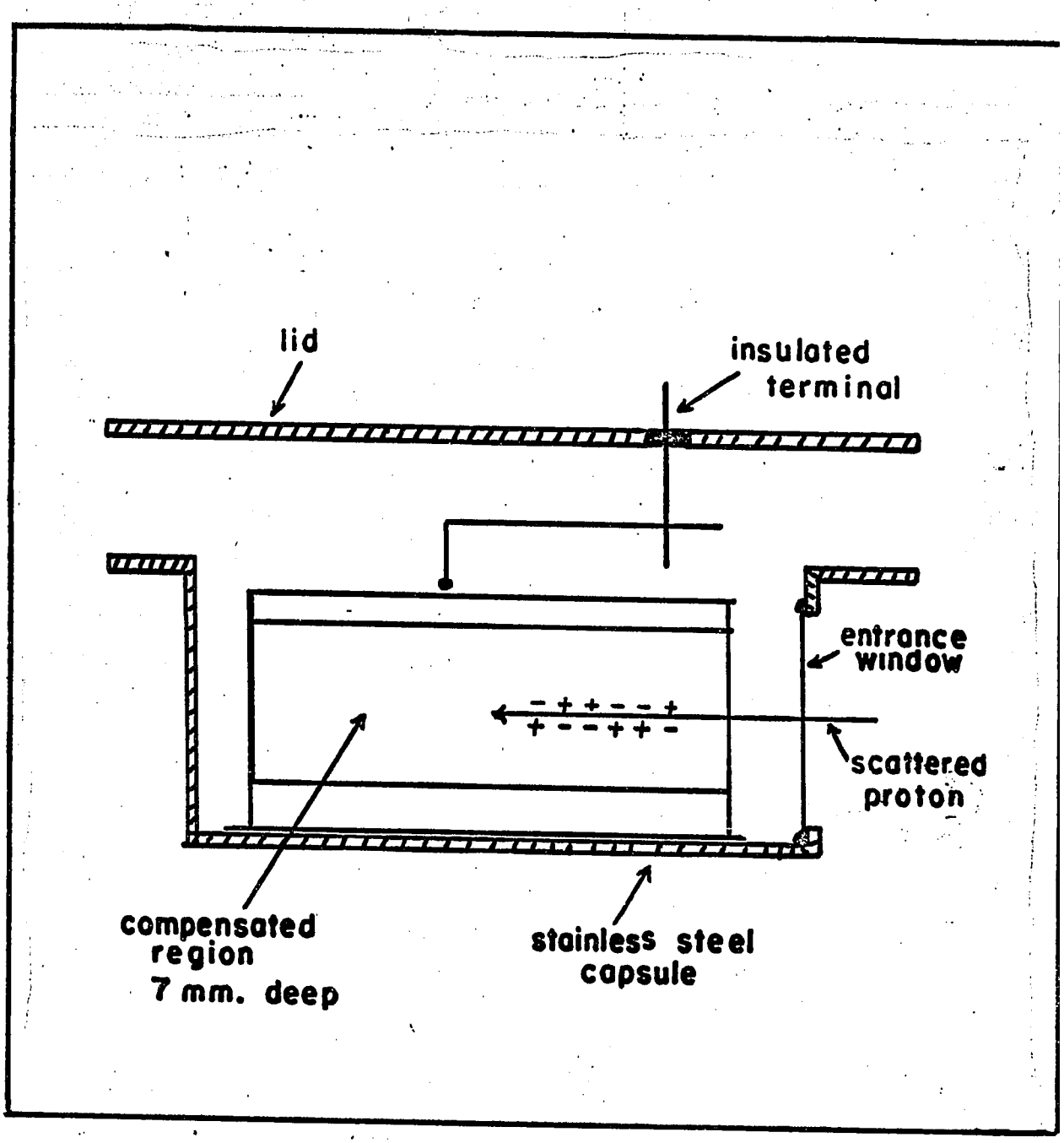

FIGURE 5

FIGURE 5

Production of Frenkel defects due to elastic collisions of protons (Dearnaley, 1963).

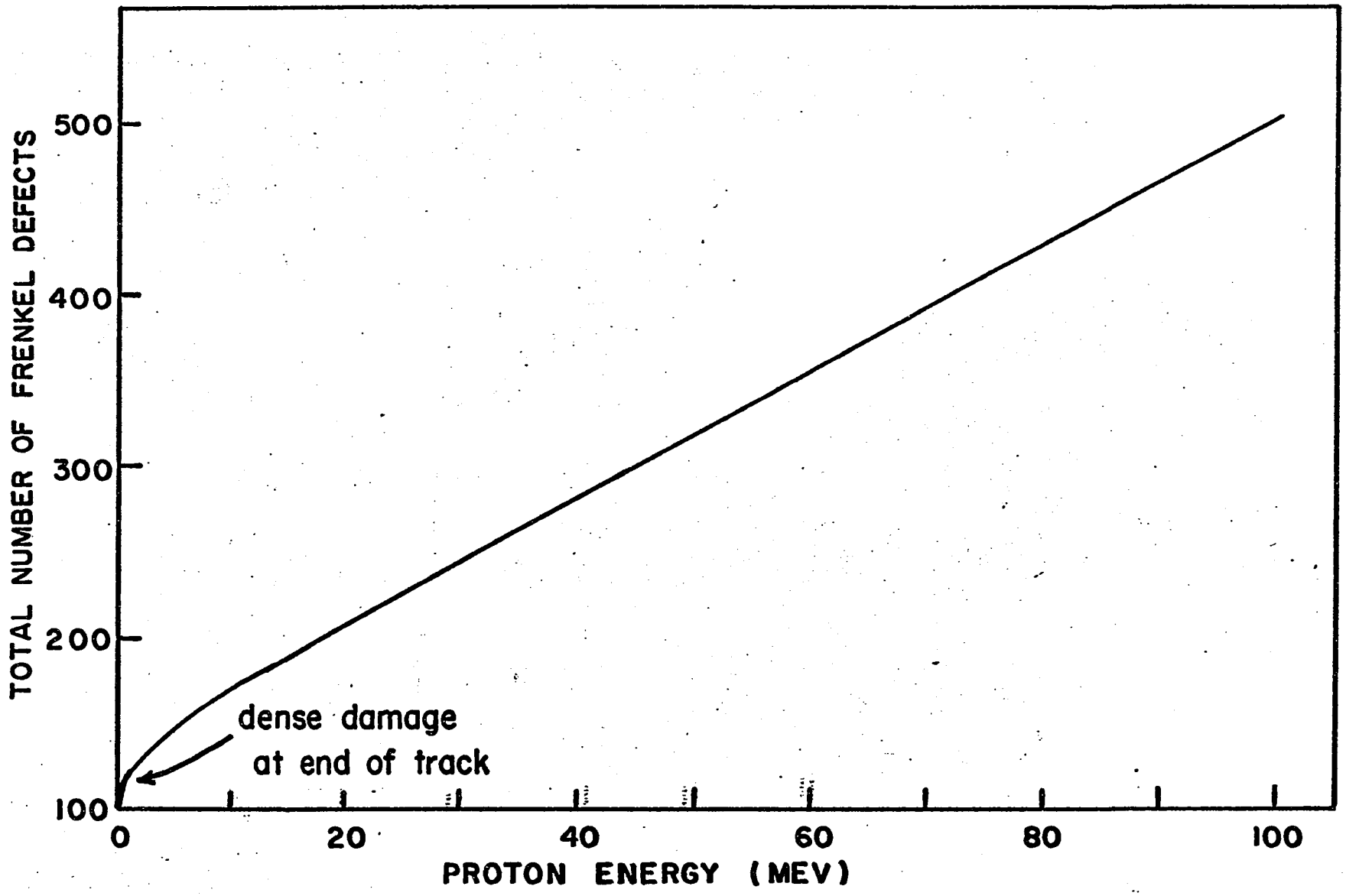
TOTAL NUMBER OF FRENKEL DEFECTS
500
400
300
200
100
dense damage
at end of track
0
20
40
60
80
100
PROTON ENERGY (MEV)

CHAPTER 3. DESCRIPTION OF THE EXPERIMENTAL APPARATUS - INELASTIC SCATTERING

3.1 THE SCATTERING CHAMBER-CRYOSTAT

From the preceding discussions it can be seen that the experimental assembly must provide the following features.

1 - A detector mount or platform cooled to approximately liquid nitrogen temperatures in an evacuated chamber. The capsule position relative to the target center to be reproducible to 0.01 inches.

2 - A method of monitoring the cold finger temperature.

3 - A telescope to limit detected events to a central portion of the detector's sensitive volume.

4 - Variability of the scattering angle without breaking the chamber vacuum.

5 - Adjustment of the detector platform relative to the target center to ensure coplanarity of the detector symmetry axis with the proton beam axis.

6 - A target holder with at least three different positions to provide facility for viewing the beam remotely, to record background spectra and to hold the actual target material. The angle between the target and the beam direction to be variable.

Two distinct types of apparatus suggested themselves which,

we believed, could satisfy the above requirements. The first would be to build a separate cryostat to house the detector and telescope and than separate vacuum chamber for the targets. The other approach would be to combine the scattering chamber and detector cryostat into a single unit.

In the first case several advantages do exist, for example: easy accessibility to the target apparatus without disturbing the detector environment, a more compact, mobile cryostat, superior cryogenic design to provide as cold as possible an environment for the detector, greater protection against possible damage to the detector due to beam accidents such as vacuum breakdown etc. We decided, however, to choose the latter approach because the extremely small volume of the detector makes the alignment of the symmetry axis of the sensitive volume with the target center critically sensitive to displacements of the order of one mm. An accurate alignment is obviously possible in a two unit system but its reproducibility to orders of fractions of a mm is highly doubtful in view of the fact that the two units would have to be movable with respect to each other. In the single unit system the alignment can be performed more accurately and its permanence is assured. A secondary advantage was the minimization of the amount of material between the detector and target in the form of air-path and chamber windows.

The details of the detector capsule were described in the preceding section. The overall dimensions of the capsule, and of

special importance the position of the window in the capsule were known to 0.01 inches. The position of the detector sensitive volume in relation to the capsule windows and walls was guaranteed by RCA to be accurate to 0.01 inches. The detector capsule was mounted on a cold finger and its position relative to the axis of the cold finger was fixed by a groove in the cold-finger platform into which the "top-hat" part of the capsule was inserted. Good thermal contact and rigidity were obtained by an allen bolt which forced the groove width to contract the necessary few thousandths of an inch. This arrangement is illustrated in figure 6.

The cold finger was constructed from copper with a 3/4 inch diameter for good thermal conductivity and silvered to minimize heat transfer due to radiative effects. Silvering of the cold finger is a standard cryogenic technique and its importance is trivial to demonstrate.

In cryostats designed for gamma ray germanium spectrometers another standard cryogenic technique is to surrond the cold finger as completely as possible in a cooled evacuated enclosure whose walls serve as a heat shield so that the detector and cold finger "see" no material at room temperature. The heat shield is usually constructed of thin stainless steel to reduce thermal conductivity across the contact points between the cold finger, heat shield and external environment.

The dual nature of our apparatus, especially the requirement

of a detector telescope and accurate detector-telescope-target center alignment compelled us to forgo the heat shield over the upper part of the cold finger. The part of the cold finger extraneous to the scattering chamber proper was enclosed in an evacuated thin-walled stainless steel tube. This arrangement is shown in figure 7. The bellows served as a flexible attachment between the heat shield and scattering chamber and consisted of three separate phosphor-bronze units resistance welded together to yield a maximum total stroke of 0.9 inches. This flexibility allowed us to adjust the cold finger platform relative to the target center and hence relative to the beam axis. This adjustment was accomplished by means of three threaded rods which supported the cold finger. These rods extended through the base of the chamber so that they could, if necessary, be adjusted externally without disruption of the chamber vacuum. Because of rapid condensation of moisture on the cold finger at atmospheric pressure any internal adjustment or maintanence required transfer of the detector to storage and dismantling of the apparatus. This procedure was clearly to our advantage to attempt to minimize. The bellows were constructed of phosphor bronze for low thermal conductivity and joined to the brass bottom of the chamber by a thin stainless steel plate (figure 7.) The cold finger and bellows were immersed in a liquid nitrogen dewar of 25 liter capacity. The rate of liquid nitrogen consumption was approximately 5 liters per day. The neck of the dewar was extended by an aluminum tube of approximately 5 inch

length so that the dewar could be refilled via a port in the extension.

In order to select the scattering angle the base of the chamber could be rotated relative to the remaining structure with the use of two long lever arms bolted to the chamber base. The physical size of the detector capsule did not allow us to go to scattering angles less than 10^{o}. The 0 - ring separating the chamber base from the aluminum walls of the chamber was large enough in diameter to ensure that the two surfaces were not in close contact with each other and hence could be relatively easily rotated under vacuum. Relative scattering angles were marked off on the base circumference of the scattering chamber in 1 degree steps with milling table precision. An overall illustration of the scattering chamber - cryostat is shown in figure 8.

A target holder was constructed with four target positions as shown in figure 8. Two target positions were occupied by the C^{12}, Mg^{24} or ^{28}Si targets, a third was empty for background measurements, and the fourth contained a zinc-sulphide fluorescent screen to allow for alignment and focussing of the beam at the target. The angle of the plane of the target with respect to the incident beam direction was adjustable so that the normal to the target plane would lie half-way between the incident beam and the scattered beam. This minimizes the difference in path lengths for protons passing through the target and thus minimizes any contribution to the overall energy resolution from energy straggle in the target thickness.

Because of the compromises in cryogenic design forced on us by the experimental requirements we did not expect the cold finger to achieve a temperature of 77 degrees K (liquid nitrogen temperature). However we were aware that several groups had successfully used germanium detectors in gamma ray investigations up to temperatures of 150 degrees K (Ewan and Tavendale, 1966; El-Shishini and W. Zobell,1966) and we hoped to achieve this temperature or better.

The temperature was measured by taking advantage of the high temperature coefficient of resistance for copper (α = 0.004) Number 44 copper wire was wound around a copper spindle and mounted in the cold finger adjacent to the detector platform. The copper thermometer was calibrated using four known temperatures: room temperature - 298 degrees K, dry ice temperature - 195 degrees K, solid-liquid cyclohexane methyl mixture - 147 degrees K and liquid nitrogen itself. The calibration curve is shown in figure 9, the insert shows the simple circuit used to measure the copper wire resistance. The actual temperature achieved at the detector platform was approximately 120 degrees Kelvin. This temperature proved to be definitely acceptable since the detector resolution for the 1333 keV gamma ray line from Co^{60} measured by us at 120 degrees K was only 7 keV compared to the 4.5 keV achieved with the same detector by RCA at 77 degrees K.

3.2 THE DETECTOR TELESCOPE

Design Considerations - As previously mentioned the basic function of the counter telescope was to restrict the entrance solid angle of the scattered protons impinging on the front face drifted region of the detector and to "veto" those proton events whose initial direction is such that they may lose only part of their energy in the active volume. The anti-coincidence window also served the normal telescope function of determining the angular acceptance and detection solid angle of the system.

In restricting the detection area of entry to a few mm^2 (out of a total depleted cross-sectional area of 70 mm^2) the design choice of either a coincidence configuration or anti-coincidence "window" configuration must be made. The coincidence technique for defining the solid angle has some advantages over the latter configuration. The number of background events appearing in the spectrum (especially in the low energy region) can be expected to be drastically reduced. Moreover a clean DE spectrum enables a dE/dx x E separation of protons from heavier mass particles so that the inelastic proton spectrum appears free of contamination due to deuterons, tritons, alphas, etc.... The most serious competition comes from the (p,d) reaction which is sufficiently strongly excited above threshold to dominate the proton spectrum so that identification of proton peaks becomes impossible. In ^{24}Mg and ^{28}Si the Q values for the (p,d) reaction are 14.3 and

14.95 MeV respectively. At these excitation energies good separation of the various proton peaks becomes intrinsically very difficult because of the high nuclear level density. Hasselgren et al. (1967) with a slightly better overall resolution than our own, were able to resolve inelastic proton peaks in these nuclei only up to an energy of 14 MeV. Thus in ^{24}Mg and ^{28}Si this region of excitation clean of deuteron or heavy particle contaminationis, in fact,quite sufficient. In ^{12}C, however, it is true that with 550 keV resolution good separation of proton peaks can be obtained up to an energy of 25 MeV whereas the Q value for the (p,d) reaction is 16.5 MeV. We have considered the possibility of using a two-element germanium range telescope (Horowitz et al. 1967), but the units were never successfully encapsulated by RCA.

A serious disadvantage of the coincidence technique is that the addition of the dE signal back to the E signal usually does not eliminate broadening of the energy resolution due to energy straggle in the dE crystal. Since our objective was to operate at the lowest energy resolution possible, this was a result which we were unwilling to concede and which is, of course, not present in the anti-coincidence window configuration.

A second serious disadvantage would be the obvious difficulty encountered in mounting and accurately aligning a minute piece of plastic measuring only 1.2 mm x 2.4 mm. Moreover the coincidence technique is not nearly as effective in reducing slit scattering from the brass collimator.

The size of the window in the anti-coincidence scintillator was dictated by two factors:

i - the minimum area on the target to which the beam can be confined. An average beam spot size, in our case, measured usually 1 1/2 mm x 2 mm, however allowing for possible wandering of the beam of the order of one mm during a run and possible detector-target misalignment we chose to define a 5 mm x 7 mm region in the center of the target as representing the minimum realistic area of confinement.

ii - the comparatively large value of 1 mm root mean square displacement due to multiple scattering of 100 MeV protons stopped in germanium in relation to the 7 mm drifted depth. In this case we decided that protons passing through the window in the plastic scintillator should not be able (if not for spreading due to multiple Coulomb scattering) to penetrate closer than 2 mm from the edge of the detector sensitive volume, the distance of 2 mm representing two root mean square displacements.

A ray diagram illustrating the target detector geometry is shown in figure 10. Based on the above considerations, the beam spot size and multiple scattering combine to restrict the size of the window in the anti-coincidence scintillator to an area of 1.2 mm x 2.4 mm = 2.9 mm^2. Moreover the above discussion makes clear the absolute necessity for accurate alignment of the detector axis-window scintillator and target center. If the detector axis and telescope window do not see a symmetric area about the target center

serious consequences such as reduced counting rate and reduced peak to total ratios would develop.

In this geometry the detection solid angle of the telescope is 0.35×10^{-3} steradians. The angle subtended by the target at the window is 0.75 degrees however the finite size of the beam spot introduces a contribution of 0.9 degrees. Additional smaller contributions come from possible beam drifts of the order of 0.5 mm ($\sim$ 0.3 degrees), the beam divergence ($\sim$ 0.3 degrees) and multiple scattering in the targets ($\sim$ 0.2 degrees). The total RMS angular resolution was therefore less than 1.3 degrees. The most serious affect of the angular resolution is the deterioration in the energy resolution due to kinematic broadening. This effect was appreciable only in ^{12}C, where a nuclear recoil contribution of $\sim$ 300 keV (corresponding to an angular resolution of 1.3 degrees) at a scattering angle of 60 degrees was observed to increase the overall resolution from 500 keV at 10 degrees to 600 keV at 60 degrees.

The cross-sectional area of the detector sensitive volume is 70 mm^2 so that a window area of 2.9 mm^2 implies a rejection rate of 70/2.9 = 24:1. Since all the events in the detector contribute to pulse pile-up this factor represents a factor 24 reduction in the maximum possible counting rate and this is clearly unacceptable.

This problem was solved by adding a brass collimator which served to reduce the flux of particles passing through the detector. The collimator was 0.625 inches thick (sufficient to stop

100 MeV protons) with a 4.5 mm x 3 mm hole in it. The area of the window in the scintillator, 2.9 mm^2, can now be compared with an area of 3 mm x 4.5 mm = 13.5 mm^2 or a rejection rate of only 3.7:1 instead of the previous 24:1.

One might ask why not simply use a brass collimator with a smaller window and eliminate the plastic scintillator. This idea is not feasible because of the serious slit scattering which would result. The thickness of the brass and its proximity to the target make the probability of a proton scattering off the inside wall of the collimator and into the detector prohibitively high. Bertrand et al. (1966), for example, with better geometry than our own (a 60 MeV proton requires roughly only half the thickness of brass) found that with the latter configuration their peak-to-total ratio decreased from 0.94 to 0.80, an undesirable result from the point of view of background contamination of proton spectra. The anti-coincidence window thus serves not only to restrict the detection solid angle to the central region of the detector sensitive volume but also to greatly reduce the probability of a proton scattering off the inside wall of the collimator and into the detector without passing through the anti-coincidence counter.

Description of the Counter Telescope - The physical layout of the detector telescope is illustrated in figure 7. The 3 mm thick plastic scintillator was mounted on a RCA 8575 photomultiplier directly in

front of and below the detector platform. To reduce γ-ray and neutron background in the anti-coincidence counter, the scintillator volume was made as small as possible by having the plastic extend only very slightly beyond the edges of the collimator hole. Optical contact was made with the photomultiplier by mounting the crystal on a lucite light pipe. The scintillator, light pipe and photomultiplier were joined together by a slow setting optical cement which allowed sufficient time to align the collimator with respect to a dummy capsule mounted in the cold finger so as to exactly reproduce the detector capsule configuration. The photomultiplier was surrounded by a magnetic shield and was held firmly in place with respect to the cold finger with special cold-resistent silicone O-rings. The window in the plastic scintillator was 2.4 mm x 1.2 mm in area and was placed as close as possible to the detector capsule window ($\sim$ 5 mm, and dictated mainly by the fact that the photocathode does not extend to the very edge of the 8575 photomultiplier. The plastic scintillator was followed immediately by the 0.625 inch thick collimator.

Collimator Slit Scattering - From the point of view of accuracy of background subtraction it is advantageous, of course, to keep slit scattering to a minimum. In our geometry, the inside walls of the brass collimator subtend at the target roughly twice the solid angle subtended by the window in the anti-coincidence counter. However the minimum scattering angle which can deflect a proton from the wall of

the collimator and through the window in the anti-coincidence counter is approximately 3 degrees. Since the angular dependence of Rutherford Coulomb scattering is very strongly forward peaked (varying inversely as $\sin^4\alpha/2$) the magnitude of the scattering angle is very much a figure of merit for the effectiveness of the arrangement in reducing the flux of slit scattered events appearing in the proton spectra. This aspect of the detector telescope was considered in the decision to make the collimator hole substantially bigger than the hole in the anti-coincidence counter. A calculation of the absolute rate of slit-scattered events appearing in the proton spectra, although desirable, is prohibitively difficult because of the many factors involved. Our experiment with the detector and telescope aligned in the beam, (section 2.4) indicates however that slit scattered events did not contribute more than 5% of the total counts in the final spectra.

3.3 E ELECTRONICS

A block diagram of the electronics used in this experiment is shown in figure 11. The detector preamplifier connection was made with RG 174-U amphenol coaxial cable, chosen for flexibility rather than low capacitance per unit length. Since external capacitance degrades the signal to noise ratio, the connection between detector and preamplifier is usually kept as short as possible, however since our overall resolution was beam limited we observed no effect on the overall resolution with more convenient cable lengths of the order of a few feet. The pulse preamplifier was the charge sensitive Tennelec

Model 100 C. The detector bias connection is accomplished through a 1000 Megohm detector load resistor. The rated charge sensitivity of the 100 C is 0.21 microvolts per ion pair or 74 millivolts per MeV energy loss in a germanium detector on X1 sensitivity. A 100 MeV energy loss therefore exceeds the specified linear dynamic range (5 volts) so that we found it necessary to reduce the charge sensitivity by increasing the feedback factor of the amplifier. This was accomplished by reducing the feedback resistance from 300 ohms to 30 ohms. The time constant of the feedback network was kept to approximately 0.015 microseconds by increasing the capacitance in the feedback loop to 480 picofarads from 47 picofarads. Only zero-temperature coefficient capacitors were used.

The linearity of the preamplifier was tested by injecting test pulse signals from a Victoreen PPG-1 pulse generator. The shape of the input test pulse was adjusted to yield an output pulse similar in shape to a proton output pulse. The preamplifier and remaining E electronics was found to be linear to 1% to energies greater than 125 MeV. The width of the test pulse (FWHM) also served as a measure of the contribution of the electronic noise and noise associated with the detector leakage current to the overall energy resolution.

To minimize undesirable effects due to pick-up, double shielded RG - 71 A/U (93 ohm) cable was used between the preamplifier and the Ortec 410 main amplifier. The remainder of the E electronics were standard logic modules to operate the anti-coincidence operation. The Ortec 410 amplifier provides one integrating time constant and

two differentiating time constants in discrete steps between 0.25 μsec and 10 μsec. The final spectra were accumulated in a 4000 channel TMC multi-channel analyser.

Anti-coincidence dE electronics - Anode pulses of duration 20 nanoseconds were produced from the anti-coincidence counter by feeding the output directly into a terminated 100 ohm cable. The pulses were stretched with a fast pulse stretcher designed and constructed by S. K. Mark (1965) and then amplified X32 by an Ortec 440 active filter amplifier, with 0.25 μsec time constant. In this manner the pulse duration at the input to the Cosmic discriminator was approximately 0.5 μsec with a rise time of approximately 100 nanoseconds in agreement with the Cosmic input specifications. Because of various delays on the dE side, proper anti-coincidence operation was obtained by delaying the E side relative to the dE side by 0.8 microseconds. To insure maximum efficiency this value was determined by taking a delayed anti-coincidence curve in which we measured the counting rate under the degraded peak as a function of delay, minimum appearance of the degraded peak corresponding, of course, to optimum efficiency of the anti-coincidence operation. With the anti-coincidence function disabled the spectrum of protons scattered from gold exhibits two peaks separated by $\sim$2.5 MeV (corresponding to the energy loss of a 100 MeV proton in 3 mm of NE 102). The lower peak contained roughly four times as many counts as the higher peak in agreement with our

expectations. (The area of the collimator hole is 3.7 times greater than the area of the window in the plastic.) A typical spectrum with and without the anti-coincidence function is shown in figure 12. Note the difference in energy resolution (430 keV compared to 750 kev) due to Landau spread in the dE crystal. To insure that every proton event in the dE triggers the Cosmic discriminator, selection of the optimum voltage for the anti-coincidence photomultiplier was performed in a similar manner by minimizing the counting rate under the degraded peak as a function of photomultiplier voltage, minimal appearance of the degraded peak again corresponding to optimum efficiency of the anti-coincidence function. The result shown in figure 12 clearly represents better than 99% efficient performance of the anti-coincidence function.

Leakage current monitor - The detector leakage current was monitored using a circuit shown in figure 13. With the detector power supply in the circuit the polystyrene low leakage capacitor is fully charged and no current flows through the picoammeter. To measure the detector leakage current the capacitor is allowed to discharge through the detector and the series connected picoammeter. Although the experiment must be interrupted to measure the leakage current, the circuit, designed by W. T. Link avoids ground loops often encountered in leakage current measurements in the picoamp to nanoamp range. The detector voltage versus leakage current characteristics were measured prior to each run

since the detector leakage current served as a qualitative indicator of the detector performance. A typical leakage curve is shown in figure 14. The leakage current is seen to increase slowly but then hits a knee and increases rapidly with further increases in applied voltage. Normal operation of the diode is at voltages smaller than the "knee" voltage, typically 120 volts/mm. As previously mentioned one of the effects of radiation damage was a decrease in the knee voltage eventually rendering the detector unuseable.

3.4 TARGETS

The ^{24}Mg target was obtained in self supporting foil form from the isotope division of the Oak Ridge National Laboratory. The target was weighed and its surface area determined accurately so that its weight of 19.1 mg/cm^2 is believed accurate to 1%. The target was enriched magnesium with the following isotopic composition

isotope	Atomic %	precision
^{24}Mg	99.7	$\pm$0.05
^{25}Mg	0.2	$\pm$0.05
^{26}Mg	0.1	$\pm$0.05

A spectrographic analysis performed by Oak Ridge showed no other elements present in quantities greater than 0.1%.

The ^{28}Si target was natural silicon (4.7% ^{29}Si, 3.09% ^{30}Si)

and was obtained by dismantling an old Ortec surface barrier detector. The detector thickness was very uniform and was measured to be $9.2 \pm 0.1 \times 10^{-3}$ inches or 56.5 ± 0.6 mg/cm^2. The dead layer thickness on Ortec surface Barrier detectors is quoted to be approximately consistent with a gold electrode thickness of 40µg/cm^2 and a dead layer on the back of the detector equivalent to 40 µg/cm^2 of aluminum. For our purposes these quantities are negligible in comparison to the measured thickness of Si.

The ^{12}C was natural carbon (1.1% ^{13}C) in graphite form and was milled to 0.013 inches thickness with parallel surfaces. The thickness of the target at its center was very uniform and was measured to be $13.4 \pm 0.1 \times 10^{-3}$ inches, or 51.5 ± 0.4 mg/cm^2.

3.5 GENERAL EXPERIMENTAL SETUP

The scattering experiments were performed with the recently operational quasi-continuous external 100 MeV proton beam of the McGill synchrocyclotron. The full beam in the experimental area has the following general properties: energy spread $\sim$400 keV (FWHM), area in phase space about 2.5 cm milliradians both horizontally and vertically, maximum intensity approximately 30 nanoamps, duty cycle of the continuous beam approximately 20:1, energy 100.3 ± 0.2 MeV with the cyclotron magnet current at 640 Amperes.

In the actual experiments described herein, the beam intensity was reduced to approximately one nanoamp by means of horizontal and vertical slits located at the entrance to the beam

transport system. In this way excellent beam qualities at the target were achieved, 1 - 2mm spot diameter as well as small divergence. The focussing and alignment of the beam was checked by closed circuit television viewing zinc sulphide fluorescent screens which could be lowered into the beam by remote control. The position of the beam spot at the target during experimental runs extending up to 24 hours was never observed to fluctuate by more than $\pm$ 0.5 mm. The experimental layout of the beam transport system and scattering facility is shown schematically in figure 15.

To extract the continuous beam optimization of the beam stretcher parameters was necessary prior to each run. To this purpose a thin dE/dX plastic scintillator was mounted in the direct beam behind the scattering chamber. The response of the scintillator displayed on a scope showed the time structure of the beam and allowed an intelligent manipulation of the stretcher controls. The operation of the stretcher was such that the pulsed structure of the beam could never be entirely removed for beam currents of the order of a nanoamp. It was therefore necessary to gate out events occurring during the beam bursts. This was accomplished by triggering the routing output of the scope with timing pulses from the cyclotron ion source which coincided in time with the beam spikes. The routing output was used in an anti-coincidence gate to remove all scattering events originating during the spiked structure of the beam.

B. ELASTIC SCATTERING

3.6 SCATTERING CHAMBER AND BEAM MONITOR

To arrive at accurate absolute elastic cross-sections an existing multipurpose laboratory scattering facility was used. The facility has been described in detail by Portner (1968), and consists of a plastic E counter preceded by a standard counter telescope and scattering chamber providing approximately 1.3 MeV energy resolution for 100 MeV protons. Several factors motivated our use of this facility to measure the absolute elastic scattering cross-sections.

The absolute efficiency correction for protons in the germanium detector is uncertain by as much as 5% however the efficiency correction difference between 100 MeV protons and lower energy protons corresponding to inelastic scattering can be estimated relatively accurately assuming only that the shape of the calculations by Makino et al. is correct. On the other hand the absolute efficiency correction for 100 MeV protons in plastic is accurately known. These corrections will be discussed in detail in sections 5.1 and 5.2

The nature of the quasi-continuous beam which makes necessary the gating out of events occurring during the residual beam bursts precludes the use of a Faraday cup alone to monitor the continuous part of the beam. No way was known of switching the Faraday cup on and off in the short time intervals under consideration. An

indirect measurement of the current in the stretched part of the beam would have involved the construction of an auxiliary calibration E x dE counter telescope and Faraday cup essentially identical to the existing facility.

The calculation of absolute differential cross-sections from the germanium detector and counter telescope would have required an accurate knowledge of the detection solid angle defined by the very small window in the plastic scintillator. Without very elaborate means this did not seem possible to achieve to an accuracy better than 10%.

A convenient solution to these problems was simply to measure the absolute elastic cross-sections for ^{24}Mg and ^{28}Si with the pulsed beam and existing laboratory scattering facility (the elastic cross-sections for ^{12}C have been previously measured in the laboratory.) and to obtain the inelastic differential cross-sections from the high resolution spectra by simply comparing the peak areas corresponding to elastic and inelastic scattering.

The beam monitor was a Faraday cup located downstream from the target with several features designed to minimize the possible sources of error in the charge collection. A pressure of 10^{-5}mm. Hg provided by a diffusion pump insured that ionization of residual gas in the cup was negligible. The cup was deep to minimize losses due to back-scattering of electrons. To avoid collection of electrons ejected from the thin aluminum entrance window was separated

from the cup entrance by 20 cm so that even the most energetic electrons could be swept out of the region by a strong magnetic field provided by permanently mounted bar magnets. Portner (1968) has studied the variation of the cup calibration as a function of telescope angle. Variations in cup efficiency could arise from changes in the beam divergence at the target due to changes in beam intensity or small deflections of the unscattered beam due to different analyser magnet positions. These effects were found to be always less than 3%, and this error has been incorporated into our estimate of the total possible error in the measurement of the elastic cross-sections.

The current collected by the Faraday cup was fed into a pico ammeter. To measure the integrated current the voltage output of the pico ammeter was fed into a voltage to frequency converter whose output was scaled with a megacycle scalar. A Keithley pico-ampere source was used to periodically check the calibration of the integrator. The absolute calibration of the picoampere source has been previously checked by Portner and found to agree to 1% using a method in which the linear ramp voltage from a Tektronix scope was fed into a standard capacitor giving an accurately determined current C dV/dt.

FIGURE 6

FIGURE 6

This diagram illustrates the cold finger platform and germanium detector configuration (not to scale).

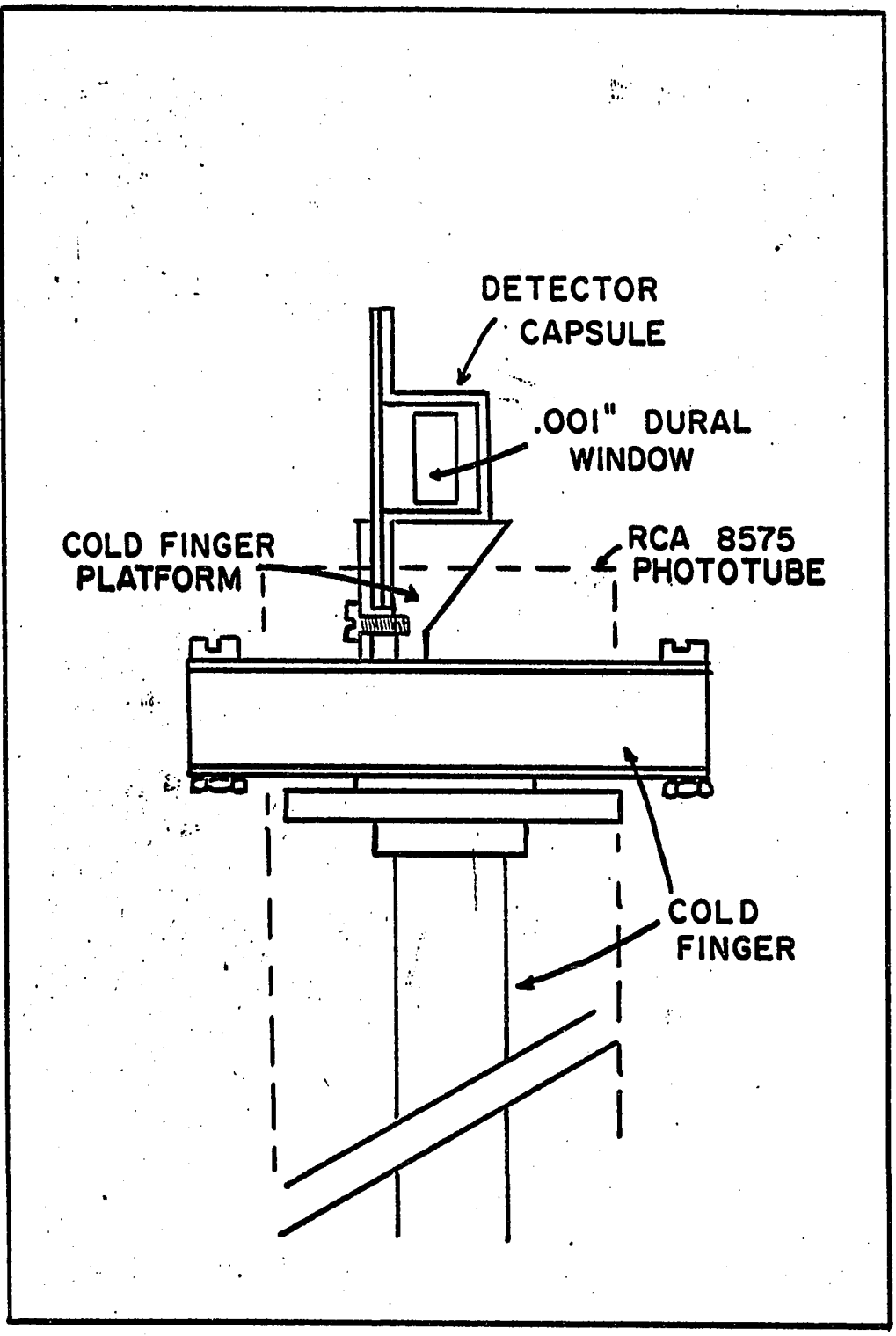
DETECTOR
CAPSULE
.001" DURAL
WINDOW
COLD FINGER
PLATFORM
RCA 8575
PHOTOTUBE
COLD
FINGER

FIGURE 7

FIGURE 7

This diagram illustrates the cold finger- detector configuration and the defining counter geometry (not to scale).

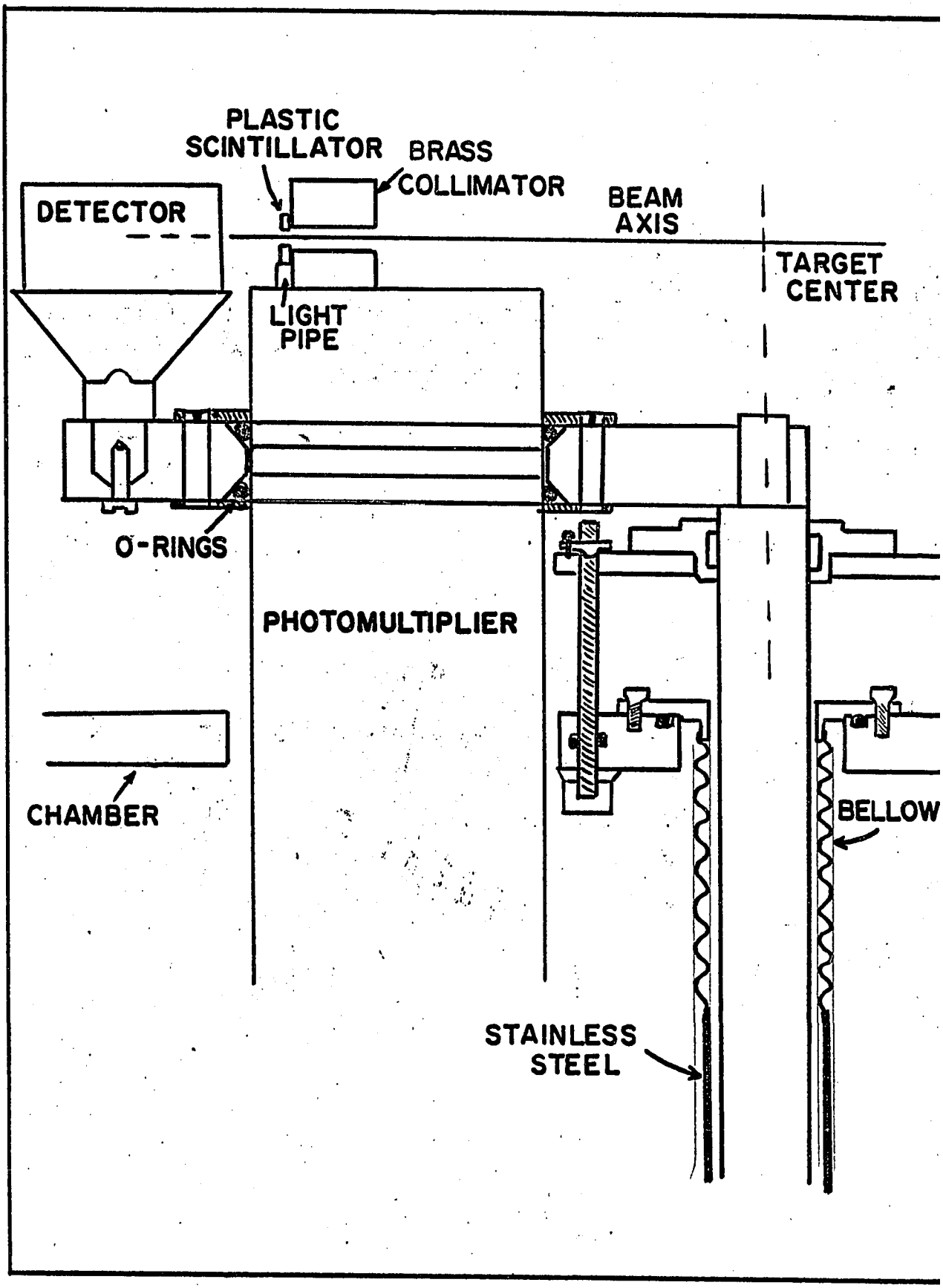
PLASTIC
SCINTILLATOR
BRASS
COLLIMATOR
DETECTOR
BEAM
AXIS
TARGET
CENTER
LIGHT
PIPE
O-RINGS
PHOTOMULTIPLIER
CHAMBER
BELLOW
STAINLESS
STEEL

FIGURE 8

FIGURE 8

Overall illustration of the scattering chamber cryostat. The target holder enabled the interchange of up to 4 targets without breaking the vacuum.

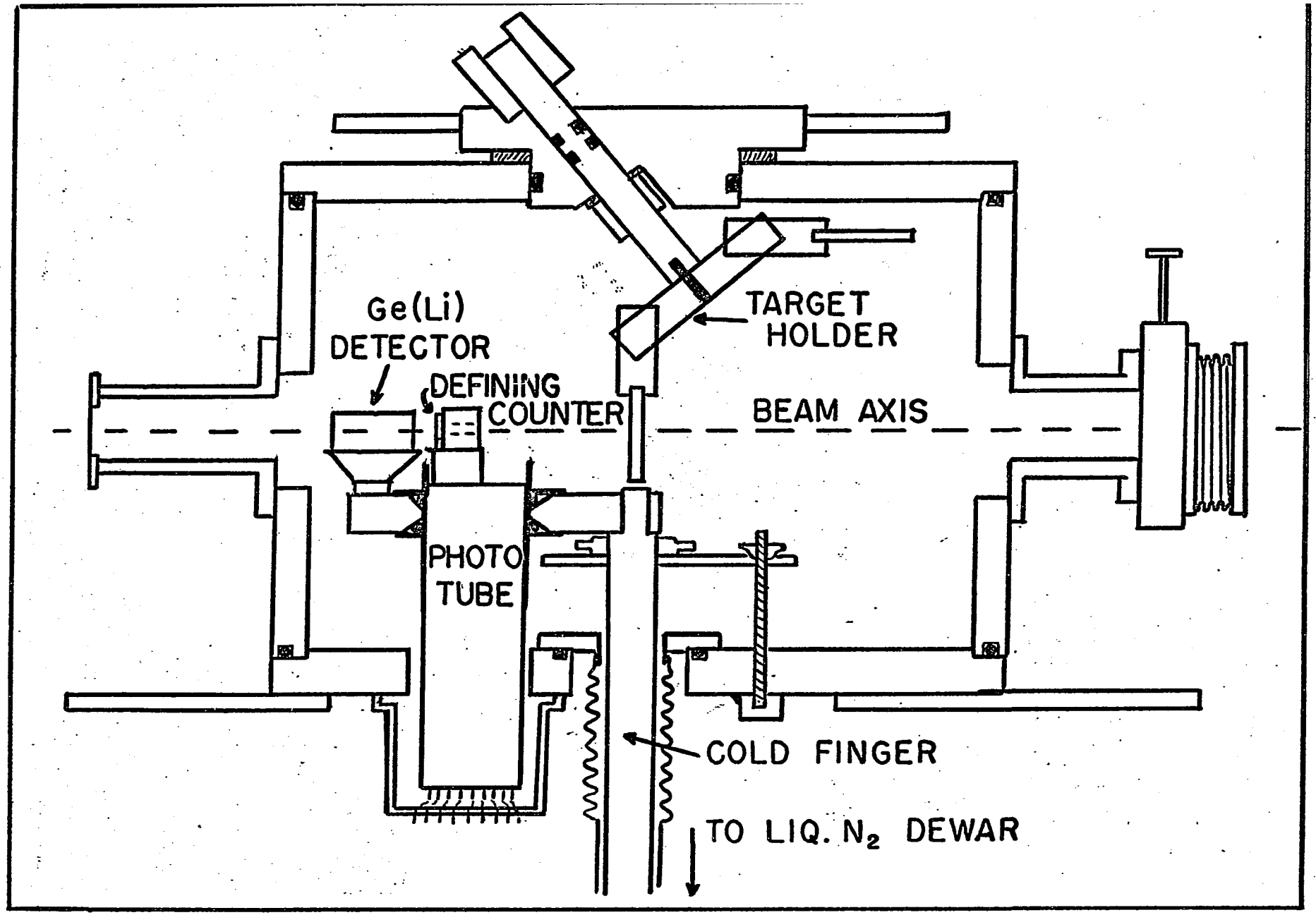
Ge(Li)
DETECTOR
DEFINING
COUNTER
TARGET
HOLDER
BEAM AXIS
PHOTO
TUBE
COLD FINGER
TO LIQ. N_2 DEWAR

FIGURE 9

FIGURE 9

Temperature calibration curve for the copper thermometer. The insert shows the simple circuit used to measure the copper wire resistance. This system measured a temperature of 120 degrees K at the cold finger platform.

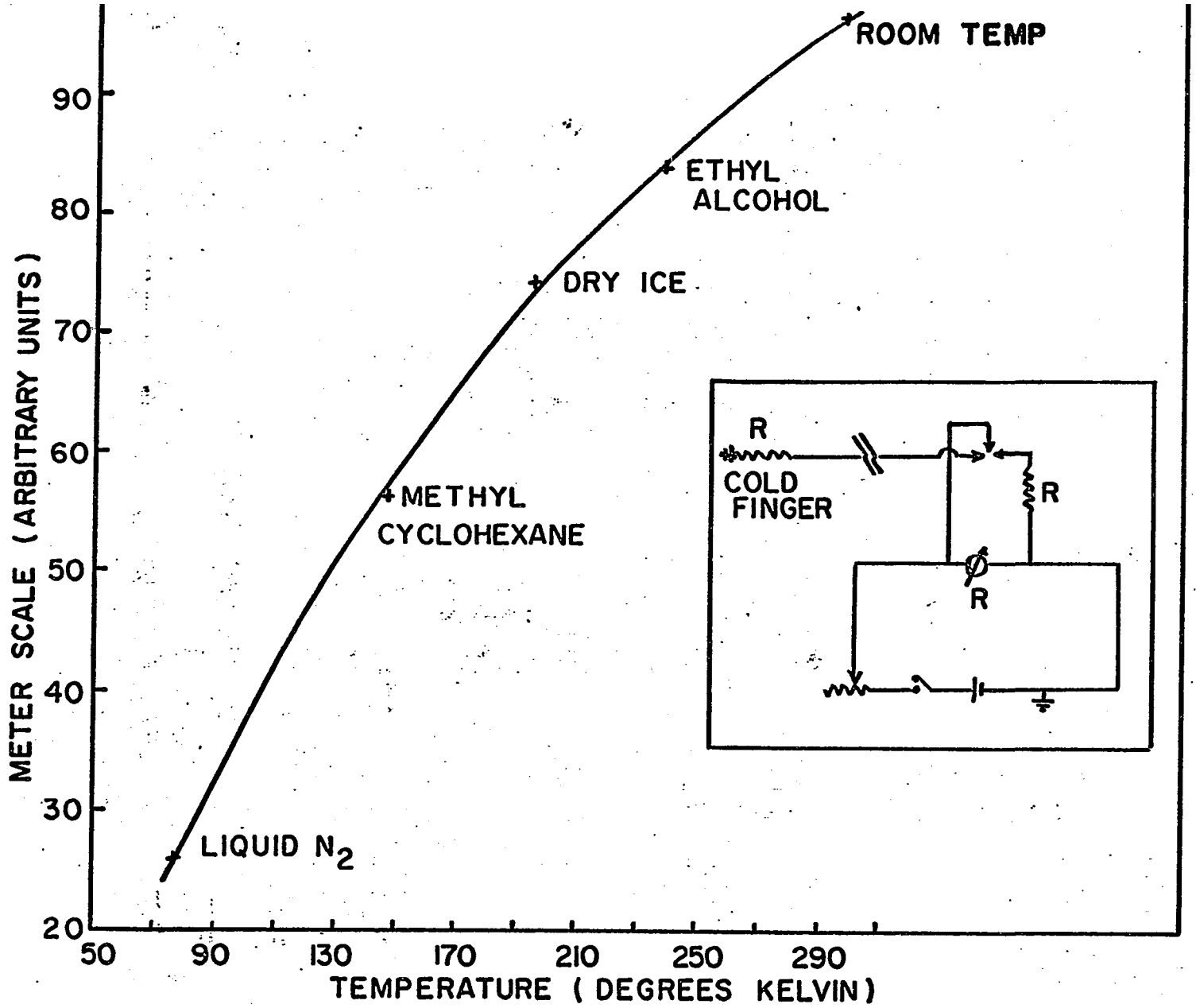
ROOM TEMP
ETHYL ALCOHOL
DRY ICE
METHYL CYCLOHEXANE
LIQUID N_2
METER SCALE (ARBITRARY UNITS)
90
80
70
60
50
40
30
20
50
90
130
170
210
250
290
TEMPERATURE (DEGREES KELVIN)
R
COLD FINGER
R
R

FIGURE 10

FIGURE 10

Ray diagram illustrating the target-defining counter-detector geometry.In this configuration no proton scattered from the 7 mm central region of the target can penetrate closer than 2 mm to the edge of the detector sensitive volume without being "vetoed".

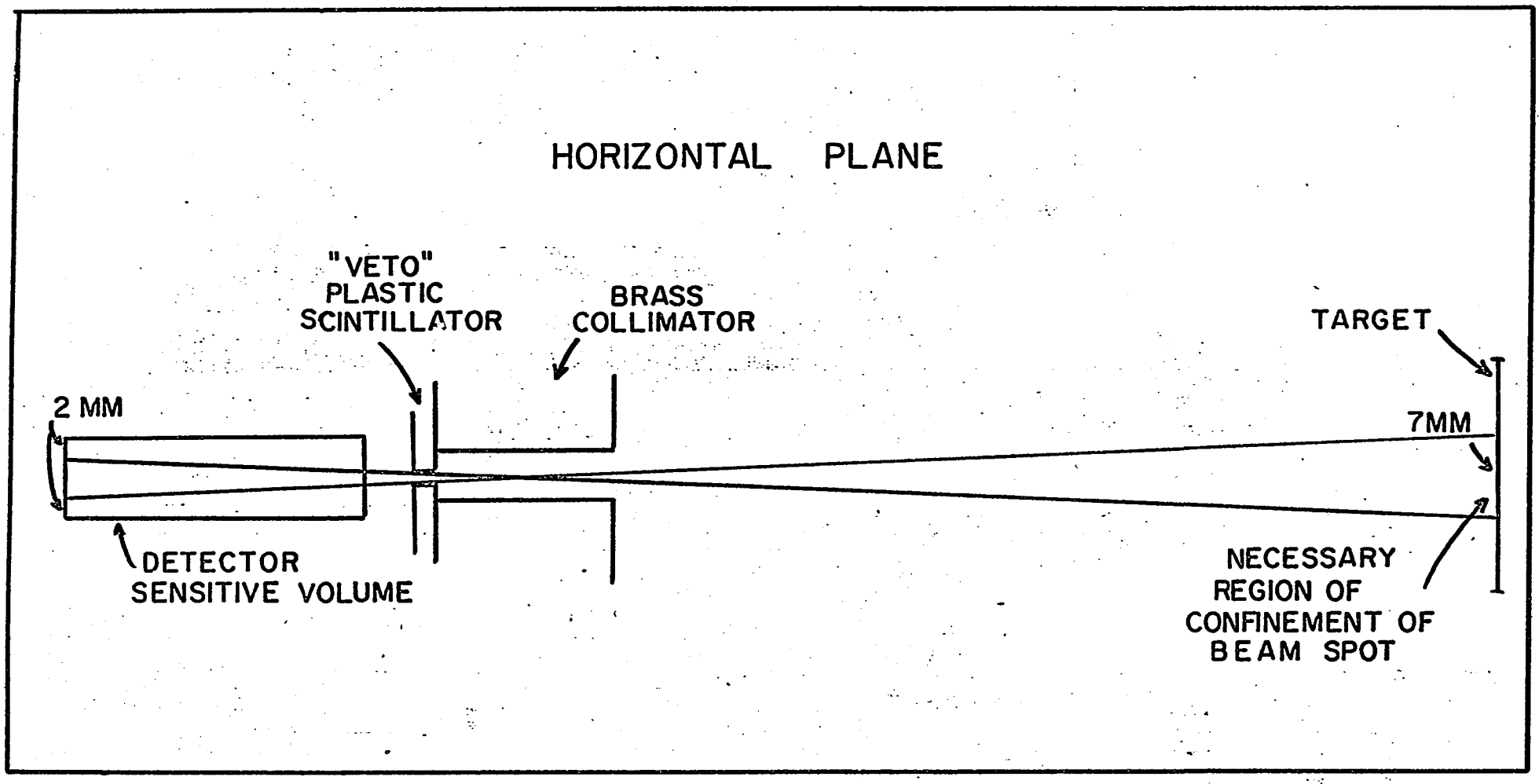
HORIZONTAL PLANE
"VETO" PLASTIC SCINTILLATOR
BRASS COLLIMATOR
TARGET
2 MM
7MM
DETECTOR SENSITIVE VOLUME
NECESSARY REGION OF CONFINEMENT OF BEAM SPOT

FIGURE 11

FIGURE 11

This figure shows a block diagram of the electronics.

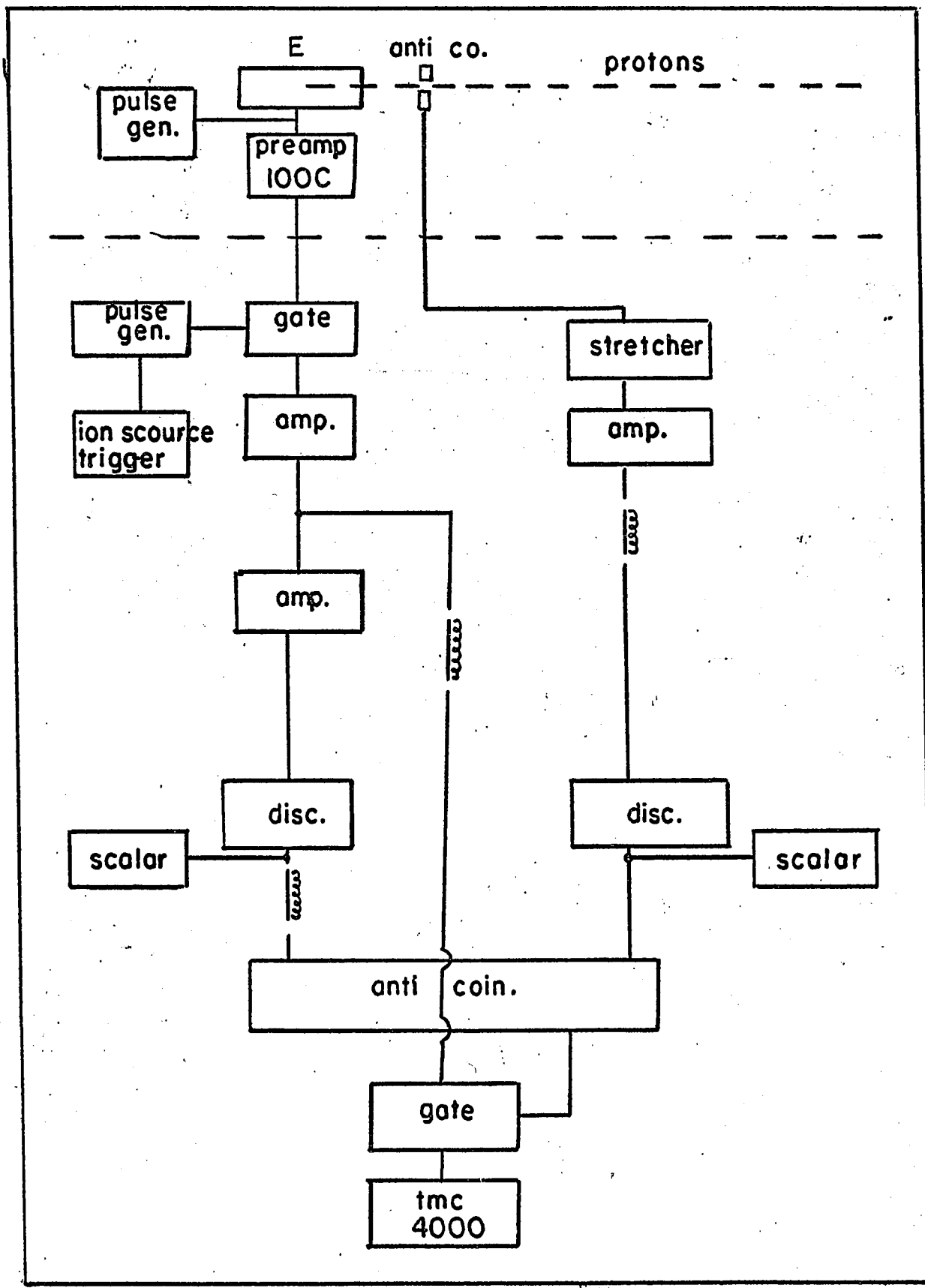
E
anti co.
protons
pulse gen.
preamp 100C
pulse gen.
gate
stretcher
ion scource trigger
amp.
amp.
amp.
disc.
disc.
scalar
scalar
anti coin.
gate
tmc 4000

FIGURE 12

FIGURE 12

Spectrum of protons scattered from gold illustrating the " veto " function. Note the increased width of the lower energy peak due to energy straggle in the plastic scintillator.

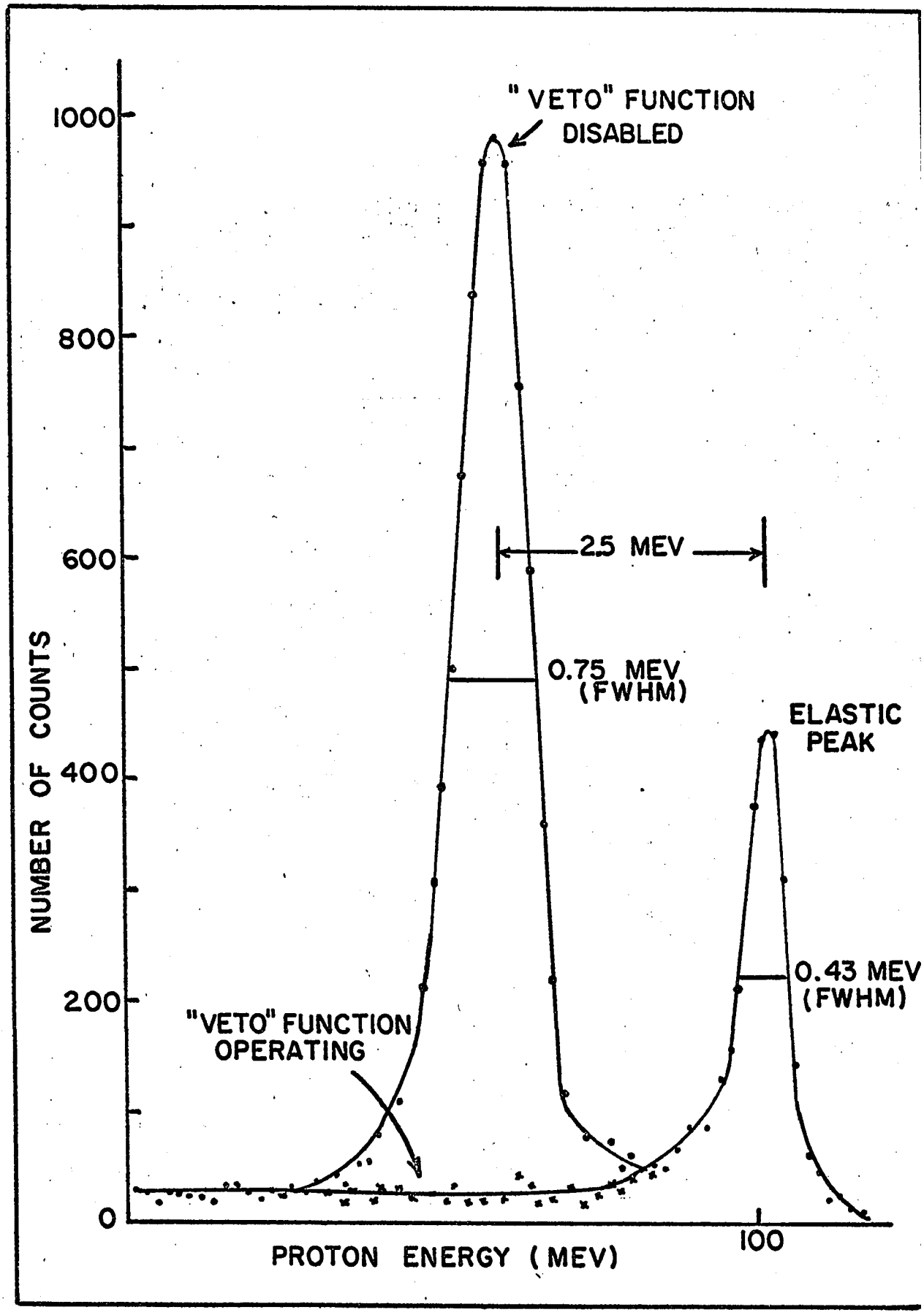
"VETO" FUNCTION
DISABLED
1000
800
600
400
200
0
NUMBER OF COUNTS
2.5 MEV
0.75 MEV
(FWHM)
ELASTIC
PEAK
0.43 MEV
(FWHM)
"VETO" FUNCTION
OPERATING
100
PROTON ENERGY (MEV)

FIGURE 13

FIGURE 13

Schematic diagram of the circuit used to control the detector bias and to monitor the detector leakage current.

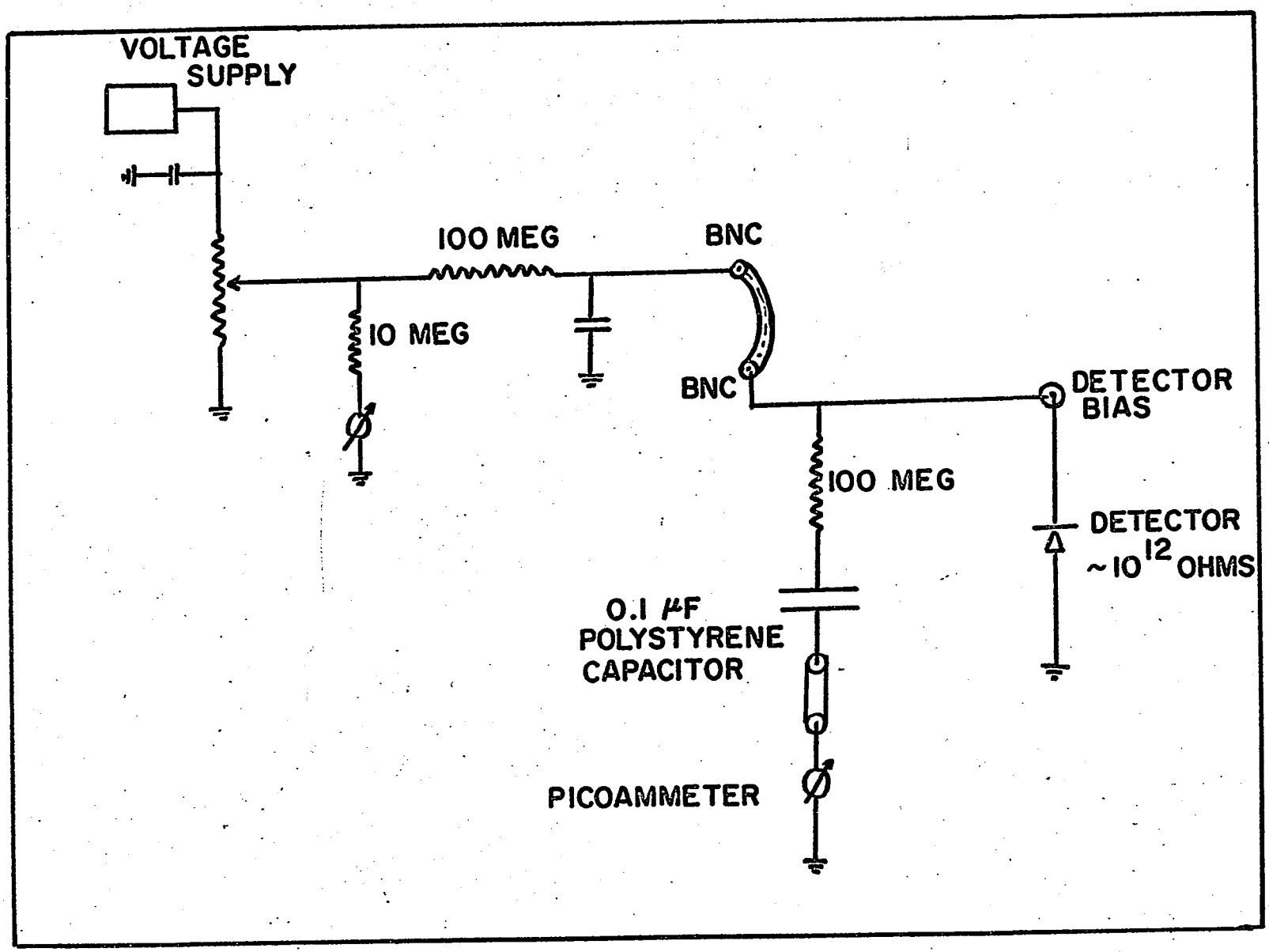
VOLTAGE
SUPPLY
100 MEG
BNC
10 MEG
BNC
DETECTOR
BIAS
100 MEG
DETECTOR
~10^12 OHMS
0.1 μF
POLYSTYRENE
CAPACITOR
PICOAMMETER

FIGURE 14

FIGURE 14

Detector bias versus leakage current characteristics for a typical detector.

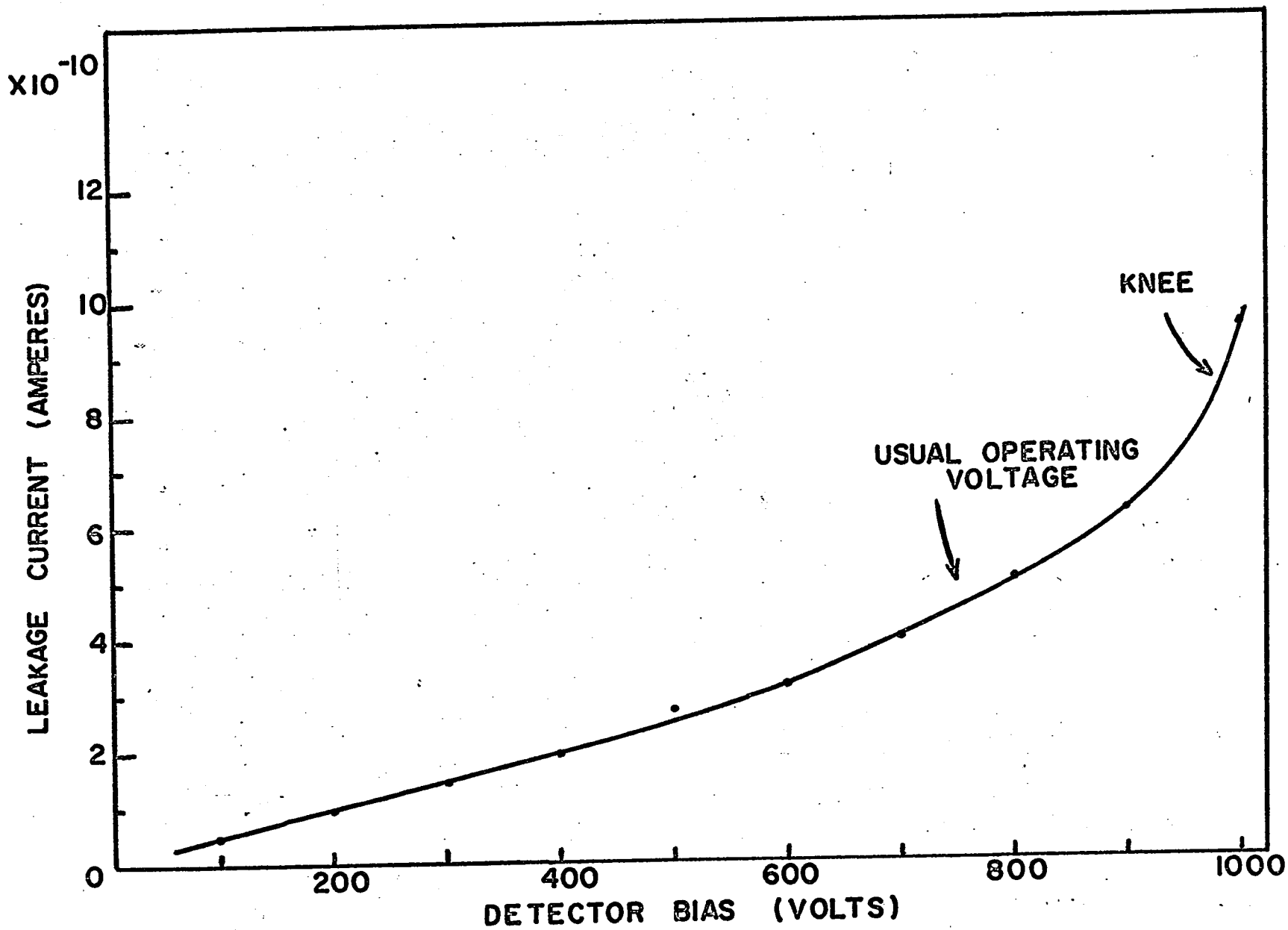
X10^-10
12
10
8
6
4
2
0
LEAKAGE CURRENT (AMPERES)
KNEE
USUAL OPERATING VOLTAGE
200
400
600
800
1000
DETECTOR BIAS (VOLTS)

FIGURE 15

FIGURE 15

Plan of the external beam system of the McGill synchrocyclotron. The labelled components are identified as follows;

A. Beam defining slits

B. Faraday Cup

C. Bending magnets

D. Quadrupole doublet

E. Television viewboxes

F. Switching magnet

G. Scattering chamber-cryostat for inelastic scattering experiment.

H. Scattering facility for elastic scattering experiment.

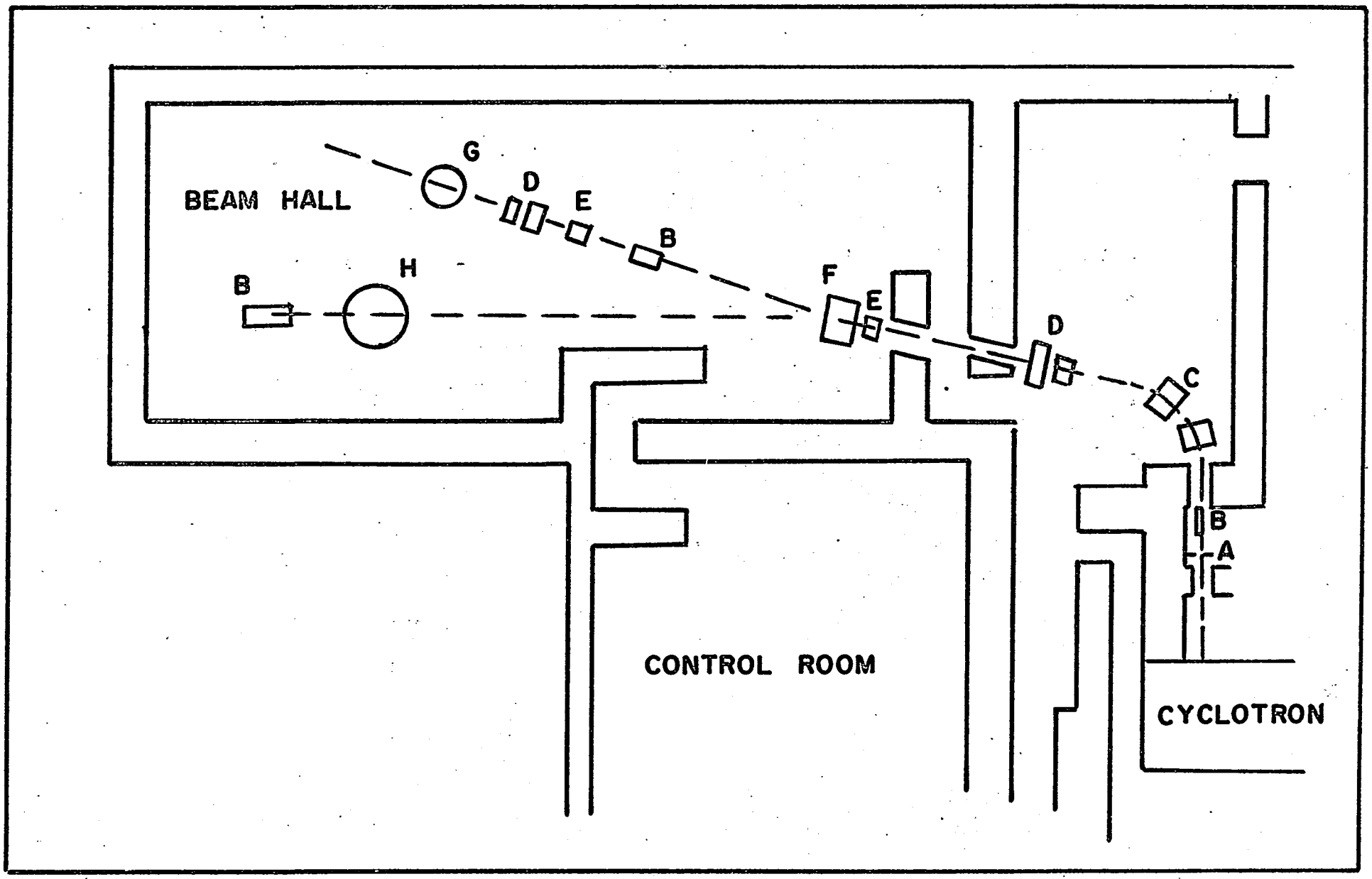
BEAM HALL
G
D
E
B
H
B
F
E
D
C
B
A
CONTROL ROOM
CYCLOTRON

CHAPTER 4. EXPERIMENTAL PROCEDURE

4.1 GENERAL EXPERIMENTAL PROCEDURE

At the beginning of each run the scattering chamber and cryostat was transported into the beam hall and raised into position to be hooked onto the external beam pipe. The beam was carefully aligned and focussed with the aid of the two view boxes and the fluorescent screen at the target position. The beam spot size was typically 1.5 mm in diameter and could be centered on the target to better than 0.5 mm. The detector during beam alignment was always kept at 90 degrees so as to intercept a minimum number of fast neutrons originating in the camera screens The beam was aligned and focussed as quickly as possible so as to reduce the accumulated dose of neutrons ejected from the screens.

The extraction of the stretched beam was normally the next step. The normal length of the beam burst is 10 microseconds, but the background activity due to the burst continues for a substantial period of time. The length of the gating pulse used to veto events occurring during the burst was adjusted so that with the stretcher off the background counting rate was negligible. This was usually accomplished by a gating pulse extending a full 100 microseconds past the beam burst. The horizontal slit at the entrance to the beam transport system was then adjusted to yield a counting rate of approximately

150 counts per second corresponding to an instantaneous counting rate of $\sim 3 \times 10^3$ counts per second (for p = 0.4%, $\tau = 1.0 \times 10^{-6}$ seconds, $p/\tau = 4 \times 10^3$). The low pile-up percentage at this counting rate is indicated by the almost negligible number of counts falling in channels above the elastic peak channels. The spectra were accumulated in a 1000 channel TMC pulse height analyser with the TMC gain adjusted to yield an energy calibration of approximately 125 keV per channel. Because of the vast difference in counting rates between the various inelastic peaks, the counting times were determined by requirements on the statistics of the counts in the weakly excited levels under study. The length of a run to acquire a minimum of 10% statistics (100 counts under the peak)varied from 3 to 6 hours.

Background measurements were taken periodically with the target out. In the region of energy excitation of interest the background counting rate was always negligible.

4.2 ZERO ANGLE CALIBRATION

In the elastic scattering experiment the zero angle calibration was determined by simply comparing the counting rates on opposite sides of the beam. ^{12}C was used as the target at a scattering angle of 25 degrees because the elastic cross-section varies very rapidly at that angle. Essentially the same method was used in the inelastic scattering experiment. A comparison was made of the ratio of elastic scattering to inelastic scattering leaving

^{12}C in its first excited state. A scattering angle of 45 degrees was chosen because at that angle the elastic cross-section is falling far more rapidly that the 4.43 MeV cross-section so that the ratio is a quickly varying function of angle. The zero angle was then determined by plotting this ratio versus angle and comparing it with the ratio observed at a standard angle on the other side of the beam. A typical zero angle calibration is illustrated in figure 16.

FIGURE 16

FIGURE 16

This figure illustrates the method used to determine the beam direction relative to the scattering chamber. In this case the left-hand right-hand difference was 0.2 degrees with a 0.15 degree associated RMS uncertainty.

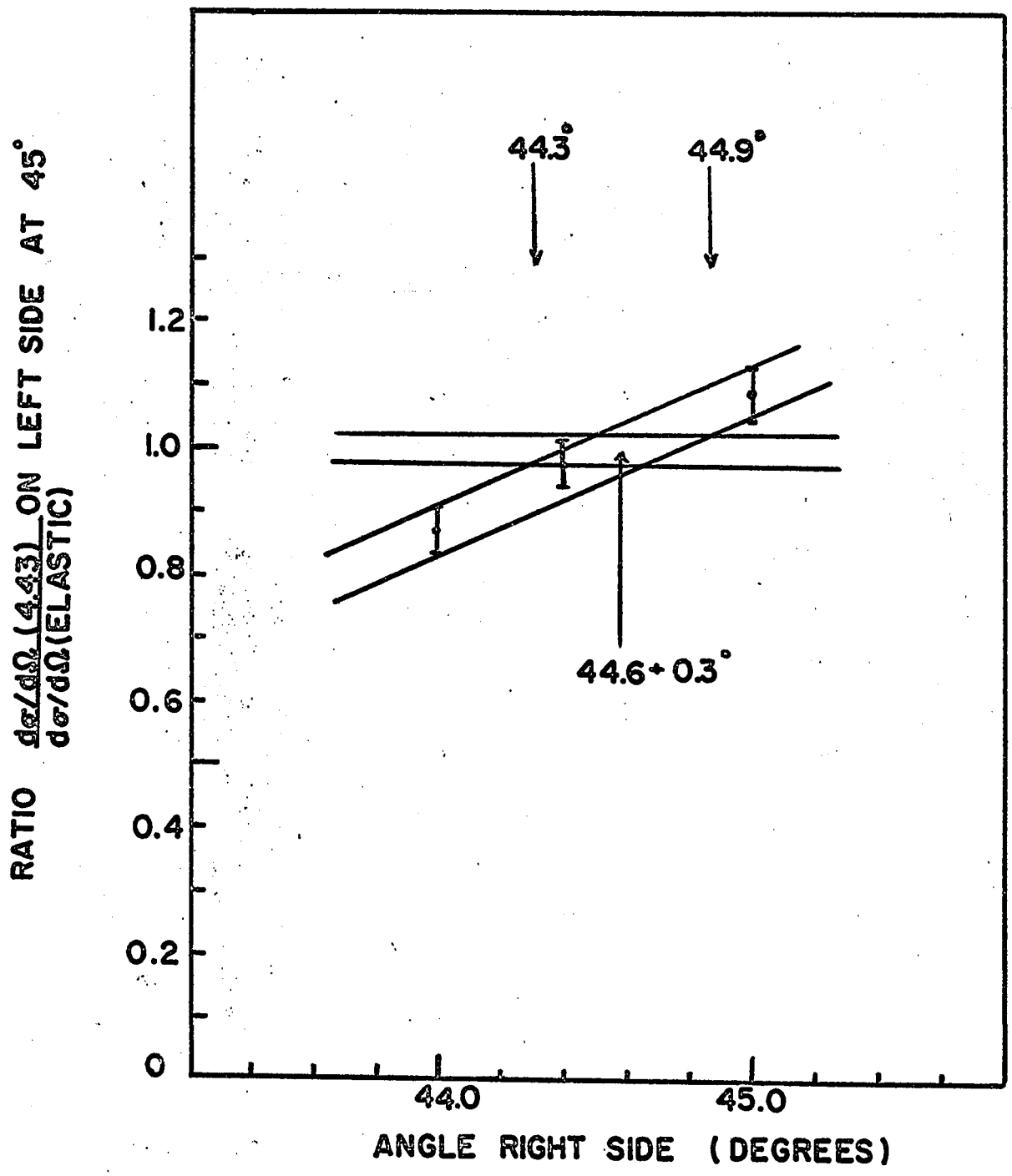
44.3°
44.9°
44.6±0.3°
1.2
1.0
0.8
0.6
0.4
0.2
0
44.0
45.0
ANGLE RIGHT SIDE (DEGREES)
RATIO dσ/dΩ(4.43) ON LEFT SIDE AT 45°
dσ/dΩ(ELASTIC)

CHAPTER 5. DATA REDUCTION AND DISCUSSION OF ERRORS

5.1 ELASTIC CROSS-SECTIONS, CORRECTIONS AND UNCERTAINTIES

The elastic differential cross-section is given by the number of particles scattered into solid angle $d\Omega$ by a corresponding incident number of particles impinging on n target nuclei per cm^2.

$$\frac{d\sigma}{d\Omega} = \frac{N_{sc}}{n\, N_{inc}\, d\Omega}$$

The actual calculation of the differential cross-section in terms of directly measureable quantities is given by

$$\frac{d\sigma}{d\Omega} = \frac{N_{sc}\, e}{Q} \left(\frac{1}{\frac{d\Omega N_o \rho t}{\cos\theta}} \right)$$

where: $N_{sc.}$ is the number of events identified as corresponding to elastic scattering.

Q is the integrated charge of the incident proton beam.

$d\Omega$ is the detection solid angle in steradians.

$t/\cos\theta$ is the effective target thickness in g/cm^2 for an angle θ between the target normal and the incident beam.

A is the atomic weight of the target material.

N_o and e are constants.

The errors involved in the measurement of the differential cross-section are thus due in large part to the uncertainties involved in the measurement of $N_{sc.}$, Q, $d\Omega$ and $t/\cos\theta$. Additional errors arise from corrections due to detector efficiency and electronic counting losses. The overall resolution of the laboratory scattering facility was 1.3 MeV for 100 MeV protons and consequently in both ^{24}Mg and ^{28}Si the elastic and first excited states were not clearly resolved. This however did not constitute a drawback because of the excellent separation of these peaks in the germanium spectra.

Corrections and uncertainties in $N_{sc.}$ - The two major corrections to the determination of $N_{sc.}$ were losses due to nuclear reactions in the E crystal and counting losses due to the dead-time of the multi-channel analyser. Minor corrections arise from pile-up and chance coincidences. The singles counting rate was kept low at 20 to 30 counts/sec. to minimize corrections due to the latter three causes. The chance coincidence rate was negligible and the pile-up rate calculated from Poisson statistics assuming an RF duty cycle of 4:1 was less than 1.5%. No systematic uncertainty was assumed for this correction.

In order to determine the dead-time correction experimentally the total number of E counts were scaled with a fast scalar and compared with the integrated number of counts collected by the pulse-

height analyser. With the previously mentioned counting rates a dead-time loss correction of approximately 4% was observed. This figure is in good agreement with the standard Cormack formula, 1962,

$$\lambda_2 t_o = 1 - (\exp)-\lambda_1 t_o$$

for an analyser dead-time longer than the beam pulse but shorter than the time between beam bursts. λ_2 and λ_1 are the observed and true counting rates and t_o is the interval between beam bursts. The experimentally determined corrections were used and we attach no significant uncertainty to their estimation.

The loss correction for protons in a plastic scintillator has been calculated by Measday (1965) for energies up to 150 MeV and has been measured experimentally in this laboratory several times with good internal consistency. Portner's measurement of the correction for the E counter in use was 14.5 $\pm$ 0.5% at 100 MeV. For A = 24 nuclear recoil results in 4 MeV difference in energy for protons elastically scattered at 10 and 60 degrees. The shape of the correction curve as a function of proton energy was estimated by fitting a smooth curve to the 100 MeV measurement and other measurements at 40 MeV and 68 MeV, (Johnston et al. 1958). This curve and the Measday calculations are illustrated in figure 17. In this way our estimate of the correction at 96 MeV (corresponding to elastic scattering at 60 degrees) was 12.5%. A systematic error of $\pm$ 1% was assigned for the uncertainty

in this correction.

An additional error involved loss of counts due to reactions or elastic scattering in the ΔE crystal. This effect has been estimated by Portner (1968) to contribute about 1% loss for the particular ΔE crystal used. No uncertainty was assigned to this correction.

Uncertainties in Q - As previously mentioned (section 3.6) the Faraday cup was specially designed to minimize possible errors in the determination of Q. Significant errors in the measurement of Q arise from possible variations in cup efficiency due to changes in the beam divergence at the target and beam deflection due to the fringing magnetic field of the analyser magnet. Portner (1968) has studied this effect using an in beam calibration Faraday cup and places an upper limit of 3% on the variation in cup efficiency due to these effects. In our case the analyser magnet was not used and the generally low beam intensities employed imply minimal changes in the beam divergence at the target. We therefore assign, somewhat arbitrarily, a total systematic error of 2% to the Faraday cup efficiency and calibration.

A Keithley picoampere source was used to periodically check the calibration of the integrator. During the course of a run the calibration was not found to vary by more than 1%. The absolute calibration of the picoampere source is believed to be correct to

1%. A total systematic error of 2% is consequently assigned to the use of the integrator. We therefore arrive at a total systematic uncertainty of 4% in the determination of Q.

Determination of the Effective Target Thickness - The thickness of the ^{28}Si target was determined by the average of a number of measurements with two micrometer gauges. The variation in thickness did not exceed 0.1×10^{-3} inches and we assign a possible error of 1% to this measurement.

The ^{24}Mg target was weighed and its surface area determined accurately so that its thickness of 19.1 mg/cm^2 is believed accurate to 1%. The target thickness was also measured with a micrometer gauge to be 4.3×10^{-3} inches. Using the density $\rho = 1.74$ gm/cm^3 (Hodgman, 1962) yields exactly 19.0 mg/cm^2. The uncertainty in the estimation of θ was estimated at $\pm$ 0.2 degrees. The greatest error in the target thickness will then occur for large angles. For a scattering angle of 60 degrees corresponding to $\theta = 30$ degrees the error is $\pm$ 0.2%. The presence of 0.3% isotopic impurities in the magnesium target introduces negligible error. In the silicon target, the presence of 4.7% ^{29}Si and 3.09% ^{30}Si introduces a non-negligible error. Assuming a maximum difference of 10% in the elastic scattering properties of the three isotopes one can assign a 0.8% uncertainty for this effect. We thus arrive at a total systematic uncertainty of 2.0 % for ^{28}Si and 1.2% for ^{24}Mg.

Uncertainty in $d\Omega$ - The solid angle of the detector telescope has been determined by Portner (1968) to be 0.293×10^{-3} steradians to an estimated accuracy of 0.4%.

Summary of Errors - Table III gives the maximum systematic error in the determination of the elastic differential cross-section for ^{24}Mg and ^{28}Si. In the case of ^{12}C the elastic differential cross-sections (Mark, 1965) are believed to be accurate to 5%. Interpolation of the elastic cross-sections to the inelastic scattering angles results in an additional error estimated to be no more than 3%.

Table III

SYSTEMATIC ERRORS IN THE ELASTIC-DIFFERENTIAL CROSS-SECTIONS

nucleus	$N_{sc.}$	Q	$t/\cos\theta$	$d\Omega$	Total
^{24}Mg	1.0%	4.0%	1.2%	0.4%	6.6%
^{28}Si	1.0%	4.0%	2.0%	0.4%	7.4%

5.2 INELASTIC CROSS-SECTIONS, CORRECTIONS AND UNCERTAINTIES

The inelastic cross-sections were determined by comparing peak areas relative to the elastic peak area. The systematic errors assigned to the measurement of the elastic cross-sections therefore also

apply to the determination of the differential inelastic cross-sections. In addition various other relative errors arise in the estimation of the ratio of the inelastic to elastic peak areas. These relative errors were treated as RMS errors and have been tabulated with the differential cross-sections.

Our procedure was to construct a standard curve for each spectrum based on the shape of the elastic peak. As previously mentioned the peaks in the energy spectra were gaussian in shape but with a distinct low energy tail due, in part, to the actual beam energy distribution. The low energy tail tended to grow slightly with detector age as would be expected from radiation damage effects.

The real background as obtained in target removed measurements was normally negligible in the excitation energy region of interest (Q = 0 to -16 MeV). However due to effects such as reactions in the crystal, outscattering from the crystal, multiple scattering in the target, collimator slit scattering and the high density of levels in the target nuclei all the spectra show a more or less smooth back - ground over which the strongly excited peaks are superimposed (for example, fig. 19). The subtraction of this background was done as carefully as possible since error in the subtraction may introduce significant relative error. Our procedure to fix the height of the background has been by inspecting well separated peaks in the energy spectrum and adjusting the level of the background so that the width of these peaks correspond to the width of the elastic peak. A great

majority of the peaks correspond to excitation of states whose intrinsic width is small compared to the overall experimental energy resolution. This procedure was, of course, supplemented by inspection of the background level and shape in peak free regions of the energy spectra.

In some instances, particularly in the s-d nuclei, the experimental resolution was insufficient to cleanly resolve neighbouring peaks. A good example is the 4.61 MeV and 4.97 MeV levels in ^{28}Si, separated by only 0.36 MeV, both strongly excited E4 and EO transitions respectively. In this particular case we were forced to assign RMS errors as large as 50% in the region of the apparent minimum of the 0^+ transition and RMS errors of 10% to 30% everywhere else. As can be seen from figure 23, however even these large RMS errors do not seriously smear out the characteristic $0^+ - 0^+$ shape of the angular distribution.

The relative RMS error in estimating the ratio of inelastic to elastic events was thus taken to be the quadratic sum of the purely statistical uncertainty in the number of inelastic events plus the estimated RMS error in the separation of poorly resolved peaks plus the statistical uncertainty in the background subtraction. In the vast majority of the cross-sections considered the statistical uncertainty in the number of elastic counts was negligible in comparison with the other uncertainties and was therefore included only in specific cases.

Corrections for Detector Efficiency - As discussed in section 2.4 we have measured a tail to peak ratio of 0.23 for our particular detector-telescope geometry of which we have assigned 0.139 to nuclear reactions of 100 MeV protons in germanium, an upper limit of 0.05 for multiple scattering out of the detector volume and approximately 0.04 for collimator slit scattering. The lowest energy protons we are interested in, 76 MeV, are those corresponding to inelastically scattered protons (Q = -16.1 MeV) from ^{12}C at a scattering angle of 60 degrees. The multiple scattering out of the detector sensitive volume is , of course, energy dependent. We have not attempted to correct for this effect. We assign for it a maximum uncertainty of $\pm$ 3% corresponding to cross-sections for highly excited (in energy) nuclear states.

The elastic cross-sections have been corrected for nuclear reactions in a plastic E counter. The remaining efficiency correction is therefore due to the energy variation of the nuclear reaction correction in germanium. We use the shape of the correction curve calculated by Makino et al. (1968) and illustrated in figure 18. The correction varies from o.3% (for the 1.37 MeV excited state in ^{24}Mg) to 2.3% for the 16.1 MeV level in ^{12}C. No systematic uncertainty is assumed for this correction,

Corrections for Isotopic Impurities - The differential cross-sections in ^{28}Si were increased by 7.8%, the ^{12}C cross-sections by 1.1% and the ^{24}Mg cross-sections by 0.3% to account for the isotopic impurities present in the three targets. No systematic uncertainty is

assigned to this correction.

5.3 ANGULAR UNCERTAINTIES

The angular uncertainty arises from two factors, error in determining the zero angle and error in the accuracy and reading of the angular scale. The former uncertainty is estimated to be $\pm$ 0.2 degrees and the latter 0.1 degrees, combining to yield a total RMS error of $\pm$ 0.22 degrees in the angular position. These uncertainties were, of course, present in both the elastic and inelastic scattering experiments. If the angular uncertainties are considered as errors in the cross-section the total RMS angular uncertainty of $\pm$ 0.33 degrees translates to an average error of $\sim$ 5% but reaches a value as high as $\sim$ 10% where the slope of the differential cross-sections are greatest.

FIGURE 17

FIGURE 17

This figure shows the predicted efficiency correction for protons in plastic due to Measday (1965). The experimental points are from Johnston et al.(1958) and Portner (1968). For this work corrections were made by fitting a smooth curve to the experimental points.

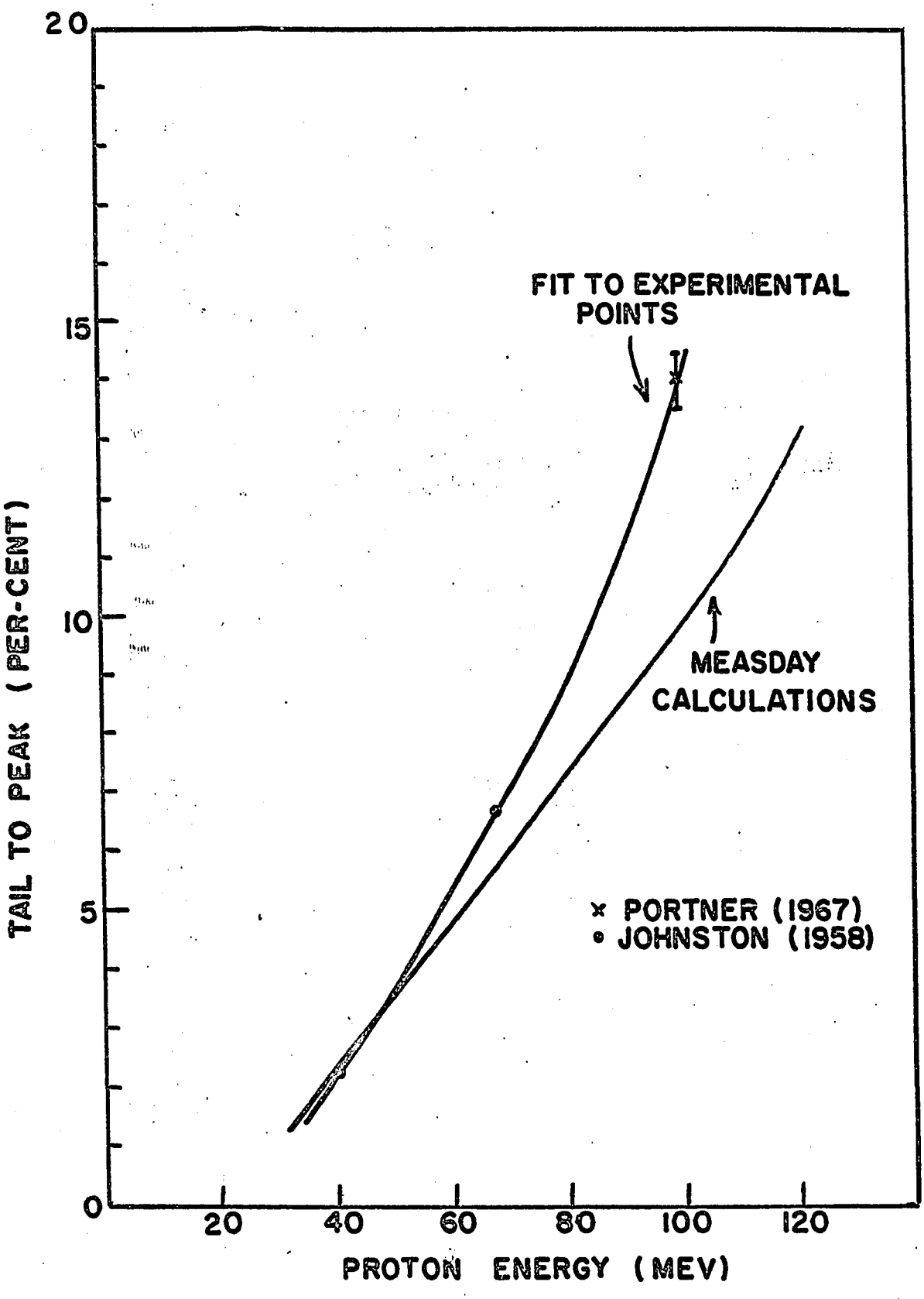
20
15
10
5
0
TAIL TO PEAK (PER-CENT)
FIT TO EXPERIMENTAL POINTS
MEASDAY CALCULATIONS
× PORTNER (1967)
• JOHNSTON (1958)
20
40
60
80
100
120
PROTON ENERGY (MEV)

FIGURE 18

FIGURE 18

This figure shows the predicted efficiency correction for protons in germanium due to Makino et al.(1968). The shape of the curve was used for relative efficiency corrections in the determination of inelastic cross-sections.

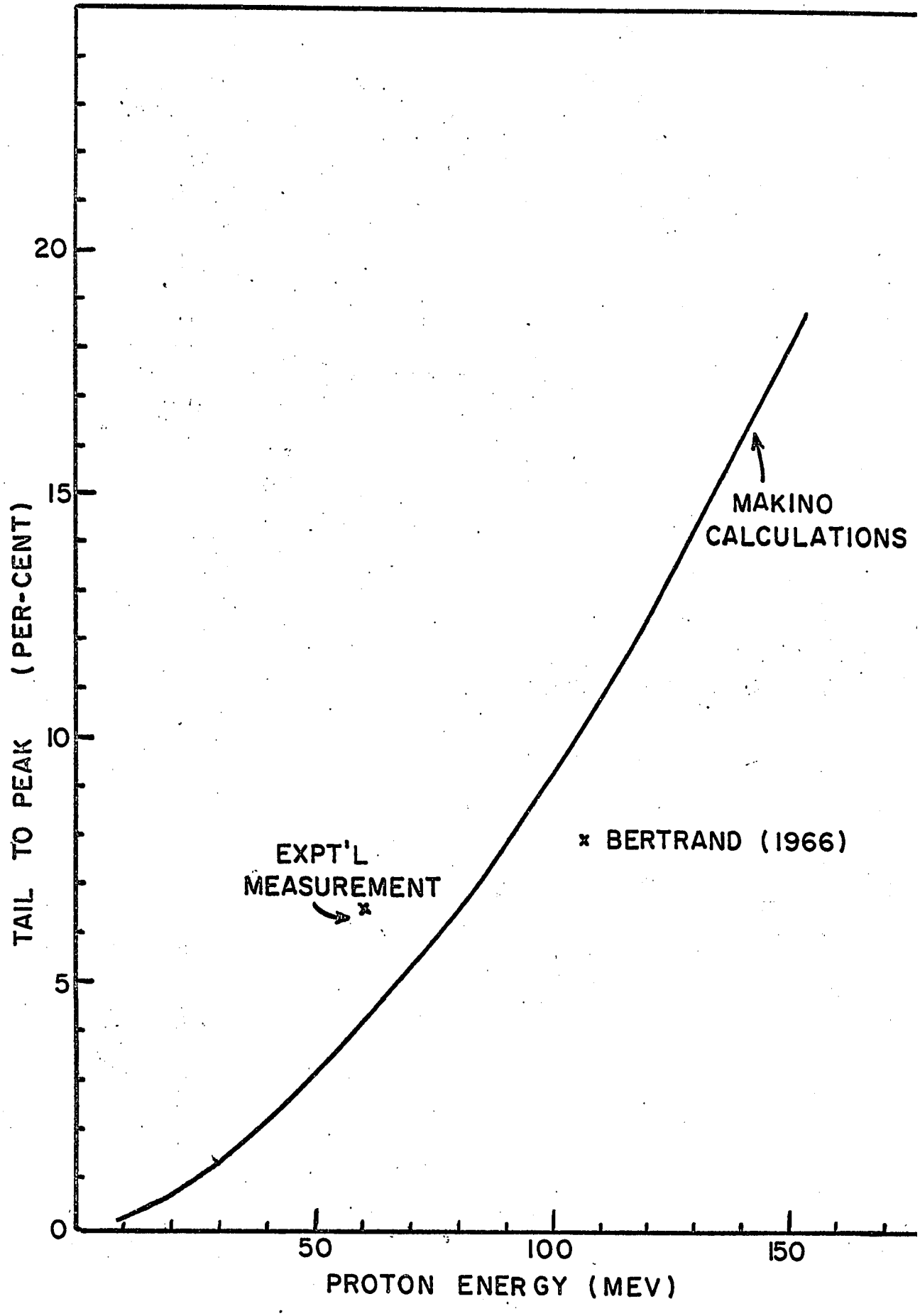
20
15
10
5
0
TAIL TO PEAK (PER-CENT)
MAKINO
CALCULATIONS
EXPT'L
MEASUREMENT
× BERTRAND (1966)
50
100
150
PROTON ENERGY (MEV)

CHAPTER 6. EXPERIMENTAL RESULTS AND DISCUSSION

6.1 INELASTIC SCATTERING FROM ^{12}C

The ^{12}C nucleus is a very suitable candidate for study via proton inelastic scattering. The Q values for the (p,d), (p,t), (p,^{3}He) and (p,α) reactions are -16.5 MeV, -23.3 MeV, -19.7 MeV and -7.5 MeV respectively so that the levels up to 16.5 MeV can be studied without recourse to particle identification. The (p,α) differential cross-section will be orders of magnitude smaller than the (p,p') cross-section. Table 4 and footnotes summarizes our present knowledge of the spin-parity assignments of the states in ^{12}C below the (p,d) Q value. It is quite surprising that in one of the most intensively studied nuclei in nuclear physics, considerable doubt still remains even in the spin-parity assignment of some of the higher-lying levels.

We have observed nine peaks in the energy spectra all of which can be identified with well known levels. The peaks observed in the proton spectra are listed in table 4 together with distinguishing characteristics of the measured differential cross-section angular distributions and properties of the corresponding excited levels.

The measurements were taken over an angular region from 10 degrees to 60 degrees with an average resolution of approximately 600 keV. Figure 19 shows a typical proton energy spectrum taken

at a laboratory angle of 34 degrees. The nine inelastic groups listed in Table 4 are easily identifiable. The differential cross-section angular distributions are shown in figures 20, 21, 23, 26, 27 and tabulated along with the relative uncertainties for the cross-sections in Tables 5 to 8. The relative errors which should be compounded with the absolute 8% uncertainty, are typically 5% for the 4.43 MeV level, 5% - 10% for the 7.66 MeV level going to 25% at the forward angles and 5% - 10% for the 9.63 MeV level. The large error typically 15% - 30% for inelastic scattering leading to the highly excited states is associated with their small cross-section and the continuum subtraction. Incorrect estimation of the background could conceivably introduce additional errors of the order of 20 - 30% for the 16.1 MeV level going to as high as 50% for the weakly excited 11.8 MeV level.

The states which did not appear to be excited in this work were the 10.1 MeV and 13.34 MeV levels. The 10.1 MeV level is a broad level but its existence is very well established from the β decays of ^{12}B and ^{12}N (Wilkinson et al. , 1963). Recent evidence seems to favor a 2^+ assignment for this state (H. Morinaga, 1963). The 13.3 MeV state is believed to have spin and parity 2^- (Brinkley et al. , 1964). Neither of these states has ever been observed in proton intermediate energy inelastic scattering.

Proton inelastic scattering from ^{12}C has been examined extensively up to 30 MeV with data also at 40 MeV (T. Stovall, 1964),

Table 4

EXPERIMENTAL RESULTS ON PEAKS OBSERVED IN THE ENERGY SPECTRA OF ^{12}C

TOGETHER WITH PROPERTIES OF THE CORRESPONDING EXCITED LEVELS

Experimental Excitation Energy (MeV) 1.	Listed Value (MeV)	Accepted Value J^π	T	Maximum Diff. $(d\sigma/d\Omega)_{c.m.}$ mb/sr	Cross-Section at angle degrees
4.4 ± 0.1	4.433	2+	0	9.2	20.9
7.7 ± 0.1	7.656	0+	0	0.76	26.3
9.6 ± 0.1	9.64	3^-	0	1.8	26.3
---	10.1	2+(0+)	0	---	-----
10.8± 0.1	10.84	1^-	0	0.46	forward
11.8± 0.2	11.83	$1^-(2^-)$	0	0.50	forward
12.7± 0.15	12.75	1+	0	0.47	16.5
---	13.3	(2^-)	0	---	-----
14.0± 0.15	14.08	4+(2+)	0	0.54	20.9
15.1± 0.15	15.11	1+	1	2.0	forward
16.1± 0.15	16.11	2+	1	0.83	forward

1- The uncertainty in the energy represents the maximum observed spread in the excitation energy over the angular region studied. Uncertainty due to possible non-linearity or error in the estimation of peak centroid positions is not included.

46 MeV (Petersen et al., 1967), 57 MeV (Nonaka et al., 1962), 96 MeV (K. Strauch et al., 1956), 150 MeV (Jacmart et al., 1962) and 185 MeV (Hasselgren et al., 1965). At energies above 100 MeV no data is available

for inelastic scattering leading to the 10.8-, 11.8- or 14.1- MeV states, and our measurements therefore constitute the first angular distribution data for these states in the intermediate energy region. Even below 100 MeV the data on the highly excited levels is extremely sparse. Only at 46 MeV (with an experimental resolution of 0.5 MeV, comparable to our own energy resolution) does data exist for inelastic scattering leading to the 10.8- and 11.8 MeV states. The Uppsala group with an energy resolution of 0.4 - 0.5 MeV (i.e., slightly better than our own results for ^{12}C) observed two small peaks in their energy spectra at 10.6 $\pm$ 0.4 and 11.1 $\pm$ 0.4 MeV but the peaks were difficult to resolve, and the former peak does not correspond to any known level in ^{12}C.

The Uppsala group did observe the 14.1 MeV level at angles beyond 20 degrees and set an upper limit of 0.2 mb/sr for the differential cross-section. In our case the level is more strongly excited and it has been possible to extract the angular distribution over the entire angular range from 10 to 60 degrees. In the forward angle region where the neighboring 15.1 MeV level is strongly excited relative errors of approximately 40% have been assigned to the differential cross-section for the 14.1 MeV level.

6.2 THE STATES AT 4.43 MeV AND 9.64 MeV

These states are unique in ^{12}C in the sense that the measured angular distributions at many incident proton energies have

been very satisfactorily predicted on the basis of the macroscopic collective model generalization of the optical model. The collective model is applied by assuming the optical potential follows the shape of the nucleus and becomes non-spherical(statically for rotations, or dynamically for vibrations). The non-spherical parts couple the ground state to the excited states and to first order yield a matrix element which takes care of both the nuclear wave functions and the effective interaction.

$$\langle\psi_f|V_{eff}|\psi i\rangle \propto \beta_\ell \frac{\partial U(r)}{\partial r}$$

where U(r) is simply the spherical part of the optical potential and β_ℓ is the 2^ℓ pole deformation parameter. In the Distorted Wave Born Approximation (DWBA) the transition amplitude for the reaction is simply

$$T_{fi} = \int \chi_f^{-*}(r_f)\langle\psi_f|V_{eff}|\psi_i\rangle \chi_i^{+}(r_i)dr_i dr_f$$

where χ_i and χ_f are distorted waves describing the motion in the entrance and exit channels. Since U(r) can be determined from elastic scattering the only free parameter in this model is β_ℓ which determines the magnitude of the cross-section.

The values of β_ℓ obtained at various proton energies agree quite well and are listed below.

Proton Energy	β_2 - 2^+, 4.43 MeV	β_3 - 3^-, 9.64 MeV
40 MeV	0.60	0.44
46 MeV	0.65	0.44
150 MeV	0.67	0.57

A comparison of deformations obtained in this manner with deformations obtained from inelastic electron scattering, Coulomb excitation and inelastic neutron scattering show good agreement,(Haybron, 1965). Our data at 100 MeV is presently being analysed by McManus, but no results were available in time for inclusion in this thesis.

Characteristic angular distributions are usually observed for the 2^+ and 3^- collective transitions successfully described by this model. In the angular distribution there is usually a dominant peak in the forward region after which the cross-section decreases more cr less monotonically as the angle decreases. The angle of the maximum is expected to increase with angular momentum transfer (Pinkston and Satchler, 1961). For the 2^+ and 3^- angular distributions that we have measured this description is accurate. The two 2^+ distributions at 4.43 MeV and 16.11 MeV peak at approximately 20.9 degrees and the 3^- distribution at approximately 26.3 degrees. The differential cross-sections decrease smoothly past these angles for all three distributions. The angular distributions are illustrated in figures 20 and 21. These same charactersitics are also observed in the inelastic scattering of 150 MeV and 185 MeV protons. This

feature of angular distributions observed in intermediate energy proton inelastic scattering is strikingly illustrated in figure 42 which shows the angular distributions we have measured for some 2^+, 3^-, 4^+ and 5^- transitions in ^{28}Si. For a discussion of the variation of peak angle with angular momentum transfer and nuclear size see section 8.1.

Cohen and Rubin (1958) were the first to observe that inelastic scattering from nuclei preferentially excites states having a collective nature. In particular they found that there is a significant correlation between the cross-sections for inelastic scattering by Coulomb excitation and by nuclear excitation. Pinkston and Satchler (1961) have shown using the direct interaction model that the matrix elements for nuclear excitation are closely analagous to those for electric multipole radiation between the same two states. Figure 22 shows the integrated cross-sections we have observed for inelastic proton scattering from ^{12}C. The 2^+ states at 4.43 MeV and 16.1 MeV, the 0^+, 3^- and 4^+ states at 7.66 MeV, 9.64 MeV and 14.1 MeV have all been interpreted as collective rotations or vibrations of the ground state (G. R. Satchler, 1967). The total cross-section for exciting these states ($\sim$15 mb) represents roughly 6% of the total reaction cross-section and roughly 90% of the inelastic cross-section leading to excited states up to 16 MeV excitation energy.

To test the correlation between the nulcear matrix elements at 100 MeV and electric multipole radiation we have followed a model

suggested by Clegg (1961, 1964) in which he compares the peak differential cross-section in the inelastic proton angular distribution with the radiative decay rates for E2 and E3 transitions. The results are consistent with Clegg's calculations for proton energies of 150 MeV and are discussed in detail in section 9.1.

6.3 THE STATE AT 7.66 MeV

Various attempts have been made to interpret the proton inelastic scattering from this 0^+ state using the collective generalized optical model. In this model the monopole L = 0 term represents a physical motion which has been called a breathing mode (Satchler, 1967). In this mode an increase in the radial extent of the nuclear density distribution must be accompanied by a decrease in the magnitude of the density. The model gives a poor description of the angular distribution of inelastically scattered protons leading to the 7.66 MeV 0^+ state, (T. Stovall, 1964, at 39.7 MeV, G. R. Satchler,,1967, at 46 MeV).

The angular distribution for the 7.66 MeV level is shown in figure 23, along with two other 0^+ --- 0^+ transitions observed in ^{24}Mg and ^{28}Si for comparison purposes. Note the vastly different shapes of the angular distributions. The s-d transitions are characterized by a clear "diffractive" pattern and deep minimum at the forward angles. In carbon both of these characteristics are absent. This difference between the 0^+ --- 0^+ transitions in the

Table 5

DIFFERENTIAL CROSS-SECTIONS FOR THE 4.43-, 7.66- and 9.64 MeV LEVELS

C.M. Angle degrees	4.4 MeV level $(d\sigma/d\Omega)^{c.m.}$ in mb/sr	7.6 MeV level $(d\sigma/d\Omega)^{c.m.}$ in mb/sr	9.64 MeV level $(d\sigma/d\Omega)^{c.m.}$ in mb/sr
12.2	3.91 ± 0.23	0.267 ± 0.088	0.524 ± 0.133
16.5	6.64 ± 0.29	0.356 ± 0.086	1.08 ± 0.12
20.9	9.16 ± 0.37	0.621 ± 0.068	1.67 ± 0.11
26.3	7.23 ± 0.35	0.755 ± 0.051	1.81 ± 0.10
31.7	4.90 ± 0.21	0.516 ± 0.029	1.71 ± 0.077
37.1	3.17 ± 0.14	0.310 ± 0.020	1.27 ± 0.060
42.5	1.96 ± 0.09	0.227 ± 0.017	1.09 ± 0.055
47.8	1.30 ± 0.06	0.0940 ± 0.0086	0.773 ± 0.039
53.1	0.873 ± 0.05	0.0477 ± 0.0054	0.590 ± 0.038
63.7	0.331 ± 0.02	0.00761 ± 0.0019	0.320 ± 0.025

different shells is accentuated by the striking similarity between the 2^+ angular distributions observed in these three nuclei with a similar very strong similarity for 3^- transitions. The 2^+ and 3^- angular distributions are shown for purposes of comparison in figures 21 and 24.

The 0^+ --- 0^+ angular distributions we have observed at 100 MeV closely resemble the angular distributions measured at 150 MeV and 185 MeV. Unfortunately the Uppsala group at 185 MeV did not carry their measurements past 30 degrees so the significant difference between the p shell and s-d shell 0^+ angular distributions was not well brought out. The Uppsala results are shown in figure 25. They choose to describe the angular distributions as "strikingly similar"

which we believe is seriously mistaken. The angular distributions are similar only in the observed rise at very small scattering angle (not shown in figure 25.) The Tokyo group at 56 MeV, (J. Kokame et al, 1967) have also commented on the similarity of angular distributions for 0^+ transitions in ^{12}C as compared with ^{24}Mg, ^{28}Si and have suggested because of the similarity that the structure and mechanism of excitation of 0^+ states may be common to the s-d and p shell nuclei. Our results at 100 MeV seem to be a strong denial of this suggestion.

Satchler, 1967, has recently attempted to interpret the 0^+ angular distribution in ^{12}C (46 MeV proton data) by a multiple excitation process. His calculations explicitly solve a set of coupled channel equations for the 4.43 MeV 2^+ coupled to the 7.6 MeV 0^+. The DWBA can be applied only to single excitation processes. The 4.43 MeV 2^+ state has most often been interpreted as the rotation of a ground state ellipsoidal nucleus. For the purposes of calculation, however, Satchler assumes that the 7.6 MeV state represents the 0^+ member of the two-phonon triplet with the 4.43 MeV level being the one phonon state. His results show an agreement in shape with the measured angular distribution which is remarkably good. The magnitude of the cross-section is out by approximately a factor two. To explain the discrepancy in magnitude a satisfactory alternative explanation is that the 0^+ state represents a β vibration of the ellipsoid about its equilibrium deformation. In addition the angular distribution is found to be very sensitive to the proportion

of multiple excitation (M) and direct excitation (D) which contributes, and any significant deviation from the M/D ratio predicted by the two-phonon model gives poor agreement in shape with the measured angular distribution.

To summarize, strong 2^+ and 3^- transitions show angular distributions which appear to be both shell and energy independent. On the other hand 0^+ transitions show angular distributions which appear to be very strongly shell dependent, and 4^+ transitions show angular distributions which are both shell and energy dependent (section 6.6). The salient fact that emerges is that the states which show angular distributions which vary with energy and from shell to shell are those which cannot be explained on a simple one-step excitation process. Moreover, contrary to the Tokyo and Uppsala suggestions, it is difficult to imagine the same excitation mechanism giving rise to the very different 0^+ shapes we have observed in carbon and in the s-d shell nuclei.

6.4 THE STATES AT 10.8- AND 11.8 MeV

The state at 10.8 MeV has definite 1^- spin and parity. The state at 11.8 MeV, however, has been reported as either 1^- or 2^- with the most recent support for the latter identification (T. A. Brinkley, 1964). Petersen *et al.* (46 MeV) however, find a resemblance between the 10.8 MeV and 11.8 MeV distributions and remark that the resemblance seems reasonable if the states are both 1^- but

is peculiar if the 11.8 MeV level is 2^-.

Our own results (figure 26) seem to corroborate Petersen's comments. Both angular distributions fall approximately one order of magnitude over the angular range from 12 to 53 degrees: however the large error bars make a more detailed comparison of shapes difficult. The more distinct forward peaking in the case of the 11.8 MeV distribution is reminiscent of the 15.1 MeV distribution which is a 1^+ spin flip transition. This could suggest a 2^- identification

Table 6

DIFFERENTIAL CROSS-SECTIONS FOR THE 10.8 MeV AND 11.8 MeV LEVELS

C.M. Angle degrees	10.8 MeV level $(d\sigma/d\Omega)^{c.m.}$ in mb./ster.	11.8 MeV level $(d\sigma/d\Omega)^{c.m.}$ in mb./ster.
12.2	0.456 ± 0.119	0.496 ± 0.123
16.5	0.262 ± 0.089	0.308 ± 0.086
20.9	0.408 ± 0.078	0.305 ± 0.057
26.3	0.221 ± 0.037	0.0701 ± 0.024
31.7	0.108 ± 0.019	0.0501 ± 0.016
37.1	0.144 ± 0.021	0.0415 ± 0.011
42.5	0.0850 ± 0.016	0.0287 ± 0.012
47.8	0.0567 ± 0.012	0.0364 ± 0.0090
53.1	0.0523 ± 0.010	0.0187 ± 0.0067
63.7	0.0383 ± 0.0056	------

for the 11.8 MeV level so that the transition would then also involve a spin-flip. Obviously no definite conclusion about the 11.8 MeV level spin-parity can be drawn from these observations.

6.5 THE STATES AT 12.7 MeV AND 15.1 MeV

The 12.7 MeV level is a 1^+, T = 0 state whereas the 15.1 MeV level is 1^+, T = 1. These states have unnatural parity and are therefore most likely to be populated via a spin-flip mechanism. In the theoretical framework of the distorted wave impulse approximation (DWIA) the states can be reached directly only through the spin and isospin dependent part of the nucleon-nucleon interaction. The angular distributions are shown in figure 26. Clegg (1965) has pointed out that under certain assumptions the difference between the two angular distributions should be due only to the different variations of the nucleon-nucleon scattering amplitudes involved. We have carried out this comparison using scattering amplitudes calculated from the BB - YLAM phase shifts. The results are discussed fully in section 8.2. The agreement with the theoretical prediction is good only in the forward angle region and consequently may be interpreted as a failure of the impulse approximation at 100 MeV for large momentum transfer.

The angular distributions of the two levels differ appreciably. The differential cross-section for the 12.7 MeV level changes by almost exactly one order of magnitude over the angular region studied whereas the 15.1 MeV level shows a variation of almost two orders of magnitude being very strongly peaked in the forward direction. This characteristic has been observed at 185 MeV and at 150 MeV but not at 46 MeV where the angular distribution levels

off at approximately 30 degrees. The difference between the angular distributions is accentuated by noting the very similar angular distributions between the 2^+ states at 4.43 MeV (T = 0) and at 16.1 MeV (T = 1). These features could be explained by attributing the difference in angular distributions in the former case to the difference in isospin and the similarity in the latter case to the predominance of the non-spin flip terms over isospin flip terms in a $0^+ \text{---} 2^+$ collective excitation.

Table 7

DIFFERENTIAL CROSS-SECTIONS FOR THE 12.7 MeV AND 15.1 MeV LEVELS

C.M. Angle degrees	12.7 MeV Level $(d\sigma/d\Omega)^{c.m.}$ in mb/sr	15.1 MeV Level $(d\sigma/d\Omega)^{c.m.}$ in mb/sr
12.2	0.367 ± 0.120	1.96 ± 0.24
16.5	0.466 ± 0.105	1.39 ± 0.17
20.9	0.349 ± 0.063	1.12 ± 0.11
26.3	0.159 ± 0.029	0.496 ± 0.050
31.7	0.129 ± 0.018	0.239 ± 0.025
37.1	0.123 ± 0.015	0.134 ± 0.019
42.5	0.116 ± 0.018	0.138 ± 0.019
47.8	0.095 ± 0.012	0.87 ± 0.014
53.1	0.080 ± 0.010	0.068 ± 0.011
63.7	0.044 ± 0.007	0.0347 ± 0.0078

Lee and McManus (1967) have investigated the 156 MeV inelastic scattering of protons from ^{12}C. They used the WKB method to compute the distorted waves and free two nucleon scattering amplitudes for the impulse approximation. The nuclear form factors

were calculated from the Gillet and Vinh-Mau (1963) wave functions based on the particle-hole model with pure j-j coupling. No free parameters are involved, so the calculation tests the accuracy of the Vinh-Mau wave functions and thus also the particle-hole model. Good fits to the differential cross-section were obtained for the 4.43 MeV, 9.63 MeV and 16.1 MeV levels. For the 12.7 MeV level there was moderate agreement in shape but the cross-section was predicted a factor 10 too high. The calculations for the 12.7 MeV level were compared with the Uppsala data since no data was available at the Orsay energy. Our own measurements in the small angle region agree in shape and magnitude with Uppsala however we have measured the differential cross-sections out to 60 degrees compared to 25 degrees for the Uppsala data. The disagreement is accentuated by our measurements at large angles, which show marked dissimilarity in shape and magnitude with the theoretical predictions. The theoretical calculations for an incident proton energy of 156 MeV are indicated by the broken line in figure 27. The conclusion is that the simple j-j coupling model is simply wrong for this spin-flip M1 transition. Similar results are obtained by Lee and McManus for the 15.1 MeV level, with the predicted cross-section being roughly three times higher than experiment. The disagreement in this case is resolved using a reduced B(M1) of 3.75 deduced from an intermediate coupling parameter $\xi = 6.0$ which has been derived from electron scattering data leading to the 15.1 MeV level (Kurath, 1964.)

Proton inelastic scattering at high energies can pick out $\Delta T = 0$ magnetic dipole collective excitations which are inaccessible in studies of radiative transitions or electron scattering. (Section 8.2) The DWIA framework should then be an excellent tool for establishing the intermediate coupling configuration wave functions for these levels, in particular the 12.7 MeV level in carbon.

6.6 THE STATES AT 14.1 MeV AND 16.1 MeV

The angular distribution for the 14.1 MeV level is nearly isotropic. This feature has also been observed in the 46 MeV inelastic scattering of protons. The level has either spin 2^+ (D. E. Alburger, 1965) or 4^+ (Petersen et al. and references therein). Recently Satchler (1967) has interpreted it as the 4^+ rotational state belonging to the ground state 0^+ --- 2^+ (4.43 MeV) band. He remarks that the energies closely correspond to the $I(I + 1)$ rule. The shape of the angular distribution (especially the isotropy for angles greater than 20 degrees) differs appreciably from the distributions for the known 2^+ levels at 4.43 MeV and 16.1 MeV. (Figure 20). Following Petersen this deviation serves as corroboratory evidence in favor of the 4^+ assignment

Satchler has studied the angular distribution for this level at 46 MeV, the only energy before the present work for which it was available. The state may be excited either by the $L = 4$ term in the generalized optical model (corresponding to a β_4 deformation),

Table 8

DIFFERENTIAL CROSS-SECTIONS FOR THE 14.1 MeV and 16.1 MeV LEVELS

C.M. Angle degrees	14.1 MeV Level $(d\sigma/d\Omega)_{c.m.}$ in mb/sr	16.1 MeV Level $(d\sigma/d\Omega)_{c.m.}$ in mb/sr
12.2	0.318 ± 0.126	0.593 ± 0.160
16.5	0.339 ± 0.104	0.615 ± 0.136
20.9	0.538 ± 0.077	0.827 ± 0.114
26.3	0.136 ± 0.031	0.374 ± 0.052
31.7	0.116 ± 0.018	0.350 ± 0.034
37.1	0.102 ± 0.016	0.233 ± 0.023
42.5	0.180 ± 0.026	0.145 ± 0.020
47.8	0.129 ± 0.019	0.090 ± 0.014
53.1	0.103 ± 0.015	0.062 ± 0.010
63.7	0.099 ± 0.014	0.031 ± 0.0063

or by double excitation via the 2^+ state at 4.43 MeV. As in the case of the 7.66 MeV state, a set of coupled channel equations must be solved coupling the 0^+ ground state to the 2^+ and 4^+ states. The angular distribution cannot be fitted by direct excitation alone and only marginal improvement is obtained by allowing a mixture of direct and multiple excitation. Figure 28 compares the 4^+ angular distribution we have measured in carbon and the s-d shell nuclei. Note the strong departure in shape from the p shell to the s-d shell as in the case of the 0^+ transitions. Unfortunately neither the Orsay nor Uppsala group extracted an angular distribution for this level. At 46 MeV the angular distribution shows a broad maximum peaking at approximately 35 degrees. This feature is not

observed in our work. The 4^+ angular distributions thus appear to be both energy and shell dependent. This observation is substantiated by a comparison in the next section of 4^+ angular distributions observed in the s-d nuclei at our energy and at 185 MeV (Figure 36.)

The angular distribution for the 16.1 MeV level 2^+, $T = 1$, is remarkably similar to the angular distribution for the 4.43 MeV, 2^+ , $T = 0$. Both cross-sections fall approximately a factor 30 over the angular region studied and the peak in the cross-sections appear at the same angle. As previously mentioned this behaviour is plausible because of the expected predominance of non-spin flip amplitudes over isotopic spin flip amplitudes in a 0^+--- 2^+ collective excitation. Petersen at 46 MeV has analysed the 16.1 MeV angular distribution using the collective optical model and obtained agreement in shape and magnitude (for $\beta_2 = 0.15$) as good as the predictions in the case of the 4.43 MeV and 9.64 MeV levels.

FIGURE 19

FIGURE 19

Typical energy spectrum of protons scattered from ^{12}C.

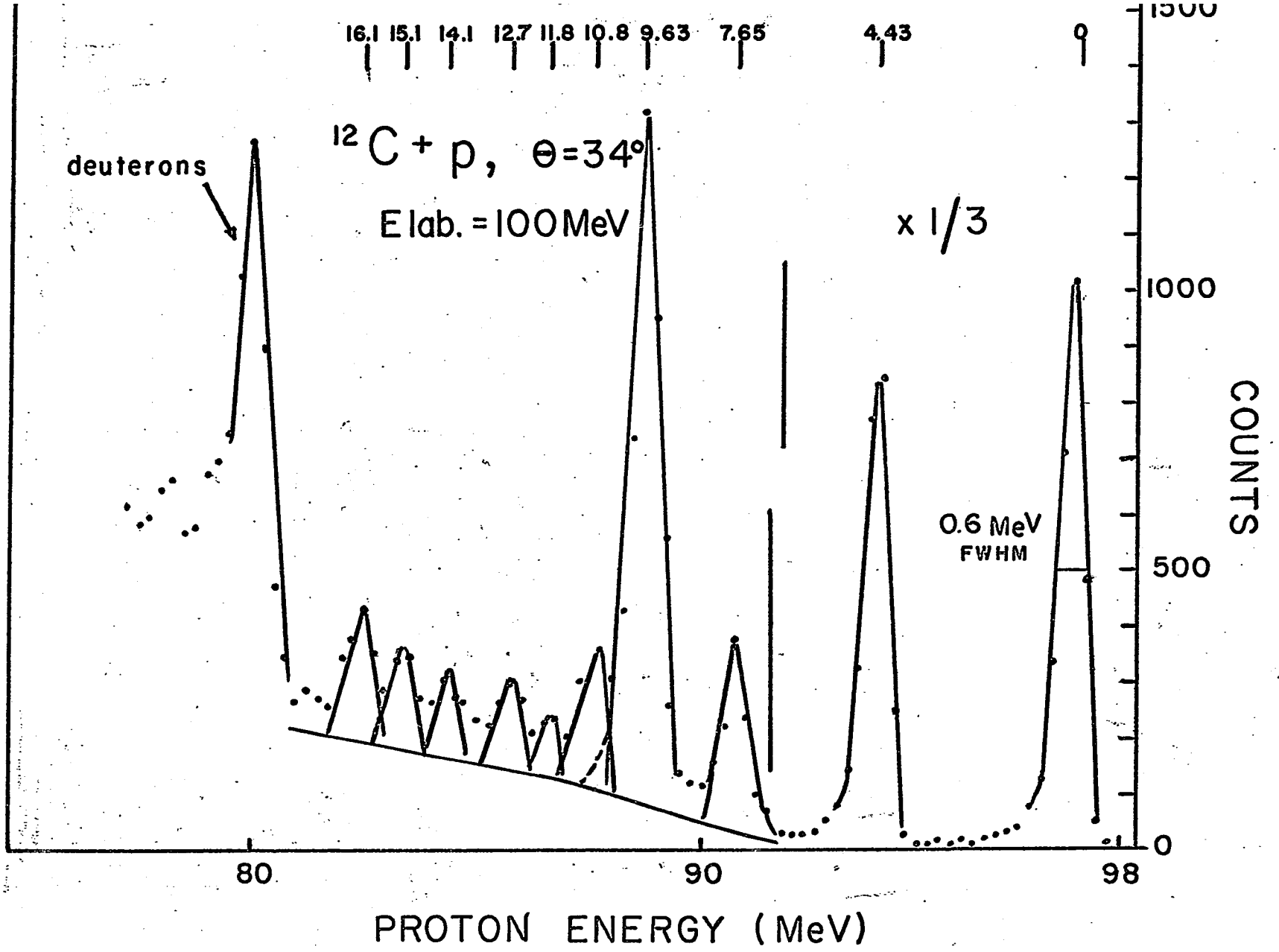
16.1 15.1 14.1 12.7 11.8 10.8 9.63 7.65 4.43 0
$^{12}C + p$, $\theta = 34°$
deuterons
Elab. = 100 MeV
x 1/3
0.6 MeV
FWHM
1500
1000
500
0
COUNTS
80
90
98
PROTON ENERGY (MeV)

FIGURE 20

FIGURE 20

Differential cross-section angular distributions for the 4.43 MeV, 16.1 MeV and 14.1 MeV states in ^{12}C. The 14.1 MeV state has J^{π} = 2+ or 4+. The error bars shown are for relative uncertainties. Note the very similar shapes of the two 2+ angular distributions.

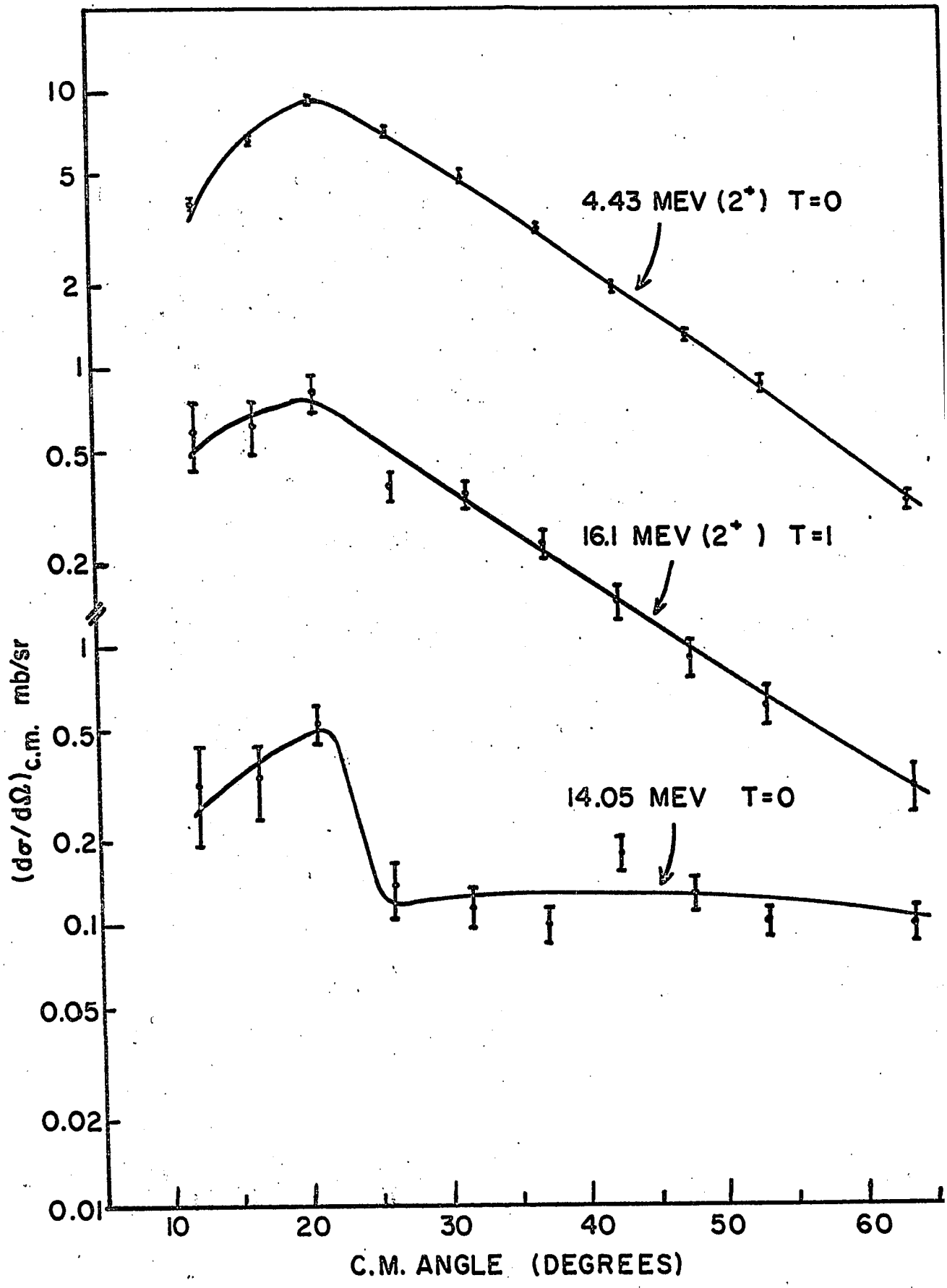
4.43 MEV (2+) T=0
16.1 MEV (2+) T=1
14.05 MEV T=0
(dσ/dΩ)c.m. mb/sr
C.M. ANGLE (DEGREES)
10
5
2
1
0.5
0.2
1
0.5
0.2
0.1
0.05
0.02
0.01
10
20
30
40
50
60

FIGURE 21

FIGURE 21

Differential cross-section angular distributions for $0^+ \text{ --- } 3^-$ transitions in the s-d and p shell nuclei. The error bars are shown for relative uncertainties. Note the similarity in shape of the angular distributions.

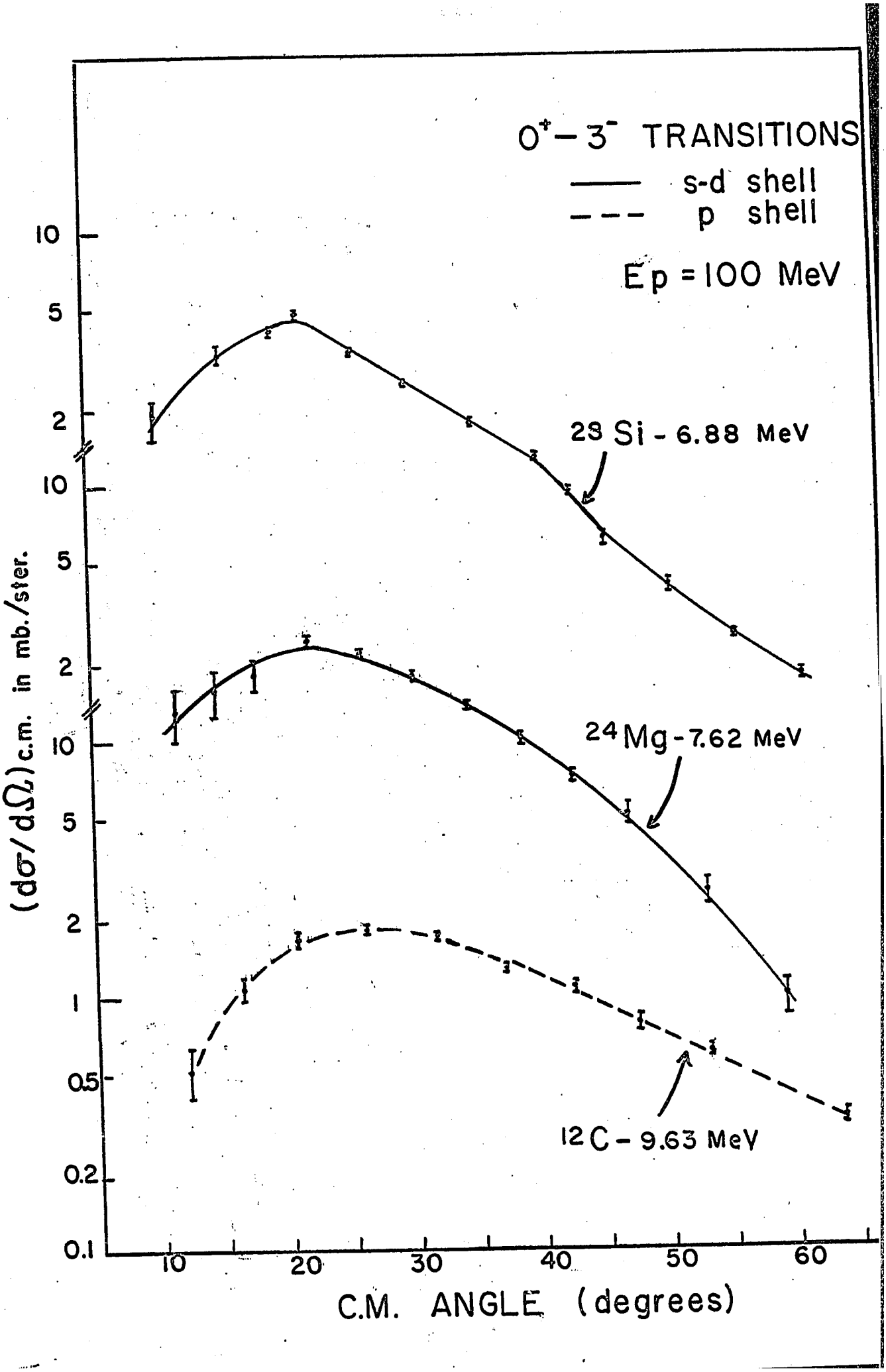
0+ – 3- TRANSITIONS
s-d shell
p shell
Ep = 100 MeV
28 Si - 6.88 MeV
24 Mg - 7.62 MeV
12 C - 9.63 MeV
(dσ/dΩ) c.m. in mb./ster.
C.M. ANGLE (degrees)
10
5
2
1
0.5
0.2
0.1
10
20
30
40
50
60

FIGURE 22

FIGURE 22

FIGURE 22

This figure shows the integrated cross-sections (10° -- 60°) for inelastic scattering leading to excited states in ^{12}C up to an excitation energy of 16.1 MeV.

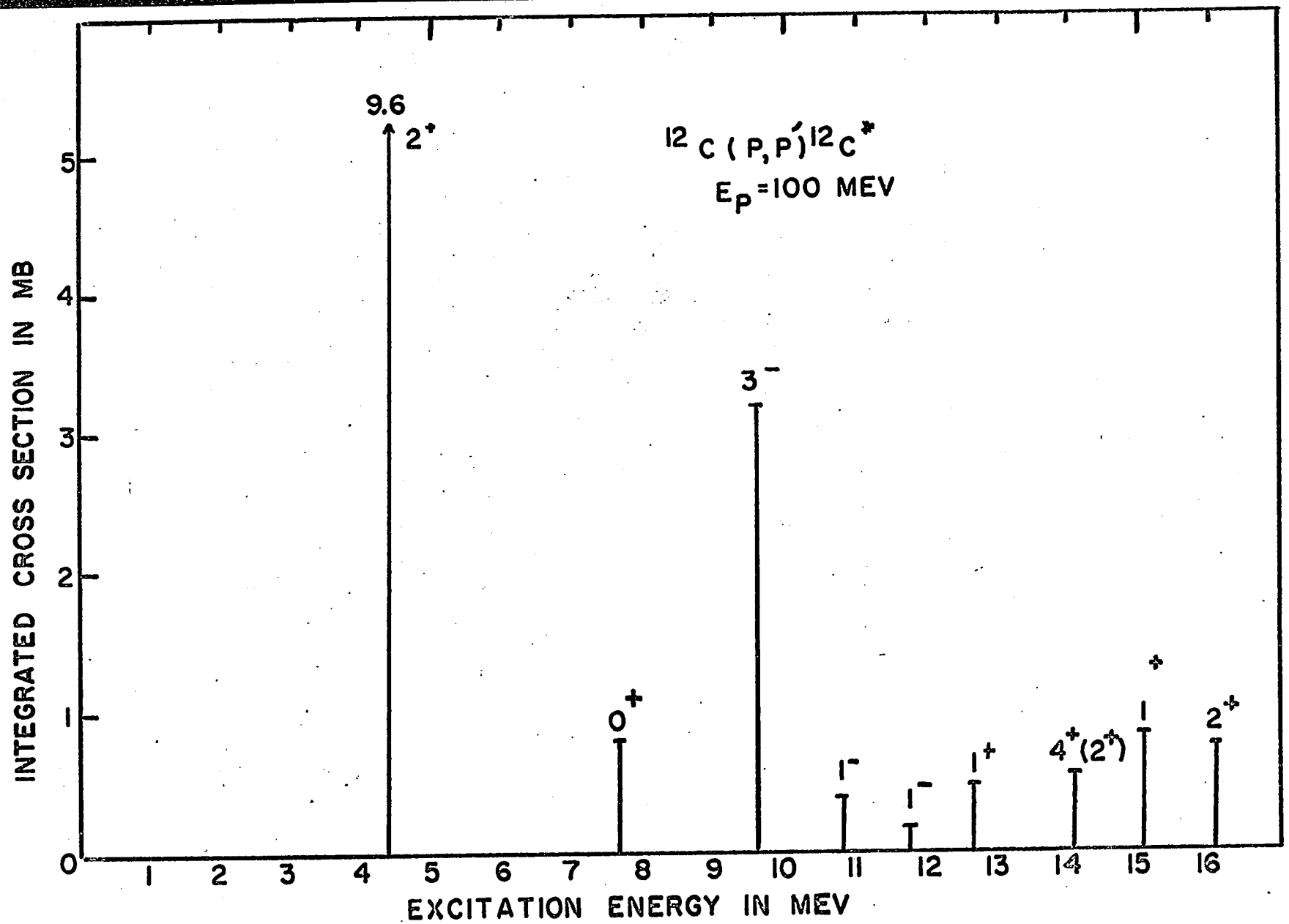
9.6
2+
12C(P,P')12C*
EP=100 MEV
3-
0+
1-
1-
1+
4+(2+)
1+
2+
INTEGRATED CROSS SECTION IN MB
EXCITATION ENERGY IN MEV
0
1
2
3
4
5
1
2
3
4
5
6
7
8
9
10
11
12
13
14
15
16

FIGURE 23

FIGURE 23

Differential cross-section angular distributions for 0+ --- 0+ transitions in the s-d shell and p shell nuclei. The error bars are shown for relative uncertainties. Note the strong dissimilarity in shape of the angular distributions in the two shells.

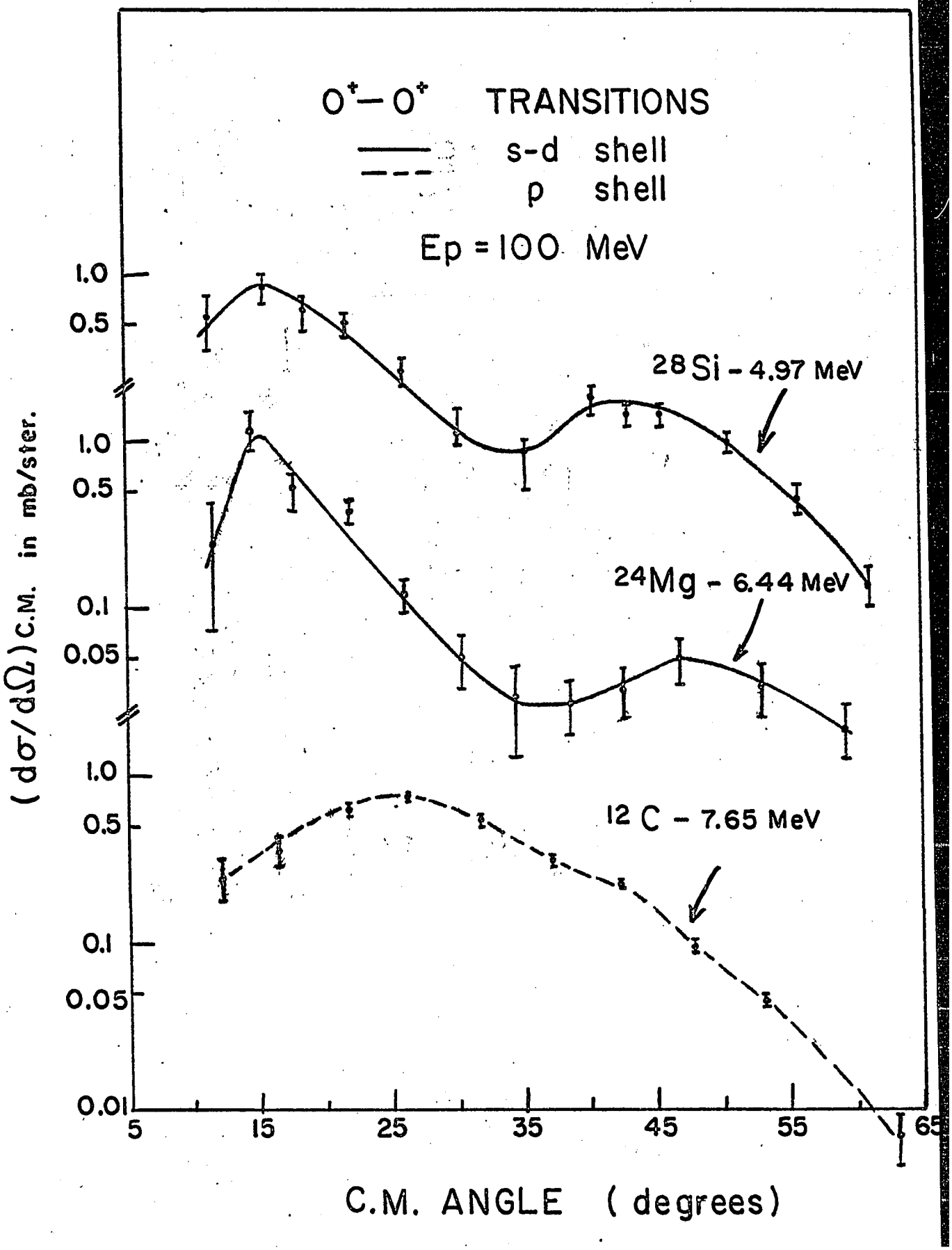
0+ — 0+ TRANSITIONS
s-d shell
p shell
Ep = 100 MeV
28Si - 4.97 MeV
24Mg - 6.44 MeV
12C - 7.65 MeV
(dσ/dΩ)C.M. in mb/ster.
1.0
0.5
0.1
0.05
0.01
5
15
25
35
45
55
65
C.M. ANGLE (degrees)

FIGURE 24

FIGURE 24

Differential Cross-Section angular distributions for 0+ - 2+ transitions in the s-d shell and p shell nuclei. The error bars are shown for relative uncertainties. Note the similarity in shape of the angular distributions.

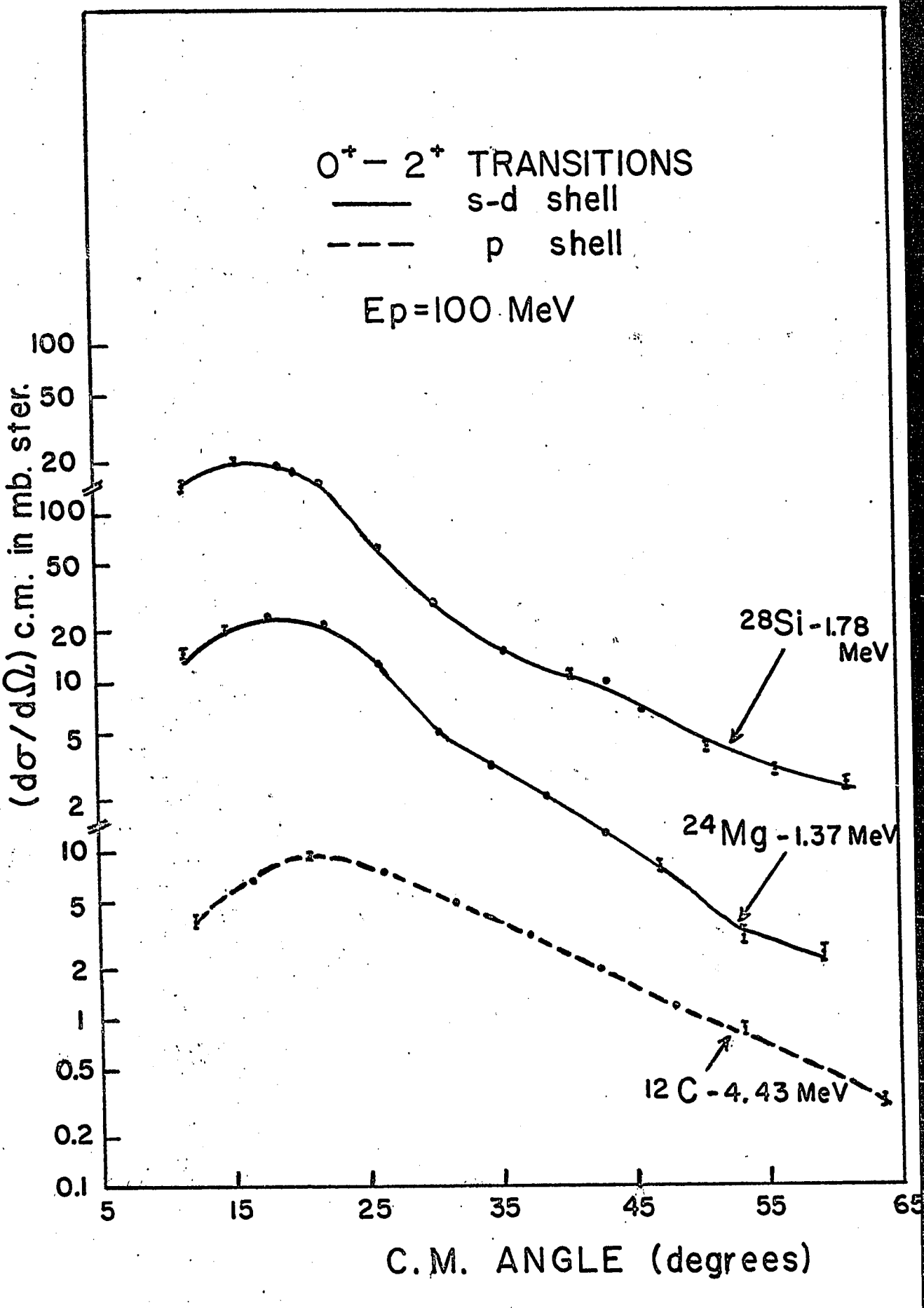
0+ – 2+ TRANSITIONS
s-d shell
p shell
Ep=100 MeV
(dσ/dΩ) c.m. in mb. ster.
100
50
20
100
50
20
10
5
2
10
5
2
1
0.5
0.2
0.1
28Si - 1.78 MeV
24Mg - 1.37 MeV
12C - 4.43 MeV
5
15
25
35
45
55
65
C.M. ANGLE (degrees)

FIGURE 25

FIGURE 25

Differential cross-section angular distributions for 0+ --- 0+ transitions measured at an incident proton energy of 185 MeV. The ^{12}C measurements were only carried out to a angle of 30° (lab). The Uppsala group has referred to all three angular distributions as "strikingly" similar. An observation which our measurements clearly refute.

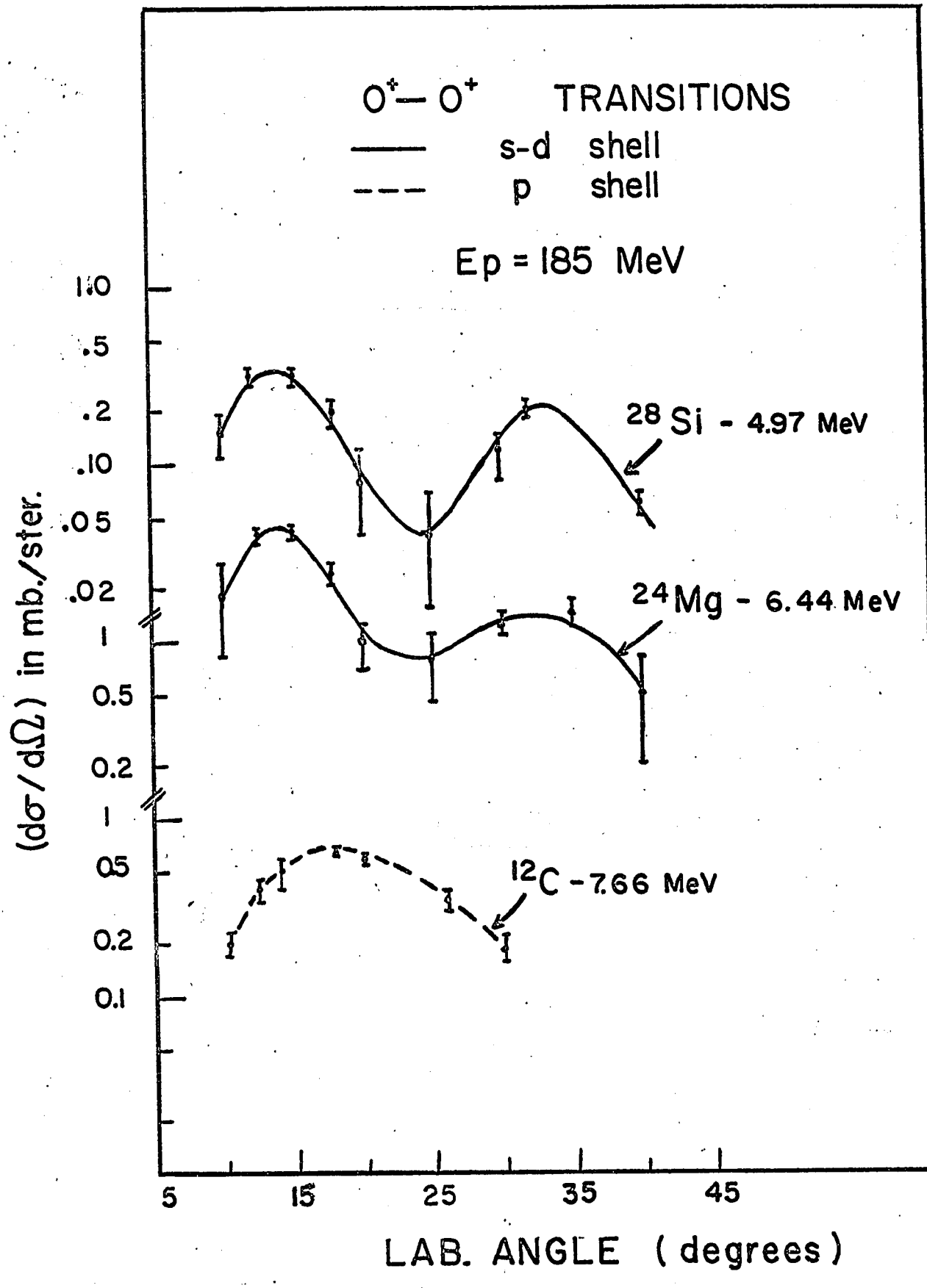
0+— 0+ TRANSITIONS
s-d shell
p shell
Ep = 185 MeV
28 Si - 4.97 MeV
24 Mg - 6.44 MeV
12 C - 7.66 MeV
(dσ/dΩ) in mb./ster.
1.0
.5
.2
.10
.05
.02
1
0.5
0.2
1
0.5
0.2
0.1
5
15
25
35
45
LAB. ANGLE (degrees)

FIGURE 26

FIGURE 26

Differential cross-section angular distributions for the 10.8 MeV and 11.8 MeV levels in ^{12}C. The error bars are shown for relative uncertainties.

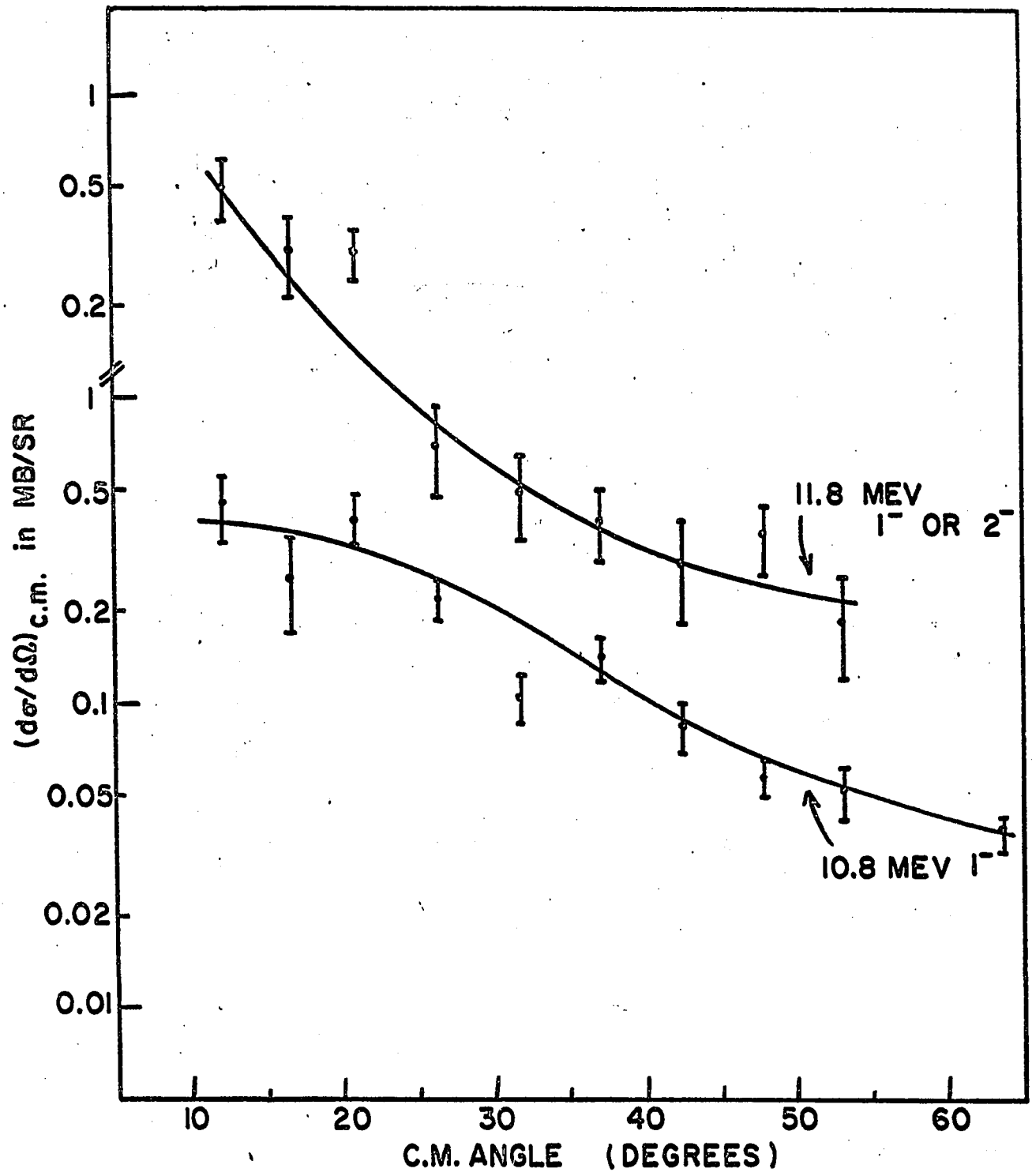
1
0.5
0.2
1
0.5
0.2
0.1
0.05
0.02
0.01
$(d\sigma/d\Omega)_{c.m.}$ in MB/SR
11.8 MEV
1⁻ OR 2⁻
10.8 MEV 1⁻
10
20
30
40
50
60
C.M. ANGLE (DEGREES)

FIGURE 27

FIGURE 27

Differential cross-section angular distributions for the 15.1 MeV and 12.7 MeV levels in ^{12}C. The error bars are shown for relative uncertainties. The dashed line represents the DWIA calculation of Lee and McManus (1967) for the 12.7 MeV level at an incident proton energy of 156 MeV.

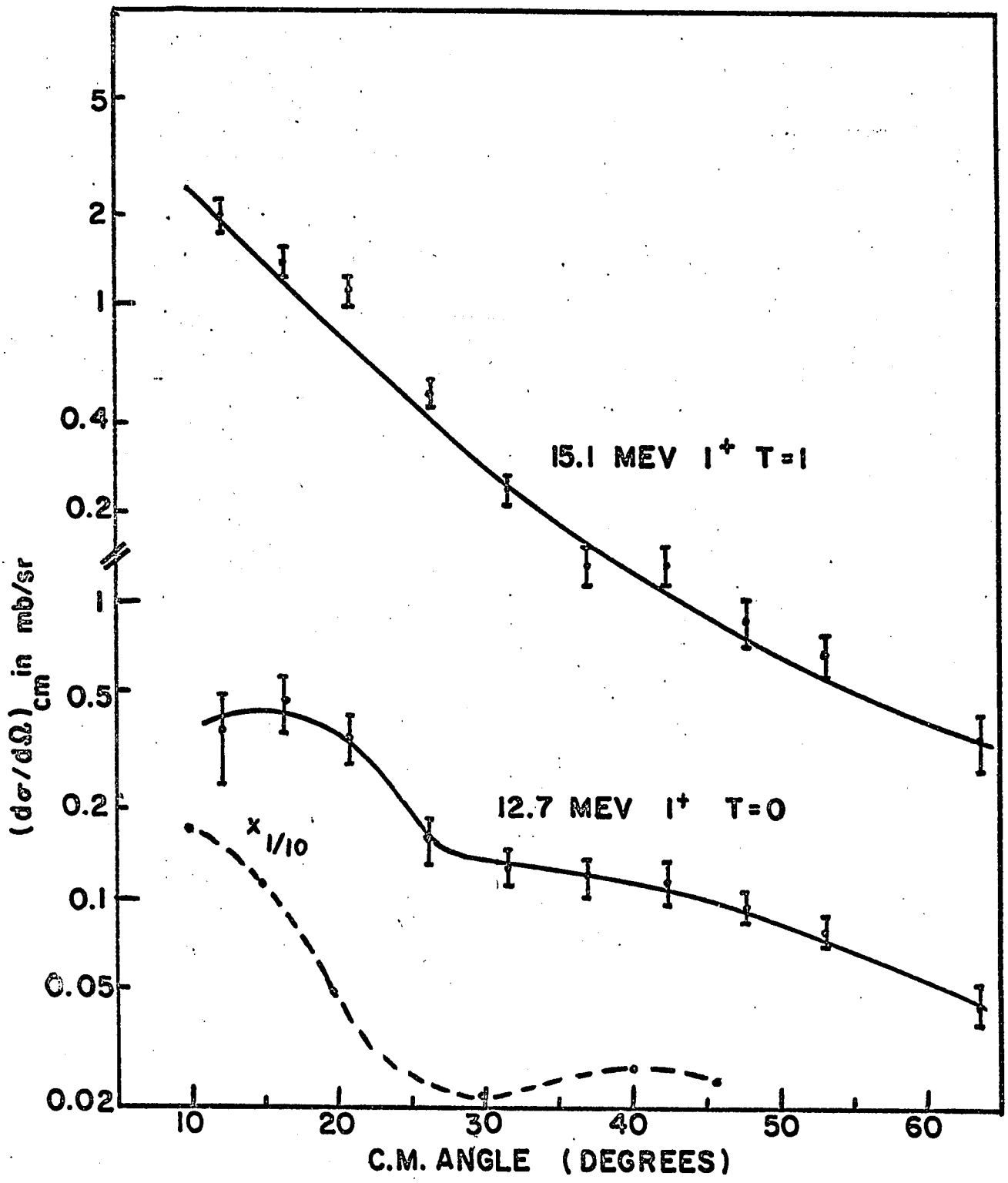
5
2
1
0.4
0.2
1
0.5
0.2
0.1
0.05
0.02
$(d\sigma/d\Omega)_{cm}$ in mb/sr
15.1 MEV 1^+ T=1
12.7 MEV 1^+ T=0
$\times 1/10$
10
20
30
40
50
60
C.M. ANGLE (DEGREES)

FIGURE 28

FIGURE 28

Differential cross-section angular distributions for 0+ --- 4+ transitions in the s-d shell and p shell nuclei. The error bars are shown for relative uncertainties. Note the dissimilarity in shape of the angular distributions in the two shells.

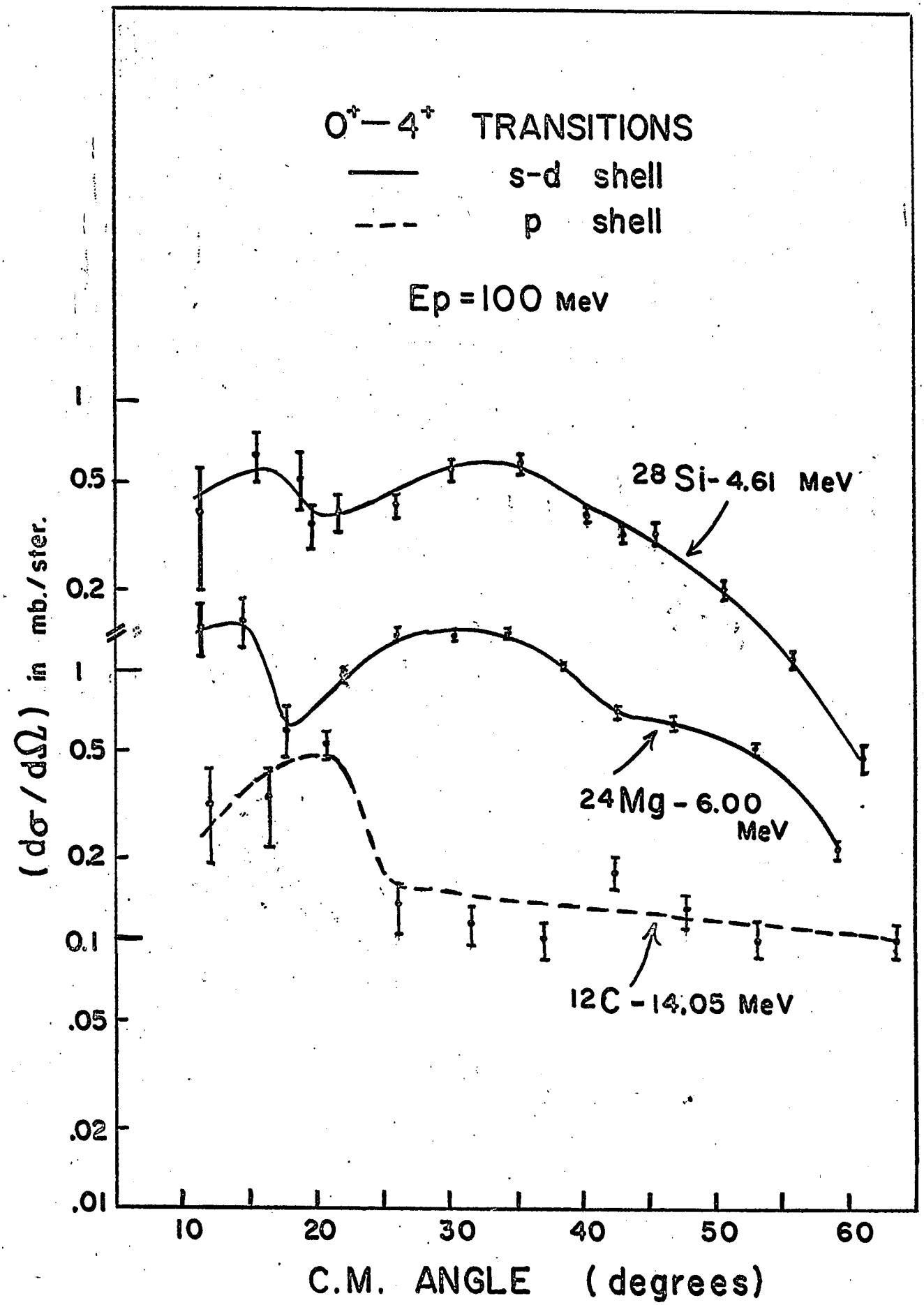
0+ — 4+ TRANSITIONS
s-d shell
p shell
Ep = 100 MeV
28 Si - 4.61 MeV
24 Mg - 6.00 MeV
12 C - 14.05 MeV
(dσ / dΩ) in mb./ster.
1
0.5
0.2
1
0.5
0.2
0.1
.05
.02
.01
10
20
30
40
50
60
C.M. ANGLE (degrees)

CHAPTER 7

7.1 ELASTIC AND INELASTIC SCATTERING FROM ^{24}Mg

^{24}Mg is considered to be a strongly deformed nucleus and many of its properties can be explained on the basis of collective motions. In particular the classic collective characteristic of considerably enhanced E2 transitions above the Weisskopf single-particle values indicates the existance of collective effects in ^{24}Mg, (S. W. Robinson, 1967). In addition the collective nature is indicated by a spin sequence and spacing of the low lying energy levels which follows the pattern of a rotational band built upon the ground state with K = 0 and another with its band head at 4.23 MeV having K = 2 (Cohen and Cookson, 1962). The low lying level scheme of ^{24}Mg illustrating the rotational aspects is illustrated in figure 29. The level scheme of ^{28}Si is included for comparison. The position and spins of the third and fourth excited states in ^{28}Si show no resemblance to the characteristic features of a K = 2 band and it has been suggested that the collective behavior in ^{24}Mg is more strongly developed than in ^{28}Si. The possible higher spin members of the two bands in ^{24}Mg have been studied by Almqvist and Keuhner (1965). Their results suggest but do not prove that levels at 8.12- and 13.2 MeV excitation are the 6+ and 8+ members of the ground state band and that levels at 8.81- and 9.52 MeV are

the 5+ and 6+ members of the K = 2 rotational band. These high spin states are difficult to populate in inelastic proton scattering and have not been observed in the present experiment.

The known collective properties of ^{24}Mg make it an interesting nucleus to study by means of proton inelastic scattering. The nuclear level density in ^{24}Mg is much greater than for ^{12}C so that considerable ambiguity exists in some cases in the identification and interpretation of proton peaks in the energy spectra especially in the energy region above 9 MeV. The interpretation is aided considerably by the fact that the cross-section for proton inelastic scattering exciting rotational levels is known to be large and expected to be larger than those for single-particle excitations. For example, it has been experimentally observed (T. Stovall, 1964) that states strongly excited via the nuclear force are also, in general, strongly excited by Coulomb excitation. This is strikingly illustrated by a comparison of our results at 100 MeV with the inelastic scattering of 42 MeV alpha particles from ^{24}Mg (I. M. Naquib and J. S. Blair, 1967). Figure 30 illustrates the energy level diagram of ^{24}Mg up to an excitation energy of 9.5 MeV. The levels labelled A ..... H are the ones which appeared to be excited in our work and correspond identically to the inelastic groups observed in the α scattering experiment. The α scattering results have been interpreted as evidence for a rotational-vibrational interpretation of the low lying levels in ^{24}Mg. In this model the 6.0 MeV level is the third member of the K = 2+ rotational band built on a γ quadrupole

vibration and the 6.44 MeV, 0+, is the first member of the K = 0+ rotational band built on a β quadrupole vibration. The authors suggest that the appearance of two strong 3^- excitations can also be accommodated in the rotational - vibrational model where the octupole strength will be distributed among 3^- levels from differing K bands.

We have observed 12 peaks in the energy spectra, 4 of them above an excitation energy of 9 MeV. The peaks observed in the proton spectra are listed in Table 9 together with distinguishing characteristics of the measured differential cross-section angular distributions and properties of the corresponding excited levels. The measurements were taken over an angular region from 10 degrees to 60 degrees with an average energy resolution of 400 keV. Figure 31 shows a typical spectrum of protons scattered from ^{24}Mg at a laboratory scattering angle of 29 degrees. Note the excellent separation of the proton peaks at 7.56 MeV and 8.35 MeV,only 790 keV apart. At this particular angle the 7.35 MeV, 2+, level does not appear to be excited and the 6.44 MeV, 0+ appears only as a small shoulder on the low energy side of the 6.00 MeV state. The separate contributions of the 4.12 MeV and 4.23 MeV levels to the observed proton group at 4.2 MeV excitation energy could, of course, not be resolved. For reasons discussed in section 7.2 we will argue that the main contribution to this peak comes from the 4.23 MeV, 2+, level. The energy region above 9 MeV is obviously quite complex and we have extracted angular distributions only for the proton peaks with an energy width comparable to the width

Table 9

EXPERIMENTAL RESULTS ON PEAKS OBSERVED IN THE ENERGY SPECTRA OF ^{24}Mg TOGETHER WITH PROPERTIES OF CORRESPONDING EXCITED LEVELS

Experimental Excitation Energy (MeV)	Listed Value (MeV)	Accepted Value J^{π}	Accepted Value T	Maximum. Diff. Cross-section $(d\sigma/d\Omega)_{c.m.}$ mb/sr	at angle degrees
1.4 ± 0.1	1.37	2+	0	2.39	17.9
4.2 ± 0.1	4.12	4+	0	2.19	17.9
	4.23	2+	0		
5.2 ± 0.2	5.23	3+	0	0.78	forward
6.0 ± 0.1	6.00	4+	0	1.54, 1.39	14.7, 34.5
6.4 ± 0.15	6.44	0+	0	1.20, 0.049	14.7, 47.0
7.3 ± 0.15	7.35	2+	0	1.68	forward
7.6 ± 0.1	7.56[1]	1^-	0	2.51	22.1
	7.62	3^-	0		
8.4 ± 0.1	8.36	3^-	0	2.53	22.1
	8.44	4^+	0		
	8.44	1^-	0		
9.3 ± 0.1	9.15	1^-		1.05	forward
	9.28	$= (-)^J$	0		
10.0 ± 0.15	---[2]	---	---	0.34	38.7
11.1 ± 0.15	---[2]	---	---	0.93	22.1
12.1 ± 0.2	---[2]	---	---	0.52	26.2

[1] Predominantly contributing level is underlined

[2] Several levels may contribute appreciably to the observed peak.

of the elastic peak. The Uppsala group at 185 MeV (S. Dahlgren, 1967) with energy resolution slightly superior to our own extracted angular distributions for five additional peaks between 12 and 16 MeV. However, the widths of these peaks are as much as two times the observed experimental energy resolution and clearly cannot be identified as due to the prominent contribution of any particular state in ^{24}Mg.

The differential cross-section angular distribution for the elastic scattering is shown in figure 32 and tabulated in table 10. The inelastic differential cross-section angular distributions are shown in figures 34 - 37 and tabulated along with the relative uncertainties for the differential cross-sections in tables 10, 11, 13, 14. The relative errors vary considerably depending on the excitation energy, scattering angle and the presence of nearby contributing levels. Typical relative errors are 3% - 10% for the 1.37 MeV state however errors as high as 25% - 30% were assigned to the 7.62 MeV level in the forward angle region because of the emergence of the 7.35 MeV peak. Similarly in the region of the minimum (30^{o} - 40^{o}) of the 6.44 MeV, 0+, errors as high as 50% - 70% were assigned because of the dominance of the 6.0 MeV peak in that angular range.

Proton inelastic scattering from ^{24}Mg has been investigated intensively at energies below 25 MeV however the data above this energy is quite sparse by comparison. Studies have been carried

out at 40 MeV (T. Stovall, 1964) with approximately 400 keV resolution: 50 MeV (A. Rush et al. , 1967) with 70 keV energy resolution: 55 MeV (J. Kokame et al., 1967) 110 keV resolution: 155 MeV (A. Willis et al. , 1968) 600 keV - 1000 keV energy resolution and 185 MeV (S. Dahlgren et al., 1967) with 350 keV resolution. The energy resolution of the Orsay group at 155 MeV is considerably inferior to the energy resolution of the Uppsala group and to the energy resolution we have achieved. The importance of good energy resolution in the study of these s-d nuclei is illustrated by the fact that the recently published results from Orsay include only inelastic scattering from the first excited state at 1.37 MeV.

Figure 33 shows the integrated cross-sections we have measured for inelastic proton scattering from ^{24}Mg. The total cross-section for scattering to the known rotational levels is ~ 25 millibarns or roughly 8% of the total reaction cross-section. This figure is somewhat higher than the 6% measured for ^{12}C which is not surprising in view of the strongly collective properties of ^{24}Mg.

7.2 THE PEAKS AT 1.37 MeV AND 4.2 MeV

The 1.37 MeV, 2+ state is clearly very strongly excited in the present work. The integrated cross-section of 15.6 mb represents almost 4% of the total reaction cross-section. At 185 MeV the integrated

cross-section is 9.2 mb or approximately 3% of the total reaction cross-section whereas at 55 MeV the corresponding figure is roughly 7% of the total reaction cross-section. In contrast to this rather strong difference in transition strength the observed shapes of the angular distributions at these three energies are very similar, characterized by a dominant peak in the forward angle region followed by a more or less monotonic decrease in differential cross-section with increasing angle. The angle at which the peak cross-section occurs is energy dependent and decreases with increasing energy. The peak angles for incident proton energies of 185 MeV, 100 MeV and 55 MeV occur at 13 degrees, 18 degrees and approximately 25 degrees respectively. As has been previously noted this characteristic E2 shape is also observed in ^{28}Si and in ^{12}C and is illustrated in figures 24 and 34.

The angular distribution obtained from inelastic proton scattering to the 1.37 MeV level has been theoretically analysed in the context of the DWBA generalized obtical model at only a few proton energies. At an incident proton energy of 17.5 MeV G.M. Crawley et al. , 1967, obtained a deformation parameter $\beta_2 = 0.52$ and at 40 MeV the same analysis yields $\beta_2 = 0.475$. These estimates of the deformation parameter are in excellent agreement with the value $\beta_2 = 0.508$ deduced frominelastic electron scattering, (R. Helm, 1956) or with the value $\beta_2 = 0.51$ obtained from electromagnetic measurements

(S. W. Robinson, 1967). A. Willis et al. , at 155 MeV have analysed the transition in the framework of the DWIA and have obtained excellent agreement in shape and magnitude with the measured E2 angular distribution.

The angular distribution corresponding to the excitation of the unresolved doublet at 4.2 MeV is shown in figure 34. The two states which contribute to this peak are 4.12 MeV (4+, K = 0) and the 4.21 MeV (2+, K = 2) levels. In the angular region from 10 degrees to 30 degrees the shape of the angular distribution is essentially identical to the shape of the E2 angular distribution observed for the 1.37 MeV level. At angles greater than 30 degrees the 4.2 MeV angular distribution does not decrease as rapidly as expected for a pure E2 transition and it is clear that the 4+ state may be contributing appreciably. The measured excitation energy of the peak, 4.24 ± 0.08 MeV, is much closer to the 4.21 MeV state and suggests a predominant contribution from the 2+ state. Because of the absence of any observed direct L = 4 multipole transition between the ^{24}Mg ground state and the 4.12 MeV state, this 4+ state would probably be excited by a double excitation mechanism through the first excited state. The excitation of the first excited state has a very large probability, as previously mentioned an integrated cross-section of 15.6 millibarns, so that if we suppose the double excitation process to be just a few per cent of this figure an integrated cross-section of roughly 0.3 mb is not unlikely for the 4.12 MeV level.

Table 10

DIFFERENTIAL CROSS-SECTIONS FOR ELASTIC SCATTERING AND THE 1.37- AND 4.2 MeV PEAKS

C.M. Angle degrees	Elastic Scattering $(d\sigma/d\Omega)_{c.m.}$ in mb/sr	1.37 MeV level $(d\sigma/d\Omega)_{c.m.}$ in mb/sr	4.2 MeV peak $(d\sigma/d\Omega)_{c.m.}$ in mb/sr
11.6	1065 ± 4	15.3 ± 0.9	1.53 ± 0.38
14.7	616 ± 4	21.0 ± 1.1	1.87 ± 0.34
17.9	304 ± 2	23.9 ± 0.6	2.19 ± 0.19
22.1	73.0 ± 0.5	22.6 ± 0.3	1.65 ± 0.10
26.2	13.6 ± 0.2	13.3 ± 0.2	1.02 ± 0.06
30.4	8.76 ± 0.17	4.92 ± 0.14	0.47 ± 0.045
34.5	8.62 ± 0.15	3.10 ± 0.09	0.174 ± 0.024
38.7	5.57 ± 0.10	2.07 ± 0.06	0.121 ± 0.016
42.8	2.51 ± 0.06	1.32 ± 0.04	0.131 ± 0.014
47.0	1.25 ± 0.05	0.795 ± 0.057	0.140 ± 0.016
53.2	0.672 ± 0.03	0.300 ± 0.025	0.101 ± 0.014
59.3	0.288 ± 0.017	0.254 ± 0.025	0.0655 ± 0.009

Thus the 4.12 MeV state could contribute approximately one-third of the integrated cross-section of the peak we observe at 4.2 MeV. Because of the similarity of the angular distribution to a characteristic E2 shape over the angular region from 10 degrees to 30 degrees it appears reasonable to suppose that the major part of the contribution from the 4.12 MeV level occurs for angles greater than 30 degrees.

The doublet has been resolved by Rush *et al.* at 49.5 MeV.

Their results more or less substantiate our conclusions. In the angular region from 10 - 40 degrees the 4.23 MeV state was excited several times more strongly than the 4.12 MeV state. Above 40 degrees the two levels were roughly equally excited. The experiment at 185 MeV was also not capable of resolving the two states however their results are very similar to ours. The angular distribution showed a characteristic E2 shape except for a slight levelling off at 35 - 40 degrees. Their measurements did not extend out beyond 40 degrees so their results are less indicative of some excitation of the 4.12 MeV state.

It thus seems very reasonable to assume that the 4.23 MeV, 2+, is excited several times more strongly than the 4.12 MeV, 4+: an upper limit for the excitation of the 4.12 MeV level would be 0.4 mb. This is quite a remarkable result because the nearby 4+, K = 2, level at 6.0 MeV is observed to be strongly excited with an integrated cross-section of 2.5 mb. The result is remarkable because it is a reasonable assumption that transitions within bands are inherently ten times more probable than those between bands, (Cohen and Cookson, 1961), thus our experimental result is roughly a factor 50 in disagreement with collective model predictions.

As pointed out previously, similar results have also been obtained by the Uppsala group who comment that since the states in question (4.12, 4+: 6.00, 4+) are of equal spin and parity distortion effects should be similar and the cross-section ratio should be

roughly equal to the square of the ratio between the electromagnetic matrix elements. Using the collective wave functions of Faessler et al. (1965), who take the rotation-vibration interaction into account very accurately, the calculated matrix elements (E4) strongly favour a transition within the ground state band as expected but in apparent strong disagreement with inelastic proton scattering experiments at 50 MeV, 185 MeV and our own energy. The disagreement may be eventually explained by the inclusion of single particle configurations in the ^{24}Mg wave functions as well as the obvious necessity of recognizing the double excitation character of these transitions.

7.3 The Peak at 5.2 MeV

The cross-section angular distribution for the peak at 5.2 MeV is shown in figure 35. The peak corresponds to the excitation of the 5.22 MeV, 3+, unnatural parity level. Because of the unnatural parity the level must be populated via a spin-flip mechanism so its cross-section is expected to be small, as observed. The importance of the spin-flip mechanism is illustrated by the complete dissimilarity of the angular distributions observed for 3+ and 3$^-$ states shown in figure 35, as well as the dissimilarity with the angular distributions observed for any other natural parity transitions. The 3+ angular distribution is strongly forward peaked as expected for a spin-flip transition (although probably accompanied by an angular momentum

transfer of 2 units). The 5.2 MeV peak has also been observed at 185 MeV, however the measured angular distribution levels off in the forward angle region. The Uppsala group used a natural magnesium target (78.7% ^{24}Mg, 10.13% ^{25}Mg, 11.17% ^{26}Mg) and both ^{25}Mg and ^{26}Mg have energy levels in the 5 MeV energy region that may contribute considerably. The angular distribution they extracted is therefore of rather dubious accuracy especially in view of the extremely weak excitation of the 5.2 MeV level in ^{24}Mg.

7.4 THE PEAKS AT 6.0 MeV AND 6.4 MeV

The angular distribution for the 6.00 MeV, 4+, level is shown in figure 28 along with two other 4+ transitions corresponding to the 4.61 MeV level in ^{28}Si and the 14.1 MeV level in ^{12}C. The two angular distributions for the s-d nuclei are very similar and are characterized by a broad maximum peaking at approximately 30 degrees with an additional maximum in the forward angle region. These results are in contrast to the Uppsala results at 185 MeV where the rise in the differential cross-section in the forward angle region was not observed. This dissimilarity for 4+ transitions is accentuated by the very similar results obtained for 2+ and 3$^-$ transitions at our energy and at 185 MeV. The 4+ angular distributions observed in the s-d nuclei at 100 MeV and 185 MeV are illustrated in figure 36. The apparent dependence of the shape of 4+ angular distributions on energy

and shell in contrast to the independence of the angular distribution shape on these factors for 2+ and 3^- transitions may, we believe, be due to the importance of multiple excitation processes in the population of the 4+ excited states. Only two DWBA analyses with collective form factors have been reported in the literature for 4+ transitions in these s-d nuclei, J. Kokame et al. at 55 MeV have reported that a preliminary DWBA calculation shows a dominant peak at about 40 degrees for 4+ transitions whereas the observed angular distribution for 4+ state in ^{28}Si at 4.6 MeV had two adjacent peaks at 15 and 40 degrees. It appears then that the 4+ angular distributions at 55 MeV, which strongly resemble our own measured angular distributions, cannot be fitted in a simple single excitation mechanism because of the rise of the cross-section in the forward angle region. This strongly supports our contention of the importance of second order excitation processes but before a definite conclusion can be reached coupled channel calculations must be performed to see whether these 4+ angular distributions can be predicted by including double excitation mechanisms. It remains to be explained why the transition at 185 MeV appears to be dominated by the single excitation mechanism. The introduction of anamalous features in (α, α') angular distributions by second order effects has been discussed by N. Austern et al. (1962) and also lends some support to the above ideas.

The angular distribution for the 0+ level at 6.44 MeV is shown in figure 23 along with two other 0+ transitions observed in

^{12}C and ^{28}Si. The angular distributions in ^{24}Mg and ^{28}Si are very similar and are characterized by a clear "oscillatory" pattern and deep minimum at the forward angles. In contrast with the 4+ angular distributions, no shape dependence of the angular distributions with energy is noted for the 0+ states - the same characteristic shape being also observed at 55 MeV and 185 MeV (table 11). The Uppsala 0+ angular distributions are illustrated in figure 25. In section 6.3 we advanced the possibility that the difference between the s-d shell and p shell 0+ angular distributions was also due to contributions from double excitation processes.

Table 11

PEAK ANGLES AND DIFFERENTIAL CROSS-SECTIONS FOR THE 2S-1d 0+ TRANSITIONS OBSERVED AT PROTON ENERGIES OF 185-, 100- AND 55 MeV

Proton Energy (MeV)	Peak Angles Degrees		Maximum ($d\sigma/d\Omega$) mb/sr	
	^{24}Mg	^{28}Si	^{24}Mg	^{28}Si
185	14.0 and 32	13.7 and 34	0.41 and 0.11	0.34 and 0.22
100	14.1 and 45	15.1 and 43	1.2 and 0.05	0.83 and 0.15
55	20 and 60	20 and 50	0.35 and 0.12	0.6 and 0.15

The 7.65 MeV 0+ transition in ^{12}C is known to be very poorly theoretically predicted in a single excitation mechanism however at 55 MeV the Tokyo group has reported that the 0+ transitions in ^{24}Mg and ^{28}Si can be explained by a DWBA analysis in which the 0+ state is created by direct two phonon excitation. This therefore supports

the explanation that the difference in shape of the 0+ angular distributions observed in ^{12}C and in the s-d nuclei is due to the importance of second order processes in the excitation of the 7.66 MeV 0+ state in ^{12}C.

7.5 THE PEAKS AT 7.35 MeV AND 7.60 MeV

The level structure of ^{24}Mg in this energy region is 7.35 MeV 2+, 7.56 MeV 1^-, 7.62 MeV 3^-, 7.75 MeV $\pi = (-)^{J+1}$ and 7.81 MeV $\pi = (-)^{J+1}$. It is reasonable to assume that the unnatural parity states are weakly excited or not excited at all, certainly no evidence for their excitation has been observed in the present work, or reported in the literature describing other (p,p') experiments. The 7.35 MeV shows a very anamalous angular distribution, very strongly forward peaked and eventually becoming impossible to resolve due to the presence of the large peak at 7.60 MeV.

At large angles the 7.35 MeV peak reappears (probably because the 7.60 MeV peak cross-section has dropped more than one order of magnitude). The angular distribution for the 7.35 MeV peak is shown in figure 34. It is obvious that there is some contribution to the 7.60 MeV peak from the 7.35 MeV peak over the angular region from 20 - 50 degrees. In this region the 7.60 MeV peak cross-section is approximately 1 - 2 mb so a contribution of the order of 0.1 mb would be difficult to detect. The measured 7.35 MeV 2+ angular

Table 12

DIFFERENTIAL CROSS-SECTIONS FOR THE 5.2-, 6.0 AND 6.4 MeV LEVELS

C.M. Angle degrees	5.22 MeV level $(d\sigma/d\Omega)_{c.m.}$ in mb/sr	6.0 MeV level $(d\sigma/d\Omega)_{c.m.}$ in mb/sr	6.4 MeV level $(d\sigma/d\Omega)_{c.m.}$ in mb/sr
11.6	0.780 ± 0.290	1.45 ± 0.35	0.249 ± 0.175
14.7	0.368 ± 0.212	1.54 ± 0.35	1.20 ± 0.33
17.9	0.395 ± 0.115	0.596 ± 0.142	0.534 ± 0.142
22.1	0.0705 ± 0.0285	0.974 ± 0.085	0.385 ± 0.069
26.2	0.0466 ± 0.0186	1.38 ± 0.073	0.130 ± 0.030
30.4	0.0606 ± 0.0266	1.35 ± 0.07	0.051 ± 0.0194
34.5	0.0526 ± 0.0155	1.39 ± 0.06	0.0315 ± 0.0162
38.7	0.0244 ± 0.0083	1.06 ± 0.04	0.0178 ± 0.0107
42.8	0.0300 ± 0.0076	0.733 ± 0.033	0.0231 ± 0.0094
47.0	0.0127 ± 0.059	0.648 ± 0.040	0.0490 ± 0.0145
53.2	-------	0.521 ± 0.036	0.0338 ± 0.0095
59.3	-------	0.220 ± 0.019	0.0181 ± 0.0066

distribution is completely uncharacteristic of an E2 transition. The Uppsala group observed this peak at 12.5 degrees with a 0.5 ± 0.1 mb/sr cross-section , i.e., roughly four times more weakly excited than in the present experiment. This satisfactorily explains why we were able to follow the peak out to 22 degrees. The 185 MeV data extends out only to 40 degrees so that the reappearance of the 7.35 MeV peak at large angles could not be observed. The 7.35 MeV level has also been observed to be strongly excited in (α, α') scattering at

42 MeV (I. M. Naquib, 1967). The transition appeared to be single excitation in character consistent with the assumption that this state is the second member of the β-vibrational band commencing with the 0+ state at 6.44 MeV.

Table 13

DIFFERENTIAL CROSS-SECTIONS FOR THE 7.35-, 7.60 AND 8.4 MeV PEAKS

C.M. Angle degrees	7.35 MeV level $(d\sigma/d\Omega)^{c.m.}$ in mb/sr	7.60 MeV Peak $(d\sigma/d\Omega)^{c.m.}$ in mb/sr	8.4 MeV Peak $(d\sigma/d\Omega)^{c.m.}$ in mb/sr
11.6	1.68 ± 0.36	1.32 ± 0.34	1.69 ± 0.34
14.7	1.86 ± 0.36	1.61 ± 0.35	2.07 ± 0.36
17.9	0.367 ± 0.151	1.79 ± 0.22	2.04 ± 0.23
22.1	0.0785 ± 0.0628	2.51 ± 0.13	2.53 ± 0.14
26.2	-------	2.18 ± 0.09	2.06 ± 0.09
30.4	-------	1.75 ± 0.08	1.49 ± 0.08
34.5	-------	1.34 ± 0.07	0.759 ± 0.053
38.7	-------	1.01 ± 0.05	0.375 ± 0.031
42.8	-------	0.709 ± 0.035	0.187 ± 0.020
47.0	-------	0.522 ± 0.034	0.135 ± 0.020
53.2	0.107 ± 0.019	0.252 ± 0.026	0.0623 ± 0.0121
59.3	0.0551 ± 0.0131	0.0962 ± 0.016	0.0630 ± 0.0099

The peak at 7.6 MeV could obviously be composed of contributions from both the 7.56 MeV 1^- and 7.62 MeV 3^- levels. The angular distribution for this peak is shown in figures 21 and 35 and clearly resembles a characteristic E3 transition. O. Sundberg et al., 1967,

have commented however, that the angular distribution for protons exciting a 1^-, T = 0 state is expected to be very similar to that for an E3 transition so that one should not be able to distinguish between the angular distributions for the excitation of 1^- and 3^- states (T =0). This statement, however, appears to be in contradiction to our results in ^{12}C in which the angular distribution corresponding to the excitation of the 10.8 MeV, 1^- state shows features quite different from the 3^- angular distributions we have measured. This observation coupled with the traditionally weak excitation of 1^- states in proton inelastic scattering[1] suggests that the major contribution to the observed peak at 7.60 MeV comes from the 7.62 MeV 3^- level. For example, G. W. Crawley et al., 1967, in 17.5 MeV proton scattering with energy resolution of 50 keV compared to the 60 keV separation of the two states in question did not observe any appreciable excitation of the 1^- state. At higher energies the Tokyo group at 55 MeV with 110 keV resolution have also not reported any excitation of the 7.56 MeV state.

Very few theoretical analyses have been performed for the 7.62 MeV 3^- transition. G. W. Crawley using DWBA with collective

---

[1] The collective electric dipole states (i.e., the giant dipole resonance are, in contrast to collective electric quadrupole and octupole states, at high excitation energies so that low-lying 1^- states are not expected to be strongly excited.

form factors obtained a value for β_3 of 0.29 in excellent agreement with β_3 = 0.28 obtained from electromagnetic measurements (T. K. Alexander et al., 1966).

7.6 THE PEAK AT 8.4 MeV

There are three states in ^{24}Mg which could contribute to this peak, the 8,36 MeV 3^-, and a doublet at 8.44 MeV with spin and parity 1^- and 4+. Any appreciable excitation of the 8.65 MeV 2+ state is rather unlikely since it would have been observed as a broadening or shoulder assymetry of the 8.4 MeV peak. The angular distribution for the peak is shown in figure 35 and again appears to be characteristic of an E3 transition. The angular distribution falls off faster with increasing angle than the angular distribution for the peak at 7.6 MeV which suggests rather minimal contribution from the 8.44 MeV 4+ state which would be expected to broaden the distribution rather than narrow it as observed. This conclusion is supported by the fact that the Tokyo group at 55 MeV have not reported any excitation of the 8.44 MeV states although their energy resolution of 110 keV would be sufficient to observe any appreciable contribution from the excitation of these levels. On the other hand the 8.44 MeV state is excited in the 17.5 MeV scattering of protons (G. W. Crawley, 1967).

The observed narrowness of the angular distribution could

also be interpreted to mean that the 7.6 MeV angular distribution is not the result of a pure E3 transition with the breadth of the distribution being an effect of appreciable excitation of the 1^- state at large angles. Very similar results to ours have been observed at 185 MeV including the observed differend widths of the two E3 distributions. Obviously some excitation of the $4+$ and 1^- states cannot be ruled out however it is clear that the dominant contribution to these angular distributions comes from the 3^- states at 7.62 MeV and 8.36 MeV.

A DWBA analysis with collective form factors has been carried out for the 8.4 MeV 3^- transition at 55 MeV and 17.5 MeV. Good fits were obtained to the angular distributions at both these energies. The group at 17.5 MeV report a value of $\beta_3 = 0.21$ in good agreement with the results reported by Naquib et al. , 1967, who report a deformation distance of 0.92 which reduces to the value $\beta_3 = 0.26$ for the deformation parameter.

Peaks with Excitation Energy Greater than 9 MeV

The level spectrum in ^{24}Mg becomes extremely dense in this energy region and we obviously can make to substantial claims concerning the unforlding of the spectra into peaks corresponding to the excitation of individual levels. Four peaks were observed at 9.3-, 10.0-, 11.1- and 12.0 MeV which remained at the same excitation energy over the angular region investigated. The angular distribution for the peak at 9.3 MeV is shown in figure 34 and obviously does not

correspond to any transition of characteristic shape. Hird et al. (1964) have suggested that the state at 9.28 MeV is most likely a doublet with both members having natural parity. The angular distribution resembles quite closely the uncharacteristic 7.35 MeV 2+ angular distribution and it is therefore possible that one of the members of the doublet is 2+.

The angular distributions for the peaks at 10.0-, 11.1- and 12.0 MeV are shown in figure 37. The peak at 11.1 MeV shows an angular distribution reasonably similar to that for a 3^- transition. P. M. Endt and C. Van der Leun (1967) list a level in ^{24}Mg at 11.165 MeV with spin and parity 1^- or 3^- which is probably the level contributing most strongly to the measured angular distribution. The Uppsala group at 185 MeV observe a similar angular distribution at the same excitation energy and also note the resemblance to an E3 transition. The peaks 10.0 MeV and 12.0 MeV show uncharacteristic angular distributions and the large angle tails indicate that several levels are contributing to the observed peak. The Uppsala group also observed peaks at these excitation energies however the angular distribution for the 10.0 MeV peak resembled a 3^- angular distribution. The Uppsala group has observed three cases of forward peaked angular distributions corresponding to M1 transitions at 10.69-, 12.71- and 13.5 MeV. Peaks at similar excitation energies have been observed in this work in the forward angle region however the widths of the peaks indicated a complex composite structure for which it did not seem worthwhile to extract the differential cross-sections.

Leaf 140 omitted in page numbering.

Table 14

DIFFERENTIAL CROSS-SECTIONS FOR THE 9.3-, 10.0-, 11.1- AND 12.0 MeV PEAKS

C.M. Angle degrees	9.3 MeV Peak $(d\sigma/d\Omega)_{c.m.}$ mb/sr	10.0 MeV Peak $(d\sigma/d\Omega)_{c.m.}$ mb/sr	11.1 MeV Peak $(d\sigma/d\Omega)_{c.m.}$ mb/sr	12.0 MeV Peak $(d\sigma/d\Omega)_{c.m.}$ mb/sr
11.6	1.05 ± 0.28	-------	-------	-------
14.7	0.754 ± 0.236	-------	-------	-------
17.9	0.296 ± 0.128	-------	0.834 ± 0.197	-------
22.1	0.218 ± 0.064	-------	0.927 ± 0.112	0.168 ± 0.068
26.2	0.103 ± 0.037	0.145 ± 0.045	0.844 ± 0.77	0.517 ± 0.065
30.4	0.193 ± 0.029	0.284 ± 0.046	0.793 ± 0.064	0.309 ± 0.056
34.5	0.183 ± 0.031	0.334 ± 0.041	0.557 ± 0.051	0.312 ± 0.044
38.7	0.199 ± 0.024	0.341 ± 0.033	0.497 ± 0.038	0.251 ± 0.033
42.8	0.163 ± 0.024	0.300 ± 0.028	0.297 ± 0.028	0.195 ± 0.026
47.0	0.149 ± 0.020	0.262 ± 0.026	0.241 ± 0.027	0.125 ± 0.023
53.2	0.110 ± 0.017	0.263 ± 0.021	0.182 ± 0.021	0.145 ± 0.018
59.3	-------	-------	0.0737 ± 0.0142	0.129 ± 0.015

FIGURE 29

FIGURE 29

Low lying energy level diagram for ^{24}Mg and ^{28}Si.

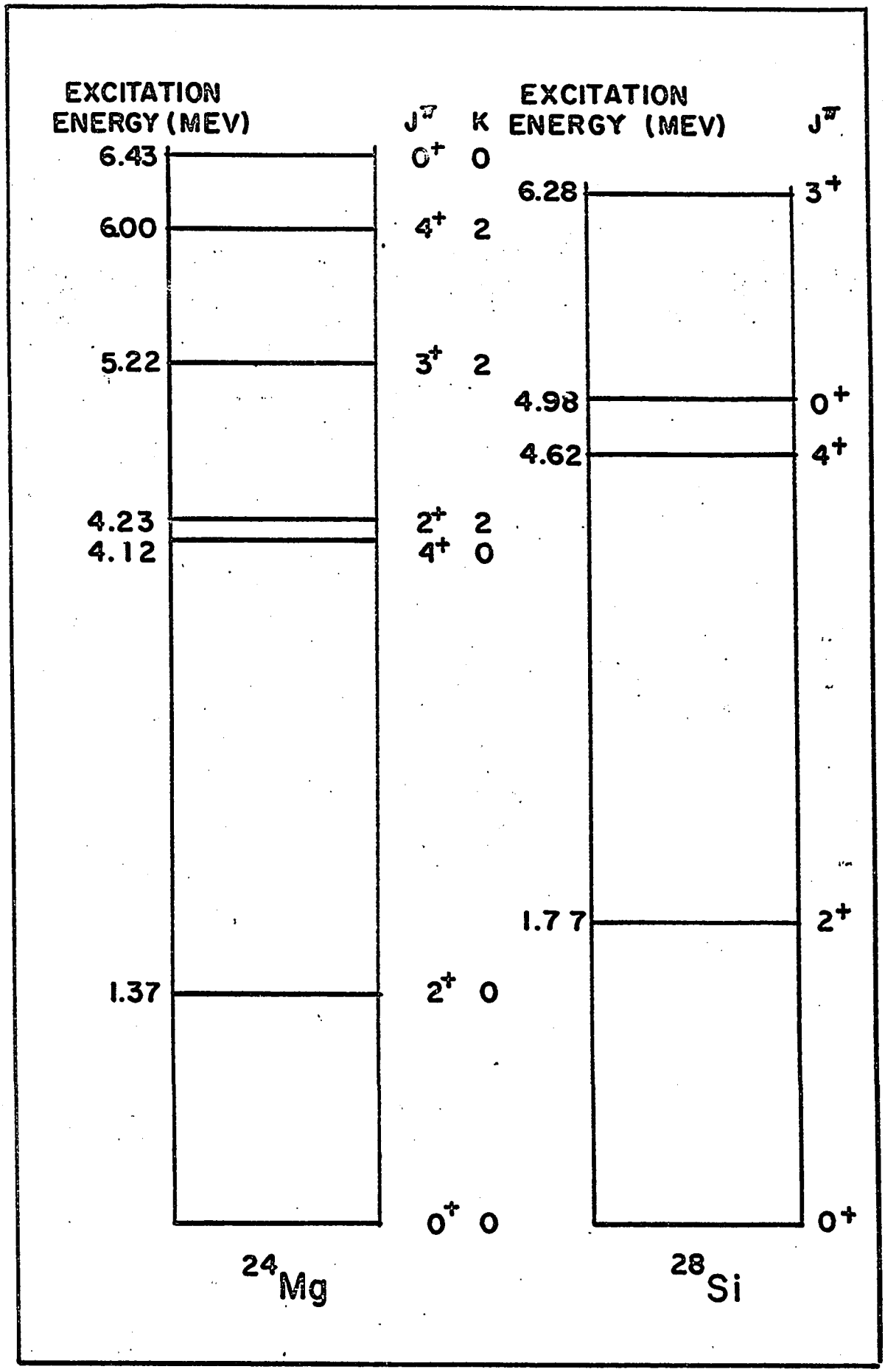
EXCITATION ENERGY (MEV)
J^π
K
6.43
0^+
0
6.00
4^+
2
5.22
3^+
2
4.23
2^+
2
4.12
4^+
0
1.37
2^+
0
0^+
0
^{24}Mg
EXCITATION ENERGY (MEV)
J^π
6.28
3^+
4.98
0^+
4.62
4^+
1.77
2^+
0^+
^{28}Si

FIGURE 30

FIGURE 30

Energy level diagram for ^{24}Mg up to an excitation energy of 9.5 MeV. Excitation energies, spins and parities are from Endt and Van der Leun (1967). The levels labelled A.....H are the ones apparently excited in the present work and also in alpha inelastic scattering at 42 MeV (Naquib and Blair, 1967).

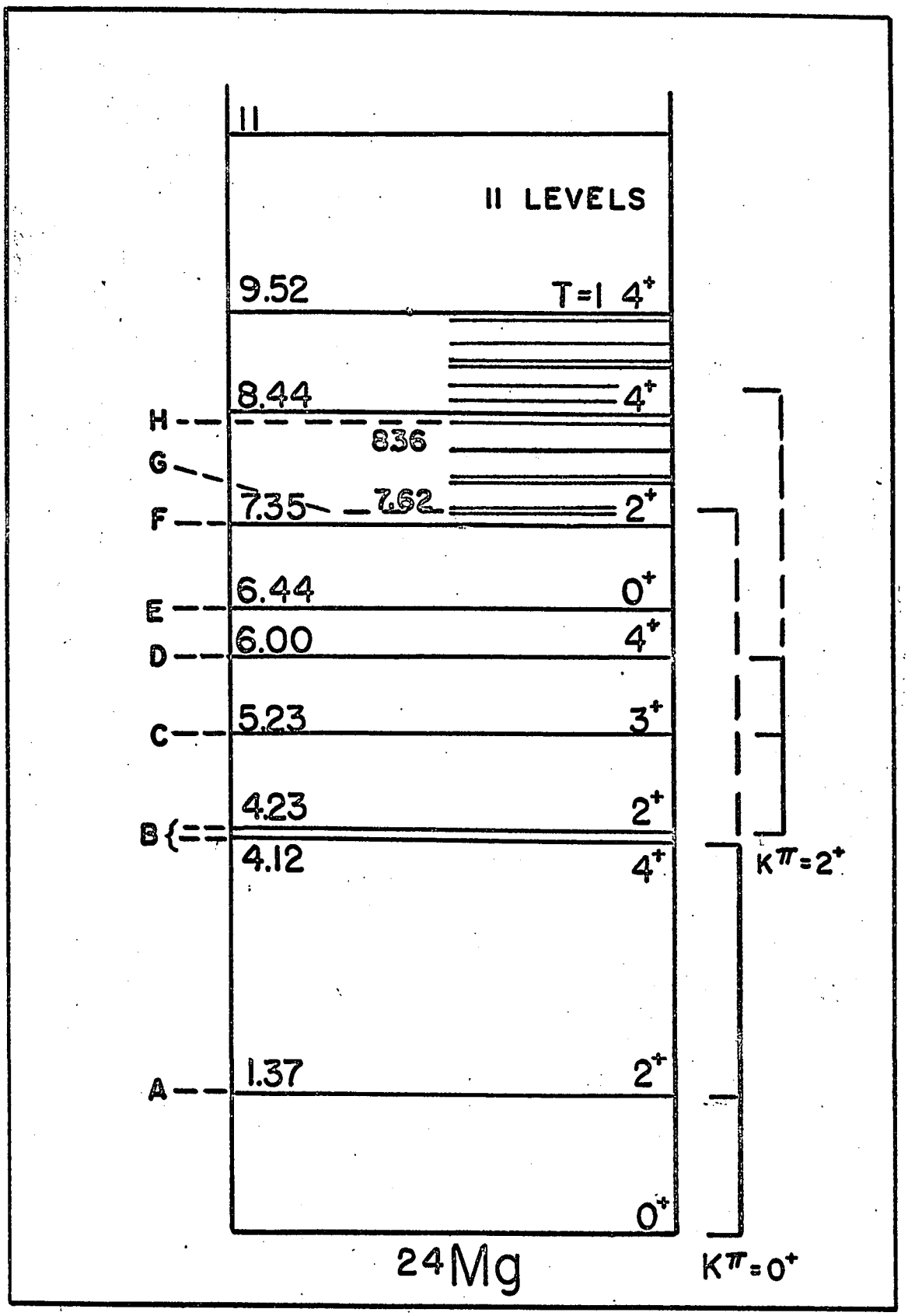
11
11 LEVELS
9.52
T=1 4+
8.44
4+
H
836
G
7.35
7.62
2+
F
6.44
0+
E
6.00
4+
D
5.23
3+
C
4.23
2+
B
4.12
4+
Kπ=2+
1.37
2+
A
0+
24Mg
Kπ=0+

FIGURE 31

FIGURE 31

Typical energy spectrum of protons scattered from ^{24}Mg. Note the dominance of the deuteron peak at high excitation energies where separation of proton peaks has become impossible due to the high nuclear level density.

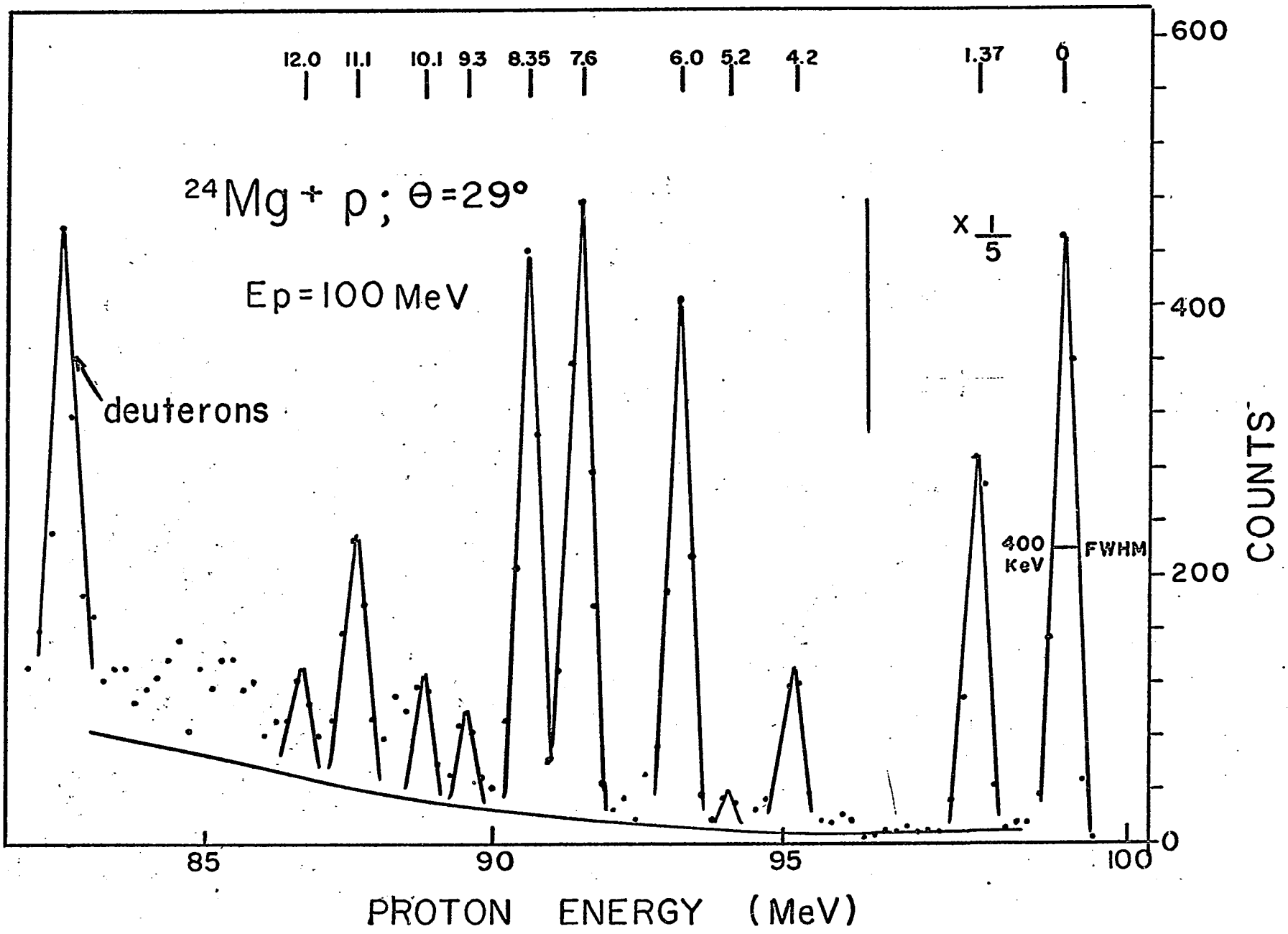
12.0
11.1
10.1
9.3
8.35
7.6
6.0
5.2
4.2
1.37
0
$^{24}Mg + p$; $\theta = 29°$
Ep = 100 MeV
X 1/5
deuterons
400 KeV FWHM
600
400
200
0
COUNTS
85
90
95
100
PROTON ENERGY (MeV)

FIGURE 32

FIGURE 32

Differential cross-section angular distribution for protons elastically scattered from ^{24}Mg.

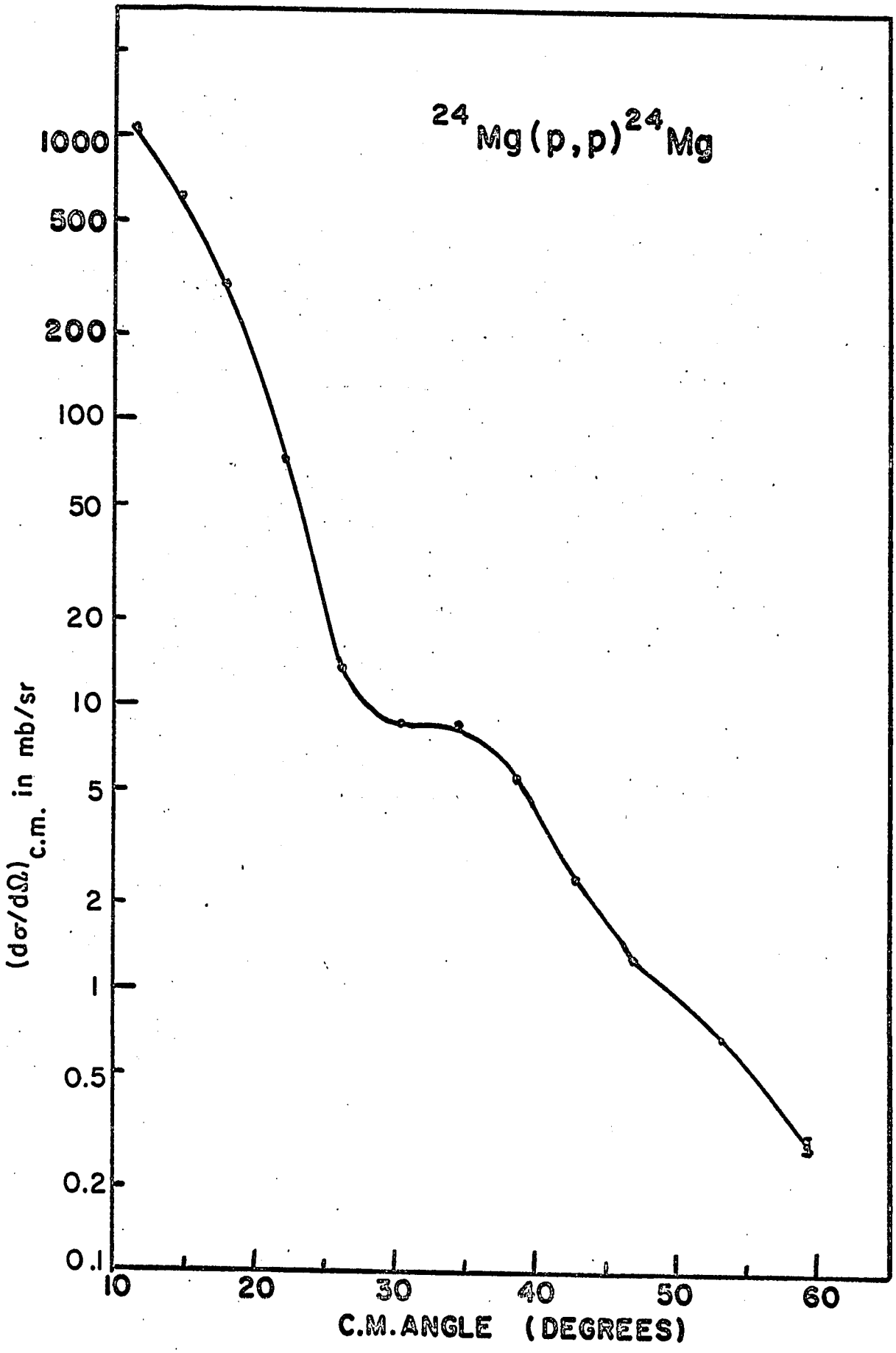
$^{24}Mg(p,p)^{24}Mg$
1000
500
200
100
50
20
10
5
2
1
0.5
0.2
0.1
$(d\sigma/d\Omega)_{c.m.}$ in mb/sr
10
20
30
40
50
60
C.M. ANGLE (DEGREES)

FIGURE 33

FIGURE 33

This figure shows the integrated cross-sections (10° - 60°) for inelastic scattering leading to excited states in ^{24}Mg up to an excitation energy of 12 MeV. Wherever identification with a particular excited state is possible the corresponding spin and parity are indicated.

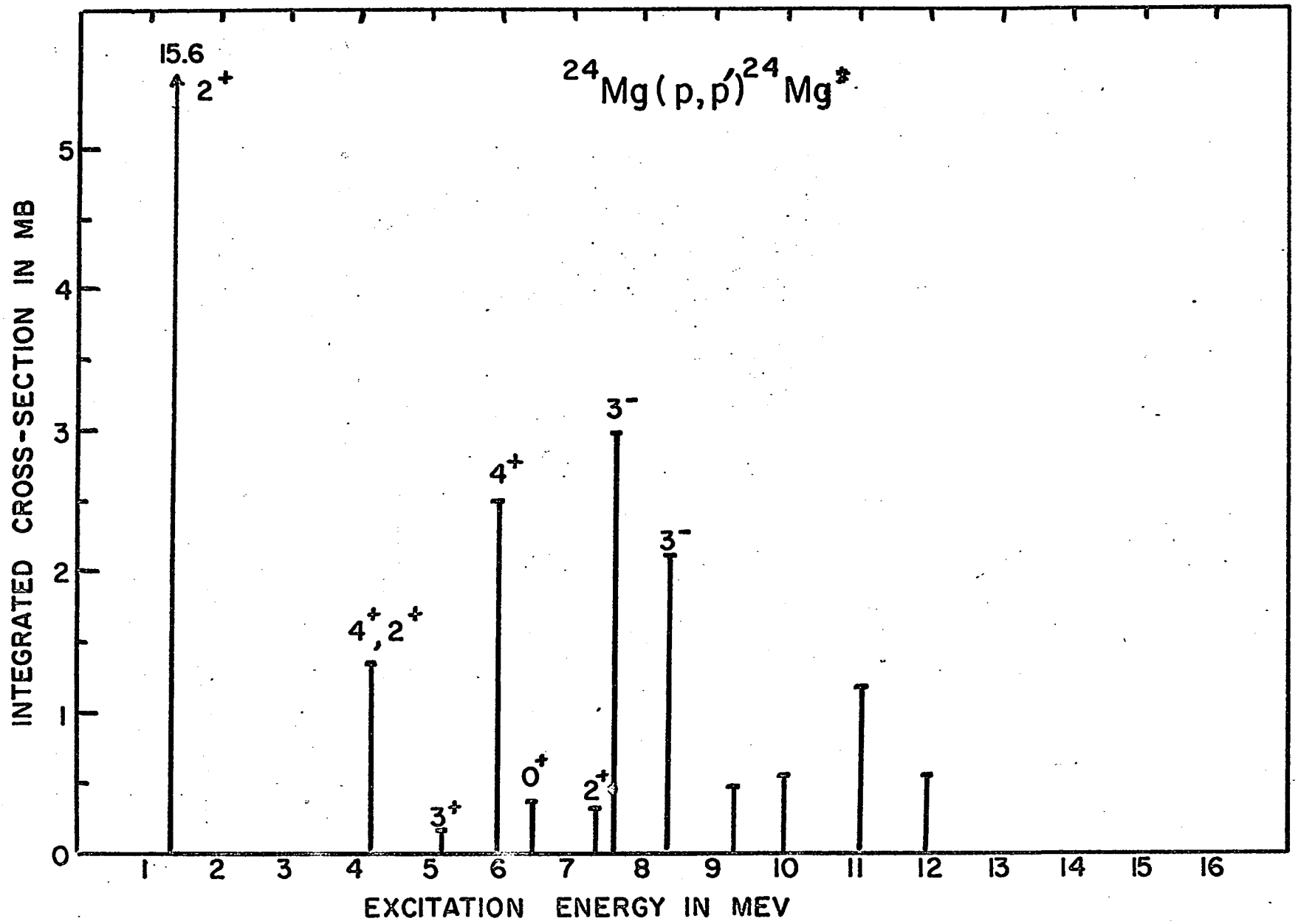
$^{24}Mg(p,p')^{24}Mg^*$
15.6
2+
4+, 2+
3+
4+
0+
2+
3-
3-
INTEGRATED CROSS-SECTION IN MB
EXCITATION ENERGY IN MEV
0
1
2
3
4
5
1
2
3
4
5
6
7
8
9
10
11
12
13
14
15
16

FIGURE 34

FIGURE 34

Differential cross-section angular distribution for the 1.37 MeV, 4.2 MeV, 7.35 MeV and 9.3 MeV peaks in ^{24}Mg. Note the re-emergence of the 7.35 MeV peak at large angles. The error bars are shown for relative uncertainties.

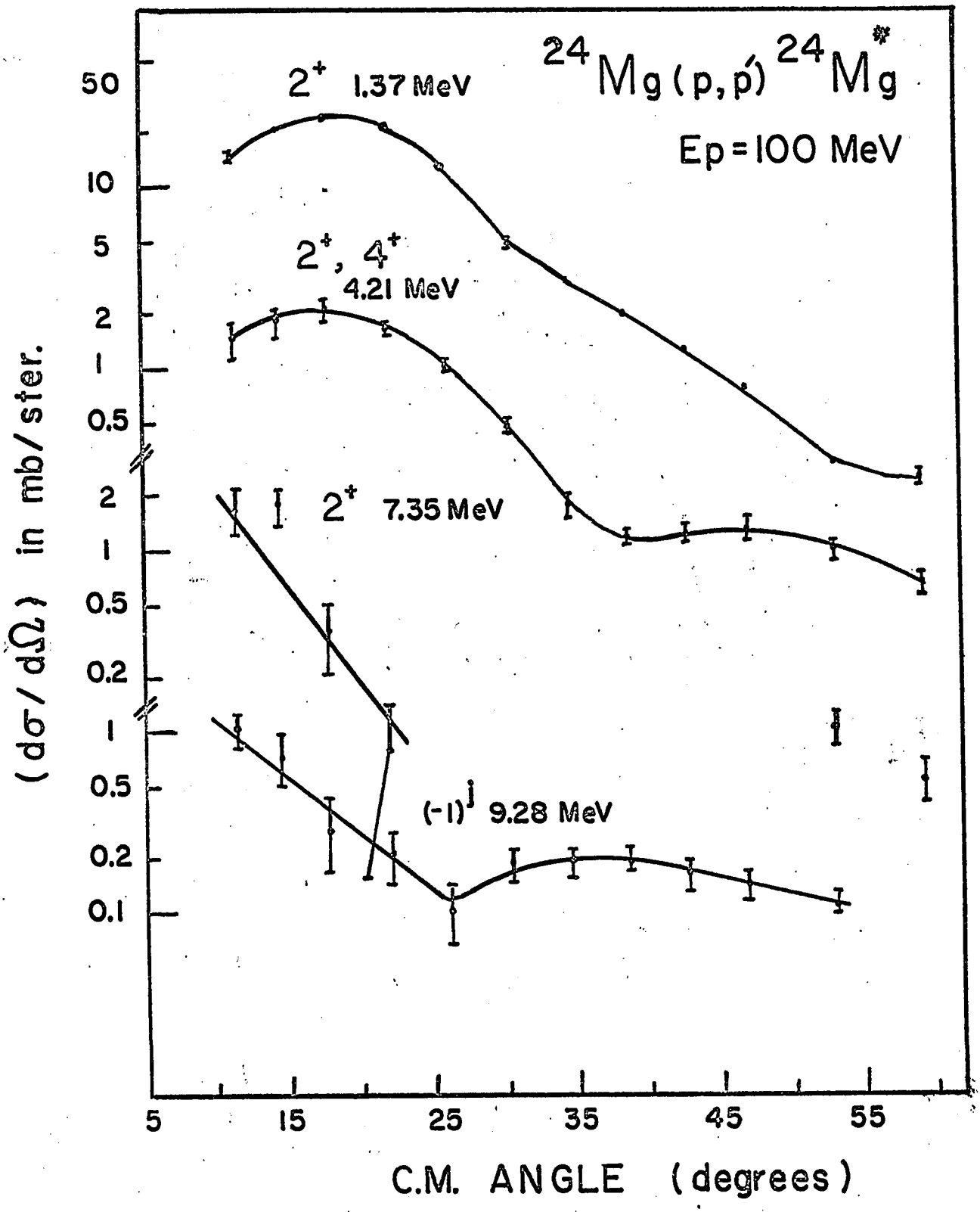
$^{24}Mg(p,p')^{24}Mg^*$
Ep = 100 MeV
2^+ 1.37 MeV
$2^+, 4^+$
4.21 MeV
2^+ 7.35 MeV
$(-1)^J$ 9.28 MeV
$(d\sigma/d\Omega)$ in mb/ster.
50
10
5
2
1
0.5
2
1
0.5
0.2
1
0.5
0.2
0.1
5
15
25
35
45
55
C.M. ANGLE (degrees)

FIGURE 35

FIGURE 35

Differential cross-section angular distributions for the 7.6 MeV, 8.4 MeV and 5.2 MeV peaks in ^{24}Mg. The 8.4 MeV angular distribution is a 3^- distribution of the narrow type. The error bars are shown for relative uncertainties.

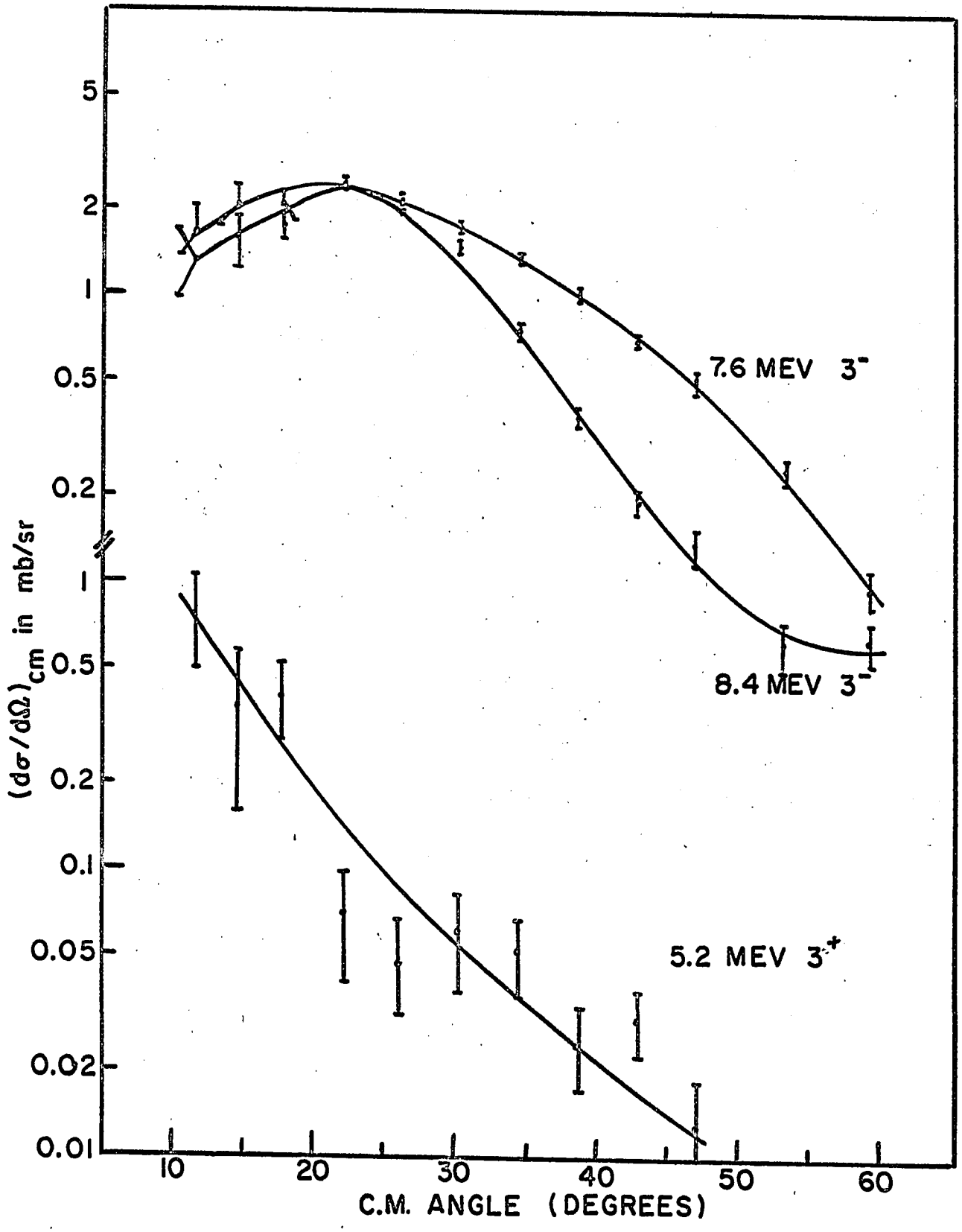
5
2
1
0.5
0.2
1
0.5
0.2
0.1
0.05
0.02
0.01
$(d\sigma/d\Omega)_{cm}$ in mb/sr
7.6 MEV 3⁻
8.4 MEV 3⁻
5.2 MEV 3⁺
10
20
30
40
50
60
C.M. ANGLE (DEGREES)

FIGURE 36

FIGURE 36

Differential cross-section angular distributions for 0+ --- 4+ transitions in ^{24}Mg and ^{28}Si observed at incident proton energies of 100 MeV and 185 MeV. No rise in the cross-section is observed at the Uppsala energy in the forward angle region. The error bars are shown for relative uncertainties.

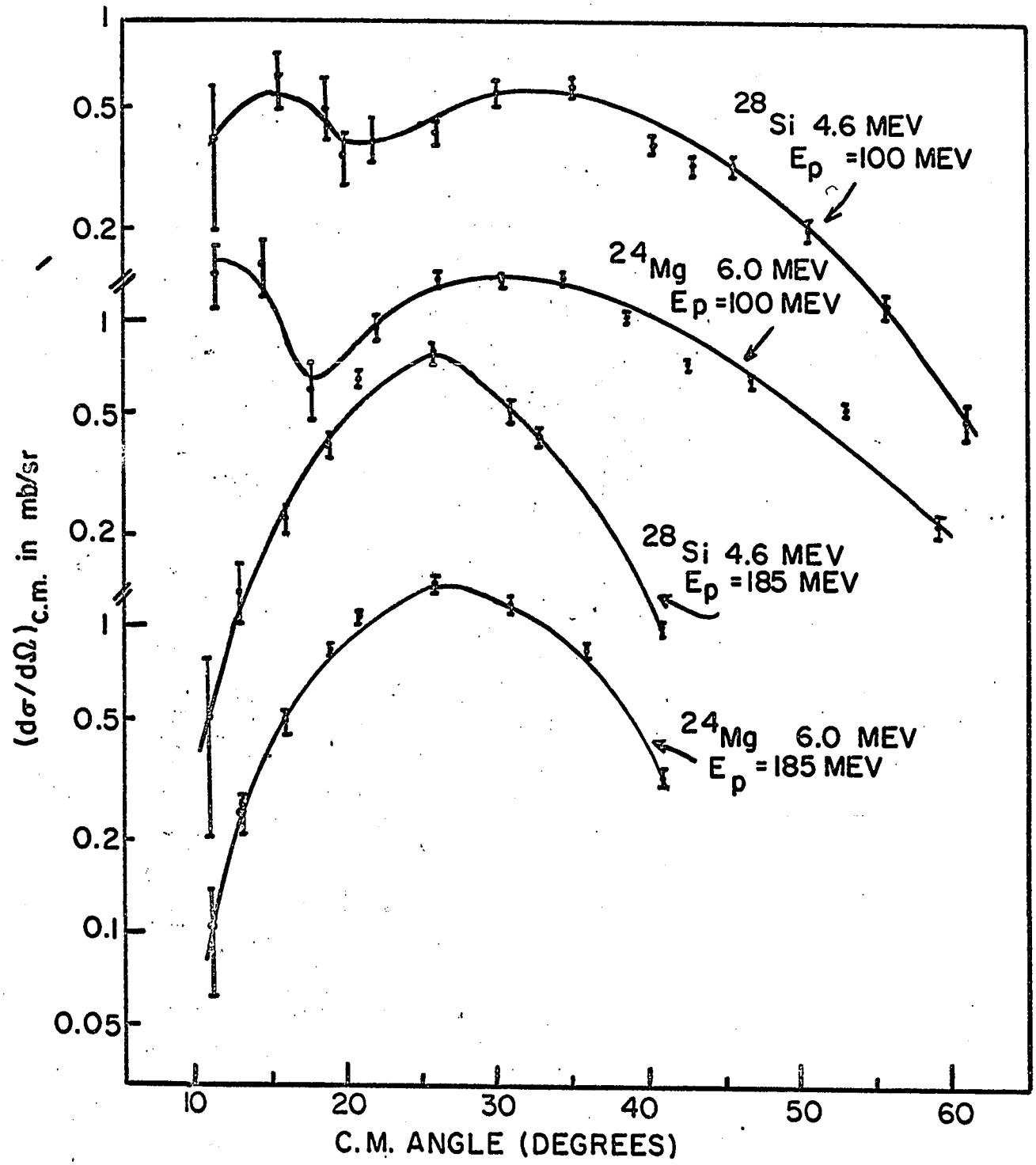
^{28}Si 4.6 MEV
E_p =100 MEV
^{24}Mg 6.0 MEV
E_p =100 MEV
^{28}Si 4.6 MEV
E_p =185 MEV
^{24}Mg 6.0 MEV
E_p =185 MEV
$(d\sigma/d\Omega)_{c.m.}$ in mb/sr
C.M. ANGLE (DEGREES)
1
0.5
0.2
1
0.5
0.2
1
0.5
0.2
0.1
0.05
10
20
30
40
50
60

FIGURE 37

FIGURE 37

Differential cross-section angular distributions for the 10.0 MeV, 11.1 MeV and 12.0 MeV peaks observed in the energy spectrum of protons scattered from ^{24}Mg. The error bars are shown for relative uncertainties.

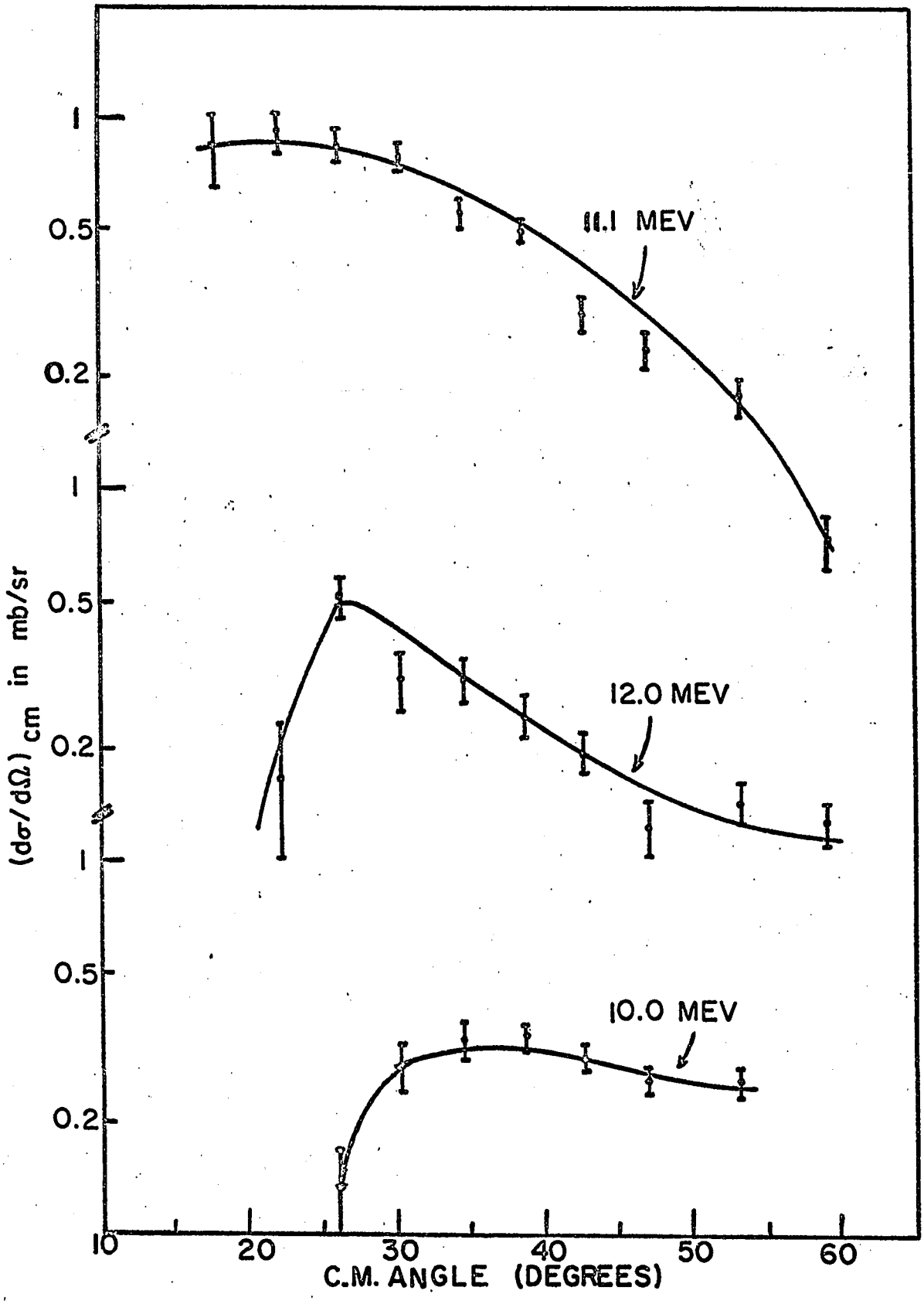
11.1 MEV
12.0 MEV
10.0 MEV
(dσ/dΩ)cm in mb/sr
C.M. ANGLE (DEGREES)
1
0.5
0.2
1
0.5
0.2
1
0.5
0.2
10
20
30
40
50
60

CHAPTER 8

8.1 ELASTIC AND INELASTIC SCATTERING FROM ^{28}Si

The evidence for rotational structure in ^{28}Si is illustrated in figure 29 and consists of the presence of a ground state rotational band which includes the levels at 1.78 MeV, 2+, and 4.62 MeV, 4+. T. R. Canada et al. , 1967, have observed a state at 8.45 MeV which decays strongly to the 4.62 MeV level and is consequently a good candidate for the 6+ member of the ground state rotational band. Additional evidence for collective properties comes from the observed enhancement of several of the electric quadrupole transitions between the low lying levels, for example, $M^2 = 10.3 \pm 0.8$ for the first excited state to ground state E2 transition. (S. W. Robinson et al., 1967). The deformation parameter obtained in this manner is 0.32, considerably smaller than the equivalent value of 0.51 for ^{24}Mg and indicative of the lesser role collective motions probably occupy in ^{28}Si.

As previously mentioned the positions and spins of the third and fourth excited states in ^{28}Si show no resemblance to the characteristic features of a K = 2 band, moreover the absence of a low lying 2+ level makes it impossible to attribute the 3+ levels at 6.28- and 6.889 MeV to a K = 2 rotational band. The role of the low-lying 0+ states in ^{28}Si is also not well understood. The 4.98 MeV state is the lowest candidate for the 0+ β - vibrational state but the 0+ state at 6.69 MeV (close to the energy of the 0+ β - vibrational state in ^{24}Mg

at 6.44 MeV) cannot be excluded as a possible candidate. Our results seem to indicate that the 4.98 MeV state in ^{28}Si plays the same role as the β - vibrational state in ^{24}Mg at 6.44 MeV. This observation is in good agreement with recent theoretical treatments of ^{28}Si in the Hartree-Fock Model (S. Das Gupta and M. Harvey, 1967) which assign an oblate shape to the ground state of ^{28}Si and associate the lower excited states to rotations of the oblate ground state and rotations of particle-hole excitations of the ground state. The state at 6.69 MeV, on the other hand, appears to be the head of a prolate shaped K = 0 excited state band. Transitions between these different intrinsic shapes should be retarded, in good agreement with our measurements in which we do not observe any appreciable excitation of the 6.69 MeV 0+ state, except at the extreme forward angles. The Hartree-Fock calculations give the positive parity levels in correct order with no additional states up to 8 MeV. The main shortcoming of the level scheme predictions is that the level spacing is compressed by approximately a factor two.

As previously mentioned Robinson et al. find that the E2 transitions within the ground state band are adequately described by the rotational-vibrational model. However the decays of the other levels appear to be in strong disagreement with this collective model. In contrast to the previous description of ^{28}Si in the Hartree-Fock model, Manning et al. (1967) using density-dependent forces with Hartree-Fock conclude that the ^{28}Si ground state is prolate rather than oblate. It follows therefore that present understanding of the rotational or particle excitation character of ^{28}Si is far from complete.

As in the case of ^{24}Mg the level scheme of ^{28}Si is very dense so that above the first three excited states the identification of proton peaks with particular levels had to be made on the basis of the characteristics of the measured angular distributions coupled with the knowledge that unnatural parity states, high spin states etc. are not expected to be appreciably excited. Figure 38 illustrates the energy level diagram of ^{28}Si up to an excitation energy of 11.5 MeV. The excitation energies, spins and parities have been extracted from Endt and Van Der Leun, 1967. Spins and parities in brackets are recent possible identifications due to this work and 185 MeV proton scattering data, (O. Sundberg et al., 1967). The levels labelled A.....K are the ones which appeared to be excited in our work and correspond identically to the proton groups observed in the (p, p') experiment at 185 MeV.

The measurements were taken over an angular region from 10 to 60 degrees with an average energy resolution of 400 keV. Eleven peaks were observed in the energy spectra, eight of which showed characteristic angular distributions and consequently are identifiable with known energy levels in ^{28}Si. The peaks observed in the proton spectra are listed in table 15 together with distinguishing characteristics of the differential cross-section angular distributions and properties of the corresponding excited levels. Figure 39 shows a spectrum of protons scattered from ^{28}Si at a laboratory angle of 49 degrees. For excitation energies greater than 7.5 MeV the level spectrum is complex and we have extracted differential cross-sections only for peaks which remained at the same excitation energy over the angular range studied and which showed widths comparable to the experimental

energy resolution.

The differential cross-section angular distribution for the elastic scattering is shown in figure 40 and tabulated in table 16. The inelastic differential cross-section angular distributions are shown in figures 42 to 44 and tabulated along with the relative uncertainties in tables 16 to 18. The relative errors, as in the case of ^{24}Mg, vary considerably depending on the excitation energy, scattering angle and the presence of nearby partially resolved peaks. Typical relative errors are 3% - 8% for the 1.78 MeV level however errors in the range of 15% - 40% were assigned to the poorly resolved peaks at 4.61 and 4.97 MeV. Relative errors for the 6.89 MeV peak were typically 5% going to 10 - 20% in the forward angle region.

Proton inelastic scattering from ^{28}Si has been recently investigated at many different proton energies with experimental energy resolution varying from 40 keV to 800 keV. Studies have been carried out at 17.5 MeV (G. M. Crawley et al., 1967) with 50 keV resolution, 21.2 MeV (R. W. Barnard et al., 1967) with 40 keV resolution, 24.9 MeV (P. J. Locard et al., 1968) with 45 - 70 keV resolution, 30.3 MeV (R. K. Cole et al., 1965) 600 keV resolution, 55 MeV (J. Kokame et al., 1967) 110 keV resolution, 155 MeV (M. Liu et al., 1965: A. Willis et al., 1968) 600 keV - 1000 keV resolution and 185 MeV (O. Sundberg et al., 1967) 350 keV resolution. From the point of view of resolving power the advantage of the low energy machines is obvious.

Figure 41 shows the integrated cross-sections we have measured for inelastic proton scattering from ^{28}Si. The integrated cross-section for scattering to the first and second excited states, presumably

Table 15

EXPERIMENTAL RESULTS ON PEAKS OBSERVED IN THE ENERGY SPECTRA OF ^{28}Si TOGETHER WITH PROPERTIES OF CORRESPONDING EXCITED LEVELS 1.

Experimental Excitation energy (MeV)	Listed Value (MeV)	Accepted Value J^{π}	T	Maximum Diff. $(d\sigma/d\Omega)_{c.m.}$ mb/sr	Cross-section at angle degrees
1.8 ± 0.1	1.779	2+	0	20.2	15.7
4.6 ± 0.1	4.61	4+	0	0.64, 0.60	15.7, 35.4
5.0 ± 0.1	4.97	0+	0	0.83, 0.18	15.7, 40.5
6.9 ± 0.1	6.69	0+	0	(observed only at 12°)	
	6.878 2.	3⁻	0	4.75	21.9
	6.887	4+	0		
7.4 ± 0.13	7.38	1+	0		
	7.41	2+	0	1.26	15.7
8.9 ± 0.15	8.90	1⁻	0	0.46	21.9
	8.94	$\pi = (-)^J$	0		
9.4 ± 0.1	9.319	(3+)	1	0.91	forward
	9.379	(2+)	1		
	9.41	---	----		
	9.49	---	----		
9.67 ± 0.1	9.70 3.	(5⁻)	0	0.35	40.5
	9.76	---	---		
10.14 ± 0.13	9.93	--- 3.	----		
	10.18	(3⁻)	0	1.47	21.9
	10.27	---	-----		
	10.31	---	----		
10.81 ± 0.1	10.71	1+	1	1.8	forward
	10.91	$\pi = +$	1		
11.36 ± 0.08	11.295	1⁻	0		
	11.418	(1,2,3)+	1	2.7	forward
4.	11.514	2+	0		
11.45 ± 0.12	11.582	3⁻	0	0.32	40.5
	11.656	2+	0		
	11.667	1⁻	0		

1. Spin and parity assignments from Endt and Van der Leun (1967).
2. Predominantly contributing level is underlined.
3. First identification due to O. Sundberg et al., 1967.
4. Possible 5^- level due to this work, section 8.7

rotations of the ground state, is approximately 12 millibarns, considerably less than the equivalent integrated cross-section of 17 millibarns measured in ^{24}Mg and indicative of the more important role of collective excitations in ^{24}Mg. The appreciable excitation of two 5^- states in ^{28}Si appears unique to high incident proton energies. In the previously cited publications only the Uppsala group at 185 MeV has observed (and identified one of) the 5^- states excited in the present work. The levels have presumably not been observed at 155 MeV because of inadequate energy resolution.

8.2 THE VARIATION OF PEAK ANGLE WITH ANGULAR MOMENTUM TRANSFER AND NUCLEAR SIZE

Figures 24 and 21 illustrate the dominant features of the characteristic E2 and E3 angular distributions we have observed in the three even-even nuclei studied. The effect of nuclear size on peak angle is very evident. For A = 12, 24, 28 the peak angles for E2 angular distributions occur at approximately 21, 18 and 16 degrees respectively. For E3 angular distributions the corresponding angles are 26, 22 and 22 degrees respectively. Figure 42 strikingly illustrates the variation of the peak angle in the angular distribution with angular momentum transfer.

In the framework of the plane wave impulse approximation it is a fairly simple matter to show how these features of the angular distributions arise. (A. B. Clegg, 1965). The matrix element for a non-spin-flip transition is

$$\int \psi_f^* M(q) e^{-iq\cdot r} \psi_i dV \qquad \text{with} \quad q = k_f - k_i$$

and becomes upon expansion of the plane wave and the assumption that the wave function of the struck nucleon is separable

$$M(q) \int j_{\ell}(qr)\phi_f(r)\phi_i(r)r^2dr$$

where ϕ_i, ϕ_f^* are the radial parts of ψ_i , ψ_f^* , $r^2\phi_f^*\phi_i$ is expected to have a comparatively narrow peak at some radius R so upon replacement by $k\,\delta(r - R)$ the integral is simply $kj_{\ell}(qR)$. This has a pronounced maximum at some value of qR and thus for some R will peak at some value of q. Since the nucleon-nucleon scattering amplitude M(q) is expected to vary smoothly with momentum transfer the angular distribution must peak at some value of q. For higher L and fixed R the spherical Bessel functions will peak at higher q values. Similarly as R increases the peak in $j_L(qR)$ occurs at a smaller value of q, so that for given L, the peak in the angular distribution will occur at smaller q for a larger target nucleus. These results are not as easy to extract in the distorted wave impulse approximation however the results are substantially the same (A. B. Clegg, 1965, pp. 48-52).

8.3 THE PEAKS AT 1.77-, 4.62 AND 4.96 MeV

The angular distribution for the 2+ state at 1.77 MeV is shown in figures 24, 42 and is of the characteristic E2 type. Various DWBA studies with collective form factors have been performed for this state at different proton energies. In general the theory gives good

fits to the measured angular distributions with values for β_2 of 0.57 (17.5 MeV), 0.57 (21.2 MeV), 0.41 (30.3 MeV) and 0.25 (155 MeV). The value of 0.25 at 155 MeV was obtained by R. M. Haybron, 1966, using volume absorption with complex coupling. The large spread in values is in contrast to the good internal consistency obtained at various proton energies for β_2 in ^{24}Mg and may be indicative of the ambiguous role collective motions play in ^{28}Si. The value for β_2(EM) of 0.32 $\pm$ 0.01 Obtained by Robinson et al. 1967, is in fairly good agreement only with the proton results at 155 MeV.

The angular distribution for the 4+ state at 4.62 MeV is shown in figures 28 and 42. The features of the angular distributions we have observed for 4+ transitions in the s-d nuclei have been discussed in the previous chapter. Only one valuefor β_4 has been reported in the literature. Bernard and Jones at 30 MeV obtain $\beta_4 = 0.33$ although the theoretical fit to the angular distribution was unsatisfactory at the extremes of the angular range. A coupled channel calculation for the transition did not reproduce the data well either.

The angular distribution for the 0+ state at 4.98 MeV is shown in figure 23. As previously discussed the DWBA with collective form factors does not succeed in describing 0+ transitions in either the p shell or s-d shell nuclei studied. Coupled channel analyses which attempt to describe the excitation of the 0+ states in ^{24}Mg and ^{28}Si allowing both direct and multiple excitation have yet to be reported in the literature. The angular distribution for the 4.98 MeV 0+ state in ^{28}Si is extremely similar to the angular distribution we have observed for the 6.44 MeV 0+ state in ^{24}Mg. The 6.69 MeV 0+ state in ^{28}Si was observed only at a laboratory

Table 16

DIFFERENTIAL CROSS-SECTIONS FOR ELASTIC SCATTERING AND THE 1.78 MeV AND 4.62 MeV LEVELS IN SILICON

C.M. Angle degrees	Elastic scattering $(d\sigma/d\Omega)_{c.m.}$ mb/sr	1.78 MeV level $(d\sigma/d\Omega)_{c.m.}$ mb/sr	4.62 MeV level $(d\sigma/d\Omega)_{c.m.}$ mb/sr
11.5	1269 ± 5	15.2 ± 1.1	0.393 ± 0.197
15.7	611 ± 2	20.2 ± 0.7	0.637 ± 0.142
18.8	257 ± 2	18.4 ± 0.5	0.519 ± 0.132
19.8	165 ± 1	17.4 ± 0.4	0.350 ± 0.076
21.9	63.2 ± 0.5	16.3 ± 0.3	0.397 ± 0.065
26.1	10.8 ± 0.2	6.03 ± 0.14	0.419 ± 0.041
30.2	12.6 ± 0.2	2.91 ± 0.11	0.572 ± 0.057
35.4	10.7 ± 0.1	1.52 ± 0.06	0.595 ± 0.048
40.5	4.73 ± 0.1	1.17 ± 0.06	0.383 ± 0.037
43.1	2.99 ± 0.06	1.05 ± 0.04	0.330 ± 0.026
45.7	1.93 ± 0.06	0.676 ± 0.041	0.328 ± 0.031
50.8	1.04 ± 0.03	0.404 ± 0.018	0.205 ± 0.016
55.9	0.489 ± 0.017	0.293 ± 0.014	0.115 ± 0.011
61.1	0.149 ± 0.009	0.265 ± 0.021	0.0477 ± 0.0068

scattering angle of 11 degrees indicative of a very strongly forward peaked angular distribution and uncharacteristic of the behavior of the 0+ transitions we have observed. The 6.44 MeV 0+ state in ^{24}Mg has been described as the 0+ β = vibrational state. Our results indicate therefore that the 4.98 MeV 0+ and not the 6.69 MeV 0+ carries this role in ^{28}Si.

The non-excitation of the 6.69 MeV 0+ state is in agreement with the Uppsala results at 185 MeV and also seems to support the Hartree-Fock calculations of Das Gupta and Harvey, 1966, in which the

low lying levels of ^{28}Si correspond to oblate configurations (the same as the ground state) whereas the 6.69 MeV 0+ state is the first excited state belonging to a prolate configuration. Transitions between the intrinsically different configurations are expected to be weak. Similar conclusions have been drawn by P. J. Locard et al., 1968, at 25 MeV incident proton energy.

8.4 THE PEAKS AT 6.3- AND 6.9 MeV

The 3+ unnatural parity state at 6.27 MeV was observed to be appreciably excited only at a laboratory scattering angle of 11 degrees. The level is analagous to the 5.22 MeV, 3+, state in ^{24}Mg which also showed a strongly forward peaked angular distribution. The level did not appear to be excited in the 185 MeV proton scattering experiment, however its appreciable excitation has been observed at various lower proton energies (R. W. Bernard et al., 1967: G. W. Crawley et al., 1967).

As previously mentioned the 6.69 MeV 0+ level appeared to be appreciably excited only at a scattering angle of 11 degrees. Two other levels which could contribute to the peak at 6.9 MeV are the 6.878 MeV, 3^-, and the 6.887 MeV, 4+, excited states. The angular distribution for this peak is shown in figures 42 and 21, and shows the features of a characteristic E3 angular distribution. This suggests that the dominant contribution to the peak comes from the excitation of the 6.878 MeV level. The angular distribution does not fall as rapidly with increasing angle as the E3 angular distribution

observed for the 8.36 MeV level in ^{24}Mg so that some excitation of the 4+ state is also indicated. In the previously cited references no experiment has succeeded in resolving this doublet however the common conclusion has been that the large yield (an integrated cross-section of 4.5 millibarns at 100 MeV) is due to the 3^- member of the doublet. The level is known to have an enhanced electric octupole decay to the ground state (A. E. Litherland et al., 1966) and thus is expected to be strongly excited in inelastic proton scattering. Recent (α, α') experiments have also indicated the strong excitation of the 3^- member of the doublet, (J. Kokame et al., 1966: F. W. Bingham, 1966).

The angular distribution for the 6.878 MeV 3^- state has been analysed in the collective model at several proton energies. Haybron at 155 MeV obtaines $\beta_3 = 0.267$ using volume absorption with complex coupling however other analyses yield $\beta_3 = 0.46$ at 17.5 MeV and $\beta_3 = 0.40$ at 30 MeV. In the 30 MeV analysis a good fit to the data was obtained over the entire angular range by assuming contributions to the angular distribution of 28% L = 4 and 72% L = 3. In contrast to the results for β_2 the low-energy proton experiments now yield values for β_3 in reasonable agreement with β_3 (EM) = 0.45, T. K. Alexander et al., 1966.

8.5 THE PEAKS AT 7.4- 8.9- AND 9.4 MeV.

The angular distribution for the peak at 7.4 MeV is shown in figure 43. The angle at which the maximum cross-section occurs is

16 degrees and is suggestive of an E2 transition, however the levelling of the angular distribution from 30 - 45 degrees is uncharacteristic. Two levels could contribute to this peak, the 7.38 MeV 1+ and the 7.40 MeV, 2+ states. The unnatural parity of the former level and the resemblance of the angular distribution to an E2 transition suggests a predominant contribution from the 2+ state. In the Hartree-Fock calculations of Das Gupta this state is also identified as belonging to an oblate configuration whereas the 7.93 MeV 2+ state is prolate. The moderately strong excitation of the 7.4 MeV 2+ in contrast to the non-excitation of the 7.93 MeV 2+ to an appreciable extent is thus consistent with these calculations. Similar results have been observed at 25 MeV, P. J. Locard et al., 1968. In the 185 MeV experiment a peak was also observed at an excitation energy of 7.4 MeV however the angular distribution peaked at approximately 18 degrees rather than the 11 degrees characteristic of an E2 transition and the breadth of the distribution was also uncharacteristic of an E2 transition.

The angular distributions for the peaks at 8.9 MeV and 9.4 MeV are shown in figure 43 and do not show the characteristic features of any particular transition. The peaks are therefore most probably composed of the contributions from several levels. Similar results have been observed at 185 MeV. except that the peak at 8.9 MeV showed an angular distribution which was reasonably similar to that for an E3 transition.

Table 17

DIFFERENTIAL CROSS-SECTIONS FOR THE 4.97-, 6.9-, 7.4- AND 8.9 MeV PEAK

C.M. Angle degrees	the 4.97 MeV level $(d\sigma/d\Omega)_{c.m.}$ mb/sr	6.9 MeV level $(d\sigma/d\Omega)_{c.m.}$ mb/sr	7.4 MeV peak $(d\sigma/d\Omega)_{c.m.}$ mb/sr	8.9 MeV peak $(d\sigma/d\Omega)_{c.m.}$ mb/sr
11.5	0.568 ± 0.206	1.86 ± 0.36	0.919 ± 0.296	---------
15.7	0.828 ± 0.166	3.27 ± 0.26	1.26 ± 0.20	0.362 ± 0.116
19.8	0.598 ± 0.085	4.09 ± 0.19	0.939 ± 0.124	0.413 ± 0.091
21.9	0.513 ± 0.069	4.75 ± 0.18	0.674 ± 0.109	0.456 ± 0.072
26.1	0.267 ± 0.035	3.28 ± 0.11	0.421 ± 0.063	0.275 ± 0.034
30.2	0.108 ± 0.058	2.51 ± 0.11	0.230 ± 0.055	0.0894 ± 0.033
35.4	0.0827 ± 0.0346	1.76 ± 0.07	0.195 ± 0.037	0.0698 ± 0.021
40.5	0.178 ± 0.030	1.27 ± 0.06	0.221 ± 0.033	0.0827 ± 0.022
43.1	0.142 ± 0.022	0.926 ± 0.036	0.195 ± 0.023	0.0633 ± 0.0155
45.7	0.147 ± 0.024	0.612 ± 0.040	0.167 ± 0.024	---------
50.8	0.101 ± 0.014	0.394 ± 0.018	0.102 ± 0.012	---------
55.9	0.0458 ± 0.0084	0.252 ± 0.013	0.0568 ± 0.0076	---------
61.1	0.0139 ± 0.0039	0.174 ± 0.010	0.0337 ± 0.0055	---------

8.6 THE PEAK AT 10.14 MeV

The angular distribution for the peak at 10.14 ± 0.13 MeV is shown in figure 43 and is very similar to a characteristic E3 transition. The Uppsala group has observed a peak at 10.19 ± 0.05 MeV which also showed an E3 angular distribution of the narrow type. They identify this peak with a known level in ^{28}Si at an excitation energy of 10.18 MeV for which there are no suggestions in the literature concerning the quantum numbers. If the identification is correct the observation of a characteristic E3 angular distribution at both incident proton energies of 100 MeV and 185 MeV is strongly suggestive that the state has $J^{\pi} = 3^{-}$.

8.7 THE PEAKS AT 9.67- AND 11.45 MeV

The angular distributions for the peaks at 9.67 ± 0.10 MeV and 11.45 ± 0.12 MeV are shown in figures 44, 42. The angular distributions are very similar, peak at approximately 40 degrees and are therefore suggestive of 5^- transitions. At 185 MeV a similar angular distribution was observed for a peak at an excitation energy of 9.66 ± 0.08 MeV. The Uppsala group identified this peak with a level at 9.70 MeV and suggested that the spin and parity of the level was 5^-. This identification of the 9.70 MeV state as 5^- has recently been supported by S. T. Lam et al., 1968, using the $^{27}Al(p,\gamma)^{28}Si$ reaction. Our results for the 9.70 MeV level serve as an additional confirmation of this spin and parity.

The apparently 5^- peak at 11.45 MeV observed at our energy is more difficult to explain. The situation is complicated by the fact that we observe a very strongly forward peaked angular distribution for another peak at 11.36 ± 0.08 MeV. However, the forward peaked nature of the angular distribution implies that the peak almost certainly corresponds to a peak at 11.4 MeV observed in 180 degree electron scattering (H. Liesem, 1966) and consequently can be identified as a M1 transition. A similar conclusion has been reached by O. Sundberg et al., 1967, at 185 MeV. Since an M1 angular distribution is definitely not expected to reappear at large angles the peak we observe at 11.45 MeV is most probably due to the excitation of a different level in ^{28}Si. The known levels in ^{28}Si in this region are listed in table 15. The T = 1 level at 11.418 MeV corresponds to the peak at 11.4 MeV observed in electron scattering. The spin-parity assignments

Table 18

DIFFERENTIAL CROSS-SECTIONS FOR THE 9.4-, 9.67- and 10.14 MeV PEAKS

C.M. ANGLE degrees	9.4 MeV peak $(d\sigma/d\Omega)_{c.m.}$ mb/sr	9.67 MeV level $(d\sigma/d\Omega)_{c.m.}$ mb/sr	10.14 MeV level $(d\sigma/d\Omega)_{c.m.}$ mb/sr
11.5	0.914 ± 0.362	----	0.467 ± 0.266
15.7	0.884 ± 0.208	----	1.044 ± 0.23
19.8	0.686 ± 0.095	----	1.23 ± 0.12
21.9	0.403 ± 0.078	0.0959 ± 0.045	1.47 ± 0.11
26.1	----	0.221 ± 0.038	1.00 ± 0.07
30.2	----	0.271 ± 0.049	0.539 ± 0.058
35.4	----	0.234 ± 0.027	0.391 ± 0.040
40.5	----	0.353 ± 0.036	0.223 ± 0.030
43.1	----	0.288 ± 0.024	0.159 ± 0.021
45.7	----	0.281 ± 0.030	0.103 ± 0.024
50.8	----	0.267 ± 0.018	0.0828± 0.012
55.9	----	0.197 ± 0.013	0.0525± 0.0098
61.1	----	0.143 ± 0.014	0.0253± 0.0068

in this region of the energy levels have been unambiguously assigned by α-γ and γ-γ angular correlation (P.M. Smulders et al.1962). No level has $J^{\pi} = 5^{-}$ nor does it appear possible that any combination of levels should give a broad rise in the cross-section at approximately 40 degrees. It thus appears possible that we are exciting a previously unknown level in ^{28}Si with $J^{\pi} = 5^{-}$. This possibility is supported by the observation that in the experiments performed by Smulders, angular correlations were carried out only for transitions to the ground state and the first excited

state, transitions which would probably not be observed for the de-excitation of a high spin 5^- state. In fact the only possibilities considered for the observed resonant states were 0+, 1^-, 2+, 3^- or 4+. We have been informed that a 5^- state at approximately 11 MeV excitation energy could fit in nicely with recent rotational interpretations of ^{28}Si (N. Anyan-Weiss, 1968)[1].

8.8 THE PEAKS AT 10.81 MeV AND 11.36 MeV

Two strongly forward peaked angular distributions have been observed for peaks at an excitation energy of 10.81 $\pm$ 0.1 MeV and 11.36 $\pm$ 0.08 MeV, figure 44. The peaks are most likely due to M1 transitions ($\Delta T = 1$) and are analagous to the excitation of the 1+ T=1 state at 15.1 MeV in ^{12}C. Endt and Van der Leun list several possible levels in the vicinity of 10.8 MeV.An appreciable part of the cross-section is probably due to the excitation of the 1+, T=1 level at 10.71 MeV also excited in a study of (p,γ) resonances (P.M. Endt et al. 1960).

A strong M1 transition has been observed at an excitation energy of 11.6 MeV in 40 MeV 180 degree electron scattering (Barber et al. 1960, 1964). H. Liesem, 1966, has apparently observed the same transition at an excitation energy of 11.42 $\pm$ 0.02 MeV in electron scattering measurements at 30- and 56 MeV. The latter excitation energy is in excellent

---

1. Recent communication by N. Anyan-Weiss (June, 1968) strongly supports the conclusion that we are indeed exciting a previously unknown 5- level at an excitation energy of 11.45 $\pm$ 0.12 MeV. We are informed that their recent lifetime measurements yield a value of $\tau > 4$ ps for the 9.70 MeV level in silicon so that this 5- level cannot be a member of the K=3- band based on the 6.88 MeV level. On the basis of the 3- to 4- level spacing the 5- of this band would be expected at approximately 10.7 MeV. Since the bands in silicon do not follow the J(J+1) rule very closely it is definitely possible that the 11.45 MeV level is the 5- level of the K=3- band. G. Walters of Strassbourg has also indicated to them that he observes a level at approximately 11.5 MeV which looks like a 5-. The question whether this 5- level is indeed the 5- level of the K=3- band obviously cannot be settled until the γ ray decay of this level has been studied.

agreement with our measured excitation energy of 11.36 ± 0.08 MeV. The Uppsala group has also observed these forward peaked angular distributions for peaks occurring at excitation energies of 10.65 ± 0.10 MeV and 11.40 ± 0.05 MeV.

Table 19

DIFFERENTIAL CROSS-SECTIONS FOR THE PEAKS AT 10.8~, 11.36~ and 11.45 MeV

C.M. ANGLE degrees	10.8 MeV Peak $(d\sigma/d\Omega)_{c.m.}$ mb/sr	11.36 MeV Peak $(d\sigma/d\Omega)_{c.m.}$ mb/sr	11.45 MeV Peak $(d\sigma/d\Omega)_{c.m.}$ mb/sr
11.5	1.80 ±0.42	2.68 ±0.47	----
15.7	0.621 ±0.130	1.14 ±0.21	----
19.8	0.331 ±0.088	0.518 ±0.092	----
26.1	0.113 ±0.034	0.184 ±0.040	----
30.2	----	----	0.125 ±0.043
35.4	----	----	0.205 ±0.039
40.5	----	----	0.316 ±0.039
43.1	----	----	0.225 ±0.024
45.7	----	----	0.229 ±0.029
50.8	----	----	0.176 ±0.015
55.9	----	----	0.101 ±0.011
61.1	----	----	0.0725 ±0.0086

The spin-flip scattering of high energy protons from s-d shell nuclei has been studied in the framework of the DWIA by M. Kawai et al. 1964. Good agreement is obtained between observed and calculated transition strengths and energies using the extreme j-j coupling shell

model. In the case of ^{28}Si the $d_{5/2}$ orbit is assumed to be full for both neutrons and protons and the spin flip level is obtained by raising a nucleon from the $d_{5/2}$ orbit to the $d_{3/2}$ orbit. The model predicts a 1+ , T=1 level at approximately 11.7 MeV in good agreement with our observed excitation energies of 10.8 MeV and 11.4 MeV. For these simple single particle transitions the DWIA yields differential cross-sections for spin-flip scattering in good agreement with the forward peaked angular distributions observed at 185 MeV. The levels populated by the spin-flip mechanism thus appear to be essentially single particle rather than collective excitations.

FIGURE 38

FIGURE 38

Energy level diagram for ^{28}Si up to an excitation energy of 11.5 MeV. Excitation energies, spins and parities are from Endt and Van der Leun (1967). The levels labelled A.....K are the ones apparently excited in the present work.

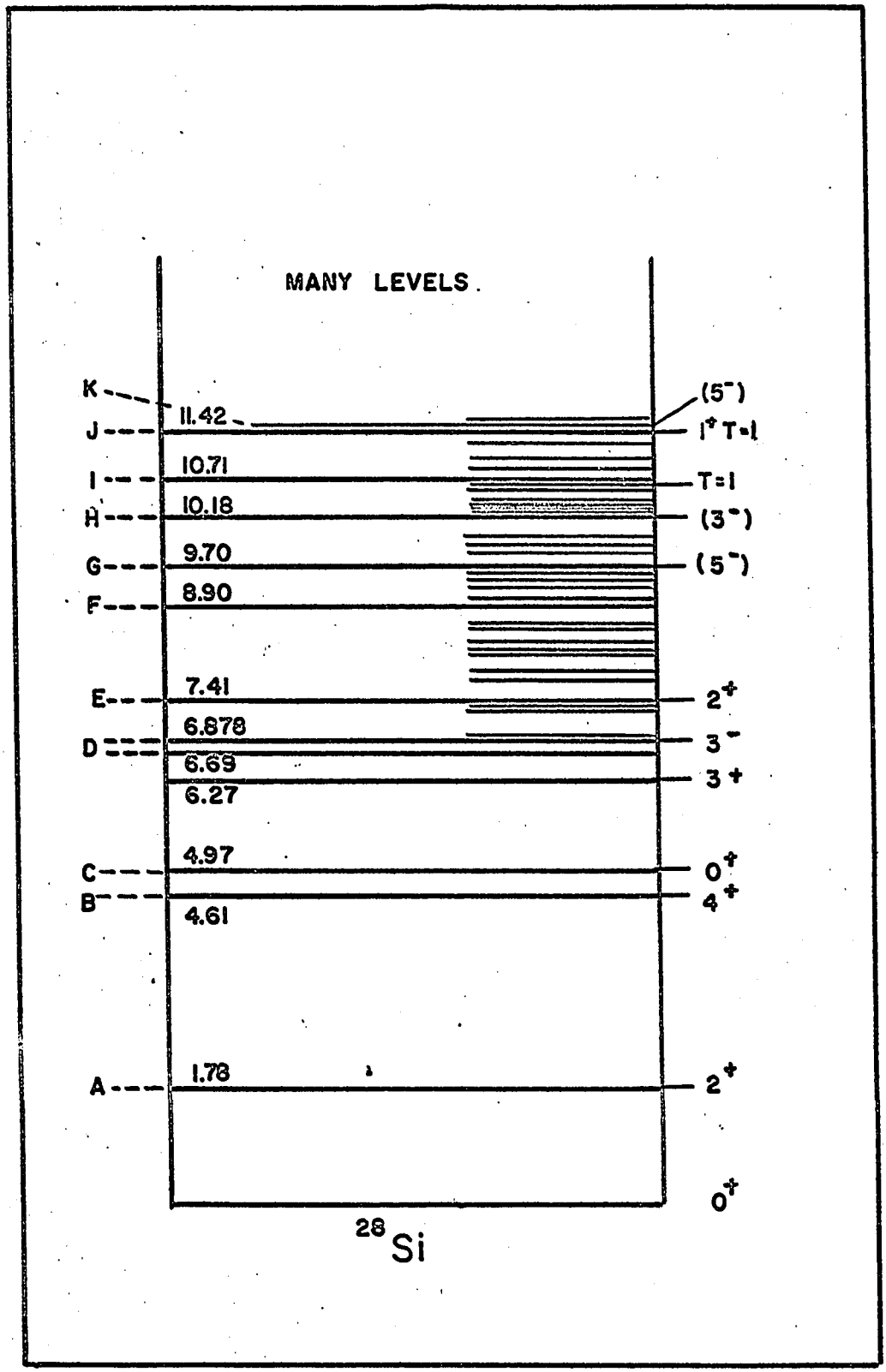
MANY LEVELS.
K
J
I
H
G
F
E
D
C
B
A
11.42
10.71
10.18
9.70
8.90
7.41
6.878
6.69
6.27
4.97
4.61
1.78
(5⁻)
1⁺ T=1
T=1
(3⁻)
(5⁻)
2⁺
3⁻
3⁺
0⁺
4⁺
2⁺
0⁺
28 Si

FIGURE 39

FIGURE 39

Energy spectrum of protons scattered from a target of natural silicon.

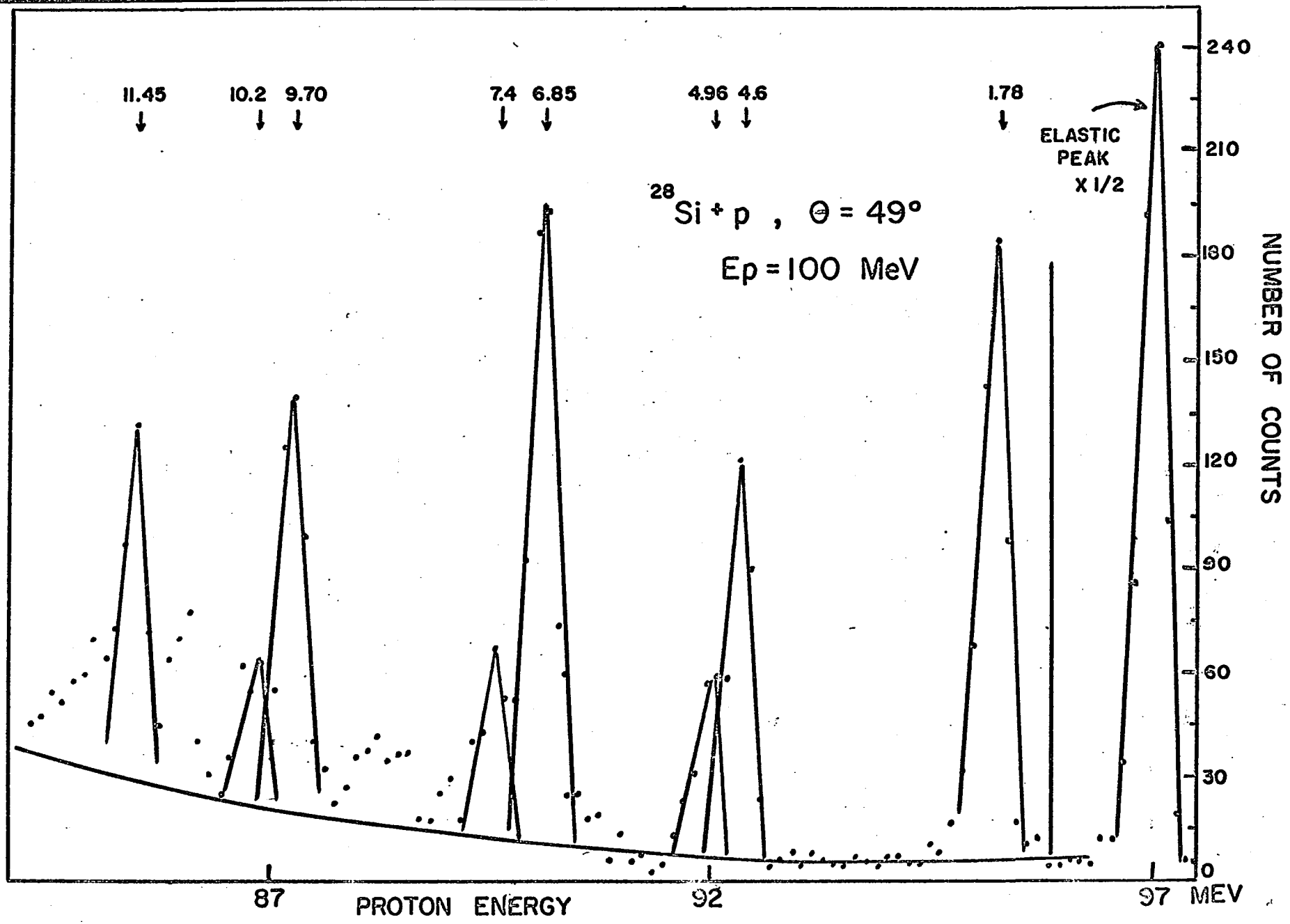
11.45
10.2
9.70
7.4
6.85
4.96
4.6
1.78
ELASTIC PEAK X 1/2
$^{28}Si + p$, $\Theta = 49°$
Ep = 100 MeV
NUMBER OF COUNTS
240
210
180
150
120
90
60
30
0
87
92
97 MEV
PROTON ENERGY

FIGURE 40

FIGURE 40

Differential cross-section angular distribution of 100 MeV protons elastically scattered from natural silicon.

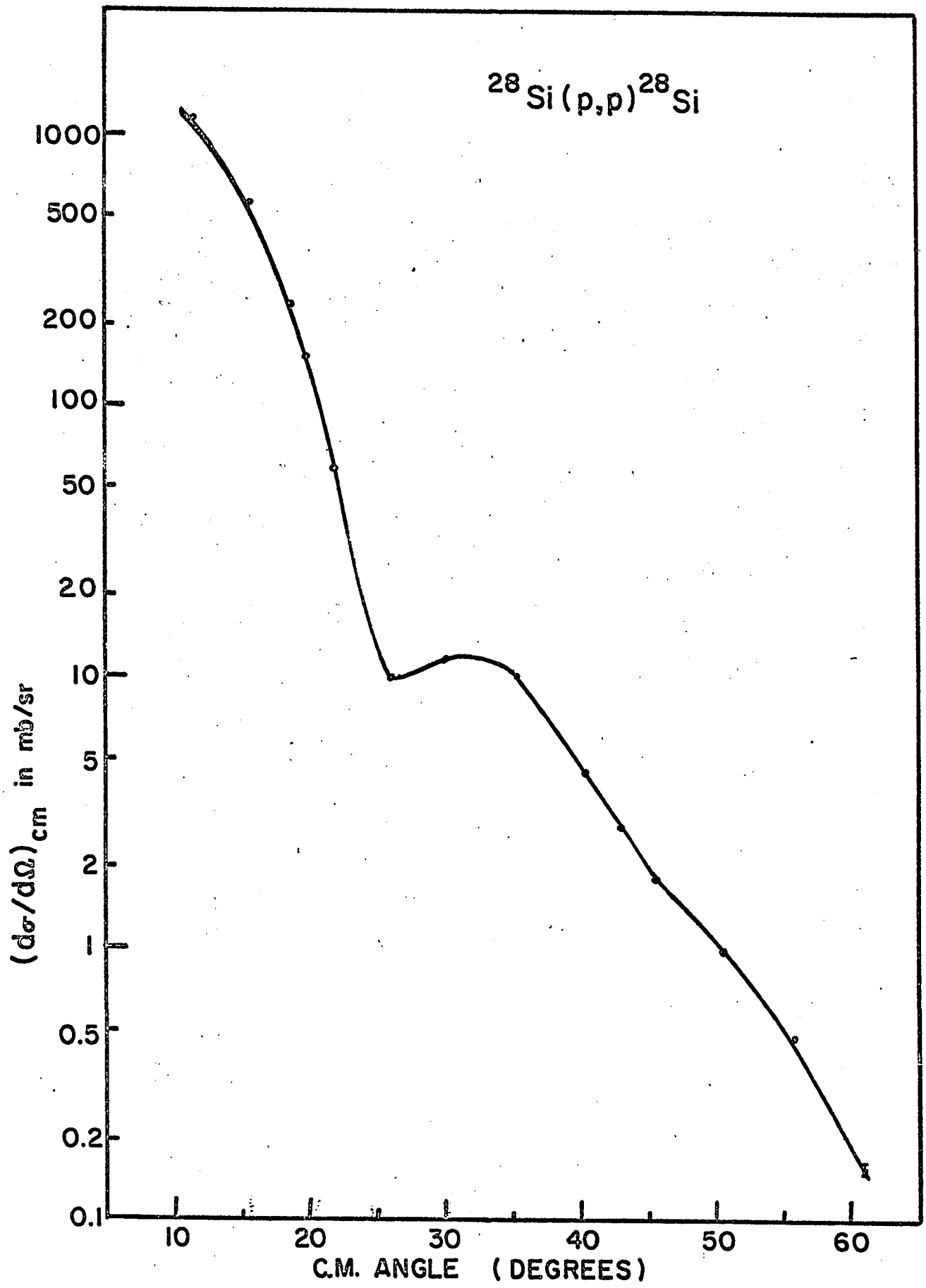
$^{28}Si(p,p)^{28}Si$
1000
500
200
100
50
20
10
5
2
1
0.5
0.2
0.1
$(d\sigma/d\Omega)_{cm}$ in mb/sr
10
20
30
40
50
60
C.M. ANGLE (DEGREES)

FIGURE 41

FIGURE 41

This figure shows the integrated cross-sections (10° - 60°) for inelastic scattering leading to excited states in ^{28}Si up to an excitation energy of 11.5 MeV. Wherever identification with a particular state is possible the corresponding spin and parity is indicated.

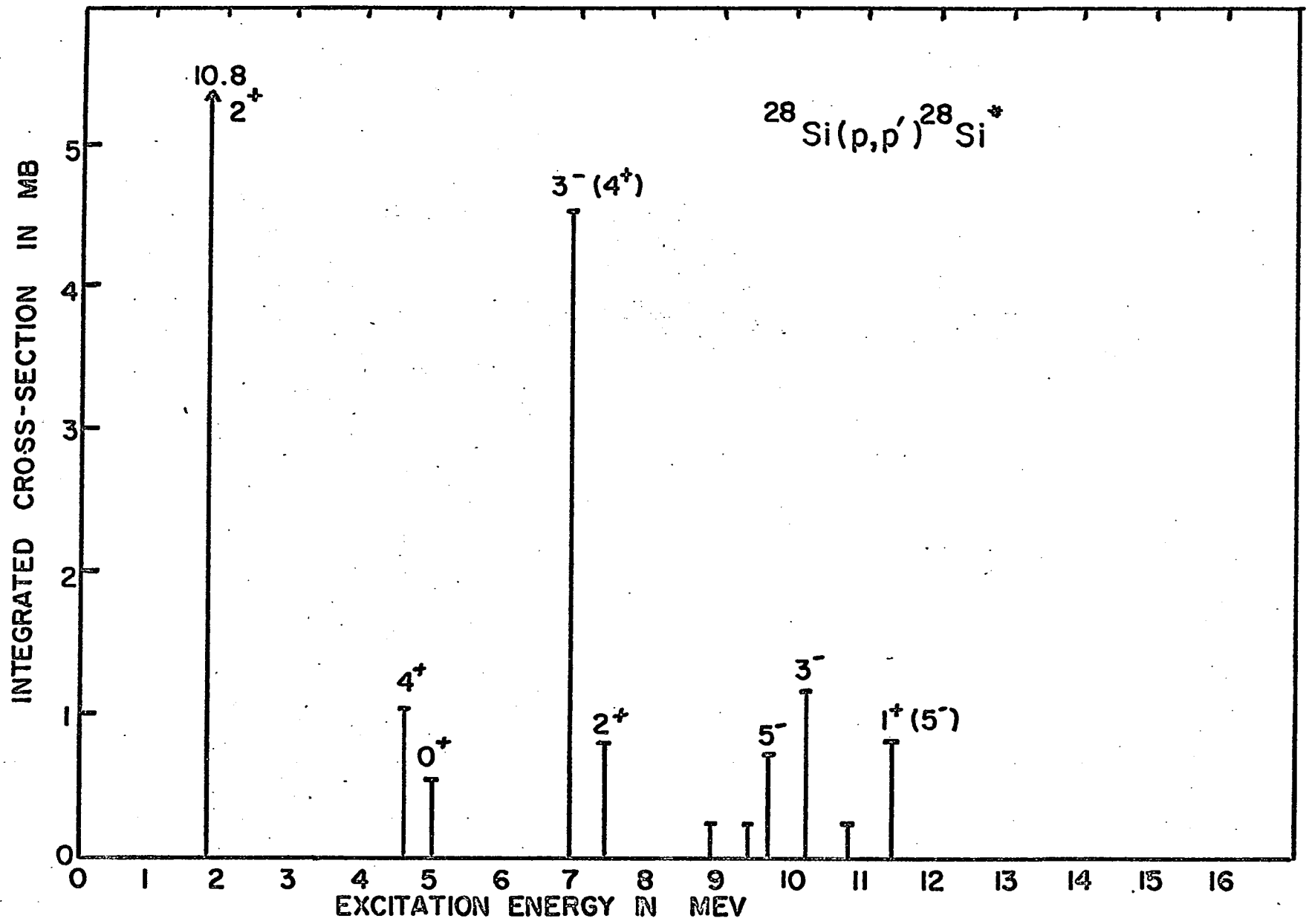
$^{28}Si(p,p')^{28}Si^*$
10.8
2+
3- (4+)
4+
0+
2+
5-
3-
1+ (5-)
INTEGRATED CROSS-SECTION IN MB
EXCITATION ENERGY IN MEV
0
1
2
3
4
5
6
7
8
9
10
11
12
13
14
15
16

FIGURE 42

FIGURE 42

Differential cross-section angular distributions for the 2+(1.78 MeV), 3^-(6.88 MeV), 4+(4.6 MeV) and 5^-(9.7 MeV) levels in ^{28}Si. This figure illustrates the dependence of the dominant peak angle on angular momentum transfer. The error bars are shown for relative uncertainties.

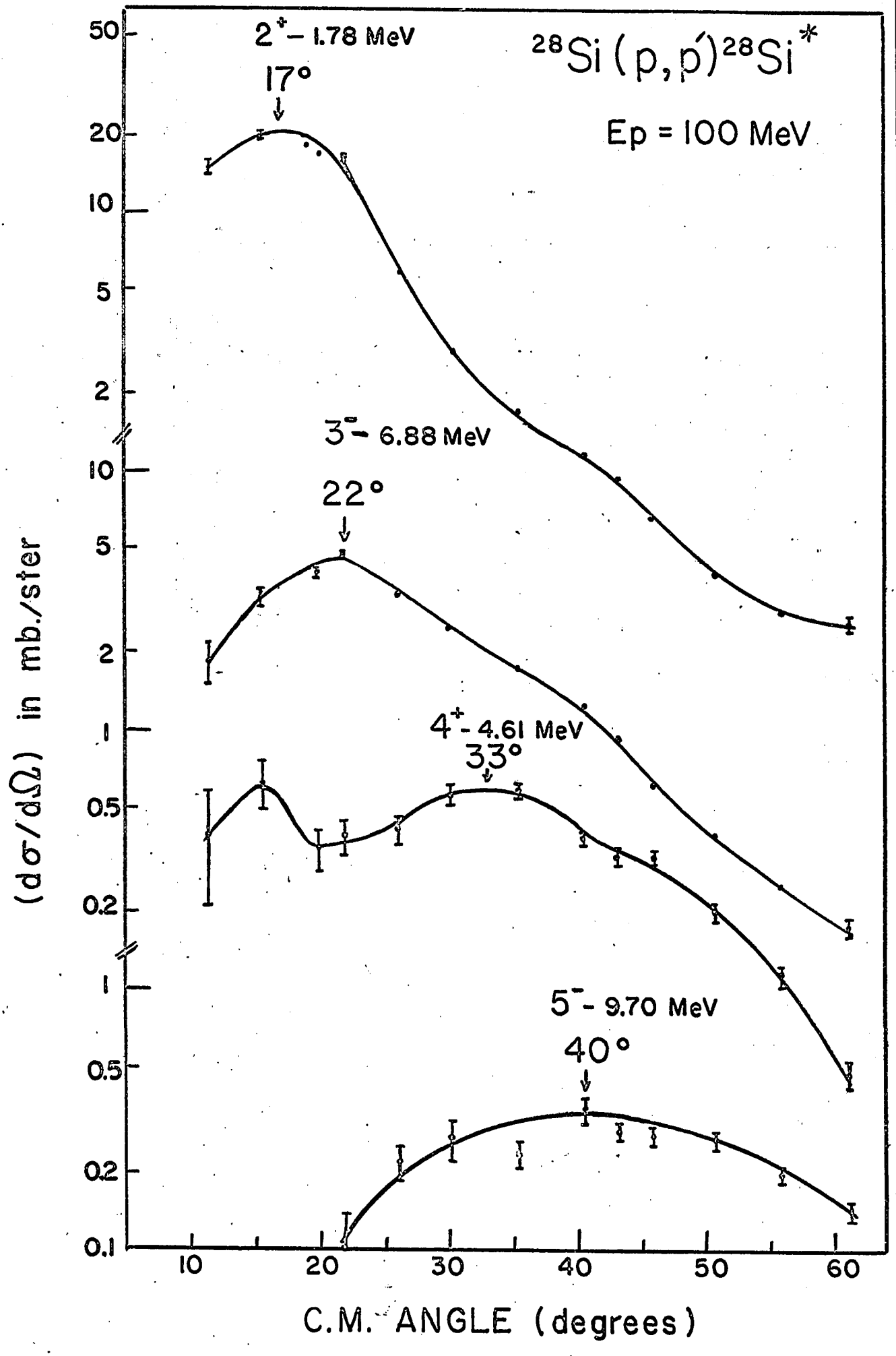
$^{28}Si(p,p')^{28}Si^*$
Ep = 100 MeV
2^+ – 1.78 MeV
17°
3^- – 6.88 MeV
22°
4^+ – 4.61 MeV
33°
5^- – 9.70 MeV
40°
$(d\sigma/d\Omega)$ in mb./ster
C.M. ANGLE (degrees)
50
20
10
5
2
1
0.5
0.2
0.1
10
20
30
40
50
60

FIGURE 43

FIGURE 43

Differential cross-section angular distributions for the 10.14 MeV, 9.4 MeV, 7.4 MeV and 8.9 MeV peaks observed in the spectrum of protons scattered from ^{28}Si. The error bars are shown for relative uncertainties.

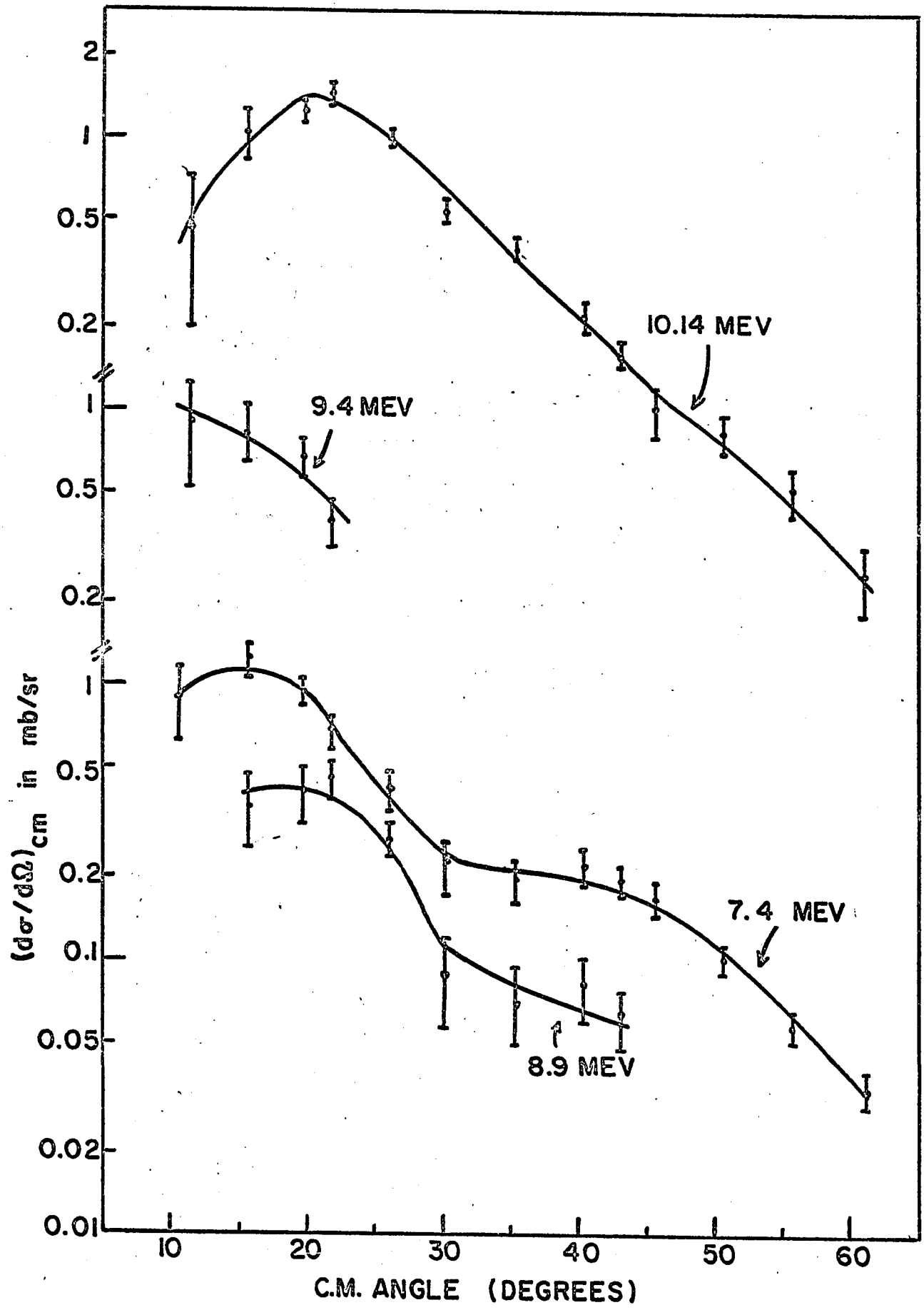
2
1
0.5
0.2
1
0.5
0.2
1
0.5
0.2
0.1
0.05
0.02
0.01
10.14 MEV
9.4 MEV
7.4 MEV
8.9 MEV
$(d\sigma/d\Omega)_{cm}$ in mb/sr
10
20
30
40
50
60
C.M. ANGLE (DEGREES)

FIGURE 44

FIGURE 44

Differential cross-section angular distributions for the 9.7 MeV, 10.8 MeV, 11.36 MeV and 11.45 MeV peaks observed in the spectrum of protons scattered from ^{28}Si. The 11.45 MeV angular distribution most probably corresponds to the excitation of a previously unreported 5^- level in ^{28}Si. The error bars are shown for relative uncertainties.

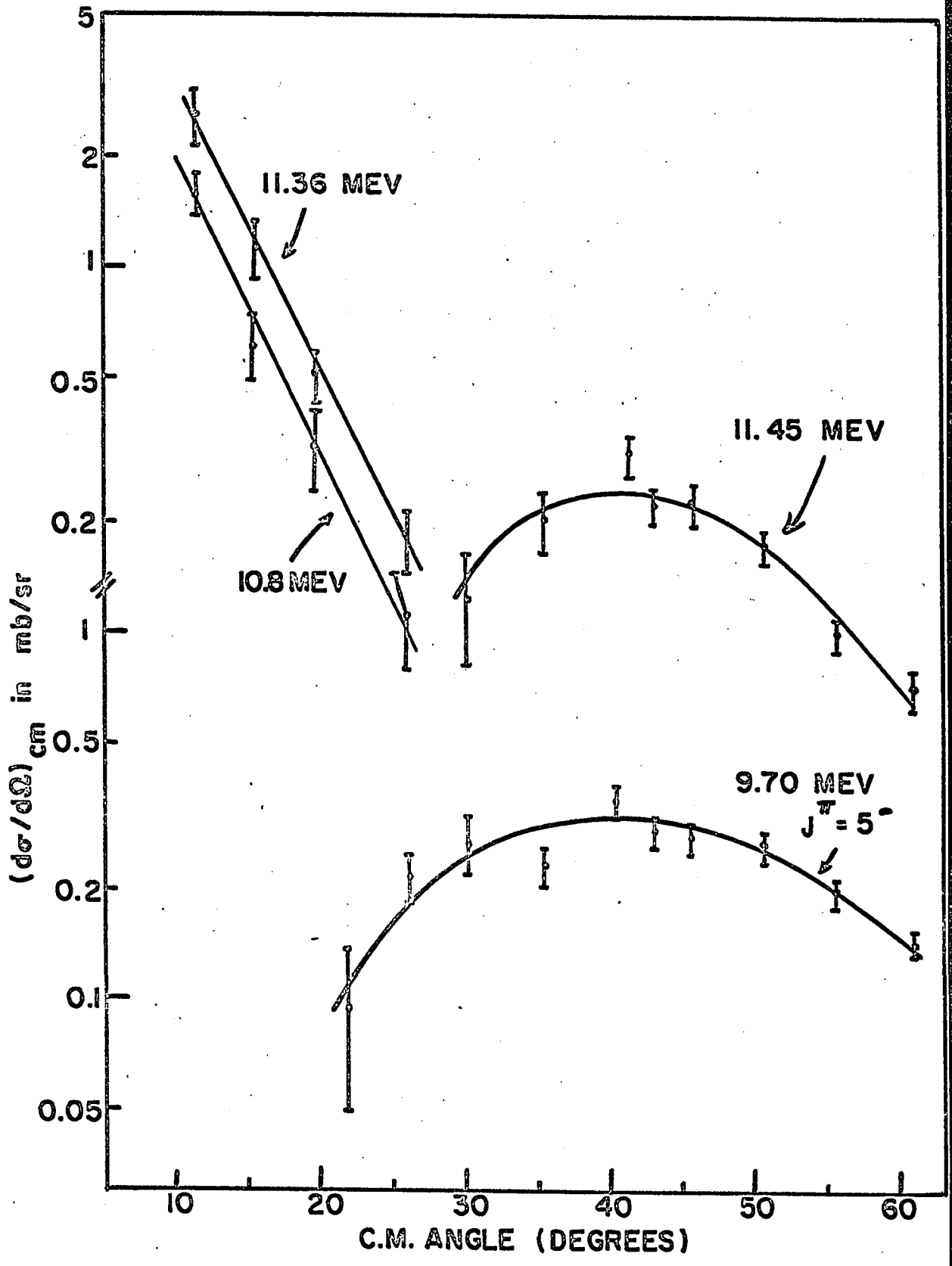
11.36 MEV
10.8 MEV
11.45 MEV
9.70 MEV
$J^{\pi} = 5^-$
$(d\sigma/d\Omega)_{cm}$ in mb/sr
C.M. ANGLE (DEGREES)
5
2
1
0.5
0.2
1
0.5
0.2
0.1
0.05
10
20
30
40
50
60

CHAPTER 9

THEORETICAL ANALYSIS

9.1 COMPARISON OF INELASTIC SCATTERING AND ELECTRIC RADIATIVE DECAY RATES

The most reliable method presently available to extract deformation parameters or equivalently transition rates (for single excitation processes) from inelastic proton scattering data is to perform a DWBA analysis with collective form factors. As previously discussed the results are usually internally consistent at various proton energies and agree reasonably well with values extracted electromagnetically or otherwise. This type of DWBA analysis has usually been restricted in its success to strongly excited E2 and E3 transitions. A. B. Clegg, 1965, however has outlined a method which suggests a comparison of the peak differential cross-section observed in (p,p') with the particular radiative transition rate involved. The approximate correctness of this comparison can be easily derived in the plane wave approximation but proceeds with somewhat more difficulty in the framework of the distorted-wave Born approximation.

Rost, 1961, has examined the effect of distortion on the relation between the $E\ell$ matrix element and the corresponding proton inelastic scattering. In a distorted wave treatment of the inelastic scattering to the 1.37 MeV 2+ state of ^{24}Mg he found the relationship holds independently of distortion. In other words collective enhancement leads to an overall multiplicative factor for the differential cross-section angular distribution if calculated from a spin-

independent nucleon-nucleon interaction.

The comparison between cross-section and radiative transition rate is of interest since it dramatically illustrates the correlation between proton ineleastic scattering and electromagnetic transitions theoretically predicted by A. Bohr, 1956.

We have for non spin-flip matrix elements in the plane wave approximation that the differential cross-section in proton inelastic scattering is proportional to the square of the integral

$$\int \psi_f^* j_\ell(qr) Y_\ell^\circ(\Theta,\Phi) \psi_i dV$$

which for small enough q, where $j_1(qr) \propto q^1 r^1$, becomes

$$q^\ell \int \psi_f^* r^\ell Y_\ell^\circ(\Theta,\Phi) \psi_i dV$$

The above integral, however, resembles very closely the radiative matrix element for the corresponding 2^1 pole transition. Unlike radiative transitions the preference factors $\sim (R/\lambda)^2$ for different multipole orders are not important. This is so because the momentum transfer in inelastic scattering varies with angle so that $\lambda = 1/q$ is under control; thus the maximum E2 cross-section will simply occur at a larger scattering angle than the corresponding maximum E1 cross-section.

If T is the radiative transition rate which goes as the square of the electromagnetic matrix element then the reduced transition rate is given by

$$B(E\ell,\ i \to f\ ) \;=\; h\ell\{\frac{(2\ell+1)!!}{8\pi(\ell+1)}\}\left(\frac{hc}{E}\right)^{2\ell+1} T$$

so that for small q, i.e., small scattering angles, the following proportionality is true:

$$\frac{d\sigma}{d\Omega} \;\propto\; q^{2\ell}\, B(E\ell)$$

The result is correct only for small q so that around the peak in the angular distribution the approximation fails. However, since j_ℓ (qR) is not expected to vary much more rapidly than r^ℓ even for larger q it is not unreasonable to expect that the ratio $B(E\ell)/\ (d\sigma/d\Omega)$ should not vary too strongly from nucleus to nucleus for larger q. This will be true only if the inelastic scattering matrix element depends on the same aspects of the nuclear wave functions as does the radiative matrix elements. Since the peak angle in the differential cross-section angular distribution varies with nuclear radius the value of q for which the angular distribution peaks also varies. In the same way the ratio, $B(E\ell\ )(d\sigma\ /d\Omega)$ at some particular q can also vary. Clegg suggests accounting for this variation by comparing $B(E\ell)$ to $(d\sigma\ /d\ \Omega\ )_{max.}$ Tables 20 and 21 compare 100 MeV inelastic scattering data and the radiative decay rates for the corresponding electric quadrupole and octupole transitions. From the previous discussion it follows that the expression

$$\tau\,(d\sigma/d\Omega)_{max}\; E^{2\ell+1}\; \frac{2I_o+1}{2I_u+1}$$

should be approximately constant, where E is the energy of the state

Table 20

COMPARISON OF INELASTIC SCATTERING AT 100 MeV AND RADIATIVE DECAY RATES FOR THE CORRESPONDING ELECTRIC QUADRUPOLE TRANSITIONS

Nucleus	Excited State MeV	τ (E2) seconds	$(d\sigma/d\Omega)_{max}$ mb/sr	Angle degrees	$\tau \frac{d\sigma}{d\Omega} E^5 \frac{2I+1}{2I_u+1} \times 10^{11}$
^{6}Li	2.18	$(1.27\pm0.13)\times10^{-12}$	7.9±0.8	12.9	15.3±2.2
^{7}Li	4.63	$(4.13\pm0.37)\times10^{-14}$	9.7±0.6	19.9	34.7±4.2
^{9}Be	2.43	$(2.5\pm0.1)\times10^{-13}$	14.9±1.5	19.7	17.0±1.9
^{9}Be	6.5	$(6.07\pm0.28)\times10^{-15}$	6.1±0.5	19.7	17.2±1.8
^{12}C	4.43	$(5.9\pm0.8)\times10^{-14}$	9.6±0.4	19.2	19.1±2.7
^{24}Mg	1.37	$(1.4\pm0.3)\times10^{-12}$	26.1±0.4	17.1	2.38±0.52
^{24}Mg	4.23	[1] $(0.102\pm0.03)\times10^{-12}$	2.4±0.2	17.1	4.5±1.3
^{28}Si	1.78	$(0.63\pm0.03)\times10^{-12}$	24.7±0.7	15.1	3.4±0.2
^{28}Si	7.4	[2] $(\lesssim 0.2)\times10^{-12}$	1.28±0.2	15.1	$\gtrsim$7.1

1,2 - T. K. Alexander et al. (1966).

Table 21

COMPARISON OF INELASTIC SCATTERING AT 100 MeV AND RADIATIVE DECAY RATES FOR CORRESPONDING ELECTRIC OCTUPOLE TRANSITIONS

Nucleus	Excited State MeV	τ (E3) seconds	$(d\sigma/d\Omega)_{max}$ mb/sr	Angle degrees	$\tau \frac{d\sigma}{d\Omega} E^7 \frac{2I+1}{2I_u+1} 10^6$
^{12}C	9.64	[1] $(0.18\pm0.02)\times10^{-11}$	2.1±0.12	24.1	4.2±0.5
^{24}Mg	8.36	[2] $(0.6)\times10^{-11}$	2.8±0.17	21.2	6.7±0.4
^{28}Si	6.88	[2] 0.84×10^{-11}	5.1±0.2	21.2	4.5±0.2
^{24}Mg	7.62	[3] 0.28×10^{-11}	2.8±0.14	21.2	1.7±0.1

1 - H. L. Crannell et al. 1964
2 - J. K. Kokame et al. 1966
3 - T. K. Alexander et al. 1966

excited, I_u its spin and I_o the spin of the ground state. The statistical factor $(2I_o + 1)/(2I_u + 1)$ simply accounts for the opposite directions of the two transitions. The radiative decay rates are from Clegg (1965) except where otherwise indicated.

From Table 20 for electric quadrupole transitions the calculated ratio is observed to be fairly constant at one value in the p shell (except for the 4.63 MeV transition in ^{7}Li) and at a considerably smaller value in the s-d shell. Note that the overall agreement in the s-d shell is improved somewhat when one recalls that the 4.23 MeV peak in ^{24}Mg almost certainly contains some contribution from the 4.12 MeV, 4+, level. Similarly the 7.4 MeV peak in ^{28}Si probably contains some contribution from the unnatural parity level at 7.38 MeV.

For electric octupole transitions the ratio is again found to be reasonably constant for the four transitions with known decay rates. For E2 transitions the ratio changes abruptly on going from the p shell nuclei to the s-d shell nuclei. This behaviour is apparently not repeated for the E3 transitions. G.Schrank et al. 1962, have suggested that the variation in the E2 ratio in going from the p shell to the s-d shell may be due to the higher angular momentum of the nucleons outside the closed shells in the s-d nuclei, and should decrease for higher angular momentum. The observation that the ratio changes abruptly on going from one shell to another is argument against the variation being due to increasing absorption as the nuclear mass increases. Similar behaviour for these ratios have been obtained by Clegg (1965) using 150 MeV proton data. Clegg points out that since

the ratio for the E3 transitions seems to show no systematic variation with mass it seems reasonable to assume that the variation in the E2 case cannot be an effect of increasing nuclear mass.

It follows that one can therefore make an estimate of an E2 or E3 transition rate from a measured proton inelastic scattering cross-section if the corresponding ratio has been determined from a transition of the same multipolarity and (for E2 only) in the same shell. Using an average value of 4.3 for the electric octupole ratio, we have extracted an estimate of 0.17×10^{-11} seconds for the octupole transition rate of the 10.18 MeV level in ^{28}Si. Because of possible contributions of other levels to the experimentally measured differential cross-sections as well as possible variation in the calculated octupole ratio no definite claim can be made to the accuracy of the estimate of this transition rate however an absolute error greater than a factor 2-3 would be surprising.

9.2 INELASTIC SCATTERING AND MAGNETIC DIPOLE RADIATIVE TRANSITIONS

In section 9.1 we showed there exists a strong correlation between (p,p') differential cross-sections and the corresponding Eℓ transition rates so that if an Eℓ transition rate is enhanced by collective effects the inelastic scattering will be also. The same correlation is not true for magnetic dipole radiative transitions. G. Morpurgo (1958) has shown that $\Delta T = 0$ M1 gamma transitions in self conjugate nuclei can be expected to be retarded by two orders of

magnitude compared to the corresponding $\Delta T = 1$ transitions. The retardation is roughly proportional to

$$\left\{ \frac{\mu_p + \mu_n - 1/2}{\mu_p - \mu_n + 1/2} \right\}^2 \simeq \frac{1}{150}$$

and is thus seen to correspond to an almost complete cancellation of the protonic, neutronic and orbital magnetic moments.

For inelastic proton scattering there does not appear to be such an inhibition. In ^{12}C two J=1+ unnatural parity states are strongly excited, one with T = 0 at 12.7 MeV and the other with T = 1 at 15.1 MeV. The unnatural parity of these levels implies that only spin-flip matrix elements can contribute to their excitation. Figure 45 illustrates the experimental ratio observed for exciting these states. For scattering angles greater than 30 degrees the measured ratio is approximately unity. It is consequently of interest to see whether the ratio for the excitation of these two levels can be explained in the framework of the impulse approximation. This approach has been investigated by Clegg (1965) who found good agreement between the theoretical and experimental ratio for 150 MeV protons over the angular range from 8 to 22 degrees (the maximum momentum transfer studied). We have carried out the same calculation for our 100 MeV data with similar results in the forward angle region. However, the agreement breaks down for scattering angles greater than 25 degrees.

A full treatment of the distorted wave impulse approximation has been given by Clegg (1965), we will give only a brief summary of the basic ideas before describing our result.

In the DWIA approximation for inelastic scattering the amplitude for scattering a proton from momentum $\vec{k}$ to momentum $\vec{k}'$ is proportional to

$$A(\vec{k},\vec{k}') = \langle J | M(q) \Phi^{-*}(\vec{k}',\vec{r}) \Phi^{+}(\vec{k},\vec{r}) | O \rangle$$

where $\phi^{-}(\vec{k},\vec{r})$ and $\phi^{+}(\vec{k},\vec{r})$ are the wave functions of the incident nucleon before and after the collision and are distorted by the optical model potential corresponding to scattering from other nucleons in the nucleus. M(q) is the free nucleon-nucleon scattering amplitude expressed as a function of the momentum transfer $\vec{q} = \vec{k}' - \vec{k}$. The differential cross-section is then given by

$$\frac{d\sigma}{d\Omega} = \left(\frac{2N}{N+1}\right)^2 \frac{k'}{k} \left| A(\vec{k}',\vec{k}) \right|^2$$

where N is the number of nucleons in the target nucleus.

The nucleon-nucleon scattering amplitude is a complicated function of the spin and isotopic spin of the nucleons involved. Assuming charge independence and invarience with respect to space and time reflection, M(q) can be expressed in the form (Wolfenstein, 1956)

$$M = A + B\vec{\sigma}_1 \cdot \hat{n} \vec{\sigma}_2 \cdot \hat{n} + C(\vec{\sigma}_1 \cdot \hat{n} + \vec{\sigma}_2 \cdot \hat{n}) + D(\vec{\sigma}_1 \cdot \hat{p} \vec{\sigma}_2 \cdot \hat{q} + \vec{\sigma}_1 \cdot \hat{q} \vec{\sigma}_2 \cdot \hat{p}) + E\vec{\sigma}_1 \cdot \hat{q} \vec{\sigma}_2 \cdot \hat{q} + F\vec{\sigma}_1 \cdot \hat{p} \vec{\sigma}_2 \cdot \hat{p}$$

where ($\hat{q}$, $\hat{n}$, $\hat{p}$) form a right-handed coordinate system given by

$$\hat{q} = \frac{\vec{k}' - \vec{k}}{|\vec{k}' - \vec{k}|} \; ; \quad \hat{n} = \frac{\vec{k} \times \vec{k}'}{|\vec{k} \times \vec{k}'|} \; ; \quad \hat{p} = \hat{q} \times \hat{n}$$

thus $\hat{q}$ is in the direction of momentum transfer to the scattered nucleon and $\hat{n}$ is perpendicular to the scattering plane. $\vec{\sigma}_1$ operates on the spin of the incident nucleon and $\vec{\sigma}_2$ on the spin of the struck nucleon.

The amplitudes A, B, C, D, E, F, are complex and are isotopic spin dependent. The amplitude D is usually taken to be zero because for D to be time reversal invariant it must be proportional to $\vec{p}.\vec{q}$ which is zero on the energy shell. In the usual KMT notation (Kerman et al. 1959) for

$$\Delta T = 0 \; ; \quad A_\alpha = \frac{1}{4}(3A_1 + A_0)$$

$$\Delta T = 1 \; ; \quad A_\beta = \frac{1}{4}(A_1 - A_0)$$

where A_1 and A_o are the T = 1, T = 0 amplitudes respectively.

For the 1+ states in ^{12}C with nearly equal excitation energy, one with T = 0 at 12.7 MeV and the other T = 1 at 15.1 MeV it is reasonable to assume that the radial wave functions as well as distortion effects will be similar. It follows therefore that the ratio of the two differential cross-sections should be approximately given by the variations of the nucleon-nucleon scattering amplitudes involved (Clegg 1965).

$$\frac{(\frac{d\sigma}{d\Omega})_{T=1}}{(\frac{d\sigma}{d\Omega})_{T=0}} \simeq \frac{(\; |C_\beta|^2+|B_\beta|^2+|F_\beta|^2 \;)}{(\; |C_\alpha|^2+|B_\alpha|^2+|F_\alpha|^2 \;)}$$

The B-B YLAM phase parameters at 100 MeV have been used by Goldstein (1967) to calculate the corresponding nucleon-nucleon scatter-

ing amplitudes as a function of θ_o (the scattering angle in the two nucleon center of mass system). An additional approximation enters here because if we treat the interaction with a bound nucleon as a nucleon-nucleon interaction, it is an interaction in which energy and momentum are not conserved (i.e., it is off the energy shell, whereas the free two nucleon interaction is one in which energy and momentum are conserved. Since the scattering amplitudes are a function of momentum transfer we have calculated the amplitude for proton-^{12}C scattering by using the nucleon-nucleon amplitudes related to the same momentum transfer. Thus if $\vec{k}$ is the momentum of theincident proton in the nucleon-nucleus center of mass system and $\vec{k}_o$ the incident momentum in the nucleon-nucleon center of mass system then

$$\frac{k}{k_o} = \frac{2A}{A+1}$$

and $$q = 2k_o \sin\frac{\theta_o}{2} \simeq 2k \sin\frac{\theta}{2}$$

therefore $$\sin\frac{\theta_o}{2} \simeq \frac{A+1}{2A} \sin\frac{\theta}{2}$$

where θ is the scattering angle in the proton-^{12}C center of mass system.

The results are illustrated in figure 45. The solid curve is the calculated ratio from the scattering amplitudes. The agreement in the forward angle region (10 - 25 degrees) is satisfactory, but the predicted ratio falls much too rapidly for angles greater than 25 degrees. D.J. Rowe et al. (1963) have studied the angular correlation

of scattered protons and gamma rays in the inelastic scattering of 147 MeV protons from the first excited state of ^{12}C. Their measurements were analysed using the DWIA and indicated a failure of the impulse approximation for angles greater than 35 degrees. Their analysis as well as ours assumed that the D scattering amplitude was equal to zero which is equivalent to assuming that off-energy-shell effects are negligible. It may be that the apparent failure of the impulse approximation for large momentum transfer is due to appreciable changes in the nucleon-nucleon scattering on going off the energy shell. This possibility offers the prospect of obtaining information about off-energy-shell scattering which cannot be obtained from nucleon-nucleon data.

To conclude, we have seen how proton inelastic scattering can pick out $\Delta T = 0$ M1 transitions which in studies of radiative transitions or electron scattering are severely inhibited and consequently inaccessible. For scattering angles less than 25 degrees the measured ratio of the $\Delta T = 1$ to $\Delta T = 0$ differential cross-sections can be explained as due mainly to the different variations of the nucleon-nucleon scattering amplitudes involved. For $\theta > 25$ degrees the disagreement between theoretical and measured values may be due to the neglect of the off-energy-shell scattering amplitudes.

9.3 OPTICAL MODEL ANALYSIS OF ELASTIC SCATTERING FROM ^{24}Mg AND ^{28}Si

This section gives the results of an optical model analysis of the elastic scattering of 100 MeV protons from ^{24}Mg and ^{28}Si. The

purpose of the analysis was two-fold. To obtain the optical potential parameters at E_p = 100 MeV as a necessary preliminary step in the theoretical analysis of the inelastic data as well as to investigate the applicability of the simple optical model for low mass highly deformed nuclei.

Theoretical fits to the experimental data were obtained using a computer program developed by Li (1968). The form of the optical potential used was

$$V(r) = V_c(r) + V_o f_o(r) + iW_v f_v(r) - i4aW_d \frac{d}{dr} f_o(r)$$

$$+ \left(\frac{h}{m_\pi c}\right)^2 \frac{1}{r} \frac{d}{dr} f_{so}(r)\, V_{so}\, \vec{S}.\vec{L}$$

where $f_x(r) = (1 + \exp(r - r_x A^{1/3})/a_x)^{-1}$ is the Saxon Woods form factor and $V_c(r)$ is the Coulomb potential for a uniformly charged sphere of radius $r_c A^{1/3}$ fm. V_o is the depth of the real potential well, W_v and W_d are the volume and surface absorption terms respectively and V_{so} is the spin-orbit potential depth. Previous studies with complex spin-orbit coupling have shown no indication of improved fits with the data so only a real spin-orbit term was used (W_{so} = 0), (Satchler, 1967; Satchler and Haybron, 1964).

The search program varies the optical model parameters so as to minimize the quantity

$$\chi^2 = \sum_{i=1}^{N} \frac{(\sigma_{exp}(\Theta_i) - \sigma_{theo}(\Theta_i))^2}{(\Delta\sigma_{exp}(\Theta_i))^2}$$

where $\sigma_{exp}\ (\theta_i)$ is the measured, and $\sigma_{theo}\ (\theta_i)$ the calculated cross-sections at angle θ_i, while $\Delta\ \sigma_{exp}\ (\theta_i)$ is the error associated with $\sigma_{exp}\ (\theta_i)$. N is the number of experimental cross-sections.

The total reaction cross-section σ_R for a wide range of nuclei at E_p = 100 MeV has been measured by Kirkby (1966). His value for magnesium (natural isotopic composition) was 399 mb. The value of σ_R for ^{28}Si has been calculated from an empirical expression which Kirkby fitted to his data with the result σ_R = 456 mb. Satchler (1967) has found in the optical model analysis of the elastic scattering of 46 MeV protons from ^{9}Be and ^{12}C that the total reaction cross-section is a useful datum for choosing between valid optical potentials i.e., between different sets of optical potentials which give equally good fits to the differential cross-section angular distributions. Our results at 100 MeV for ^{24}Mg and ^{28}Si are in striking agreement with this finding. This is in contrast to the results of analyses on heavy nuclei where it has been found that different good fits to the differential cross-sections usually predict the absorption cross-section equally well (G. R. Satchler, 1967; F. G. Perey, 1963).

Because of the rather limited range of angles we have studied (10^{o}-60^{o}) as well as the unavailability of polarization data it was imperative to limit the number of varying parameters in the optical potential as much as possible. To this end we have used as a starting point the optical model radius and diffuseness parameters obtained by Rush et al. (1967) in a study of the elastic scattering of 50 MeV protons by ^{24}Mg. Their data extended over an angular retion from 10 to 140 degrees and polarization data was also available over the same

region. Most recent analyses (Fricke et al. 1967; Satchler, 1967; Ruch et al. 1967) indicate that the spin-orbit form factors need to be different from the real central form factors. This result is indicated only when polarization data is also being analysed. In order to parallel the analysis of Ruch (1967) we also use independent spin-orbit coupling ($r_{so} \neq r_o$, $a_{so} \neq a_o$). Table 22 shows the best fit 100 MeV proton optical potentials we have obtained for ^{24}Mg.

Table 22

OPTICAL POTENTIALS FOR 100 MeV PROTONS SCATTERED FROM ^{24}Mg

Columns c, f, and i are the best-fit optical potentials for E_p = 100 MeV. Columns a, d and g are best-fit optical potentials at 50 MeV from Rush et al. (1967).

	a	b	c	d	e	f	g	h	i
V_o(MeV)	44.68	27.88	22.09	39.98	28.25	23.14	45.71	35.37	27.03
r_o(fm)	1.10	(1.10)	1.27	1.14	(1.14)	1.25	1.10	(1.10)	1.21
a_o(fm)	0.74	(0.74)	0.68	0.724	(0.724)	0.70	0.694	(0.694)	0.44
W_v(MeV)	7.90	10.87	7.23	6.80	11.13	10.23	--	--	--
r_v(fm)	1.50	(1.50)	(1.50)	0.76	(0.76)	(0.76)	--	--	--
a_v(fm)	0.53	(0.53)	0.53	0.274	(0.274)	(0.274)	--	--	--
W_d(MeV)	--	--	--	5.94	8.14	5.15	7.45	10.14	12.09
r_d(fm)	--	--	--	1.21	(1.21)	(1.21)	1.17	(1.17)	1.248
a_d(fm)	--	--	--	0.639	(0.639)	(0.639)	0.697	(0.697)	0.563
V_{so}(MeV)	5.61	14.18	9.89	6.03	11.81	8.51	7.71	13.64	6.04
r_{so}(fm)	1.00	(1.00)	(1.00)	1.03	(1.03)	(1.03)	0.98	(0.98)	0.788
a_{so}(fm)	0.60	(0.60)	(0.60)	0.588	(0.588)	(0.588)	0.647	(0.647)	0.664
χ^2/n	24.6	1.17	1.01	6.65	1.76	0.41	23.2	23.4	3.07
σ_R(mb)	588.6	542	429	591	556	428	649	618	600

1 - r_c = 1.25fm following Rush et al. (1967)

2 - Parameters in brackets were held constant.

Our procedure in obtaining these optical potentials was to adopt the Rush radius and diffuseness parameters and only allow the potential depths to vary. In the volume absorptive case (column b) the resulting fit to the elastic angular distribution was excellent ($\chi^2/N = 1.17$), however the theoretically predicted total reaction cross-section was 542 mb in comparison with the experimental value of 399 ± 40 mb. The expected increase in the total reaction cross-section as E_p goes from 100 MeV to 50 MeV, furthermore, cannot account for the predicted value of 589 mb for σ_R at 50 MeV. Rush et al. were apparently unaware of Kirkby's measurements and accept 500-600 mb as a reasonable value for σ_R at 50 MeV. The 40% difference between the experimental and theoretically predicted raction cross-sections at 100 MeV was, however, clearly unacceptable. Column c shows the optical potential parameters which give excellent agreement with both the elastic differential cross-sections and the experimental value of σ_R. Note that the radius and diffuseness parameters for the spin-orbit and imaginary potentials are unchanged.

The procedure which led us to this optical potential is as follows. Li et al. (1968) have recently completed an optical model analysis of 100 MeV elastic proton scattering from 1p shell nuclei. The average predicted absorption cross-sections were from 200 mb to 300 mb with an average value of 1.33 fm for r_o and 0.64 fm for a_o. These values suggested to us the possibility of reducing the predicted absorption cross-section by increasing r_o and decreasing a_o in discrete steps and at the same time allowing the potential depths to vary for each discrete choice of a_o and r_o. The results are shown in column c

and the fit to the angular distribution in figure 46. Both the total reaction cross-section and the differential cross-sections are extremely well predicted.

The same procedure was carried out in columns d-f with a mixture of volume and surface absorption with identically good results. Columns g - i show the best-fit optical potentials obtained using surface absorption only. As before we used the 50 MeV parameters and allowed the potential depths to vary. This time, however the resulting fit to the differential cross-sections was poor ($\chi^2/N = 23.4$). Allowing all nine parameters to vary gave an improved fit to the differential cross-sections but did not improve the discrepancy between the theoretical and experimental values for σ_R, nor did the procedure previously outlined improve this discrepancy. Figure 47 illustrates the fit to the differential cross-sections using surface absorption only. This result (preference for volume absorptive potentials at 100 MeV) is in agreement with analyses of elastic data at 180 MeV which also preferred volume absorption for all but very light nuclei. (G.R. Satchler and R. M. Haybron, 1964).

Table 23 shows the best-fit 100 MeV proton optical potentials we have obtained for ^{28}Si. The corresponding optical potentials for ^{24}Mg are listed for comparative purposes. As can be seen the difference between the ^{24}Mg and ^{28}Si parameters is small. Several different sets of initial parameters were tried for ^{28}Si. R. M. Haybron (1965) has obtained optical potentials (constrained spin-orbit coupling) for 155 MeV proton scattering from ^{28}Si. We attempted to fit our 100 MeV data using the radial and diffuseness parameters of Haybron and

allowing the potential depths to vary, but this procedure did not yield good fits. A similar attempt using the parameters obtained from the ^{24}Mg analysis also failed in the volume absorptive case. Good fit to the differential cross-sections was finally obtained by allowing all nine parameters to vary. As in the case of ^{24}Mg it was then found necessary to change r_o and a_o in discrete steps and allow the potential depths to vary in order to obtain agreement with the expected value of the total reaction cross-section.

For surface absorptive potentials and potentials with a mixture of volume and surface absorption the ^{24}Mg parameters served as a good starting point and it was necessary only to vary the potential depths to obtain good fits to the differential cross-sections. These fits to the angular distribution are illustrated in figures 48 and 49. The final χ^2 fit in the surface absorption case obtained by varying all nine parameters showed no improvement over the fit obtained by varying only the potential depths.

To conclude, we have obtained optical model potentials for ^{24}Mg and ^{28}Si using both volume absorptive potentials (W_d=0), surface absorptive potentials (W_v = 0) and a mixture of volume and surface absorptive potentials. Definite preference to volume absorptive potentials is indicated in agreement with the analysis of Satchler (1964) who found that at 180 MeV nuclei above A = 40 definitely prefer volume absorption. The inferior surface absorptive fits led us to include in the analysis optical potentials using a mixutre of volume and surface absorption. Following Rush et al. (1967) excellent fits were

obtained both to the differential cross-sections and the total reaction cross-section. It should be remembered, however, that recent results (Satchler, 1967; Satchler and Haybron, 1964) indicate that when a mixture of volume and surface absorption is used the individual values of W_v and W_d are very poorly determined.

An interesting and possibly very useful effect we have observed is that the total reaction cross-section may provide a means of reducing the ambiguities in the parameters defining the optical model potential. Satchler (1967) has recently observed the same result in an analysis of 46 MeV elastic proton scattering from ^{9}Be and ^{12}C. Li et al. (1968) however have not observed this effect in a recently completed analysis of 100 MeV proton elastic scattering from 1p shell nuclei. The procedure we have adopted to obtain good fits to both the differential cross-sections and the total reaction cross-sections appears to be physically reasonable for several reasons. The fits to the experimental data are very good, moreover, the induced variation in the optical model parameters was very similar for both ^{24}Mg and ^{28}Si. An interesting extension of this analysis would be to see if the radial and diffuseness parameters in the 100 MeV optical model potentials would give good fits to the 50 MeV elastic scattering, polarization and total reaction cross-section data for ^{24}Mg.

Table 23

OPTICAL POTENTIALS FOR 100 MEV PROTONS SCATTERED FROM ^{28}Si AND ^{24}Mg

V_o(MeV)	21.73	22.09	23.26	23.14	27.33	27.03
r_o(fm)	1.27	1.27	1.26	1.25	1.21	1.21
a_o(fm)	0.68	0.68	0.68	0.70	0.44	0.44
W_v(MeV)	6.18	7.23	11.00	10.23	--	--
r_v(fm)	1.55	1.50	0.76	0.76	--	--
a_v(fm)	0.42	0.53	0.27	0.27	--	--
W_d(MeV)	--	--	5.32	5.15	12.57	12.09
r_d(fm)	--	--	1.21	1.21	1.25	1.25
a_d(fm)	--	--	0.64	0.64	0.56	0.56
V_{so}(MeV)	9.54	9.89	8.76	8.51	3.05	6.04
r_{so}(fm)	1.08	1.00	1.03	1.03	0.78	0.79
a_{so}(fm)	0.61	0.60	0.59	0.59	0.67	0.67
χ^2/N	5.1	1.0	4.6	0.4	9.5	3.1
σ_R	447	429	480	428	667	600
	^{28}Si	^{24}Mg	^{28}Si	^{24}Mg	^{28}Si	^{24}Mg

FIGURE 45

FIGURE 45

Ratio of the measured differential cross-sections for exciting the J = 1+, T=1 state of ^{12}C at 15.1 MeV to that for exciting the J = 1+, T=0 state at 12.7 MeV. The solid curve is the corresponding ratio of the nucleon-nucleon scattering interaction.

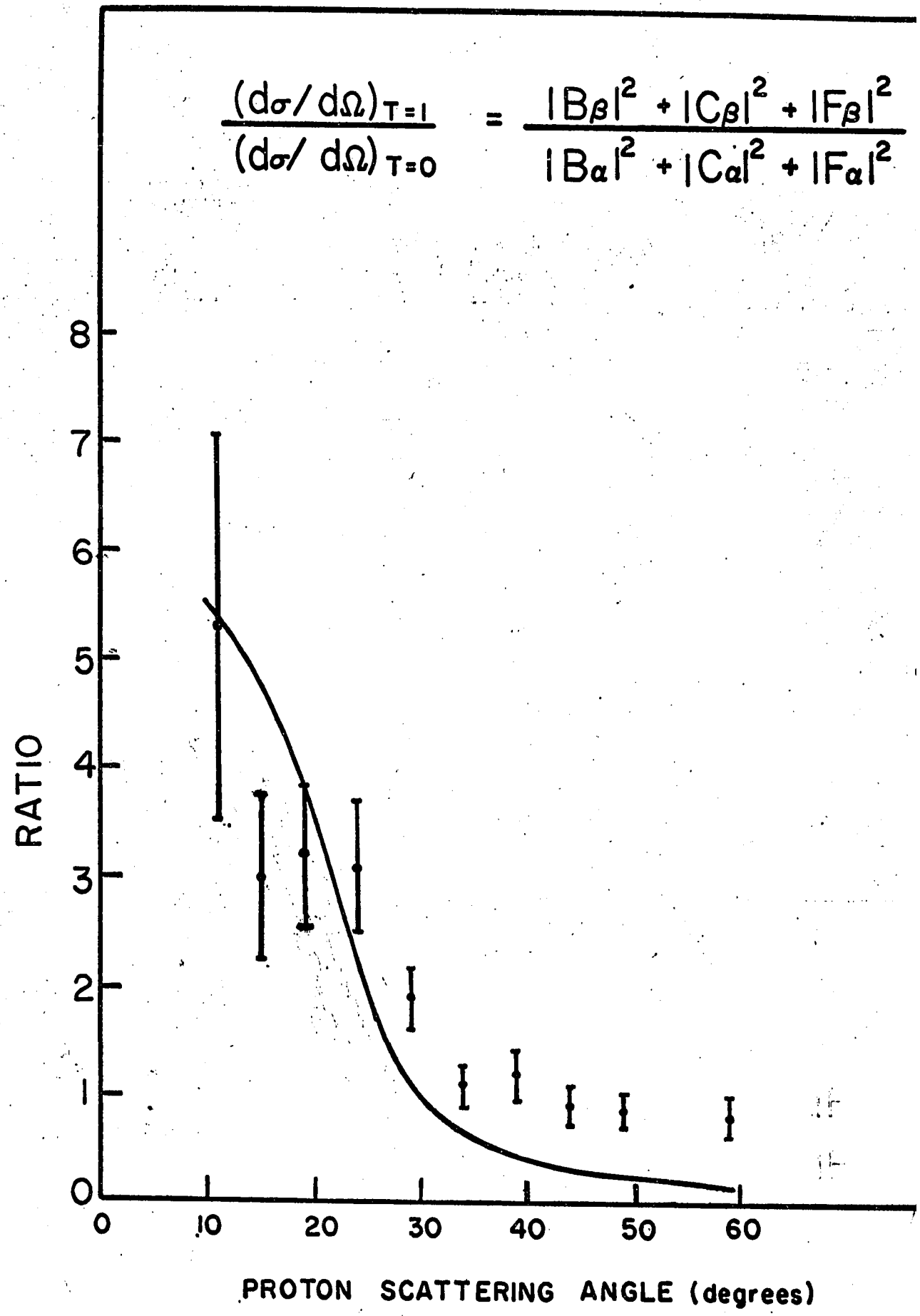
$\frac{(d\sigma/d\Omega)_{T=1}}{(d\sigma/d\Omega)_{T=0}} = \frac{|B\beta|^2 + |C\beta|^2 + |F\beta|^2}{|B\alpha|^2 + |C\alpha|^2 + |F\alpha|^2}$
RATIO
0
1
2
3
4
5
6
7
8
0
10
20
30
40
50
60
PROTON SCATTERING ANGLE (degrees)

FIGURE 46

FIGURE 46

Optical model fit to $^{24}Mg(p,p)^{24}Mg$ using an optical potential containing a volume imaginary term.

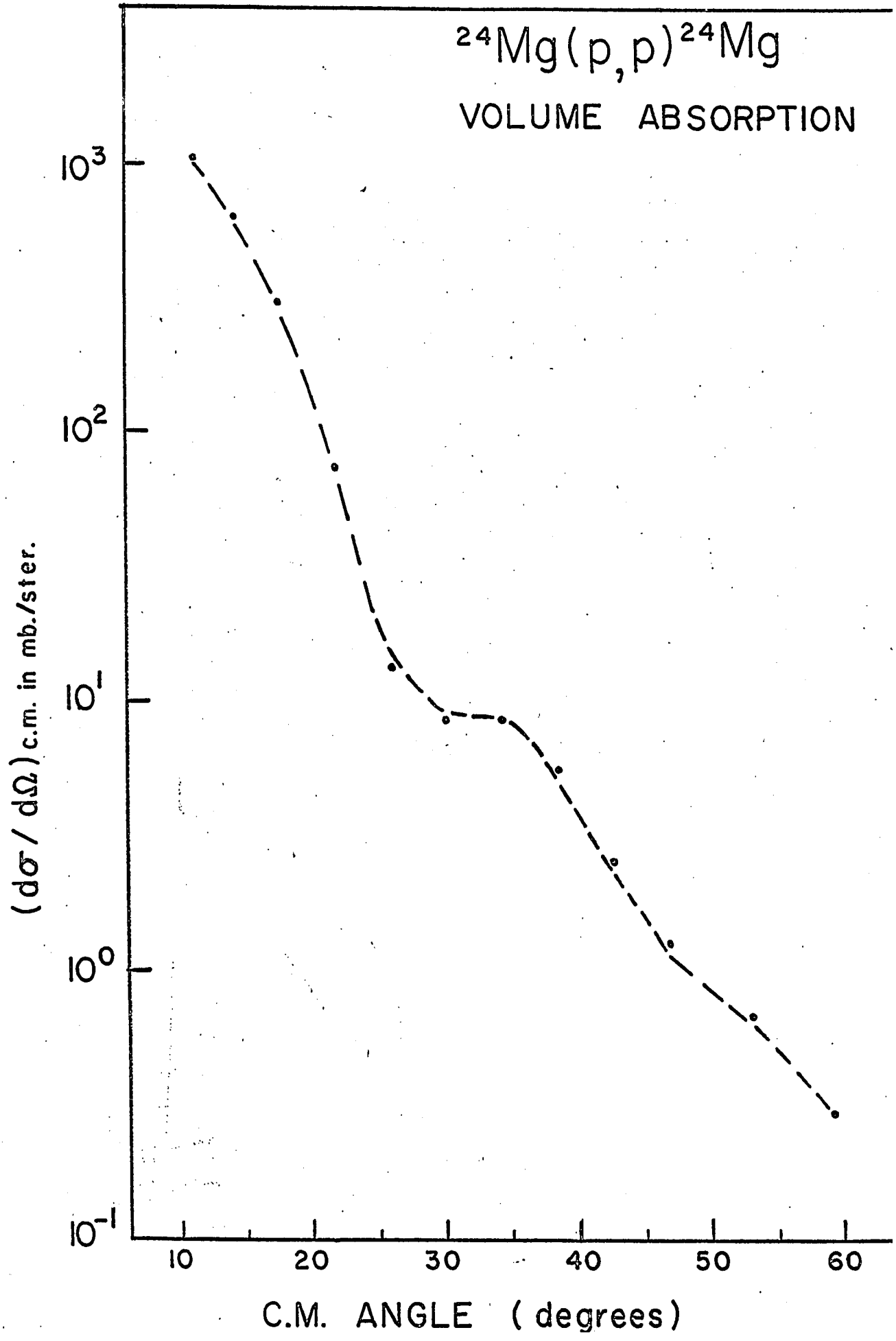
$^{24}Mg(p,p)^{24}Mg$
VOLUME ABSORPTION
10^3
10^2
10^1
10^0
10^{-1}
$(d\sigma / d\Omega)_{c.m.}$ in mb./ster.
10
20
30
40
50
60
C.M. ANGLE (degrees)

FIGURE 47

FIGURE 47

Optical model fit to $^{24}Mg(p,p)^{24}Mg$ using an optical potential containing a surface imaginary term.

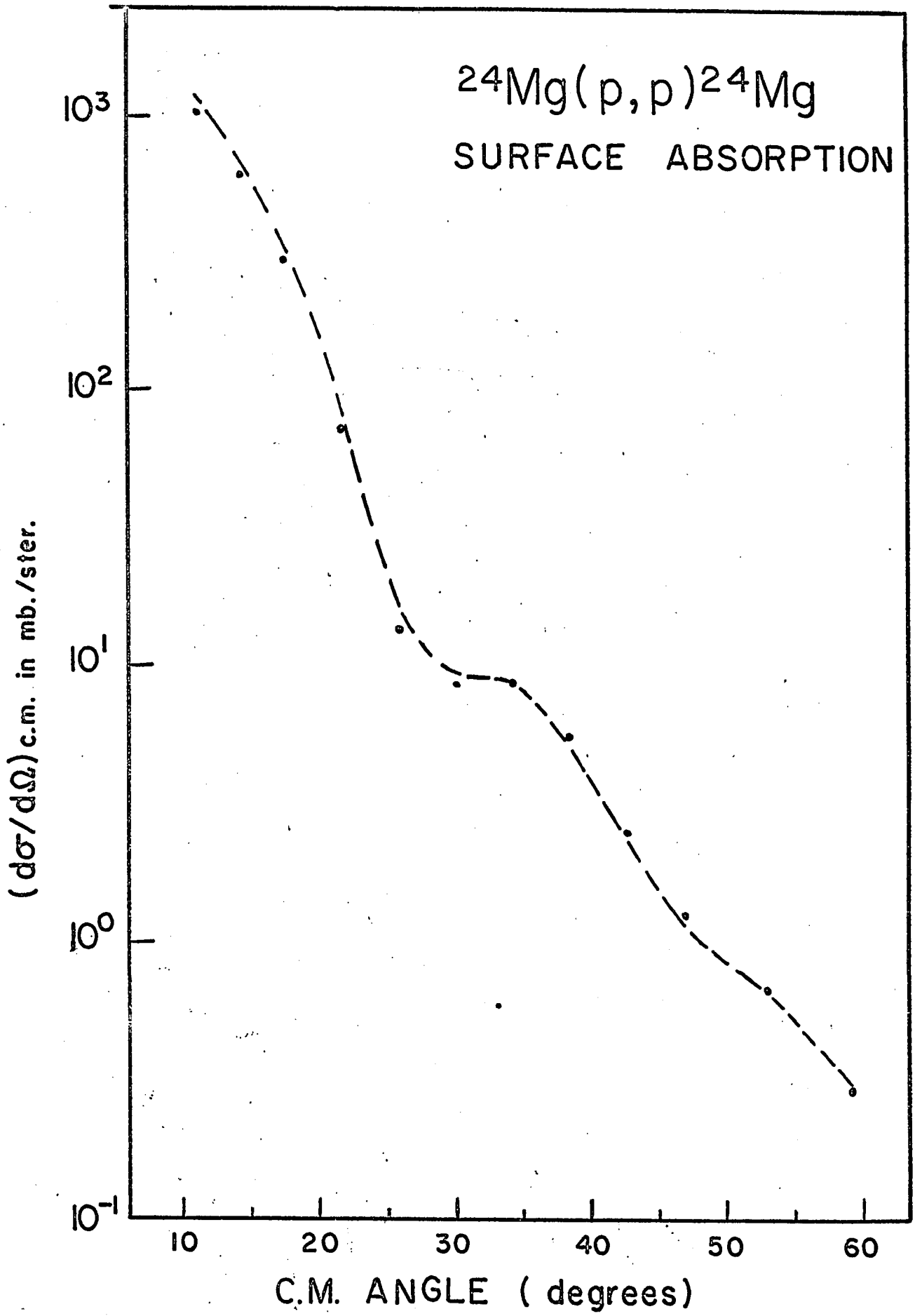
$^{24}Mg(p,p)^{24}Mg$
SURFACE ABSORPTION
10^3
10^2
10^1
10^0
10^{-1}
$(d\sigma/d\Omega)$ c.m. in mb./ster.
10
20
30
40
50
60
C.M. ANGLE (degrees)

FIGURE 48

FIGURE 48

Optical model fit to $^{28}Si(p,p)^{28}Si$ using an optical potential containing a volume imaginary term.

FIGURE 49

FIGURE 49

Optical model fit to $^{28}Si(p,p)^{28}Si$ using an optical potential containing a surface imaginary term.

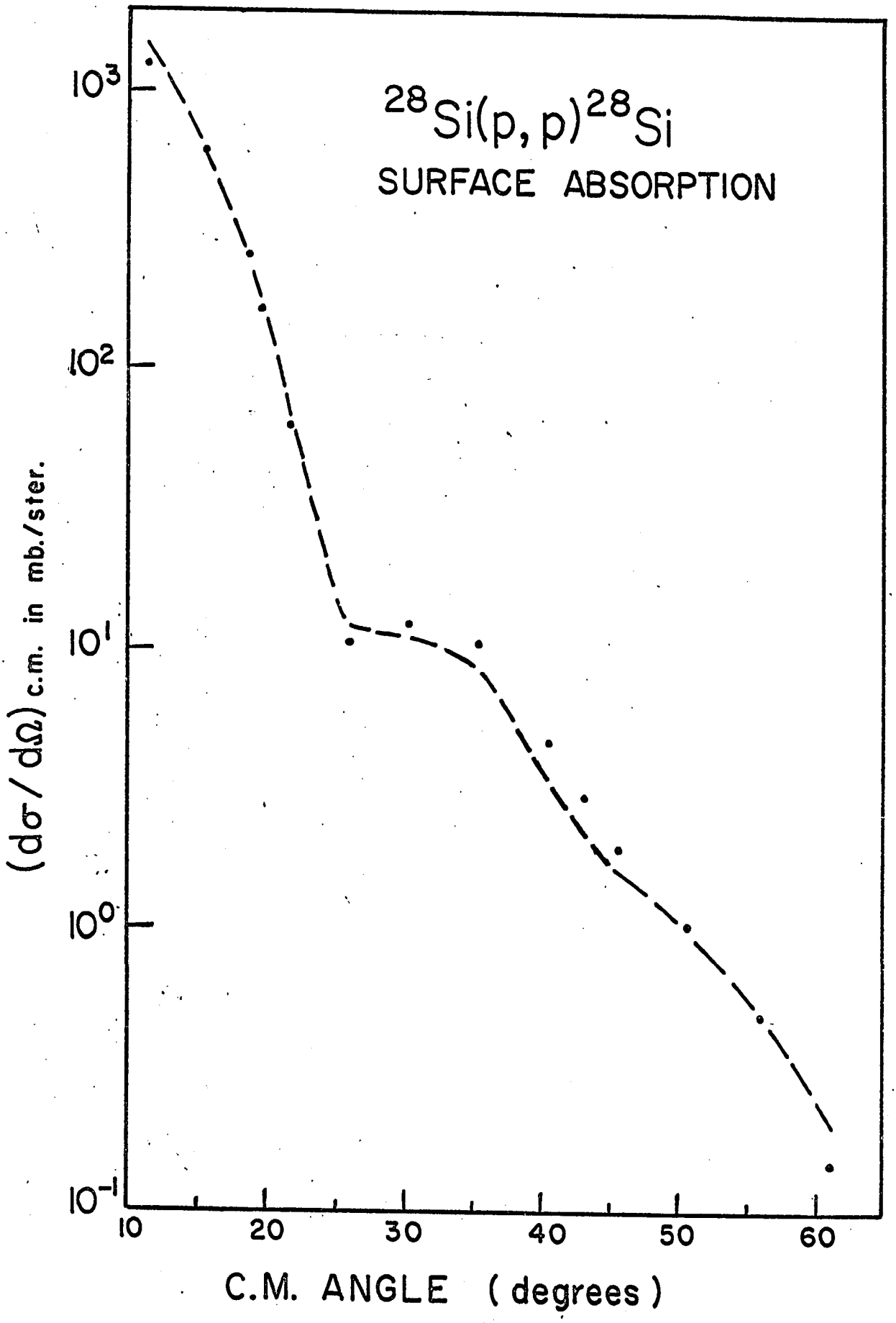
$^{28}Si(p, p)^{28}Si$
SURFACE ABSORPTION
10^3
10^2
10^1
10^0
10^{-1}
$(d\sigma / d\Omega)$ c.m. in mb./ster.
10
20
30
40
50
60
C.M. ANGLE (degrees)

CHAPTER 10 - SUMMARY AND CONCLUSIONS

10.1 Germanium Detectors as Total Absorption Proton Counters

Intermediate Energy proton scattering experiments using total absorption scintillation counters are severely disadvantaged because of inadequate energy resolution. The need for a 100 MeV proton total absorption counter with good energy resolution prompted our investigation into the use of lithium drifted germanium detectors as total absorption counters. Because of limitations in the depth of the depleted region the detectors are used in side-entry orientation to acquire sufficient thickness to stop 100 MeV protons. A single unit scattering chamber-cryostat was designed and constructed so as to allow the efficient use of these detectors in inelastic proton scattering experiments. Our experiment with these detectors constitutes the first use of germanium detectors as total absorption counters for proton energies above 60 MeV.

An overall experimental energy resolution of 0.4 MeV has been achieved almost all of which we believe is due to beam spread. This figure is as good as the best energy resolution presently attainable with magnetic spectrometers in the 100 MeV to 200 MeV energy region and roughly three times better than the energy resolution presently obtainable with NaI(Tl) counters at 100 MeV. The germanium detectors have a great advantage over magnetic spectrometers in that the entire energy spectrum is obtained simultaneously in one detector. In contrast the Uppsala group at 185 MeV obtain their energy spectra in steps of 0.4 MeV. This improved data collection rate has, for example, allowed us to easily extend the region of measurement out to 60° whereas the spectrometer experiments at 155 MeV and 185 MeV have been carried out to only 30° - 40°.

Our inadequate knowledge of the beam energy spread has hampered our study of the detector's intrinsic response to 100 MeV protons however we have extracted a tentative estimate of 0.160 ± 0.060 MeV for the detector's energy resolution for 100 MeV protons. With the advent of new intermediate energy accelerators having high resolution proton beams the use of these detectors should yield overall experimental resolutions of approximately 0.1% - 0.2%.

One unfortunate aspect of the germanium detectors is their sensitivity to radiation damage, however improved methods of recovery may eventually eliminate this drawback. The small sensitive volume of the detectors also presents special problems (multiple scattering of protons out of the sensitive volume - the severity of this problem increases with increasing proton energy; alignment problems etc..) however as we have shown these difficulties are by no means insurmountable. Our conclusion is that present "state of the art" lithium drifted germanium detectors can serve as excellent total absorption counters for intermediate energy proton scattering experiments.

10,2 Summary of Experimental Results

Two nuclei in the 2s-1d shell, ^{24}Mg and ^{28}Si, as well as ^{12}C in the p shell were studied by means of elastic and inelastic scattering of 100 MeV protons. The measurements cover an angular region from 10° to 60° degrees and excitation energies up to 16.5 MeV. Differential cross-section angular distributions have been presented for 35 peaks in the energy spectra. At energies above 100 MeV no data is available for proton inelastic scattering leading to the 10.8 MeV, 11.8 MeV or 14.1 MeV states

in ^{12}C and our measurements therefore constitute the first angular distribution data for these states in the intermediate energy region. The shape of the angular distribution for the 14.1 MeV level in ^{12}C is strongly dissimilar to the two 2+ angular distributions for the 4.43 MeV and 16.1 MeV states in ^{12}C and is therefore suggestive of a 4+ assignment to the 14.1 MeV level. The excitation of a previously unknown level in ^{28}Si at an excitation energy of 11.45 $\pm$ 0.12 MeV has been observed. The level most probably has $J^{\pi} = 5^-$ and may therefore be the 5^- level belonging to the $K=3^-$ band in ^{28}Si. Definite identification however, must await a study of the γ ray decay of the level. Our measurements also confirm the $J^{\pi} = 3^-$ (with an outside possibility of 1^-) assignment to the 10.18 MeV level in ^{28}Si and the 5^- assignment for the 9.70 MeV level also in ^{28}Si. An interesting observation is that the levels in ^{28}Si assigned an oblate shape the same as the ground state (Das Gupta and Harvey, 1967) appear to be strongly excited whereas the prolate shaped configurations are very weakly excited. The measurements thus seem to confirm the Hartree Fock calculations of Das Gupta.

A qualitative discussion of the excited states which correspond to the observed peaks has been presented and was based mainly on shapes of angular distributions. Several interesting features have emerged. Shapes of angular distributions for strongly excited $0+ - 2+$ and $0+ - 3^-$ transitions appear energy and shell independent. The angular distributions have a dominant peak at an angle which increases with angular momentum transfer and then are observed to decrease more or less monotonically with increasing angle. These features are observed at 100 MeV, 155 MeV and

185 MeV. Significant differences exist however for 0+ - 0+ and 0+ - 4+ transitions. In the s-d nuclei the 0+ - 0+ angular distributions are characterized by a clear oscillatory pattern and deep minimum at the forward angles. This characteristic shape is also observed at 55 MeV and 185 MeV in the s-d nuclei. In ^{12}C however the 0+ - 0+ angular distribution we observe is very broad and shows no oscillatory structure. The 185 MeV 0+ - 0+ angular distribution in ^{12}C shows the same characteristics however the difference between the s-d shell and p shell 0+ - 0+ angular distributions is not as well brought out because their measurements extend out to only 40°. For 0+ - 4+ transitions the angular distributions at 100 MeV show a rise in the cross-section in the forward angle region in addition to the expected characteristic maximum at larger angles. This feature is observed at 55 MeV but not at 185 MeV. The salient correlation which emerges is that 0+ - 2+ and 0+ - 3^- transitions which are expected to be direct excitation processes show essentially identical characteristic angular distributions at many different incident intermediate proton energies (55 MeV, 100 MeV, 155 MeV and 185 MeV) and also for different nuclei irrespective even of shell (^{24}Mg and ^{28}Si in the s-d shell, ^{12}C in the p shell). On the other hand 0+ - 0+ and 0+ - 4+ transitions which are expected to be a mixture of multiple and direct excitation processes show angular distributions with characteristics which are both shell and energy dependent.

A comparison between proton inelastic scattering and radiative decay rates has been presented. The comparison successfully illustrates the correlation between proton inelastic scattering and electric quadrupole and octupole transitions. The E3 transition rate for the 10.18 MeV level

in ^{28}Si is estimated to be approximately 0.17×10^{-11} seconds. The correlation between inelastic proton scattering and radiative decay rates is shown to fail for M1 transitions in self-conjugate nuclei. No retardation is experimentally observed for M1 $\Delta T = 0$ transitions compared to M1 $\Delta T = 1$ transitions in inelastic proton scattering. For scattering angles less than 25° the measured ratio of the M1 $\Delta T=1$ to $\Delta T =0$ differential cross-sections in ^{12}C can be explained as due mainly to the different variations of the nucleon-nucleon scattering amplitudes involved. For scattering angles greater than 25° the disagreement between theoretical and measured values may be due to neglect of the off energy shell scattering amplitudes.

An optical model analysis was carried out for 100 MeV proton elastic scattering from ^{24}Mg and ^{28}Si. A definite preference for volume absorptive potentials was found in agreement with other recent analyses at 180 MeV. An additional interesting effect we have observed is that the total reaction cross-section can provide a means of reducing ambiguities in the parameters defining the optical model potential. A similar effect has been observed by Satchler in the 46 MeV elastic scattering of protons from ^{9}Be and ^{12}C. This result is in contrast to the results of analyses on heavy nuclei where it has been found that different good fits to the differential cross-sections usually predict the absorption cross-section equally well.

REFERENCES

ALEXANDER T.K., BROUDE C., LITHERLAND A.E., SMULDERS P.J.M., Atomic Energy of Canada Ltd. PR-70,71 (1966)

ALEXANDER T.K., et al., "Proceedings of the International Conference on Nuclear Physics", Gatlinburg,Tennessee 1966 (unpublished)

ANTMAN S.O.W., LANDIS D.A., PEHL R.H., Nucl. Inst.& Meth. 40 (1966)272

ANYAN-WEISS N., 1968 (private communication)

AUSTERN N., DRISKO R.M., ROST E., SATCHLER G.R., Phys. Rev. 128 (1962) 733

BALDINGER E., FRANZEN W., "Advances in Electronics and Electron Physics", N.Y., 1956 Academic Press Inc., 255

BARBER W.C., BERTHOLD F., FRICKE G., GUDDEN F.E., Phys. Rev. 120 (1960) 2081

BARBER W.C., GOLDEMBERG J., LEWIS JR.F.H., WALECKA J.D., Phys. Rev. 134 (1964) B1022

BARNARD R.W., JONES G.D., Nucl. Phys. A108 (1968) 655

BERTRAND F.E., PEELE R.W., LOVE T.A., FOX R.J., HILL N.W., TODD H.A., IEEE Trans. Nucl. Sci. NS-13 (1966) 279

BETHE H.A., Z. Phyzik 76 (1938) 293

BINGHAM F.W., Phys. Rev. 145 (1966) 901

BOHR A., Physica 22 (1956) 963

BRINKLEY T.A., ROBSON B.A., TITTERTON E.W., Proc. Phys. Soc. 84 (1964) 201

CANADA T.R., BENT R.D., HASKETT J.A., Bull. Amer. Phys. Soc. 12 (1967) 570

COHEN A.V., COOKSON J.A., Nucl. Phys. 29 (1962) 604

COHEN B.L., RUBIN A.G., Phys. Rev. 111 (1958) 1568

CLEGG A.B., "Proceedings of the Rutherford Jubilee International Conference", Heywood & Co.Ltd., Ed. Birks J.B., (1961) 96

CLEGG A.B., "High Energy Nuclear Reactions", Clarendon Press, Oxford (1965)

COLE R.K., WADDELL C.N., DITTMAN R.R., SANHU H.S., Nucl. Phys. 75 (1966) 241

CONWELL E.M., Proc. IRE 46 (1958) 1281

CORMACK A.M., Nucl. Inst. & Meth. 15 (1962) 268

CRANNELL H.L., GRIFFY T.A., Phys. Rev. 136 (1964) B1580

DAHLGREN S., JOHANSSON A., RENBERG P.U., SUNDBERG O., TIBELL G., Nucl. Phys. A90 (1967) 673

DAS GUPTA S., HARVEY M., Nucl. Phys. A94 (1967) 602

DEARNALEY G., NORTHROP D.C., "Semi-conductor Counters for Nuclear Radiations", E. & P.N. Spon Ltd., London (1963)

DICKSON J.M., SALTER D.C., Nuovo Cimento 6 (1957) 235

EL-SHISHINI M.M., ZOBEL W., IEEE Trans. Nucl. Sci. NS-13 (1966) 359

ENDT P.M., VAN DER LEUN C., Nucl. Phys. A105 (1967) 1

EWAN G.T., TAVENDALE A.J., Can. Jour. of Phys. 42 (1964) 2286

FAESSLER A., GREINER W., SHELINE R.K., Nucl. Phys. 70 (1965) 33

FANO U., Phys. Rev. 72 (1947) 26

FRICKE M.P., GROSS E.E., MORTON B.J., ZUCKER A., Phys. Rev. 156 (1967) 1207

GILLET V., VINH MAU N., Nucl. Phys. 54 (1964) 321

GOLDSTEIN N.P., PhD Thesis (unpublished) 1967 McGill University

GOULDING F.S., Nucl. Inst. & Meth. 43 (1966) 1

GRUHN C.R., KUO T.K., GOTTSCHALK B., KANNENBERG S., WALL N.S., Phys. Lett. 24B (1967) 266

HASSELGREN D., RENBERG P.U., SUNDBERG O., TIBELL G., Nucl. Phys. 69 (1965) 81

HAYBRON R.M., Nucl. Phys. 79 (1966) 33 and references therein

HIRD B., KUEHNER J.A., ALMQVIST E., BRASSARD C., Can. Jour. of Phys. 42 (1964) 153

HODGMAN C.D., Ed., "Handbook of Chemistry and Physics", Chemical Rubber Publishing Co. (1962)

HOROWITZ Y.S., SHERMAN N.K., Bull. Amer. Phys. Soc. 12 (1967) 632

HOROWITZ Y.S., SHERMAN N.K., Can. Jour. of Phys. 45 (1967) 3265

HOROWITZ Y.S., SHERMAN N.K., Nucl. Inst. & Meth. 56 (1967) 106

HOUDAYER A., MARK S.K., BELL R.E., Nucl. Inst. & Meth. 59 (1968) 319

JACMART J.C., GARRON J.P., RIOU M., RUHLA C., Phys. Lett. 8 (1964) 269

JOHNSTON L.H., SERVIDE D.H., SWENSON D.A., IRE Trans. Nucl. Sci. NS-5 (1958) 95

KAWAI M.,TERASAWA T., IZUMO K., Nucl. Phys. 59 (1964) 289

KERMAN A.K., MCMANUS H., THALER R.M., Annals of Physics 8 (1959) 551

KIRKBY P., LINK W.T., Can. Jour. of Phys. 44 (1966) 1847

KOKAME J., NONAKA I., KOIKE M.,MATSUDA K., KAMITSUBO H., AWAYA W., WADA T., "Proceedings of the International Conference on Nuclear Structure", Tokyo (1967) 351

KOKAME J., FUKUNAGA F., NAKAMURA H., Phys. Lett. 20 (1966) 672

KUEHNER A.J., ALMQVIST E., Bull. Amer. Phys. Soc. 10 (1965) 37

KURATH D., Phys. Rev. 134 (1964) B1025

LAM S.T., AZUMA R.E., LITHERLAND A.E., Bull. Amer. Phys. Soc. 13 (1965) 673

LEE H.K., MCMANUS H., Phys. Rev. 161 (1967) 1087

LI T.Y., MARK S.K., to be published in Nucl. Phys. (1968)

LIESEM H., Z. Phys. 196 (1966) 174

LINDHARD J., NIELSEN V., Phys. Lett. 2 (1962) 209

LITHERLAND A.E., ALEXANDER T.K., SMULDERS P.J.M., Bull. Amer. Phys. Soc. 11 (1966) 65

LIU M., JACMART C., RICCI R.A., RIOU M., RUHLA C., Nucl. Phys. 75 (1966) 481

LOCARD P.J., BENENSON W., AUSTIN S.M., Bull. Amer. Phys. Soc. 13 (1968) 674

MAKINO M.Q., WADDELL C.N., EISBERG R.M., Nucl. Inst. & Meth. 60 (1968) 109

MANN H.R., BILGER H.R., SHERMAN I.S., IEEE Trans. Nucl. Sci. NS-13 (1966) 252

MANN H.M., YNTEMA J.L., IEEE Trans. Nucl. Sci. NS-11 (1964) 201

MANNING M.R., VOLKOV A.B., Phys. Lett. 26B (1967) 60

MARK S.K., PORTNER P.M., MOORE R.B., Can. Jour. of Phys. 44 (1966) 2961

MEASDAY D.F., Nucl. Inst. & Meth. 34 (1965) 353

MEYER O., LANGMAN H.J., Nucl. Inst. & Meth. 39 (1966) 119

MORINAGA H., Internal Report, BNL 10027 (1963)

MORPURGO G., Phys. Rev., 110 (1958) 721

NAQUIB I.M., BLAIR J.S., Phys. Rev. 165 (1967) 1250

PEHL R.H., LANDIS D.A., GOULDING F.S., JARRET B.V., Phys. Lett. 19 (1965) 495

PEHL R.H., LANDIS D.A., GOULDING F.S., IEEE Trans. Nucl. Sci. NS-13 (1966) 274

PEREY F.G., Phys. Rev. 131 (1963) 745

PINKSTON W.T., SATCHLER G.R., "Proceedings of the International Conference on Nuclear Structure", Eds. BROMLEY D.A., VOGT E.,(University of Toronto Press, Toronto 1961) p.394

PORTNER P.M., MOORE R.B., Can. Jour. of Phys. 43 (1965) 1904

PORTNER P.M., PhD Thesis (unpublished) 1967 McGill University

ROBINSON S.W., BENT R.D., Phys. Rev. 168 (1967) 1266

ROST E.S., University of Pittsburgh Thesis , 1961 (unpublished)

ROWE D.J., SALMON G.L., CLEGG A.B., NEWTON D., Nucl. Phys. 54 (1964) 193

RUSH A.A., BURGE E.J., LEWIS V.E., SMITH D.A., GANGULY N.K., Nucl. Phys. A104 (1967) 340

SATCHLER G.R., Nucl. Phys. A100 (1967) 497

SATCHLER G.R., Nucl. Phys. A92 (1967) 273

SATCHLER G.R., HAYBRON R.M., Phys. Lett. 11 (1964) 313

SCHRANK G., WARBURTON E.K., DAEHNIK W.W., Phys. Rev. 127 (1962) 2170

SEITZ F., Discussions, Faraday Society 5 (1949) 271

SIFFERT P., COCHE A., HIBOU F., IEEE Trans. Nucl. Sci. NS-13 (1966) 225

SERBER R., Phys. Rev. 72 (1947) 1114

SIMON G.W., DENNEY J.M., DOWNING R.G., Phys. Rev. 129 (1962) 2454

SMULDERS P.J.M., ENDT P.M., Physica 28 (1962) 1093

STOVALL T., HINTZ N.M., Phys. Rev. 135 (1964) B330

STRAUCH K., TITUS F., Phys. Rev. 95 (1954) 854

STRAUCH K., TITUS F., Phys. Rev. 103 (1956) 200

STRAUCH K.,TITUS F., Phys. Rev. 104 (1956) 191

SUNDBERG O., JOHANSSON A., TIBELL G., DAHLGREN S., HASSELGREN D., HOISTAD B., INGEMARSSON A., RENBERG P.U., Nucl. Phys. A101 (1967) 481

TYREN H., MARIS A.J., Nucl. Phys. 3 (1957) 52

TYREN H., MARIS A.J., Nucl. Phys. 4 (1957) 637

TYREN H., MARIS A.J., Nucl. Phys. 6 (1958) 82

VAN ROOSBROECK W., Phys. Rev. 139 (1965) A1702

WILKINSON D.H., ROBSON B.A., TITTERTON E.W., Phys. Rev. 130 (1953) 1963

WILLIAMSON C.F., BOUJOT J.P., PICARD J., CEA - R3042 (1966)

WILLIS A., GEOFFRION B., MARTY N., MORLET M., ROLLAND C., TATISCHEFF B., Nucl. Phys. A112 (1968) 417

WOLFENSTEIN L., Ann. Rev. Nucl. Sci. 6 (1956) 4

APPENDIX 1

Germanium Total Absorption Spectrometer for 100 MeV Proton Scattering.

Published in the Canadian Journal of Physics, Vol. 45 (1967)

GERMANIUM TOTAL ABSORPTION SPECTROMETER FOR 100-MeV PROTON SCATTERING

Y. S. HOROWITZ AND N. K. SHERMAN
Foster Radiation Laboratory, McGill University, Montreal, Quebec
Received May 15, 1967

A lithium-drifted germanium total absorption spectrometer has been constructed and used to achieve an energy resolution of 0.49 ± 0.05 MeV in proton-scattering experiments at 100 MeV.

I. INTRODUCTION

Recently several authors, in patricular Bertrand *et al.* (1966) at 60 MeV, and Gruhn *et al.* (1967) at 160 MeV, have indicated that significant improvements in the energy resolution of intermediate energy proton-scattering experiments, while maintaining good data-taking rates, may be achieved by the use of lithium-drifted germanium detectors. We wish to report the successful use of these detectors in studies of the $^{12}C(p, p')$ and $^{197}Au(p, p)$ reactions produced by 100-MeV protons from the McGill synchrocyclotron. In previous experiments at this laboratory, an energy resolution of 1.1 MeV (FWHM) has been achieved with NaI(Tl) scintillation counters. We find, on the other hand, that lithium drifted germanium counters yield an overall resolution of 0.49 ± 0.05 MeV (FWHM) for protons scattered from gold, and 0.38 ± 0.05 MeV (FWHM) with the detector directly aligned in the beam. The latter value is essentially the incident beam width.

II. EXPERIMENT AND RESULTS

The depletion region of the detector is 0.6 × 1.0 × 2.6 cm³. (The range of 100-MeV protons in germanium is 2.5 cm.) The detector is used in a side-entry orientation in which the scattered protons traverse the detector in a direction at right angles to the direction of the electric field in the crystal. To protect the germanium detector from the environment of the scattering chamber vacuum system it was encapsulated in mild steel with an end window of 0.001-in-thick aluminium. The encapsulated crystal is mounted in a scattering chamber whose main features are: cooling of the detector to 140 °K, variability of the scattering angle, remote selection of targets, and television monitoring of the beam position. An anticoincidence telescope consisting of a brass collimator and a window scintillator preceding the germanium crystal completes the spectrometer.

A rather unfortunate feature of the data collected by Gruhn *et al.* was a considerable tail below the full energy peak which must have contained at least three times as many events as the peak itself. They estimated that the tail arose from roughly equal contributions of reactions in the crystal, slit scattering into the crystal, multiple scattering out of the crystal, and scattering from parts of the cryostat and other extraneous sources. We have minimized the contribution due to the second and third processes by collimating

the scattered protons with a slit 3 mm by 4.5 mm in area in a brass block thick enough to stop 100-MeV protons, followed directly by an anticoincidence plastic scintillator with a 2 mm by 0.8 mm hole in close proximity (~1 cm) to the germanium detector itself. With the incident beam spot kept about 3 mm in diameter, scattered protons which pass through the hole in the anticoincidence telescope impinge on the detector within a central area only very slightly greater than the physical size of the hole itself. We calculate that not more than 2% of the protons passing through this window can be lost from the sensitive volume through multiple scattering.

It is more difficult to estimate the effectiveness of our arrangement in eliminating slit scattering from the brass collimator. However, the results shown in Figs. 1 and 2 indicate good success. The peak-to-valley ratio in

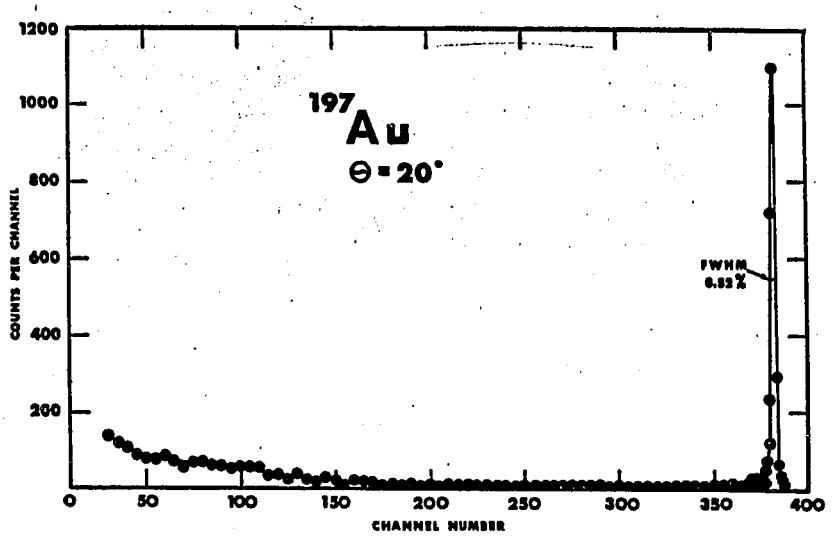

FIG. 1. Energy spectrum of protons scattered from ^{197}Au at a scattering angle of 20°. The figure shows the overall resolution before correcting for finite channel width.

Fig. 1 is 110 to 1, and the ratio for the case where the detector was in the direct beam was 250 to 1, compared with the Gruhn *et al.* value of 20 to 1. Furthermore, a Gaussian fit to the elastic and 4.43-MeV peaks in the ^{12}C spectrum (Fig. 2) indicates only a 10% deviation from Gaussian symmetry on the low-energy side of these peaks. Previous studies of the McGill cyclotron beam profile have indicated similar deviations from Gaussian symmetry on the low-energy side of the beam energy distribution which could account for much of the low-energy asymmetry in our spectra. The energy resolution in the ^{12}C spectrum is 0.63 ± 0.04 MeV, slightly worse than in the gold case. We attribute this mainly to kinematic broadening since our angular acceptance of 2.5° introduces a kinematic spread of 0.45 MeV (total width) for ^{12}C at a scattering angle of 35°.

The first detector tested showed massive deterioration in resolution after approximately four weeks in the neutron background environment of the

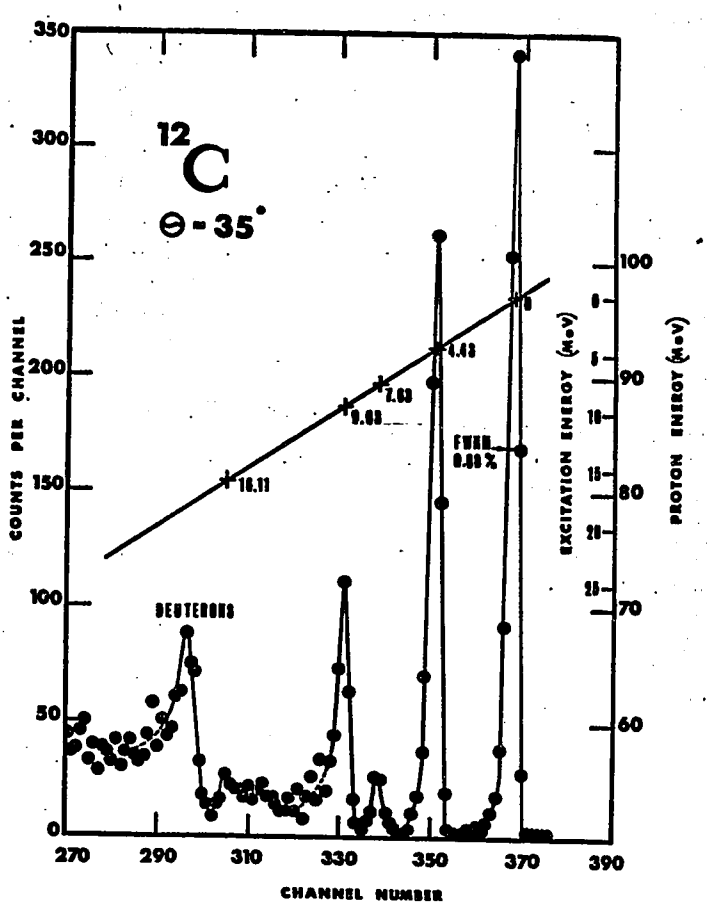

FIG. 2. Energy spectrum of protons scattered from ^{12}C at a scattering angle of 35°. The figure shows the overall resolution before correcting for finite channel width.

beam hall. To minimize possible radiation damage to the detectors now in use, the scattering chamber is removed from the cyclotron beam hall after each run. An accumulated dose of 10^7 protons/cm^2 has not resulted in any observable deterioration in resolution.

III. CONCLUSION

The results of our experiments indicate that Ge(Li) detectors can be used to achieve substantially improved energy resolution in intermediate energy proton-scattering experiments. The acceptance area of our spectrometer of 1.6 mm^2 represents a detection solid angle of 0.3×10^{-3} steradians; hence this improved resolution can be achieved with only a moderate sacrifice in the rate of data accumulation compared with present systems using NaI(Tl) scintillators. The energy resolution we have achieved is comparable to the resolution obtained with magnetic spectrometers, but is combined with a

much greater rate of data accumulation. The use of these detectors in inelastic proton-scattering experiments on light and intermediate nuclei is now underway in this laboratory.

ACKNOWLEDGMENTS

The detector was made and encapsulated (Webb 1966) at the RCA Victor Laboratories in Montreal. We wish to thank J. Annecou, S. Smith, R. Belley, S. Doig, R. H. Mills, and E. Yablonovitch for their technical support, and Professor R. E. Bell for helpful discussions. This work was supported by the Atomic Energy Control Board (Canada) and the National Research Council of Canada.

REFERENCES

BERTRAND, F. E., PEELLE, R. W., LOVE, T. A., FOX, R. J., HILL, N. W., and TODD, H. A. 1966. IEEE Trans. Nucl. Sci. NS-13, No. 3, 279.

GRUHN, C. R., KUO, T., GOTTSCHALK, B., KANNENBERG, S., and WALL, N. S. 1967. Phys. Letters, 24B, 266.

WEBB, P. P., GREEN, R. M., FOWLER, I. L., and MALM, H. L. 1966. IEEE Trans. Nucl. Sci. NS-13, No. 3, 351.

APPENDIX 2

Separation of Particles at Intermediate Energies in a Germanium Range Telescope Spectrometer.

Published in Nuclear Instruments & Methods, Vol.56 (1967)

NUCLEAR INSTRUMENTS AND METHODS 56 (1967) 106–108; © NORTH-HOLLAND PUBLISHING CO.

SEPARATION OF PARTICLES AT INTERMEDIATE ENERGIES IN A GERMANIUM RANGE-TELESCOPE SPECTROMETER

N. K. SHERMAN and Y. S. HOROWITZ

Foster Radiation Laboratory, McGill University, Montreal, Canada

Received 26 June 1967

At intermediate energies, clean proton scattering spectra and heavy particle reaction spectra can be obtained simultaneously using a two-detector range telescope. The method is based on the large difference between the range of protons and the range of all heavier particles of comparable energy. Its application at 100 MeV using germanium detectors to study ^{12}C and ^{9}Be is described.

1. Introduction

Long lithium-drifted germanium detectors with deep depletion layers are coming into use as spectrometers for inelastic proton scattering in the 50 to 200 MeV energy region[1-3]). These detectors provide energy resolution comparable to that obtained in practice with magnetic spectrometers (better than 0.5%), with comparable acceptance solid angle (about 10^{-3} sterad) and with the great advantage of providing a complete energy spectrum in a single detector. However, the advantage lies with the magnetic spectrometer when it comes to separating the several different particle species, each with a spectrum exhibiting many peaks, which can be produced in proton-nucleus reactions. Earlier workers in the intermediate energy region, using plastic scintillators or NaI(Tl) crystals as detectors (with about 1.6% resolution), have resorted to $(E+\mathrm{d}E/\mathrm{d}x)$ particle sorting. We wish to describe a technique which we are applying to germanium detectors, whereby we will obtain clean proton spectra by range discrimination in the detector against deuterons and heavier particles. In addition, simultaneously with the proton spectrum from the (p,p′) reaction, an energy spectrum of all the other reactions, frequently dominated by the deuteron spectrum from the (p,d) reaction, will be obtained. In other cases, (p,d), (p,t), (p,^{3}He) and (p,α) reaction peaks can be identified by subsequent kinematic analysis of angular distributions.

The technique takes advantage of the widely-differing ranges of scattered protons and pickup deuterons in the intermediate energy region. It applies to experiments in which the incident beam energy is kept fixed. We suggest using a two-counter telescope in which the front detector is long enough to stop emitted deuterons and heavier particles, and the second detector is long enough to stop protons transmitted by the first. In the explanatory examples which follow, we will restrict our remarks to reactions produced by 100 MeV protons. The method can be applied at other energies as well and, of course, to detectors other than germanium. We refer to germanium detectors having depletion layers several millimeters deep used in end-entry orientation.

2. Example I: carbon-12

Table 1 shows the calculated energy losses by protons in each segment of a double germanium detector designed for use with carbon targets. Both detectors will be contained in the same capsule. The front counter must be long enough to stop deuterons having the highest energy that can be produced at 100 MeV from ^{12}C, namely 82.46 MeV. To allow for range straggling (about 5% of the range) and uncertainty in the range-energy relations, the front counter is designed to stop deuterons of 7% higher energy, whose range in germanium ($Z=32$, $\rho=5.32$ g/cm^3) is 6.0 g/cm^2, or 11.3 mm. This length is the range of a 64 MeV proton. The sum of the two counter lengths must be greater than 25 mm in order to stop 100 MeV protons. We have already obtained energy resolution of 0.38% using a counter which is 26.1 mm long[3]). To obtain the scattered proton spectrum, the pulse heights recorded by the front and rear counters are added when they register a coincidence. This can be done either by analog addition before pulse height analysis, or by digital addition after analysis. The sum spectrum of the front and rear counters will be a pure proton spectrum extending down to 64 MeV from the ^{12}C elastic peak. In practice a rear counter coincidence threshold might raise this figure slightly. (The threshold in the front counter could be set as high as 32 MeV.) Even at 180° laboratory angle, the elastic peak is above 70 MeV. At 70°, it is at 89 MeV; and at 50° it lies at 94 MeV, allowing an energy band of 30 MeV in which to study excited levels of ^{12}C.

When the mass number A of the target nucleus is small, the peaks in the reaction spectra move rapidly towards lower energies as the detector angle relative to the incident beam direction increases. This target

TABLE 1
Proton energy losses in front and rear counters when front counter is 11.3 mm long.

Incident proton energy (MeV)	Loss in front counter (MeV)	Loss in rear counter (MeV)
100	32	68
95	33	62
90	35	55
85	36	49
80	39	41
75	41.5	33.5
70	48	22
65	56	9
64	64	0

recoil effect nearly vanishes at large A; however, for the light nuclei it reduces the width of the excitation energy band which can be studied at large angles, since the proton range cutoff in the front detector is constant. This is not a real limitation because nuclear level spacings at excitation energies near the cutoff are usually smaller than the detector's energy resolution. Furthermore, in published (p,p') work at intermediate energies[4]), 45° is about the largest laboratory angle which has been studied.

It should be emphasized that if a detector is designed to study a nucleus of mass A having a (p,d) reaction Q-value equal to Q, it can be used to study the (p,p') reaction in nuclei having $A' \geqq A$ and $Q' \leqq Q$. Carbon is an unusually favorable example. Its large and negative $Q(-16.49$ MeV) offsets its low A.

Now let us discuss the deuteron spectrum. A heavy-particle spectrum can be obtained from the front counter without demanding an anticoincidence with the rear counter since no proton can lose more than 64 MeV in the front counter. With this proton cutoff, at small detection angles the front counter provides a proton-free spectrum extending more than 18 MeV away from the ground-state peak of ^{11}C at 82.46 MeV. The ground-state deuteron peak moves down in energy as the emission angle is increased, but is still 10 MeV above the proton cutoff at 52.5°. Care in analyzing the heavy-particle spectrum is required, since for example at 37°, alpha particles corresponding to the ground-state of ^{9}B produced in the (p,α) reaction lie under the deuteron peak corresponding to the ground-state of ^{11}C. The two energy-vs-angle loci cross at this angle. (In ^{40}Ca for example, none of the loci intersect.) The band of excitation energy of the (p,d) daughter nucleus and the range of deuteron emission angles which can be observed compare favourably with the energy and angle regions previously studied using poorer-resolution detectors.

3. Example II: beryllium-9

The more positive the Q-value of the (p,d) reaction becomes, the more energetic the observed deuterons can be, and the thicker the front counter must become. The proton cutoff therefore rises and reduces the available energy band over which a pure proton spectrum is obtainable. One of the worst cases is that of ^{9}Be, which has a positive Q-value (+0.56 MeV) and in addition has small A, so that the proton elastic peak moves rapidly in the direction of the cutoff energy with increasing angle. But even here the method is very useful. The maximum deuteron energy is 98.6 MeV. Again adding 7% to the energy, which is more conservative than adding it to the range, we obtain 15.4 mm as the length of the first detector. The proton cutoff is therefore 76 MeV. The rear detector from example I can of course be used as the rear detector in this example as well.

With this spectrometer the elastic (p,p) reaction can be studied from 0° to 99° in the laboratory. If we accept 0° to 50° as the maximum angular range which it is practical to study (the cross sections become very small at larger angles), then the elastic proton peak will fall from 100 MeV to 92 MeV as the angular region is traversed. When the detector is at forward angles, nuclear structure can be observed over a band of 24 MeV in the inelastic spectrum. At 50°, this band has shrunk to 16 MeV, which is still very useful. In addition, at any angle out to and beyond 90°, the ground-state deuteron peak corresponding to ^{8}Be formation lies at least 9 MeV above all the other (p,x) reactions, and lies 10 MeV above the proton cutoff in the first counter out to 52.5°. Hence the front counter gives a clean deuteron spectrum, and the sum of the

TABLE 2
Proton energy losses in front and rear counters when front counter is 15.4 mm long.

Incident proton energy (MeV)	Loss in front counter (MeV)	Loss in rear counter (MeV)
100	45	55
95	49	46
90	52	38
85	56	29
80	65.5	14.5
76	76	0

pulses from the front and rear detectors provides a clean proton spectrum.

4. Conclusion

These two examples show that clean proton spectra are obtainable by range discrimination in a two-counter germanium spectrometer when the double detector is tailored to one particular target nucleus. Enclosing two detectors having separate signal leads in one capsule having a thin entrance window should cause no essential difficulties. It may seem wasteful to require a different front detector for each target studied. Radiation damage, however, limits the lifetime of lithium-drifted germanium detectors to about 10^8 detected 100 MeV protons which is comparable to the number needed for good statistics in a study of one nucleus. Nevertheless, since techniques for restoring radiation-damaged detectors are improving, we are examining the possibility of optimizing one two-detector combination to study a range of nuclear masses.

We wish to thank Professor R. E. Bell for discussions on range straggling. This work was supported by the National Research Council and the Atomic Energy Control Board (Canada).

References

[1] F. E. Bertrand, R. W. Peelle, T. A. Love, R. J. Fox, N. W. Hill and H. A. Todd, IEEE Trans. Nucl. Sci. NS-13, no. 3 (1966) 279.

[2] C. R. Gruhn, T. Kuo, B. Gottschalk, S. Kannenberg and N. S. Wall, Phys. Lett. 24B (1967) 266.

[3] Y. S. Horowitz and N. K. Sherman, Bull. Am. Phys. Soc. 12 (1967) 632.

[4] D. Hasselgren, P. U. Renberg, O. Sundberg and G. Tibell, Nucl. Physics 69 (1965) 81.